UNIVERSITÀ
DEGLI STUDI
DI PADOVA

Università degli Studi di Padova

Department of Medicine

Ph.D. COURSE IN: CLINICAL AND EXPERIMENTAL SCIENCES

CURRICULUM: HEPATOLOGY AND TRANSPLANTATION SCIENCES

SERIES XXXI

CONFINED EXTRACELLULAR ENVIRONMENT AFFECTS PLURIPOTENCY MAINTENANCE AND ACQUISITION

Coordinator: Prof. Paolo Angeli

Supervisor: Prof. ssa Patrizia Pontisso

Co-Supervisor: Prof. Nicola Elvassore

Ph.D. student: Erika Torchio

SUMMARY

Human pluripotent stem cells represent a model to study early embryonic stages *in vitro*. Pluripotent stem cells are characterized by the ability to proliferate continuously and to differentiate in all cells and tissues composing the human body. Pluripotent stem cells, are not only a potentially unlimited source of any desired cell, but represent also a powerful tool to recapitulate *in vitro* early embryogenesis.

In vitro, two stages of pluripotent stem cells have been isolated, named naïve and primed states. The first represents a more primitive stage, and is linked to the pre-implantation stage of the embryo, while the latter is linked to the post-implantation stage. Differences between the two stages are important to be examined because may shed light on mechanisms underlying embryo implantation failures.

Moreover, *in vitro*, pluripotency can be acquired by somatic cells thanks to cell reprogramming. This technique radically rewrites cell expression program and represents a revolutionizing tool for patient-specific therapies because gives access to a patient-specific unlimited source of any required cell type. Among different reprogramming strategies, the use of microfluidic platforms represents a boost for cell reprogramming, allowing cost-effective and high-efficiency experiments, but the reasons behind this increase in efficiency have not been uncovered yet.

Indeed, the outcome of a revolution in cell expression program similar to the one occurring in cell reprogramming is diagnosed every day in hospitals, under the name of cancer. In fact, at the basis of cancer onset there are abnormal gene mutations that allow the de-differentiation of somatic cells and the re-acquisition of stem-like features such as proliferation and motility. Cells that undergo this process are named cancer stem cells. To counteract cancer de-regulated gene expression, cell

reprogramming could act as a tool to reset cancerous epigenetic state and re-establish the correct expression program.

Current studies on pluripotent stem cells *in vitro* maintenance and on pluripotency acquisition by reprogramming focus mainly on gene expression differences between naïve and primed stem cells or between somatic and pluripotent cells, without considering the extracellular environment surrounding those cells, the extracellular matrix contribution and the spatial organization of these cells in the 3D space. Nevertheless, those factors have been proved to be fundamental for embryo development.

In this work, thanks to microfluidic platforms, *in vitro* cell culture environment has been miniaturized to better simulate *in vivo* conditions and confined environment contribution to pluripotency maintenance and acquisition has been evaluated.

To gain a broad view on the complex phenomena of cell pluripotency and cell heterogeneity, molecular target-driven approaches have been set aside in favor of multi-omic, unsupervised approaches and the whole secretome and transcriptome of pluripotent stem cells have been analyzed. Moreover, single-cell approaches have been applied to dissect cell heterogeneity. Guided by proteomic and transcriptomic results, this work focuses then on extracellular matrix analysis along pluripotency maintenance and acquisition.

The first chapter presents an introduction to naïve and primed pluripotency stages, cell reprogramming techniques and cancer stem cells concept, with an insight on cancer reprogramming and on SERPINB3 role in cancer aggressiveness. Then the chapter introduces the structure of extracellular matrix and a state-of-the-art update on matrix role in stem cells culture and reprogramming. Afterward microfluidic platform features and advantages are presented and finally the chapter introduces the concept of single-cell RNA-sequencing and the main approaches to study cell heterogeneity.

The second chapter focuses on the aim of this work, while the third chapter presents all the materials and methods employed in this thesis.

The fourth chapter presents the results obtained in this work: initially the colony structure and extracellular matrix organization in naïve and primed pluripotent stem

cells, as well as in differentiated fibroblasts is analyzed in conventional cell culture devices, reporting a striking difference in matrix organization among the different stages. Then the influence of confined environment on the above-mentioned stages is investigated, revealing the role of confined environment in inducing matrix production. Afterward, the link between colony shape, mechanotransduction and matrix deposition has been examined for the first time in naïve pluripotent stem cells, revealing that 3D spatial organization is linked to higher extracellular matrix deposition and naïve pluripotency marker expression. Next, extracellular matrix organization after cell reprogramming has been analyzed in newborn pluripotent colonies, both in conventional devices and in confined environment, showing a different organization of matrix deposition in the two conditions that can contribute to explain the high reprogramming efficiency obtained in microfluidic platforms. Aiming at simulating cancer reprogramming and studying possible SERPINB3 influence on cancer reprogramming, this serpin has been administered during cell reprogramming of a model cell line, resulting in drastic reduction of reprogramming efficiency. The possible reasons for this outcome have been investigated also thanks to transcriptomic database analysis. Finally, the chapter reports the setup of Drop-Seq single-cell RNA-sequencing: a cost-effective, microfluidic-based single-cell analysis system.

In conclusion, this work contributes to pluripotent stem cells knowledge by giving for the first time a portrait of extracellular matrix organization in naïve and primed pluripotent stem cells. Moreover, it shows how extracellular matrix and 3D colony organization is linked to pluripotency gene expression in naïve pluripotent stem cells, and to pluripotency acquisition via cell reprogramming. Finally, it reports how SERPINB3, a protein which is highly expressed in aggressive tumors, inhibits cell reprogramming, suggesting an inhibition of this protein if approaching reprogramming of tumors with high SERPINB3 expression.

RIASSUNTO

Le cellule staminali pluripotenti umane rappresentano un modello per lo studio *in vitro* dei primi stadi di sviluppo embrionale. Le cellule staminali pluripotenti sono caratterizzate dalla capacità di proliferare in maniera illimitata e di poter differenziare in qualunque tipo cellulare che compone il corpo umano. Le cellule staminali pluripotenti non sono solo una fonte potenzialmente infinita del tipo cellulare d'interesse, ma sono anche un ottimo strumento per ricostruire e studiare l'embriogenesi *in vitro*.

In vitro sono stati isolati due stadi di cellule staminali pluripotenti, denominati stadio naïve e primed. Il primo rappresenta uno stadio più primitivo nell'embriogenesi ed è collegato allo stadio di embrione pre-impianto, mentre il secondo è collegato allo stadio post-impianto. È importante analizzare le differenze fra i due stadi perché potrebbero contribuite a comprendere i meccanismi alla base dell'alto tasso di fallimenti negli impianti degli embrioni nell'utero.

La pluripotenza può anche essere riacquisita *in vitro* da parte di cellule somatiche differenziate, grazie ad una tecnica nota come riprogrammazione cellulare. Questo metodo consente di riscrivere radicalmente il programma di espressione genica delle cellule e rappresenta uno strumento rivoluzionario per terapie paziente-specifiche, poiché dà accesso ad una fonte illimitata di cellule paziente-specifiche. Fra le diverse strategie di riprogrammazione cellulare, l'utilizzo di piattaforme microfluidiche garantisce un sostanziale potenziamento del il processo, consentendo di riprogrammare cellule ad alta efficienza e con costi ridotti. Tuttavia le ragioni per questo incremento nell'efficienza di riprogrammazione non sono ancor noti.

Il risultato di un processo simile a quello della riprogrammazione cellulare viene diagnosticato quotidianamente nei nostri ospedali, sotto la definizione di cancro. Infatti, alla base dello sviluppo della massa tumorale si trovano mutazioni alterano la normale espressione genica delle cellule, promuovendo un de-differenziamento delle cellule coinvolte con riacquisizione di caratteristiche tipiche di cellule staminali, come la proliferazione illimitata e riacquisizione di motilità, portando alla nascita delle cosiddette cellule staminali del cancro. Per contrastare l'espressione genica alterata dal cancro, la riprogrammazione cellulare potrebbe rivelarsi uno strumento in grado di resettare lo stato epigenetico tumorale e ristabilire il corretto programma di espressione genica.

I recenti studi riguardanti il mantenimento *in vitro* di cellule staminali pluripotenti o la riacquisizione di pluripotenza mediante riprogrammazione cellulare si focalizzano principalmente sulle differenze di espressione genica fra cellule staminali naïve e primed o fra cellule somatiche e riprogrammate, senza considerare l'ambiente extracellulare che circonda le cellule stesse, il contributo della matrice extracellulare e l'organizzazione spaziale tridimensionale di queste cellule. È importante notare che questi fattori si sono dimostrati fondamentali per lo sviluppo embrionale *in vivo*.

In questo studio, grazie a piattaforme microfluidiche, l'ambiente di coltura extracellulare è stato miniaturizzato per simulare al meglio le condizioni *in vivo* ed è stato valutato il contributo di tale ambiente confinato al mantenimento e all'acquisizione di pluripotenza.

Per avere una visione d'insieme su fenomeni complessi come la pluripotenza e l'eterogeneità cellulare, sono stati messi da parte approcci basati su specifici bersagli molecolari in favore di approcci multi-omici come l'analisi completa del secretoma e del trascrittoma delle cellule staminali pluripotenti e differenziate. Inoltre, per analizzare l'eterogeneità del sistema, sono stati utilizzate tecniche single-cell. Guidato dai risultati dell'analisi proteomica e trascrittomica, questo lavoro si focalizza anche sull'analisi della matrice extracellulare nell'ambito del mantenimento e dell'acquisizione di pluripotenza.

Il primo capitolo fornisce un'introduzione sugli stadi di pluripotenza naïve e primed, sulle tecniche di riprogrammazione cellulare e sul concetto di cellule staminali del cancro, con riferimento anche alla riprogrammazione di cellule tumorali e sul ruolo della proteina SERPINB3 nei tumori più aggressivi. In seguito il capitolo presenta la struttura generale della matrice extracellulare e un aggiornamento sullo stato dell'arte riguardante il ruolo della matrice nelle colture di cellule staminali e nella riprogrammazione. Inoltre riporta le principali caratteristiche e vantaggi delle piattaforme microfluidiche. Infine il capitolo introduce il concetto di single-cell RNA-sequencing e i principali approcci allo studio dell'eterogeneità nella popolazione cellulare.

Il secondo capitolo presenta lo scopo del lavoro di tesi, mentre il terzo capitolo descrive tutti i materiali e metodi impiegati.

Il quarto capitolo espone i risultati ottenuti in questo lavoro: innanzitutto è stata analizzata la struttura della matrice extracellulare di cellule staminali pluripotenti naïve e primed e di fibroblasti differenziati cresciuti in supporti convenzionali di crescita cellulare, dimostrando una sostanziale differenza nell'organizzazione della matrice extracellulare nei diversi stadi di differenziamento. In seguito è stata valutata nei sopracitati stadi l'influenza dell'ambiente confinato garantito dall'utilizzo di piattaforme microfluidiche, rivelando un ruolo dell'ambiente confinato nell'indurre produzione di matrice. Successivamente è stato esaminata in colonie naïve, la relazione tra forma 3D della colonia, meccanotrasduzione e deposizione di matrice, rivelando che a una maggior organizzazione 3D della colonia corrisponde a maggior produzione di matrice e di espressione di marcatori di pluripotenza naïve. Inoltre l'organizzazione della matrice extracellulare è stata analizzata alla fine del processo di riprogrammazione cellulare in colonie riprogrammate sia in supporti convenzionali sia in piattaforme microfluidiche, mostrando una deposizione molto dissimile nei due ambienti. Questa osservazione può contribuire a spiegare l'alta efficienza di riprogrammazione ottenuta in piattaforme microfluidiche. Allo scopo di simulare la riprogrammazione di cellule tumorali e studiare la possibile influenza di SERPINB3 su tale processo, questa proteina è stata somministrata durante esperimenti di riprogrammazione di cellule modello, portando al crollo dell'efficienza di riprogrammazione. Le possibili spiegazioni di questo risultato sono

state approfondite anche grazie ad analisi di database trascrittomici. Infine il capitolo descrive la messa a punto del sistema Drop-Seq per single-cell RNA-sequencing: uno strumento economico e basato su piattaforme microfluidiche per analisi single-cell.

Questo lavoro contribuisce ad accrescere le attuali conoscenze sulle cellule staminali pluripotenti realizzando per la prima volta un ritratto dell'organizzazione della matrice extracellulare in cellule staminali pluripotenti naïve e primed. Inoltre mostra come la matrice extracellulare e l'organizzazione tridimensionale della colonia siano collegati all'espressione di geni di pluripotenza in cellule naïve e all'acquisizione di pluripotenza in caso di riprogrammazione cellulare. Infine riporta come SERPINB3, proteina maggiormente espressa nei tumori più aggressivi, inibisce la riprogrammazione cellulare, suggerendo la possibilità di inibire questa serpina prima di affrontare la riprogrammazione di cellule derivate da tumori con elevata espressione di SERPINB3.

INDEX

FIGURE INDEX

CHAPTER 1: INTRODUCTION

CHAPTER 2: AIM OF THE THESIS

CHAPTER 3: MATERIALS AND METHODS

CHAPTER 4: RESULTS AND DISCUSSION

TABLES INDEX

CHAPTER 1: INTRODUCTION

CHAPTER 3: MATERIALS AND METHODS

CHAPTER 1: INTRODUCTION

1.1. PLURIPOTENCY *IN VIVO* AND *IN VITRO*

In cell biology, potency is defined as the ability of a cell during development to divide asymmetrically and differentiate into daughter cells with and lower potency level and distinct characteristics compared to the mother cell[1]. Therefore, the wider the range of commitment options, the greater the pluripotency is.

In this scenario, totipotency identifies cells able to give rise to every cell type sufficient to form the entire organism and represents the highest differentiation potential achievable. Other potency levels that have been observed are defined as pluripotency, multipotency, oligopotency and unipotency, in a descending loop of potency narrowing[1].

In particular, pluripotency is defined as the ability of a cell, which takes the name of stem cell, to give rise to daughter cells that belongs all three embryonic germ layers, but not to every extra-embryonic tissue[1,2]. This stage is considered of great interest for both basic science and translational applications. Indeed, a full picture of human pluripotency will not only help in understanding why embryogenesis fails at least three times as often as it succeeds[3], but will also open new doors to a more efficient cell differentiation for regenerative medicine, drug screening or tissue engineering[4].

1.1.1. *In vivo* embryogenesis is a continuous process

1.1.1.1. From zygote, to blastocyst, to germ layer specification

In vivo, during human embryogenesis, differentiation proceeds as a continuum, starting from the totipotent zygote, as represented in fig.1.1.

Right of after fecundation, the zygote begins to exist in the oviduct as a single cell and in the first 3 days of gestation, it undergoes a series of mitotic divisions without growing in size, becoming a compact cell mass, called morula, composed by 16 cells. By the stage of morula, the embryo has reached the uterus. The following divisions of the morula are marked by the beginning of cell self-organization and fluid production, where it is possible to observe a difference in gene expression between the cells in the center of the mass and the outer layer.

By day 5, the 32-cells morula cell mass becomes a blastocyst that it is organized as a hollow sphere composed by an outer shell layer called trophoblast and an inner group of cells called the inner cell mass. The remaining hollow cavity is the blastocoel and is filled with fluid produced by the cells themselves. The passage from 16-32 cells morula to blastocyst represents the end of embryo totipotency: the cells of the trophoblast will become the fetal portion of the placenta, while the cells composing the inner cell mass will give rise to all body tissues and therefore are considered pluripotent.

After the formation of the blastocyst, by the end of the first week of gestation, the embryo implants in the uterine wall. The implantation marks the distinction between two phases of embryogenesis: the pre-implantation and the post-implantation embryo. After implantation, the cells of the inner cell mass differentiate into two layers of cells: the epiblast and the hypoblast, which represents two layers of the bilaminar disc that divide the blastocyst into two cavities. The cavity on the hypoblast side will become the extraembryonic yolk sac, while the cavity on the epiblast side will become the amniotic cavity that will surround the growing fetus.

The third week of gestation is the week of gastrulation, when the epiblast loses its pluripotency state and differentiates in the three germ layers: endoderm, mesoderm and ectoderm. Each germ layer is considered multipotent because it will differentiate into a limited number of tissues. For example, endoderm will give rise to stomach, liver, lung, pancreas, bladder

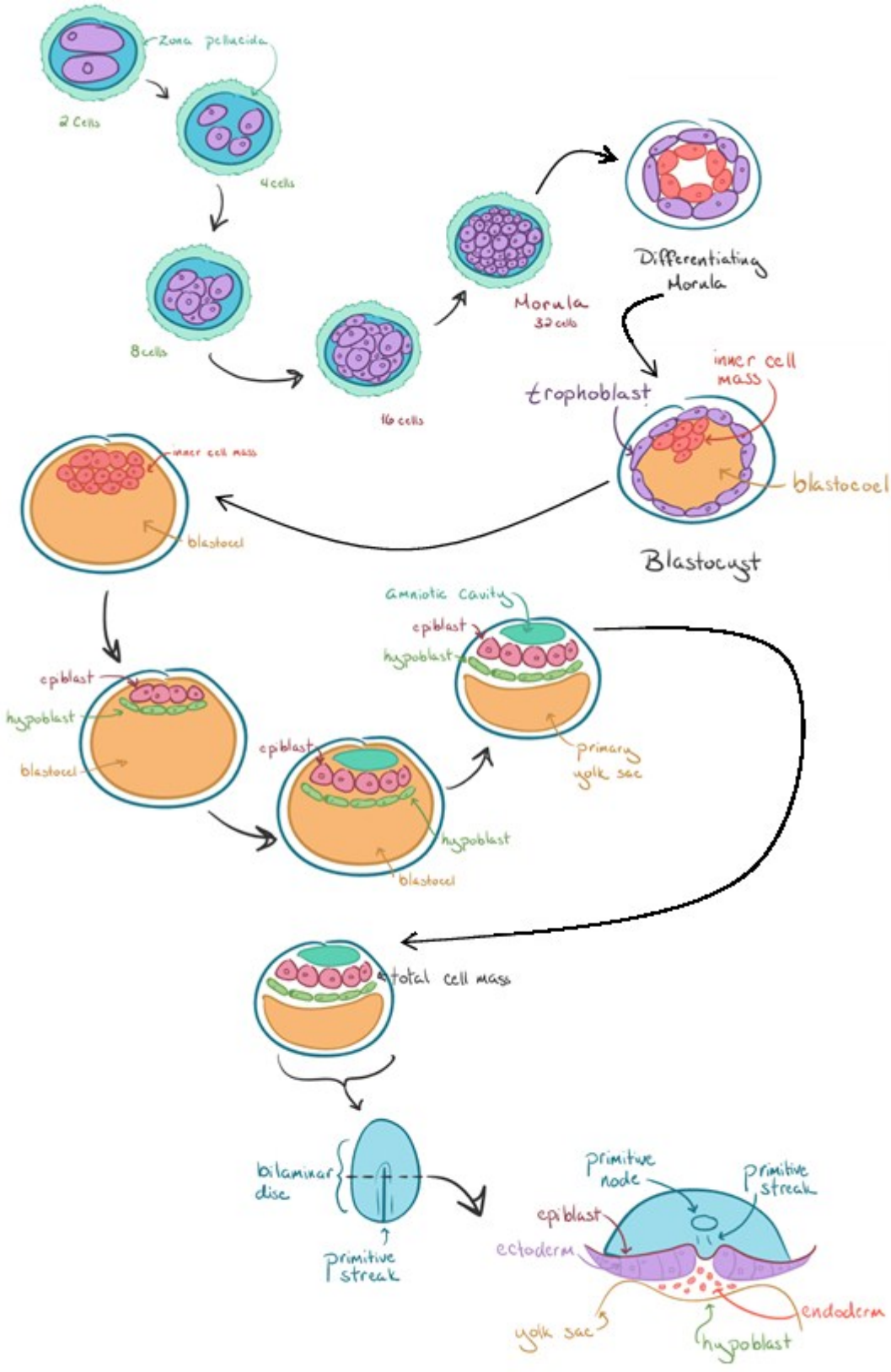

***Figure 1.1: Human embryo development, from fecundation to gastrulation**. Modified from "Human Embryogenesis", Khan Academy, under CC-BY-NC-SA 4.0 creative common license.*

and colon, mesoderm to muscle, connective tissue, bone and circulatory system and ectoderm to brain, peripheral nervous system, spinal cord and skin. Gastrulation begins with the formation of the primitive streak: an indentation along the dorsal surface of the epiblast with specific rostral-caudal orientation. The primitive streak divides the left and right sides of the body and a node at the caudal end of the primitive streak emits growth factors that direct cells to multiply and migrate. Thus, the primitive streak is composed by very motile cells moving toward and through the primitive streak, from the top of the original epiblast to the hypoblast, then moving laterally, creating invaginations. The cells that invaginate first and move deeply toward the hypoblast form the endoderm, those who remain between the original epiblast and the endoderm form the mesoderm and those that continue to border the amniotic cavity form the ectoderm. Ectoderm and endoderm are characterized by tightly connected epithelial sheets, while the mesodermal cells are less organized loosely connected.

Following gastrulation, organ formation starts, in a process called organogenesis. By week eight the embryonic period ends, the rudimental organs are formed and the embryo is about 3 cm long and weighs about 8 g. Organogenesis is characterized by continuous decrease of cell potency that will leave in the adult only few niches of precursor cells, called adult stem cells[3].

1.1.1.2. Intrinsic and environmental cues trigger cells self-organization

Since every cell in an organism shares the same DNA of the zygote, an alternative source of variability needs to be taken into account to explain cell differentiation. Indeed it's the epigenetic state of the cell, controlled by modifications to DNA and histones, that alters gene expression patterns and is responsible for cell identity[5]. During embryo development, the fine control of gene expression patters allows the proper transitions between cellular states by regulating gene expression networks responsible for maintenance of pluripotency or differentiation. Recent single-cell analysis methods are starting to shed light to the complexity of embryo heterogeneity revealing that a small number of functional modules of co-expressed genes,

also known as morphogens, can define each developmental stage[6], but the current understanding of the molecular pathways and their interconnections and crosstalk with the environment is far from complete[7]. Here, only few examples of cell-fate determinants and morphogens will be explained and the main concept of gradient-driven lineage specification is summarized in fig.1.2.

As a general mechanism, polarity acquisition and fate decision depends on gradients of signaling molecules and on mechanical sensing of cell position. For example, when the morula becomes a blastocyst, specific signals play their role to distinguish cells that will become the inner cell mass from the cells that will become the trophoblast. In this first cell fate decision, known as first lineage specification, the outer cell layer of the morula (8-16 cells stage) maintain expression of TEAD4, which is a strong activator of CDX2 and blocks OCT4, thus becoming trophoblast cells, while the inner cells will maintain OCT4 expression that inhibits TEAD4 and will become the inner cell mass. $OCT4^{+}$ cells will then secrete FGF4 to signal to the neighbor cells to remain trophoblast cells and proliferate[8]. It has been demonstrated that this mutual repression depends only on the position of the cells in the morula mass. In fact, outer cells have fewer contacts with the other cells and are more subject to mechanical stress; this results in YAP nuclear localization. Instead, in the inner cell mass cells have more contacts with the cells and are not subjected to polarizing stimuli, therefore the HIPPO pathway is active and YAP is inactive. TEAD4 requires YAP nuclear localization to activate CDX2 transcription, therefore in the inner cell mass TEAD4 cannot activate CDX2 and OCT4 signaling prevails[9]. In this mechanism, a combination of mechanical stimuli and FGF4 gradient is responsible for the first cell fate decision of embryo development.

At the late blastocyst stage, a second lineage specification occurs and the inner cell mass divide into epiblast and primitive endoderm layer. The players involved in this fate decision are NANOG and GATA6, which are mutually exclusive. In the inner cell mass, cells are randomly expressing one of these two factors in a salt-and-pepper fashion, but at the late

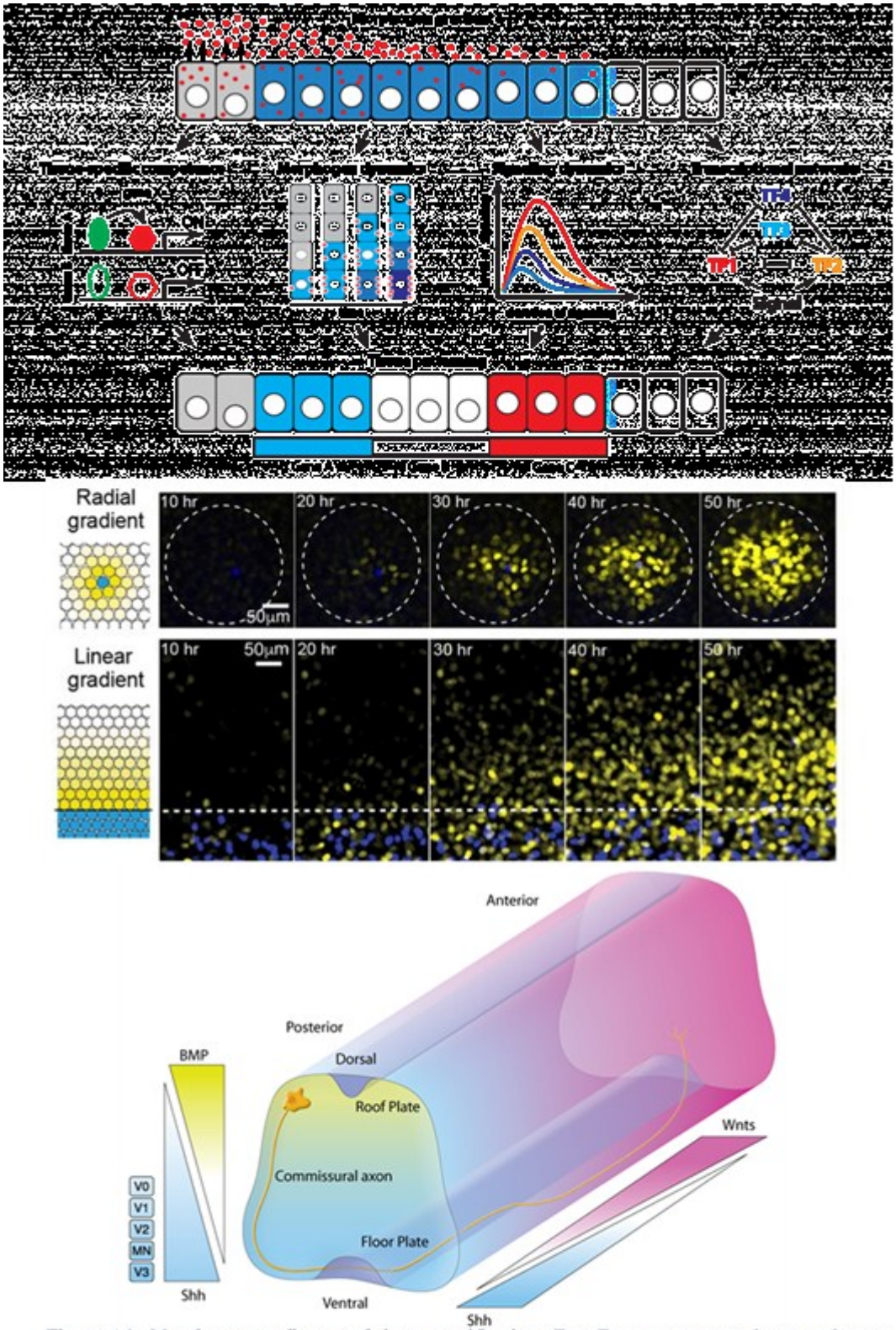

Figure 1.2: Morphogen gradients and tissue specification. ***Top****: Tissue patterning during embryonic development relies on the differential induction of target genes by morphogen gradients. Induction of target genes depends not only on the level of the morphogen, but also the specific competence of receiving cells, the ability of cells to decode dynamics of morphogen signaling, and the regulatory logic of downstream transcriptional networks. Modified from: Sagner et al. 2017.* ***Middle****: Time-lapse images of representative radial and linear SHH signaling gradients. Modified from: Li et al. 2018.* ***Bottom*** *: Example of Shh, BMP, and Wnt gradients that help guide axon orientation. Adapted from R&D Systems Inc. (www.rndsystems.com/resources/articles/sonic-hedgehog-morphogen-involved-axon-guidance).*

blastocyst stage the expression becomes patterned due to cell migration or cell apoptosis[10]. This is another example of cell ability to self-organize and give rise to patterns, even if the complete mechanism is not fully understood.

During gastrulation, gradient of secreted BMP4 will determine the dorso-ventral orientation of the embryo, while NODAL and WNT gradient define the anterior-posterior orientation. In presence of high NODAL and BMP4 expressions, cells will undergo epithelial-to-mesenchymal transition and migrate forming the primitive streak, where more motile cells will then become mesoderm, while less motile cells will become endoderm cells. The migration direction and the migration speed is determined by the gradient intensity. In the region of the embryo where both NODAL and BMP4 gradients are low, cells do not migrate and will become ectoderm.

Another pathway fundamental for body segment development and in formation of adult appendages is sonic hedgehog (SHH). In a recent work it is possible to appreciate how SHH gradients can direct morphogenesis[11,12].

Taken together, these examples show how molecular gradients, cell-cell contacts and, in general, the microenvironment that surrounds the cells is able to shape cell fate.

1.1.2. *In vitro* pluripotency cell models establishment

Studying pluripotency cannot rely only on the observation of embryos at different stages of development, especially where human embryos are concerned, therefore pluripotency models needed to be established. The first pluripotent cell line was derived in 1976 from a mouse teratocarcinoma, a germline tumor[13], followed by the isolation of embryonic stem cells from mouse embryos(mESCs) in 1981[14]. The first human embryonic stem cell line (hESC) was established in 1998 from the cells of the inner cell mass of a human blastocyst and represented the foundation of human stem cell biology[15].

Conversely to *in vivo* development, where pluripotency is a continuum of transient states, *in vitro* distinct pluripotent stages can be established and propagated. Pluripotent cells can be maintained indefinitely in culture by

promoting artificially self-replication thanks to the supplementation of exogenous factors[16]. Notably, self-renewal is only a transient feature of *in vivo* embryo development, but it is a fundamental aspect of *in vitro* cell models because it allows the propagation of everlasting cell lines.

The establishment of embryonic pluripotent cell lines must satisfy the following criteria[15]:

- Derivation from the inner cell mass of the blastocyst of a preimplantation embryo;
- *In vitro* prolonged self-replication in undifferentiated state;
- Ability to differentiate cells belonging to all three germ layers, even after prolonged *in vitro* culture.

According to those criteria, both for human and mouse embryonic stem cells, two different pluripotent cell stages have been established *in vitro*. By comparing their morphological and molecular features to their *in vivo* embryonic counterparts they have been named primed and naïve pluripotent stem cells. Their features are compared in Table 1 and in fig.1.3.

1.1.2.1 Primed pluripotent stem cells

The subtype of primed human embryonic stem cell line (hESC) has been the first one to be established from the inner cell mass of a human blastocyst[15]. At first primed hESC were cultured on a layer of mitotically inactivated (by mitomycin or γ-irradiation treatment) mouse embryonic fibroblast (MEF) as feeder layer, but recently many surrogates have been developed to substitute the MEF layer[15,17,18].

Short after hESC establishment, many differences between human and mouse ESC (mESC) have been noticed[19], starting from morphology: primed hESC grow as colonies of cells with flat, epithelial-like morphology, where cells show a high nucleus to cytoplasm ratio and prominent nucleoli. In contrast, mESC have a compact, dome-like 3D shape and cells cannot be distinguished from the mass.

In primed hESC, the core pluripotency network that maintains cells in undifferentiated state is composed by the transcription factors OCT4, SOX2

and NANOG, the same genes responsible for mESC, but in mESC OCT4 requires the activation of its distal enhancer, while in primed hESC the preferred enhancer is the proximal one. Moreover, primed hESC rely on fibroblast growth factor 2 (FGF2) and transforming growth factor-β1 (TGF-β1) / ActivinA signaling for proliferation and self-renew but are not dependent on LIF signaling, differently from mESC. Thus, in primed hESC, pluripotency is dependent on MEK/ERK pathway. Other typical markers of primed hESC are SSEA4, TRA-1-60, TRA-1-81[20].

In contrast to mESC, primed hESC show low clonogenicity and have low tolerance to single-cell passaging, requiring Rho-associated kinase inhibition to survive this procedure[21]. Moreover, primed hESC have low capability of colonization of the pre-implantation ICM to form mixed-species chimeras[22,23].

When looking at epigenetic features, more differences between human and mouse ESC can be detected: primed hESC show tendency to maintain X chromosome inactivation (XiXa state) in female cells and high H3K27me3 methylation is observed on developmental regulators. DNA is globally hypermethylated[24]. Instead, in mESC, both X chromosomes are active (XaXa state) and epigenetic methylation on DNA and histones is widely erased.

From a metabolic point of view, primed hESC rely on glycolysis and grow in high oxygen growth culture conditions, while mESC have active mitochondria and their metabolism rely on oxidative phosphorylation and on low oxygen growth culture conditions.

At the beginning, differences between human and mouse ESC were attributed to species-specific differences but in 2007 the derivation of a new pluripotent cell state from the post-implantation mouse epiblast (EpiSC)[23,25] suggested that differences between human an mouse ESC were due to a different developmental stage. In fact, primed hESC share the above-mentioned features with EpiSC[19] and it has been hypothesized that the

process of derivation of hESC from embryos could involve the progression of the explanted culture to the equivalent of a post-implantation state[16].

From this observation, the distinction between naïve and primed pluripotent states was suggested[26], where the naïve state, also called ground state, identifies the pluripotency features present in mouse ESC, while the primed state identifies the features described in mouse EpiSC and human ESC.

1.1.2.2 Naïve pluripotent stem cells

In 2009, the interconversion between naïve and primed state in mouse cells[27] raised the hypothesis that also naïve human stem cells could be isolated in the appropriate culture conditions. In fact, short after, naïve hESC lines were established, both by conversion of primed hESC to naïve state[22,28] and by de-novo derivation from the inner cell mass of human blastocyst[22,29]. Naïve human pluripotent stem cells (PSC) share common features with mouse ESC.

Naïve human PSC can be grown *in vitro* as packed dome-shaped 3D colonies on inactive MEF feeder layer, colonies can be disaggregated to single cells with high clonogenicity. Naïve human PSC rely on medium supplementation with specific naïve state promoting and primed state inhibiting small molecules or growth factors:

- Leukemia inhibitory factor (LIF), which activates JAK-STAT3 pathway and promotes naïve pluripotency;
- PD035901, an inhibitor of MEK-ERK;
- CHIR9902, an inhibitor of WNT-GSK3β;
- Gö6983, an inhibitor of PKC pathway;
- SP600125, an inhibitor of JNK pathway;
- SB203580, an inhibitor of p38 pathway;
- Y-27632, an inhibitor of ROCK pathway;

Naïve human PSC growth media lack of FGF2 and TGF-β1, promoters of primed pluripotency.

Naïve human PSC maintain both X chromosomes in the active XaXa state in female cells and their epigenetic state is globally hypomethylated[30]. In fact, naïve human PSC have been proved to be able to integrate in mouse blastocyst forming mixed-species chimeras and contributing to organogenesis[22].

In naïve human PSC, the pluripotency network is enhanced by overexpression of OCT4 (from its distal enhancer), NANOG, KLF17 KLF4, KLF2, TBX3, GBX2, LIN28, TFCP2L1 and SOCS3 compared to primed cells[28]. Moreover TFE3 is reported to be strictly nuclear[22,31] in naïve human PSC, in contrast to primed cells where TFE3 has also a cytoplasmic localization[20,22,28,32,33]. Nevertheless, naïve human PSC are not identical to mESC: human naïve cells have downregulated expression of OTX2, ZIC2 and CD24 if compared to mESC and exclusive nuclear localization of TFE3[22,31,34].

Naïve human PSC metabolism can rely also on oxidative phosphorylation and show active but immature mitochondria; therefore, they have higher oxygen consumption rate compared to primed cells. To fully sustain naïve human PSC metabolism, physiological oxygen concentration (5%) should be used when cultivating naïve cells[35,36]. Low oxygen conditions (compared to standard air concentration of 21%, also referred as high oxygen conditions) helps also the maintenance of active X chromosome[37].

Due to the above-mentioned features, naïve human PSC are of extraordinary interest not only to study early embryo development, but also to model epigenetic-related and X-inactivation-related diseases such as Fragile-X Syndrome[38]. Nevertheless, even if large amount of data is now available on naïve state transcriptome and epigenome, little is known on microenvironment and extracellular matrix contributions to naïve state maintenance.

Table 1: Comparison between naïve and primed pluripotent stem cells features[39,40].

	NAÏVE STATE	PRIMED STATE
Corresponding embryonic state	Pre-implantation blastocyst	Post-implantation blastocyst
Morphology	3D Dome-shape	Flat 2D monolayer
Required growth factors	LIF	FGF2, TGF-β or ActivinA
MERK/ERK dependence	No	Yes
Pluripotency factors	KLF17, KLF4, NANOG, SOX2, ESRRβ, OCT4	OCT4, SOX2, NANOG,
Dominant OCT4 enhancer	Distal	Proximal
Molecular identification markers	Nuclear TFE3, TFCP2L1, SSEA1	Cytoplasmic TFE3, SSEA3/4, TRA-1-60, TRA-1-81
DNA methylation and H3K27me3	Low	High
X-Chromosome activation	XaXa	XaXi
Metabolism	Oxidative phosphorylation, glycolysis	Glycolysis
Mitochondrial activity	High	Low
Growth rate	High	Low
Chimera contribution	High	Low

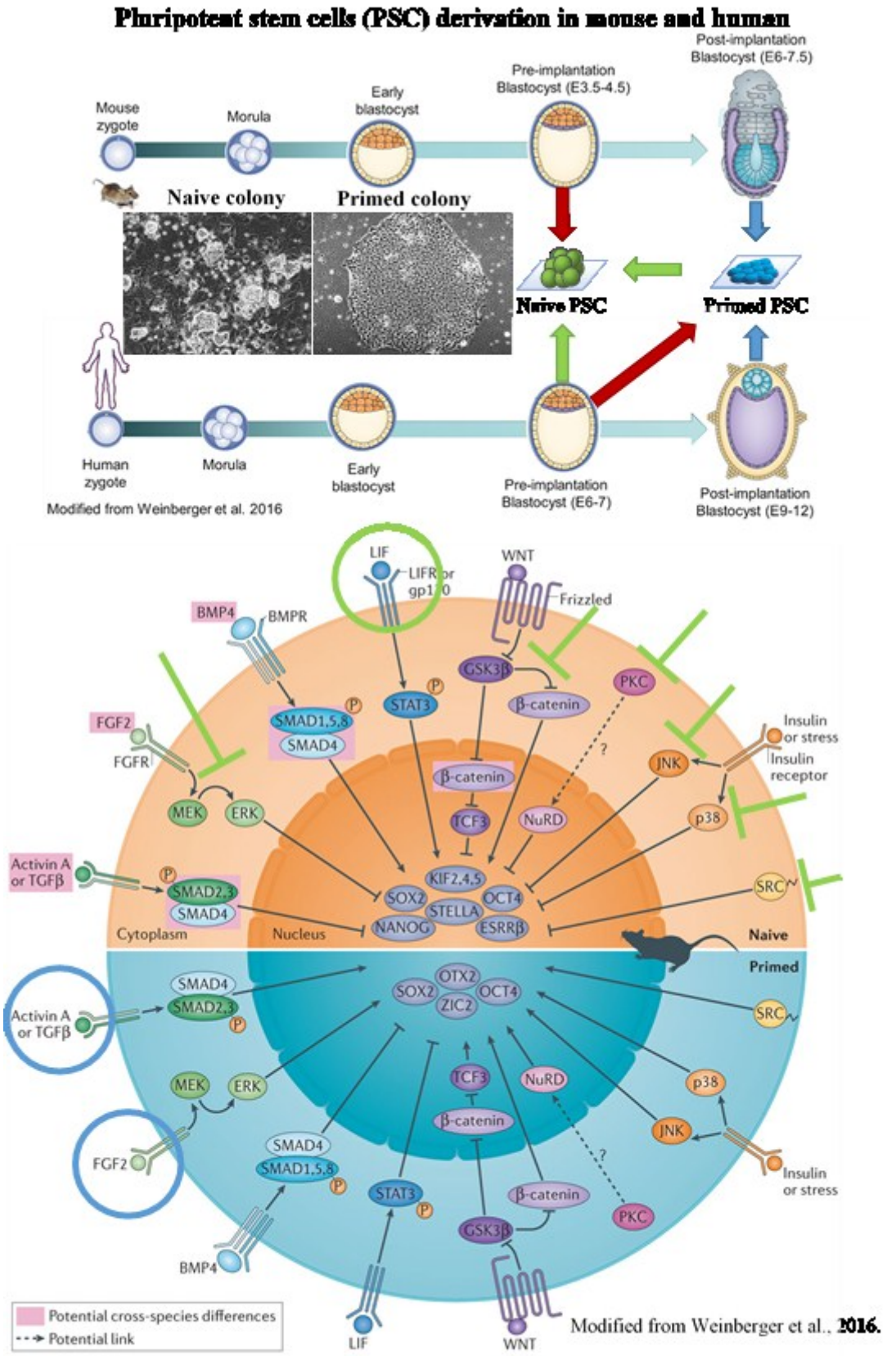

***Figure 1.3: Differences between naïve and primed PSC. Top**: parallelism between human and mouse PSC derivation. **Bottom**: molecular pathways in naïve and primed PSC. In green are highlighted the pathways recognized also in human naïve cells, in blue those recognized in human primed cells. Modified from Weinberger et al. 2016.*

1.1.3. Cell reprogramming is a tool to rewrite cell fate

In the late 19th century, August Weismann theorized that, since inheritance is only mediated by gametes, unnecessary genetic codes must be deleted or terminally inactivated in somatic cells that are committed to a specific state. This theory is known as the Weismann barrier and implies that the destiny of lineage-committed cells was permanent[41]. Only in 1962 this rigid scheme was dismantled, thanks to the milestone work by Sir John Gurdon, who reported the first example of cell fate subversion thanks to the somatic cell nuclear transfer (SCNT) technique[42,43]. In SCNT, the nucleus of a somatic cell is transferred to an enucleated egg. The new egg then starts to divide, generating an embryo that is genetically identical to the donor of the somatic cell. This demonstrated that genetic information needed for pluripotency is not lost in differentiated somatic cells, but it's maintained inactive in the nuclei and it can be re-activated with the proper conditions (granted by the egg cytoplasm). Despite this important discovery, Gurdon's work was followed by limited progresses for the next 40 years, in which time SCNT was applied to other animals, including mammals (e.g. Dolly the sheep[44]), but without a molecular understanding that could explain Gurdon's results. In early 2000 it was demonstrated that enucleated pluripotent stem cells could rejuvenate somatic cells nuclei, obtaining the re-expression of pluripotency genes[45,46]. This suggested that PSC contain factors that can erase the memories of somatic cells and re-establishing pluripotency. In parallel, transdifferentiation experiments by the administration of specific transcription factors (e.g. MYOD-driven conversion of fibroblasts into myoblasts[47]) provided stronger evidences that transcription factors, especially the master regulators of cell identity, can modify cell fate.

The confluence of these efforts led to the breakthrough discovery of cell reprogramming by Professor Shinya Yamanaka in 2006 (murine cells, 2007 with human cells)[48,49].

1.1.3.1 Reprogramming process and strategies

Cell reprogramming allows the conversion of adult somatic cells into pluripotent stem cells thanks to the administration of defined transcription factors, therefore called reprogramming factors. The ectopic administration of Yamanaka's reprogramming factors is sufficient to completely rewrite cell expression program, restoring the pluripotency state. Pluripotent stem cells obtained with this method are called induced pluripotent stem cells, or iPSC (hiPSC when human cells are used). Not surprisingly, Professor Shinya Yamanaka, won the Nobel Prize for medicine in 2012. Yamanaka identified a pool of 24 transcription factors important for the maintenance of PSC *in vivo* and *in vitro* and set up a screening to verify if a combination of those factors could induce pluripotency in somatic cells. Indeed OCT4, SOX2, KLF4 and C-MYC were sufficient to convert adult fibroblasts into hESC-like cells. Months later the discovery was confirmed by other labs[50] and the era of iPSCs begun. As years went by, many other reprogramming factors have been proposed to improve cell reprogramming process, such as NANOG[51] and LIN28[52,53].

hiPSC represented a revolution in different fields, among others: disease modelling, regenerative medicine, drug screening and developmental biology. In fact, hiPSC represent a potentially infinite source of PSC with the unique feature of being donor-specific, carrying along the genetic features of the somatic cell donor. Thus, in the past decade hiPSC have been extensively used to model diseases in patient-specific fashion and to understand the influence of genetic background on disease phenotype heterogeneity[54]. Moreover, as years went by, reprogramming has been performed not only from fibroblasts, but also from more accessible cell sources, such as from renal epithelial cells derived from urine[55] and from $CD34^+$ cells derived from blood[56]. This improvement, linked to the ability of hiPSC to be differentiated in every cell type originated from the three germ layers, turned hiPSC into an easily accessible source of patient-specific, non-immunogenic spare parts for regenerative medicine. In fact, some hiPSC-based therapies are already undergoing clinical phase I or II

trials[4,57,58], flanking the clinical trials that apply human embryonic stem cells, even if some concerns are arising from cell culture conditions- or reprogramming-induced DNA mutations observed in some hiPSC cultures[59]. Furthermore, having a source of patient-specific PSC that can be differentiated *in vitro* represents a perfect platform for pre-clinical *in vitro* high-throughput drug screenings, also in combination with recent advancements in 3D tissue bioprinting or organoid formation[54,60]. In fig.1.4. it is possible to appreciate hiPSC influence in literature and clinical trials, together with a summary of hiPSC potential applications[61]. In the last decade, different methods to deliver reprogramming factors have been developed, as summarized in Table 2[57,62]

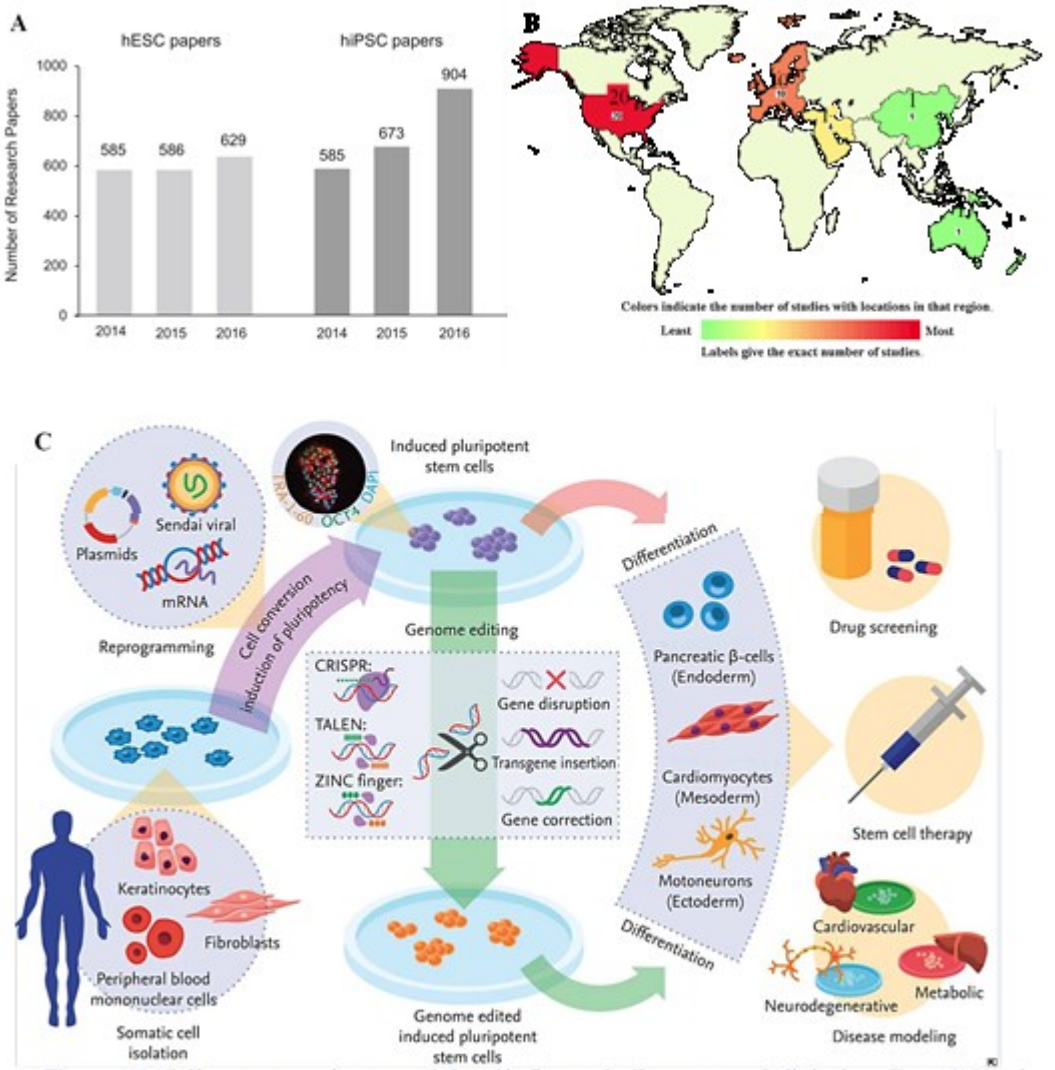

Figure 1.4: Cell reprogramming potential and influence in literature and clinical studies. *(A) Number of original research papers published from 2014 to 2016. (B) Currently ongoing clinical trials featuring human PSC. From www.clinicaltrials.gov. Last update, August 2018 (C) hiPSC potential applications. Modified from Diecke et al. 2014.*

Table 2: Cell reprogramming strategies, relative efficiency and features.

STRATEGY		EFFICIENCY	NOTES
DNA INTEGRATION	Retrovirus	0.001-1%	Incomplete viral silencing and slow kinetics
	Lentivirus	0.1-1.1%	Transduces dividing and non-dividing cells
	Inducible lentivirus	0.1-2%	Controlled expression of factors, requirement for transactivator expression
REVERSIBLE INTEGRATION	Transposons	0.1%	Labour-intensive screening of excised lines
	Cre/Lox lentivirus	0.1-1%	loxP sites retained in the genome
NO DNA INTEGRATION	Adenovirus	0.001%	Low efficiency
	Plasmids	0.001%	Low efficiency and occasional vector genomic integration
DNA FREE	Sendai virus	1%	Difficulty in purging cells of replicating virus
	Proteins	0.001%	Short half-life, requirement for large quantities of proteins
	miRNA	0.1%	miR-200c, miR-302s or miR-369s
	Modified mRNA	4%	Bypasses innate antiviral response, multiple transfection
	Nonmodified[63] mRNA+miRNA	3%	Fewer transfections, faster protocol.

From Table 2, it emerges how cell reprogramming is indeed an inefficient process, where efficiency is calculated as the ratio between the

number of hiPSC colonies obtained over the total number of somatic cells seeded at the beginning of the reprogramming experiment.

Two main models have been proposed to explain the mechanism of reprogramming process and its efficiency[64]. According to the "deterministic" model, individual somatic cells synchronously convert into iPSCs with a constant latency represented by a constant number of cell divisions (models i and ii in fig.1.5)[65,66]. According to the "stochastic" model instead, somatic cells will give rise to iPSCs with variable latencies or after going through different numbers or cell division (models iii and iv in fig.1.5)[66,67]. Moreover, it's debated whether all somatic cells or only a few "elite" cells will yield iPSCs, such as somatic stem or progenitor cells that may persist in explanted cell populations. As low efficiency of hiPSC generation points out, reprogramming is unlikely to follow a purely deterministic process. On the other hand, models based exclusively on an elite are also unlikely because iPSCs derivation has been achieved also from fully differentiated cells. It has been observed that cell proliferation improves cell reprogramming efficiency because it allows rare cells in almost every clonal

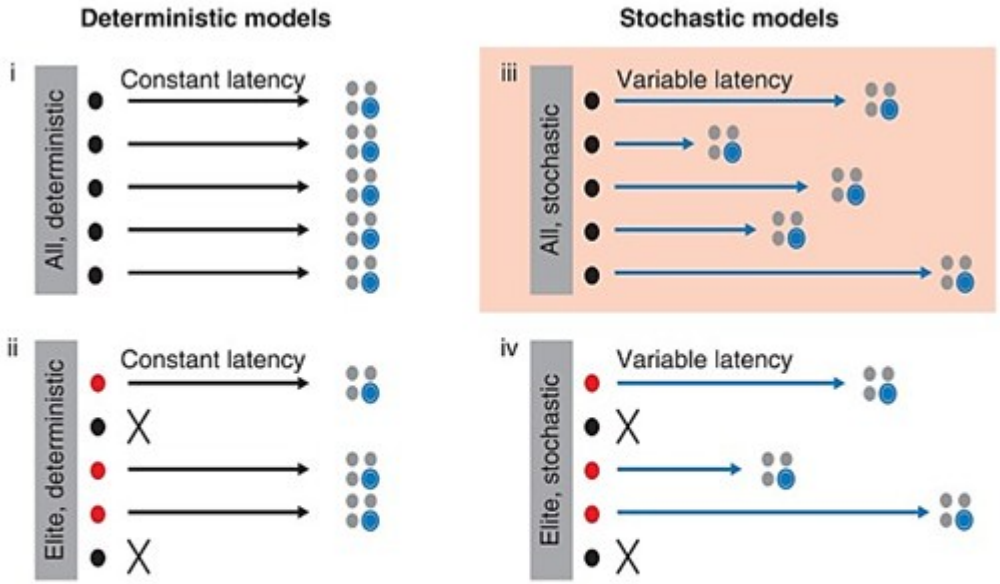

Figure 1.5: Stochastic and deterministic models of cellular reprogramming into iPSCs. *The deterministic model posits that (i) all somatic cells or (ii) a subset of somatic cells termed elite founder cells gives rise to iPSCs with the same predetermined latency. In contrast, the stochastic model predicts that (iii) all cells or (iv) a subpopulation of "elite" cells produces iPSCs with different latencies. Latency can be measured in elapsed time or number of cell divisions necessary to activate pluripotency genes. Modified from Hanna et al. 2009 and from Hochedlinger et al. 2015.*

cell population to acquire molecular changes that facilitate their conversion into a pluripotent state, supporting the stochastic model of cellular reprogramming[2]. Indeed, original Yamanaka's reprogramming process can be accelerated by additional treatments to promote proliferation or chromatin remodeling with transcription factors (e.g., Tbx3, Sall4, Glis1), chromatin regulators (e.g., UTX, BAF, Dnmt1, Mbd3), microRNAs (e.g., miR-294, miR-302/367), and signaling molecules (e.g., Wnt, Tgf-β, Jak/Stat)[68–70].

From the first studies it appeared that reprogramming follows an organized sequence of events, each of which represents a bottleneck that aspiring iPSCs have to pass[71]. In fibroblasts, cell model for reprogramming, it all starts with the down-regulation of somatic markers and somatic changes that have been defined mesenchymal-to-epithelial transition (MET), where fibroblasts lose the typical elongated morphology and become more round-shaped and compact, expressing the epithelial marker E-Cadherin[72,73]. Unexpectedly, before embarking on the essential MET, fibroblasts undergoing reprogramming transiently become more mesenchymal[74]. These events are followed by the activation of the early pluripotency markers such as SSEA-1, alkaline phosphatase, and Fbxo15 and only in later stages bona fide pluripotency genes such as NANOG or OCT4 become expressed. The telomerase enzyme is reactivated at the same time as endogenous NANOG and OCT4. Interestingly, even if expressing the pluripotency markers, during a reprogramming process, the majority of cells fails to proceed to iPSC, suggesting that they are or have become refractory to reprogramming[75]. To successfully complete pluripotency acquisition, pluripotency genes such as OCT4 and NANOG must be epigenetically reactivated by removing repressive histone modifications such as histone H3 lysine 27 trimethylation (H3K27me3) and DNA methylation and restoring the activating histone mark H3 lysine 4 trimethylation (H3K4me3)[75,76]. In general, reducing global genomic methylation levels boosts cellular reprogramming[75]. In parallel, the silencing of the somatic program must be carried on during the first phase of reprogramming[77].

1.1.3.2 Naïve resetting and reprogramming

In the above-mentioned studies, reprogramming of human somatic cells led to human primed PSC, with the classic flat 2D-shaped morphology, dependent on FGF2 and TGF-β1 supplementation. When the possibility of stabilizing human naïve PSC emerged, a great effort has been put in developing protocols to convert different cell types into naïve PSC. These methods can be divided into two categories: human primed PSC resetting to ground state pluripotency and somatic cells reprogramming to naïve PSC[78].

Primed PSC resetting to ground state pluripotency has been achieved by transgene mediated overexpression of naïve markers such as NANOG and KLF2 in combination with naïve PSC-specific medium development[22,28,79]. To prevent transgene integration and dependency from exogenous transcription factors transgene free strategies to convert primed PSC into naïve PSC have been developed by combinatory screening of small molecules or growth factors able to block the primed PSC regulatory network and restoring ground state pluripotency. These studies helped to define naïve PSC-specific medium composition, based on medium supplementation with LIF, ERK-GSK3β-p38-PKC-SRC inhibitors and FGF2-TGF-β1 removal, as previously described in paragraph 1.2.2[80–82]. Notably, different resetting methods led to different transcriptomic, epigenetic or proteomic profiles of naïve PSC, making it difficult to establish an unique naïve PSC signature[35,78,82].

In parallel, the possibility to directly convert somatic cells into induced naïve PSC via cell reprogramming was investigated and different studies demonstrated the feasibility of naïve reprogramming starting from fibroblasts, by delivery of defined reprogramming factors[35,78]. In these studies Sendai virus and mRNA were used to deliver four reprogramming factors (OCT4, SOX2, KLF4 and c-MYC) to human fibroblasts for several day, thereafter reprogramming medium was switched to naïve medium to allow naïve colonies formation. Naïve colonies arouse directly from reprogrammed fibroblasts, without the need for a primed intermediate (Article under revision).

Considering the recent advances in the field, cell reprogramming emerges therefore as a fundamental tool to rewrite cell fate and grant access to primed and naïve pluripotency without ethical concerns related to the use of human embryo for hESC isolation.

1.1.4. Cancer is an alteration of cell fate *in vivo*

As seen in paragraph 1.1.1, in physiological conditions, differentiation from a pluripotent state to a specialized one is unidirectional process driven by the complex interplay between lineage-specific transcription factors and epigenetic rearrangements that determine spatial and temporal gene expression patterns. Indeed, even if cell reprogramming represents a trick to access pluripotency *in vitro*, it is possible to find a parallel process *in vivo*: cancer[83]. Solid and liquid tumors are characterized by pathological re-acquisition of immortality and self-renewal, with deregulation of molecular mechanisms that are remarkably similar to those that allow iPSC generation. Cancer hallmarks in parallel with cells undergoing reprogramming are, for example, acquired hyperproliferation, senescence bypass, c-MYC overexpression, metastasis formation with epithelial-to-mesenchymal transition (EMT) to leave the primary tumor couplet with MET to colonize new sites[84], aberrant DNA methylation patterns[85]. The most striking parallelism between cancer insurgence and cell reprogramming is indeed the formation, at the very beginning of tumor onset, of a subset of cancer cells with stem-like features, known as cancer stem cells (CSCs).

1.1.4.1 Cancer stem cells

In 1997 Bonnet and Dick described for the first time the existence within a tumor (acute myeloid leukemia) of a subset of cells, representing less than 1% of the tumor mass, with the unique and specific ability of recreating the tumor in immunocompromised mice[86]. Indeed, as few as 5000 cells of the subpopulation could form tumors in host mice, whereas 500,000 cells from the complete population where unable to form tumors. In 2003 a similar population of cells with tumor-initiating capacity was described also in breast and brain tumors[87] and in the next years massive amount of data

demonstrated the existence of tumor-initiating cells in all types of solid and liquid tumors[88–90]. This sub-population of cells is called Cancer Stem Cells (CSCs) and according to CSCs model, it has the ability to self-renew and differentiate in a variety of different sub clones, giving rise to the total tumor mass[91,92]. Clinically, this highly dynamic subpopulation (accounting 2-40% of tumor mass[93]) is responsible for tumor onset, regeneration, resistance to radiochemotherapy, metastatic spread, and overall poor patient outcome[94]. The juxtaposition of cancer cells with stem cells is due to the main common features between CSCs and stem cells: the ability to self-renew (promoting therapy resistance) and the ability to differentiate in a heterogeneous population of less competent cells (the tumor mass)[91,92]. CSC are therefore responsible of hierarchical organization of cancer that results in cell heterogeneity inside the primary tumor mass and metastasis[95], thus becoming marker of tumor aggressiveness and poor prognosis after treatment[96]. It is important to notice that CSCs do not necessarily arise from the adult stem cells resident in the tissue, but rather de-differentiate from somatic cells[97] by mutations in key cell fate maintenance genes such as KRAS and c-MYC[98].

In this scenario, CSC-related heterogeneity relies not only in the genetic mutations that gives origin to the tumor, but mostly on epigenetic factors, such as epigenetic regulation and noise in gene expression that can give survival advantages to the cells in the tumor environment[85,99]. Notably, not all cancers strictly conform to the unidirectional hierarchical CSC model, but rather rely on "tumor cell plasticity", where non-CSC can dedifferentiate and acquire CSC-like properties under certain conditions, in a dynamic epigenetic reprogramming[100]. Moreover, also the tumor microenvironment plays a fundamental role in CSCs dedifferentiation, for example by secreting hepatocyte growth factor that induces nuclear β-catenin localization and elicits Wnt signaling activity[101].

As represented in fig.1.6, addressing solid tumors taking into account the heterogeneous and hierarchical organization of their cell mass

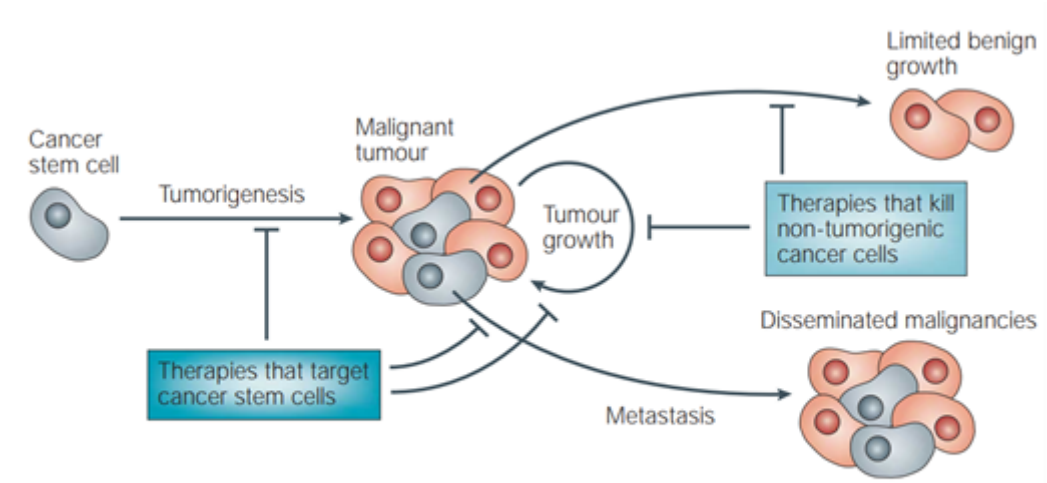

Figure 1.6: Therapeutic implications of cancer stem cells. *Conventional therapies target prevalently proliferating cells that derive from CSCs, but do not target directly CSCs, leading to tumor relapse. New therapies that target directly CSCs are needed. Adapted from Pardal et al. 2003.*

constitutes a novel approach to cancer treatment, not aimed at shrinking tumor bulk, but rather at exterminating CSCs by direct targeting[102,103].

1.1.4.2 Cancer reprogramming

Yamanaka's work demonstrated how transcription factors, acting on cell's epigenetic regulation, could completely reverse cells phenotypes. From this observation, cell reprogramming technique has also been applied to cancer studies, with the generation of iPSC from malignant patient tissues[104,105]. Several studies on solid tumors reported the generation of iPSC from cancers, even in presence of irreversible genetic alterations.

The study of cancer-derived iPSC has multiple purposes, summarized in fig.1.7: first, current cancer models are derived from *in vitro* cell culture of cells explanted at specific cancer progression stages, therefore these models allow only the analysis of late cancer hallmarks and are not representing the mechanisms driving cancer onset. With cancer-derived iPSC it could be possible to go through cancer development and understand in a patient-specific fashion the evolution of the tumor[105,106]. Moreover, cancer-derived iPSC could offer a platform for studying tumor heterogeneity and a source for cancer type-specific drug discovery studies to identify agents that inhibit the stemness and self-renewal properties of CSCs[107]. Finally, the most promising application of cancer reprogramming is the possibility to normalize the malignant phenotype of cancer stem cells

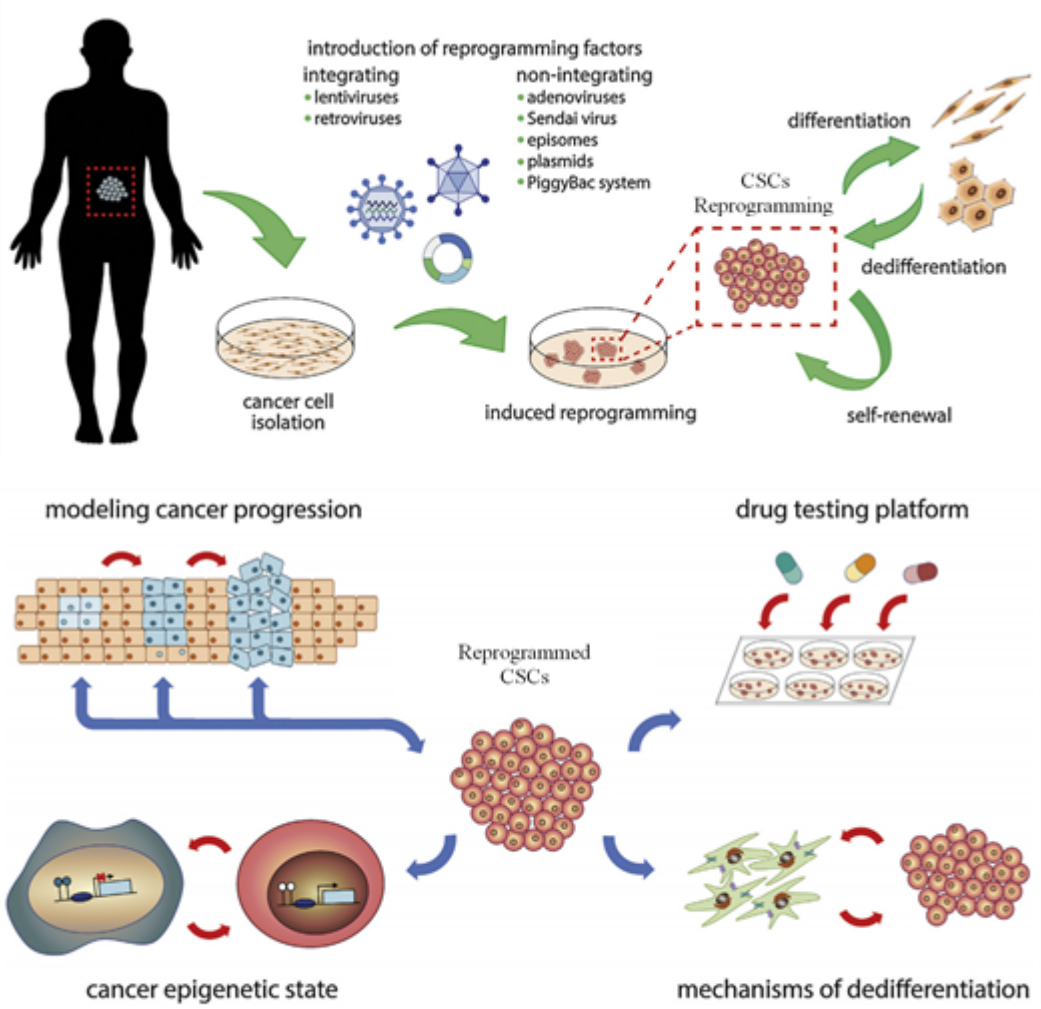

Figure 1.7: Generation of cancer-derived hiPSCs and potential applications. *Cancer-derived hiPSCs can be obtained by reprogramming patient-specific tumor masses and can be used to model cancer progression, for drugs testing or to clarify cancer epigenetic state. Adapted from Czerwinska et al. 2018.*

via epigenetic resetting, as an alternative to conventional therapeutic protocols. Several studies on solid tumors reported that, even in presence of irreversible genetic alterations, the malignancy of cancer cells was suppressed after cell reprogramming and subsequent differentiation[108–112].

So far, the reprogramming efficiency of cancer cells is extremely low, suggesting that some barrier impedes reacquisition of pluripotency, derived from the accumulation of DNA damage and cancer-specific mutations, epigenetic modifications and reprogramming-triggered cellular senescence. Application of reprogramming into cancer studies may therefore help to determine the epigenetic state of cancer cell and to evaluate the relative contribution of reversible epigenetic and irreversible genetic changes that occur during carcinogenesis[113,114]. Moreover, uncovering the epigenetic

stability of cancer cells may ultimately contribute to the development of therapeutics that effectively target epigenetic modifications in cancer cells.

1.1.4.3 Tumors with high SERPINB3 expression have a more aggressive phenotype and stem features

Recently, the serine-protease inhibitor SERPINB3 has been proposed as a marker of poor prognosis in several types of tumors, including liver[115,116], esophagus[117] and colorectal[118] cancers. The molecular mechanism that SERPINB3 exploits to promote oncogenesis is complex, multifactorial and unfortunately not completely understood, but it has been demonstrated that SERPINB3 has an anti-apoptotic role[119] by blocking the release of cytochrome c[120], a protective effect to radiotherapy and low oxygen environments[121–123], it promotes invasiveness by inducing EMT[124,125]. In general, as reported in fig.1.8, its overexpression gives rise to poorly differentiated tumors, with enhanced stem characteristics, that are known to be more aggressive and prone to relapse[123,126,127]. The protein acts both as paracrine and endocrine signal[124,128].

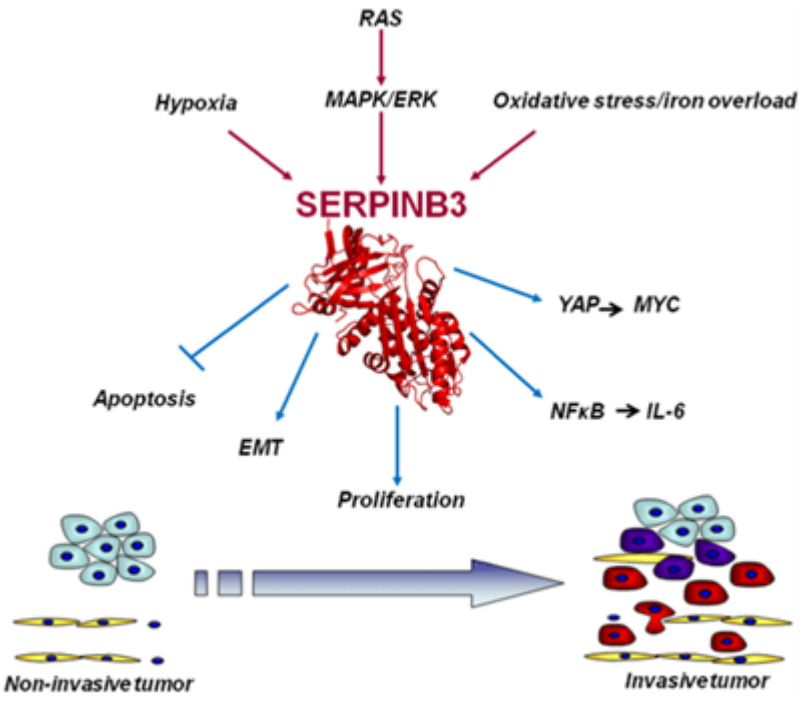

Figure 1.8: Biological activities of SERPINB3. Adapted form Turato et al. 2017.

1.2 CELLS INTERACTION WITH THE ENVIRONMENT

Cells are not isolated, self-sustaining entities, but rely on interactions with the environment to survive, proliferate and absolve their encoded functions. To form tissues and ultimately organisms, different specialized cells need to be coordinated and organized structurally and functionally. In fact, all tissues contain an acellular portion known as extracellular matrix (ECM) to fulfill this goal[129].

Until the first half of twentieth century, the ECM was thought to provide only structural support for cells in tissues, only later the complex cell-ECM inter-talk and cross-influence begun to be investigated and the current view of "dynamic reciprocity" was postulated[130]. Indeed, a growing amount of data indicated that ECM molecules could interact with specific receptors on the cell surface, which then would initiate an intracellular signaling cascade through the cytoskeleton to the nucleus resulting in gene expression regulation, whose products, in return, would affect the ECM structure or composition in various ways. Thus, the ECM provides not only essential physical scaffolding for the cells, but also initiates crucial biochemical and biomechanical cues that are required for tissue morphogenesis, differentiation and homeostasis. Although, fundamentally, the ECM is composed of water, proteins and polysaccharides produced by the cells themselves, each tissue has an ECM with a unique composition and topology that is generated during tissue development through a dynamic and reciprocal, biochemical and biophysical dialogue between the various cellular components and the evolving cellular and protein microenvironment. This continue cross-talk makes the ECM a highly dynamic structure that is constantly being remodeled, either enzymatically or non-enzymatically, and its molecular components are continuously subjected to post-translational modifications and re-arrangements[129].

Among the many functions of ECM, the most notable are:

- definition of the mechanical proprieties of organs (e.g. stiffness, elasticity, tensile and compressive strength);

- regulate cell adhesion, migration, growth, differentiation and apoptosis by binding growth factors (GFs) and cytokines and interacting with cell-surface receptors;
- maintaining extracellular homeostasis (buffering salts and sugars) and water retention;

Indeed, deregulations in ECM homeostasis results in a variety of diseases, including connective tissue disorders, muscular dystrophy, fibrosis, and cancer[131].

In this paragraph, ECM composition and structure will be described, with focus on cell-ECM cross-talk and especially on stem cells interactions with ECM. Fig.1.9 represents the most common ECM components.

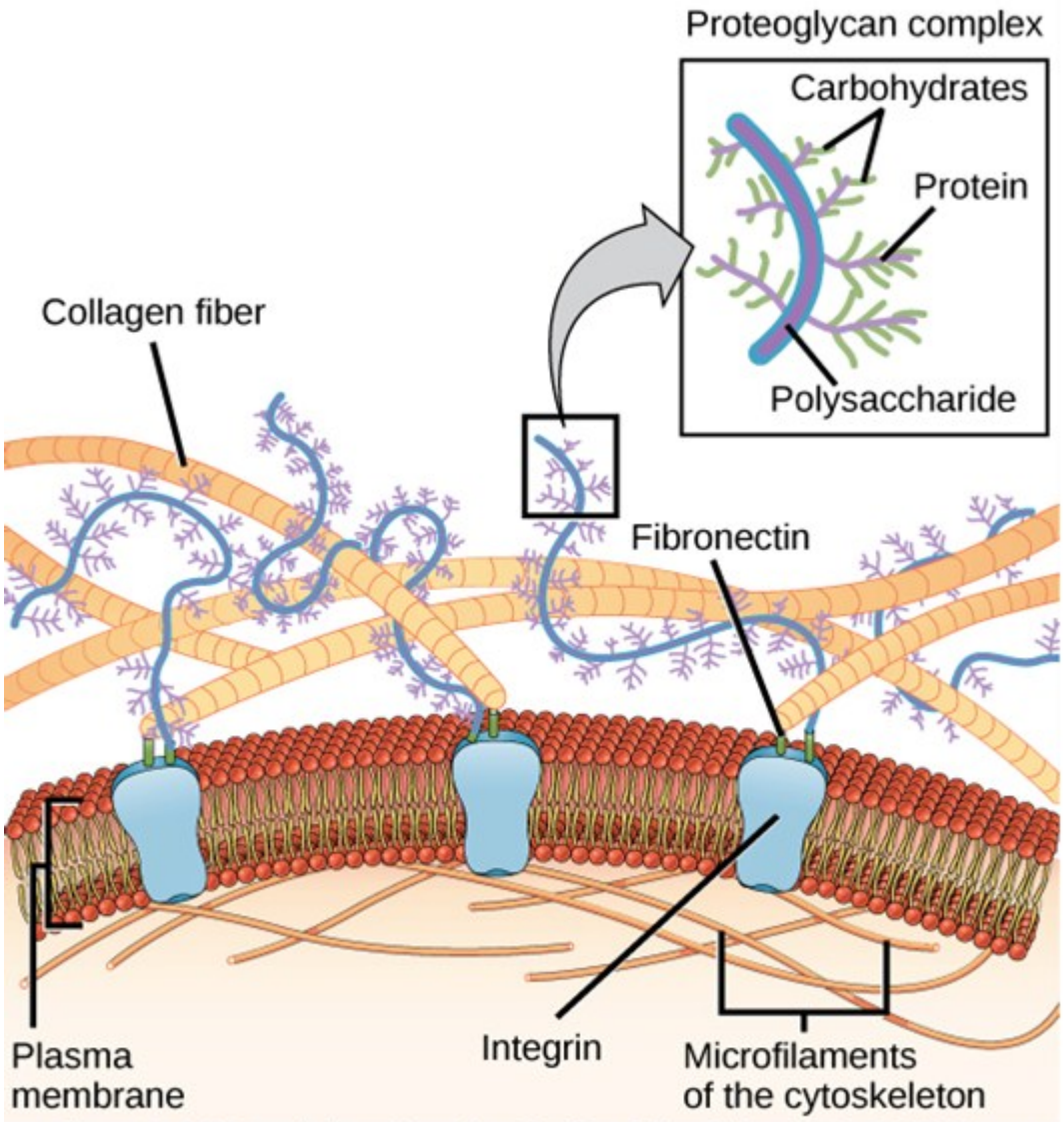

Figure 1.9: ECM organization. *Adapted from* OpenStax College Biology, *under CC-BY 3.0 creative common license.*

1.2.1 ECM composition and organization

The ECM is composed of two main classes of polymer-forming macromolecules: fibrous proteins and proteoglycans (PGs). As a general feature, the macromolecular components are secreted by the cells as precursor molecules and modified during ECM remodeling to be assembled with other components into functional polymers.

ECM dynamic changed are ensured by extracellular proteinases such as metalloproteinases and ADAMTS (a disintegrin-like and metalloproteinase domain with thrombospondin type 1 repeat) proteinases[132,133].

The main fibrous ECM proteins are collagens, elastins, fibronectins and laminins:

- Collagens. Collagens are the most abundant proteins in mammalian tissues (up to 30% of total human proteins). To date, 28 types of collagens have been identified[134]. Collagens can be divided into different groups according to their structure and function.
    - Fibrillar collagens are formed by the combination of different chains (α-chain), which share a characteristic domain composed of about 300 repetitions of the Gly-X-Y tripeptide, where Y is often a proline or hydroxyproline. α-chain can coil into left-handed helix and, by combining thee collagen α-chains, a collagen molecule is formed, with the typical right-handed triple helix structure. Single collagen molecules are then subsequently assembled into supramolecular complexes, such as fibrils and networks, depending on the type of collagen. Collagen molecules can be homotrimeric (three identical α-chains) or heterotypic and in total, 11 α-chain-coding genes have been identified.

      Thanks to their rigid structure, summarized in fig.1.10[135], fibrillar collagens are responsible for the structural support to resident cells. In fact, a characteristic feature of fibrillar collagens is their precise 3D organization that follows

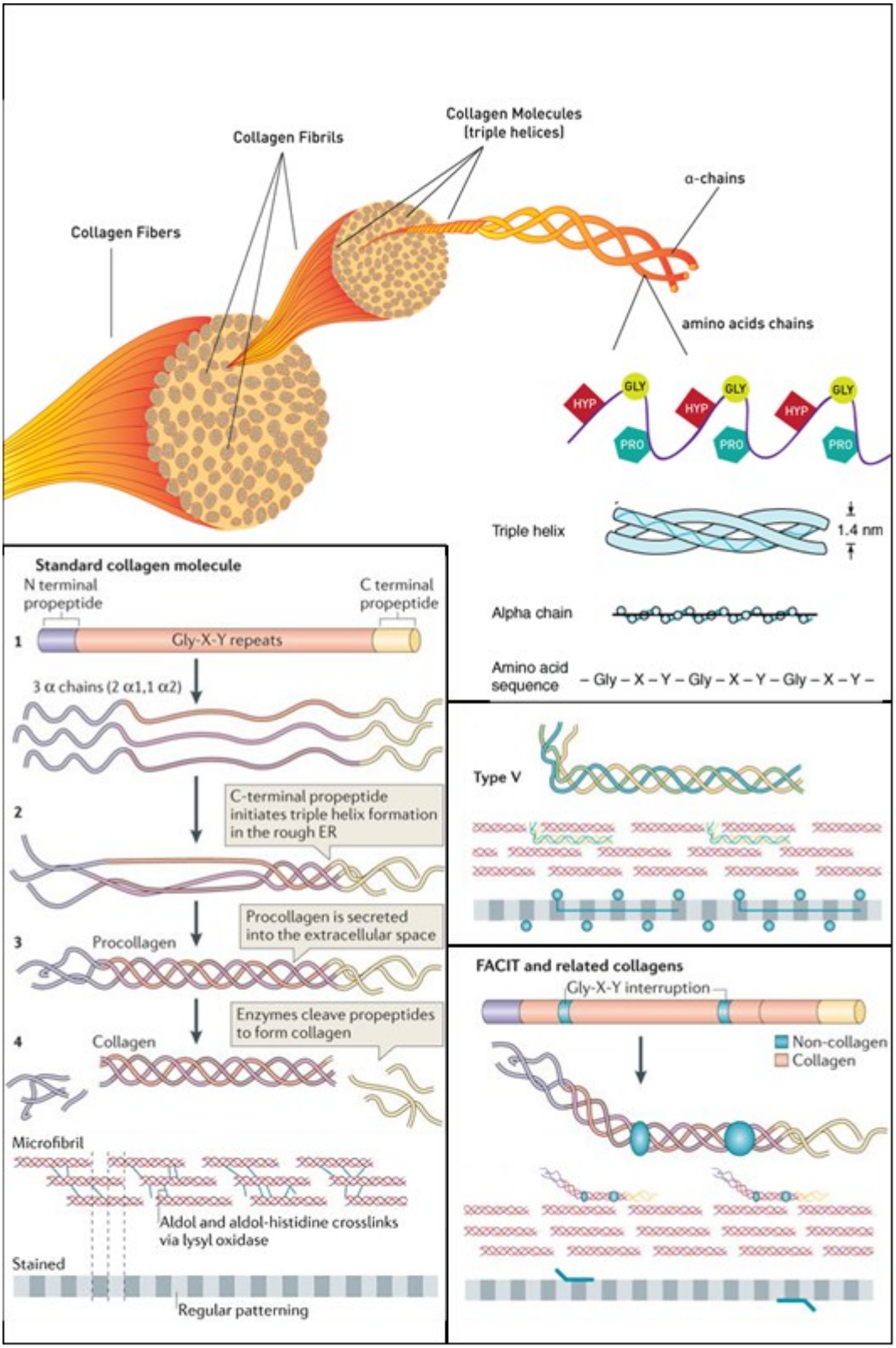

Figure 1.10: Collagen structure. ***Top****: Collagen fiber organization: regular amminoacid sequences are assembled in α-chains, then in triple helix, collagen fibrils and finally collagen fibers.* ***Bottom left****: Fibrous collagen I assembly and regular patterning.* ***Bottom right****, collagen V intercalates collagen I regular pattern while FACIT collagens regulate collagen I assembly. Adapted from Mouw et al. 2014.*

mechanical stress lines to ensure maximum tensile strength with minimum material. Ultimately, cells themselves are responsible for establishing these patterns.

Collagens belonging to this category are type I, II, III, V, XI, XXIV and XXVII. Among others, collagen type I and V are remarkably notable: collagen type I is the most abundant collagen in the human body, found in skin, tendon, bone, cornea, lung and vasculature; collagen type V is a quantitatively minor collagen associated with collagen type I, serving as regulator of fibril assembly. Indeed, the diameter of collagen fibrils are determined by the ratio of the minor component (collagen V) and the major component (collagen I): a high ratio results in thin fibrils, a low ratio results in thick fibrils[136].

- Basement membrane collagens represent a specialized ECM area for cell attachment and compose the 40-50 nm thick basal laminae typical of tissue boundaries. Collagens belonging to this group are type IV, VII, XV and XVIII, but collagen type IV is the most abundant and well known. Collagen IV molecules are longer than fibrillar collagens but contain several discontinuities in the Gly-X-Y repeats, thus they are not able to form a tight triple helix. Collagen IV forms a network-like scaffold by both end-to-end and lateral interactions and it interacts with various non-collagenous molecules such as laminin[137].
- Beaded microfilament forming collagen type VI is the unique member of this group and has the peculiarity of containing a short triple-helix domain of 335–336 amino acid residues, which are flanked by large N- and C-terminal globular region. This peculiar structure results in the typical beaded filament net structure. Collagen VI has been

demonstrated to be involved in the maintenance of stemness in different adult stem cell niches[138].

- Fibril associated collagens with interrupted triple helix (FACIT collagens) have flexible hinges and are needed to bridge fibrils, other matrix constituents and cells. This group includes collagen type IX, XII, XIV, XVI, XIX, XX, XXI and XXII[136].
- Transmembrane collagens or MACIT (Membrane associated collagens with interrupted triple helix) are collagens with single trans-membrane domain, short cytosolic N-terminal domain and long interrupted triple helical extracellular domains. They have cell adhesive properties and occur on numerous cell types, including malignant cells. The group includes type XIII, XVII, XXIII, and XXV. In particular, Collagen XIII is component of cell adhesion structures such as focal adhesions[139] and collagen XXIII was associated with carcinogenesis[140].

- Elastin. Elastin is the major component of elastic fibers and has the ability to recoil after transient stretch, thus providing tissues with elasticity. Elastin is composed by alternating hydrophobic elements and α-helical Ala- and Lys- rich sequences. Lysins form extensive lateral crosslinking between different elastin chains, while hydrophobic segments tend to adopt a folded, random-coil conformation. After stretch, the hydrophobic residues are exposed and tend to fold to minimize water exposition, thus compressing the whole elastin molecule. Elastin structure is represented in fig.1.11.
- Fibronectin. Fibronectin (FN) is a glycoprotein composed by two nearly identical monomers bound together by disulfide-bond. Although FN is the product of a single gene, by alternative splicing as many as 20 FN variants can be originated. There are two types of FN: soluble plasma FN which is a major component of blood plasma and is secreted by hepatocytes, and insoluble cellular FN, major

ECM component secreted by cells (primarily fibroblasts) as a soluble protein dimer and then assembled into its insoluble form[141]. FN chain is composed by three types of multiple repeats of modules, named Fn1, Fn2 and Fn3. Fn1 modules have adhesion sites for heparin and fibrin, Fn2 modules represent the collagen-binding domains while Fn3 modules contain the integrin-recognition sequences to allow cell adhesion to FN. Among the cell-adhesive domains, the most diffused is the RGD (Arg-Gly-Asp) motif and it is the site of cell attachment via cell integrin α5β1. The functional form of FN in vivo is in its fibrillar state where FN molecules are assembled into fibers. Cells can assemble soluble FN derived from plasma or produce the insoluble form directly in the ECM. The main feature of FN is the ability to bind different ECM components and cells, thus acting as glue of the extracellular matrix and as main substrate for cell adhesion, proliferation and migration[142]. Physiologically, FN is fundamental for correct wound healing, but de-regulated overexpression of FN has a role in promoting carcinogenesis[131]. FN structure is represented in fig.1.11.

- Laminin. Laminins are cross-shaped, heterotrimeric basement membrane molecules formed by different combinations of α, β and γ chains. In basal laminae, laminins provide interaction sites for other ECM components and cells. Notably, laminin does not bind directly to collagen IV, but they are connected thanks to bridging molecules such as nidogen. Laminins play crucial roles in early embryonic development and organogenesis and are among the most used proteins for *in vitro* cell adhesion[143,144]. Laminin structure is represented in fig.1.11.

Proteoglycans (PGs) fill the majority of the extracellular interstitial space within the tissue in the form of a hydrated gel[145,146]. PGs are composed of glycosaminoglycan (GAG) chains covalently linked to a specific protein core and have been classified in three main families: small leucine-rich proteoglycans, modular proteoglycans and cell-surface proteoglycans. The

GAG chains are unbranched polysaccharide chains composed of repeating disaccharide units that can be sulphated or non-sulphated. PGs are highly polar, extremely hydrophilic and adopt extended conformations that are not only essential for hydrogel formation, but also enable matrices to withstand high compressive forces. PGs have a wide variety of functions that reflect their unique buffering, hydration, binding and force-resistance properties, moreover have been implied in genetic disorders and cancer[147]. Most PGs act predominantly in the extracellular space, not only as structural elements, but also as ligands for the many small protein growth factors, cytokines, chemokines, and morphogens that regulate embryonic development, inflammatory responses to pathogens and injury, and communication between cells[145,146]. PGs structure (as an example lecticans and small leucine-rich repeat proteoglycans SLRP) is represented in fig.1.11.

In some cases, GAGs can be found unbound to protein cores. The most common and well known is hyaluronic acid (HA), a non-sulfated high-molecular-weight GAG composed of repeating N-acetylglucosamine and glucuronic acid disaccharides. The physical and mechanical properties of HA contribute to maintenance of tissue hydration, mediation of solute diffusion and the lubrication. The diverse biological functions of HA are manifested through its complex interactions with matrix components and resident cells. Binding of HA with cell surface receptors activates various signaling pathways, which regulate cell function, tissue development, inflammation, wound healing and tumor progression and metastasis.

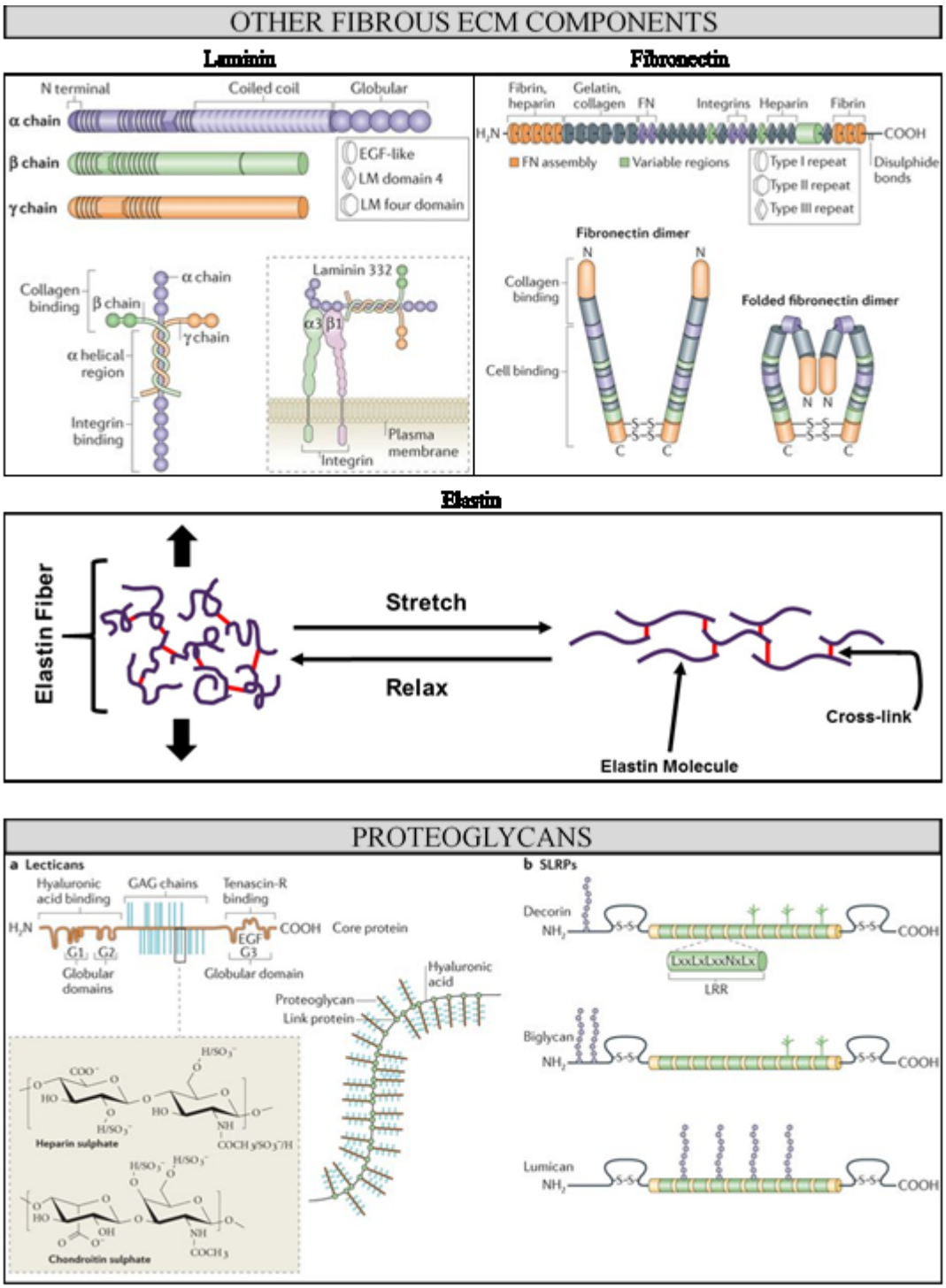

Figure 1.11: Laminin, fibronectin, elastin and proteoglycans general structure. Adapted from Mouw et al. 2014.

1.2.2 Cell-ECM interactions

As mentioned before, the ECM is not only a mechanical scaffold that allows cells 3D organization, but it is also actively interacting with cells in a dynamic and reciprocal influence. Therefore, cells need specific adaptors to catch ECM cues, transduce them to intracellular signaling and elaborate a specific cellular response.

- Integrins. The first contact between cells and ECM is mediated mostly by integrins, alongside other receptors such as cadherins. Integrins are heterodimeric, glycosylated, transmembrane cell adhesion receptors that link the ECM to the cytoskeleton. In humans, the integrin family accounts of 24 members, composed by different combinations of noncovalently bound α- and β- subunits. To date, 24 α- and 9 β-subunits have been identified and in all reported cases, integrins are formed by the combinations of one α- with one β-subunit. The specific α- and β-subunits combination determines the ligand specificity of the integrin and the type of intracellular response, as shown in fig.1.12[148,149]. For example, integrins containing the α4-, α5-, α8-, αIIb-, or αV- subunits bind to ECM components that contain the RGD (Arg-Gly-Asp) sequence, such as fibronectin and vitronectin; integrins containing the α3-, α6-, or α7-subunits are laminin-binding receptors, while the α1-, α2-, α10-, or α11-subunits are collagen-binding receptors. Integrin monomers have a large extracellular domain, also called the globular head domain, a single transmembrane domain and a generally short cytoplasmic tail. Integrin extracellular domains can exist in bent 'closed' conformations, intermediate extended conformations with a closed headpiece, and extended 'open' conformations. These states may correspond to low affinity, activated, and activated and ligand occupied integrins, where the ligand binding site is formed by the assembly of the globular head domains from the two α- and β-subunits[148,150,151].

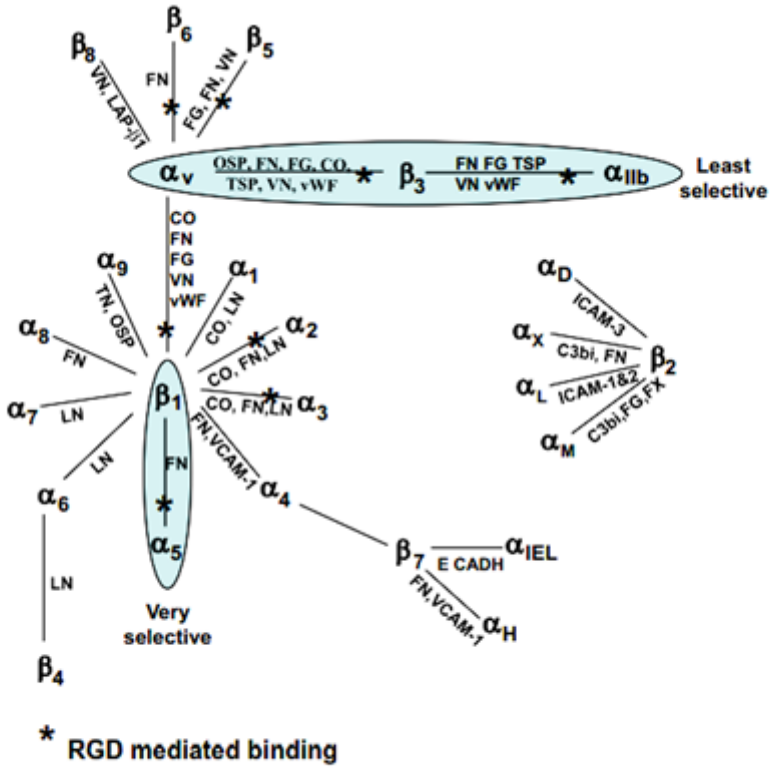

Figure 1.12: Dimers of the integrin family and their most common ligands. Adapted from Olsen et al. 2014.

There are two directions of integrin signaling: inside-out and outside-in signaling. During 'inside–out' signaling, an intracellular activator, such as talin, binds to the β-integrin tail, which is inhibited by the cytoplasmic domain of the α-subunit, leading to conformational changes that result in increased affinity for extracellular ligands, also referred as integrin 'activation'. This conformational rearrangement splits α and β cytoplasmic domains. Certain cations (e.g., Mn^{2+}) and antibodies may activate integrins by stabilizing or inducing their active conformation[148]. Inside–out signaling controls adhesion strength and enables sufficiently strong interactions between integrins and extracellular matrix (ECM) to allow integrins to transmit the forces required for cell migration and ECM remodeling and assembly. The outside-in signaling instead is related to the traditional receptor activity of integrins, where information is transmitted from the extracellular environment to the cell. Binding of integrins to their extracellular ligands changes the

conformation of the integrin and contributes to integrin clustering. Integrin conformational rearrangement and bidirectional integrin signaling are summarized in fig.1.13. The combination of these two events leads to intracellular signals that control cell polarity, cytoskeletal structure, gene expression and cell survival and proliferation. Although the two signaling directions are described

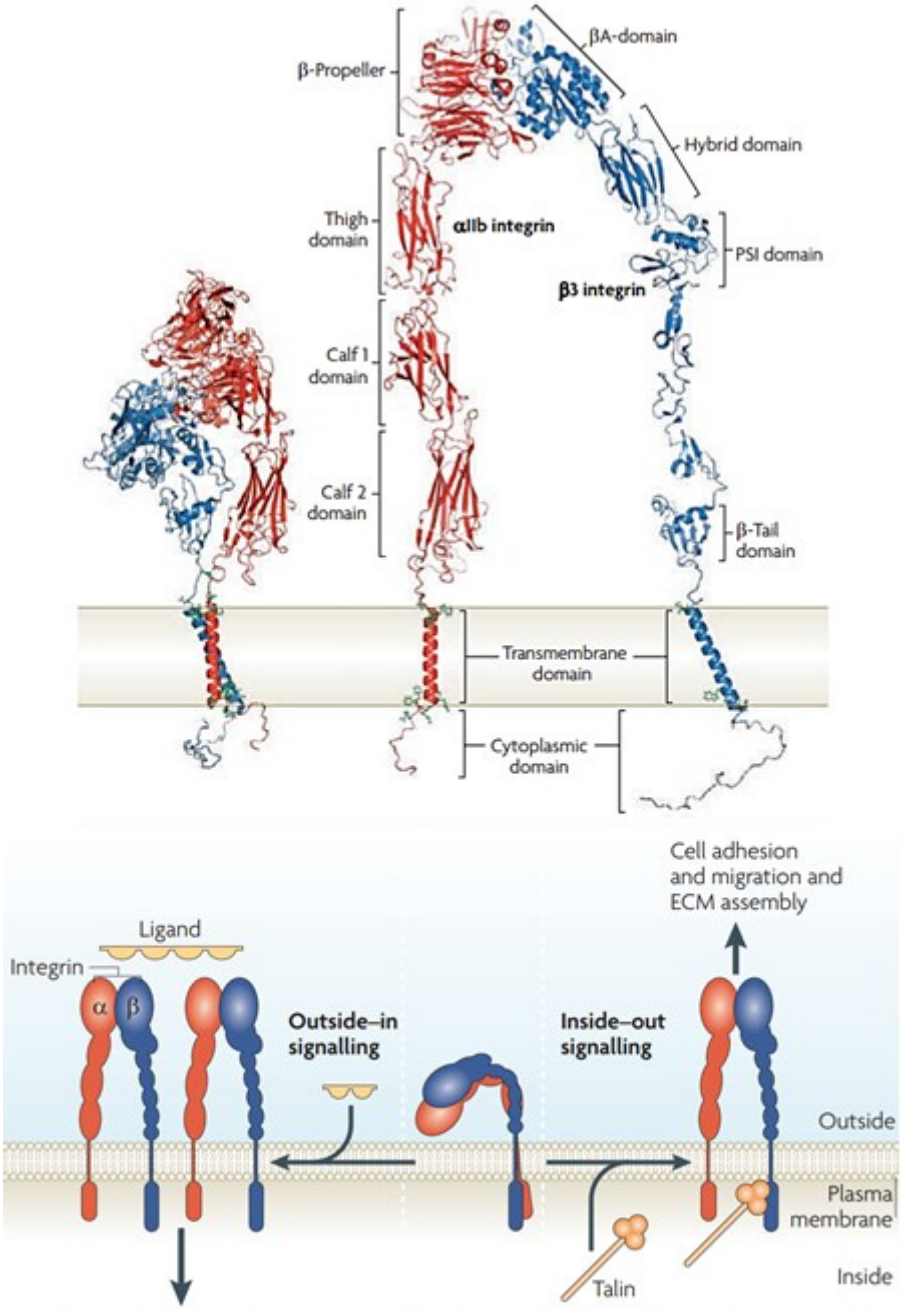

Figure 1.13: Integrin activation. ***Top****: integrin bent (inactive) conformation with α-cytoplasmic domain inhibiting β-chain compared to integrin open (active) conformation where α- and β- cytoplasmic domains are separated.* ***Bottom****: integrin bidirectional signaling. Adapted from Shattil et al. 2010.*

separately, they are closely linked: on one hand integrin activation can increase ligand binding, resulting in outside–in signaling, while on the other hand ligand binding can generate signals that cause inside–out signaling[150,151].

- Focal adhesions. Following integrin activation, ligand binding and oligomerization, a variety of proteins including integrins, signaling molecules and cytoskeletal proteins are recruited to form a specialized structure in adherent cells named focal adhesions. Average focal adhesion contact area is about 200 nm and the dimension of the protein complex that connects integrins to the cytoskeleton (also known as adhesome) is about 40 nm[152]. Are least 232 proteins are involved in the formation of the integrin adhesome as represented in fig.1.14[153,154]. From a structural point of view, as represented in fig.1.14, the focal adhesion is organized in layers: in contact with the membrane there is the first layer containing integrin cytoplasmic tails, FAK and paxillin; then an intermediate force transduction layer containing talin and vinculin; and an uppermost actin-regulatory layer containing zyxin, vasodilator-stimulated phosphoprotein and a-actinin[152]. As the layer structure suggests, indeed focal adhesions components are recruited in a hierarchical fashion after integrin activation and aggregation: the first proteins to be recruited are the adaptor protein tensin and focal adhesion tyrosin kinase (FAK), then cytoskeletal components such as vinculin, talin, and α-actinin are recruited, and the signaling cascade is initiated. Notably, various adhesion structures that differ in their morphology and subcellular localization as well as in their protein composition and mechanical properties can be recruited following distinct integrin combinations[155], but a key player of integrin signaling through focal adhesions is FAK[156]. As represented in fig.1.15, FAK exists as an auto-inhibited monomer, a conformation maintained by interactions between its amino terminal FERM domain and the

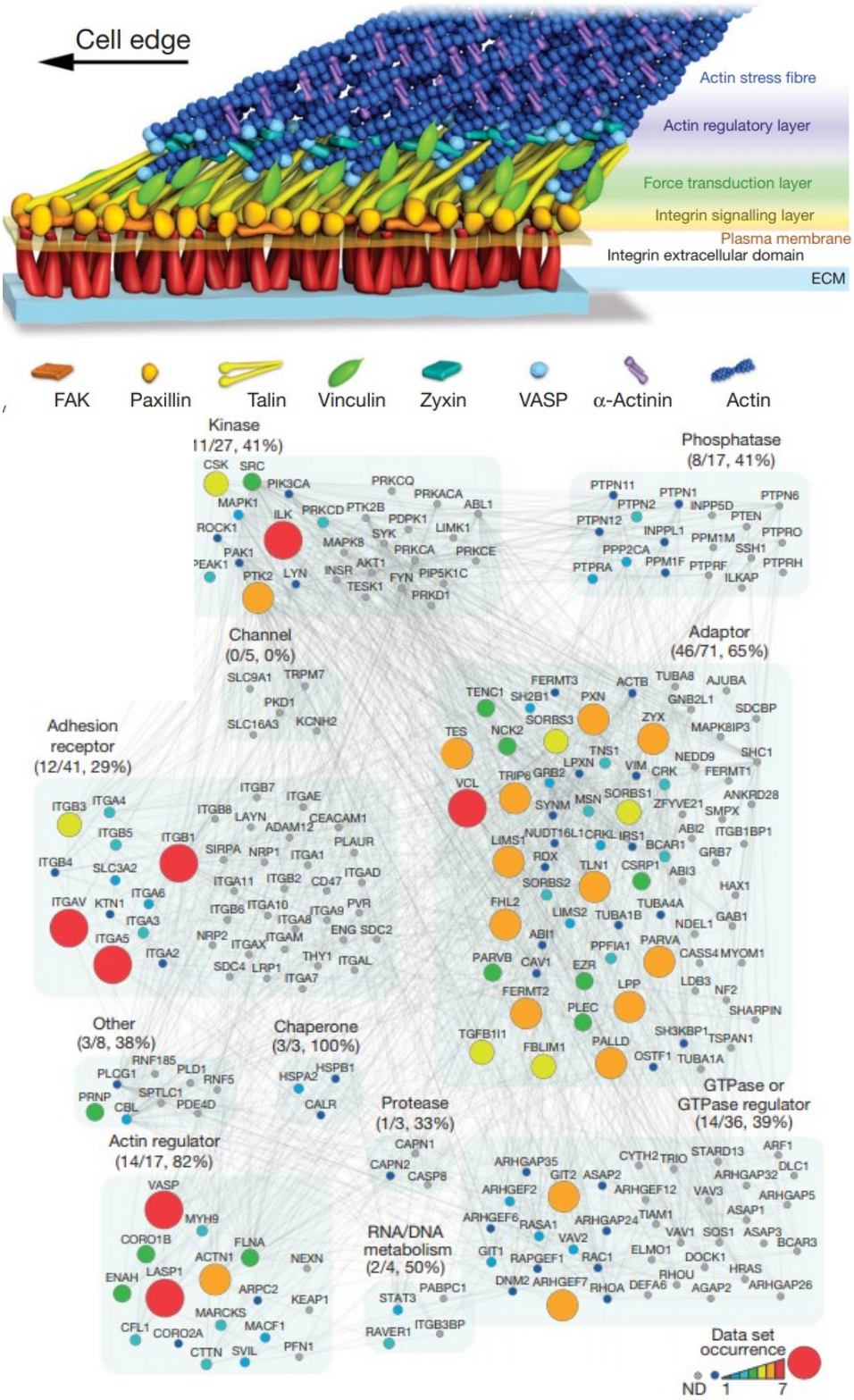

Figure 1.14: Focal adhesion layer organization and consensus adhesome proteins. ***Top***: *different layers that compose focal adhesions.* ***Bottom***: *the 232 proteins involved in the formation of the integrin adhesome. Adapted from Kanchanawong et al. 2010 and from Horton et al. 2015.*

central kinase domain. Upon PIP5KIγ-mediated phosphatidylinositol-4,5-biphosphate [PI(4,5)P2] release in focal adhesions[157], [PI(4,5)P2] induces a relaxed conformation in FAK, followed by FAK clustering and dimerization. FAK dimerization allows FAK autophosphorylation at Y397 in trans. Y397 FAK phosphorylation creates a binding site for the SH2 domain of Src kinases and the FAK-Src complex initiates multiple downstream signaling pathways through phosphorylation of other proteins to regulate different cellular functions.

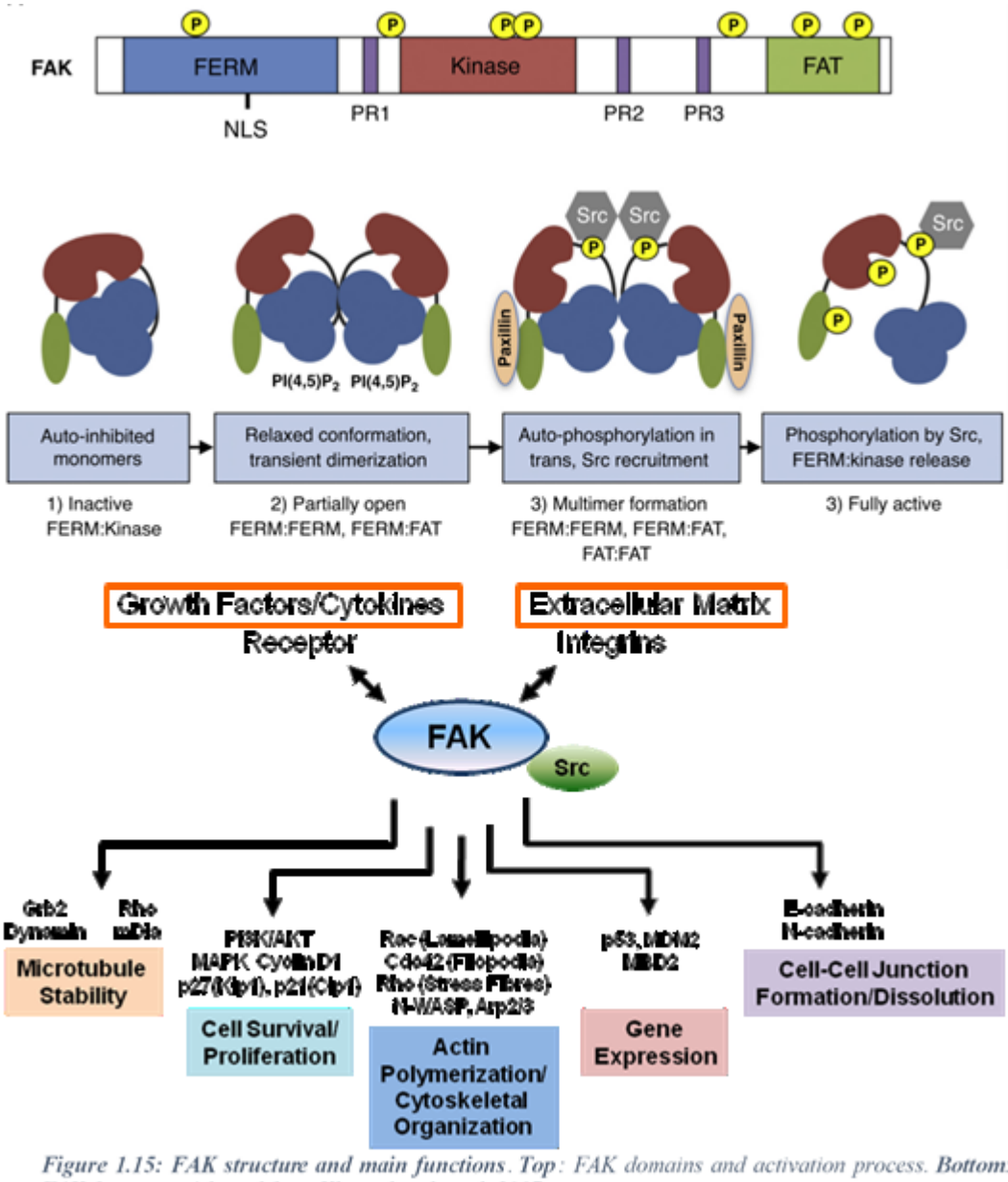

Figure 1.15: FAK structure and main functions. Top: FAK domains and activation process. Bottom: FAK functions. Adapted from Kleinschmidt et al. 2017.

- Mechanotransduction. Besides recognizing the different ECM proteins and respond accordingly as previously described, integrins and focal adhesions are also main players in cell mechanosensitivity. Indeed, integrin adhesome proteins are the first sensors of the physical state of the extracellular environment, transmitted to the cells by ECM stiffness and tension or by the neighbor cells. The process of reacting to the biophysical properties of the extracellular environment through integrin-based adhesion sites is called mechanotransduction[155]. During mechanotransduction, force alters the function and structure of mechanosensitive proteins within focal adhesions to initiate signaling cascades that regulate both rapid responses in cellular mechanics and long-term changes in gene expression. In the cell, force is transmitted by a continuous flow of actin polymerization against the membrane. At the membrane edge, actin monomers are polymerized and the growing actin filaments is pushed inside, in a continuous actin flow called 'retrograde flow' since it moves from the cell edge where cell–ECM adhesions form towards the cell center, driven by myosin powered contractions. The speed of actin flow determines the force load on the focal adhesions, and the integrin adhesome that connects ECM to the force-generating actomyosin cytoskeleton can be compared to a molecular clutch that transmits the force between the ECM and the actin filaments[158]. Binding proteins such as talin and vinculin mediate the interaction between integrins and actomyosin cytoskeleton. F-actin and myosin are held together by crosslinking proteins in structures called stress fibers (SFs)[159].

  When the clutch senses force, the mechanical stretch on integrins activates FAK and Src family kinases and induces immediate cell stiffening through the Rho pathway: RhoA promotes stress fiber formation and myosin II activity through the activation of Rho-associated kinase (ROCK). Rho pathway activation ultimately results in the activation of Yes-associated protein (YAP) and WW

Domain-Containing Transcription Regulator Protein 1 (WWTR1 or TAZ), generally referred to as YAP/TAZ, even if the direct molecular link has yet to be clarified[160]. YAP/TAZ are transcriptional co-regulators well characterized in the context of the Hippo pathway, but recent findings suggested a new role for YAP and TAZ as master regulators of mechanotransduction[161,162]. Notably, YAP and TAZ respond to very diverse biomechanical signals with cell type- stress-specific biological effects as represented in fig.1.16.

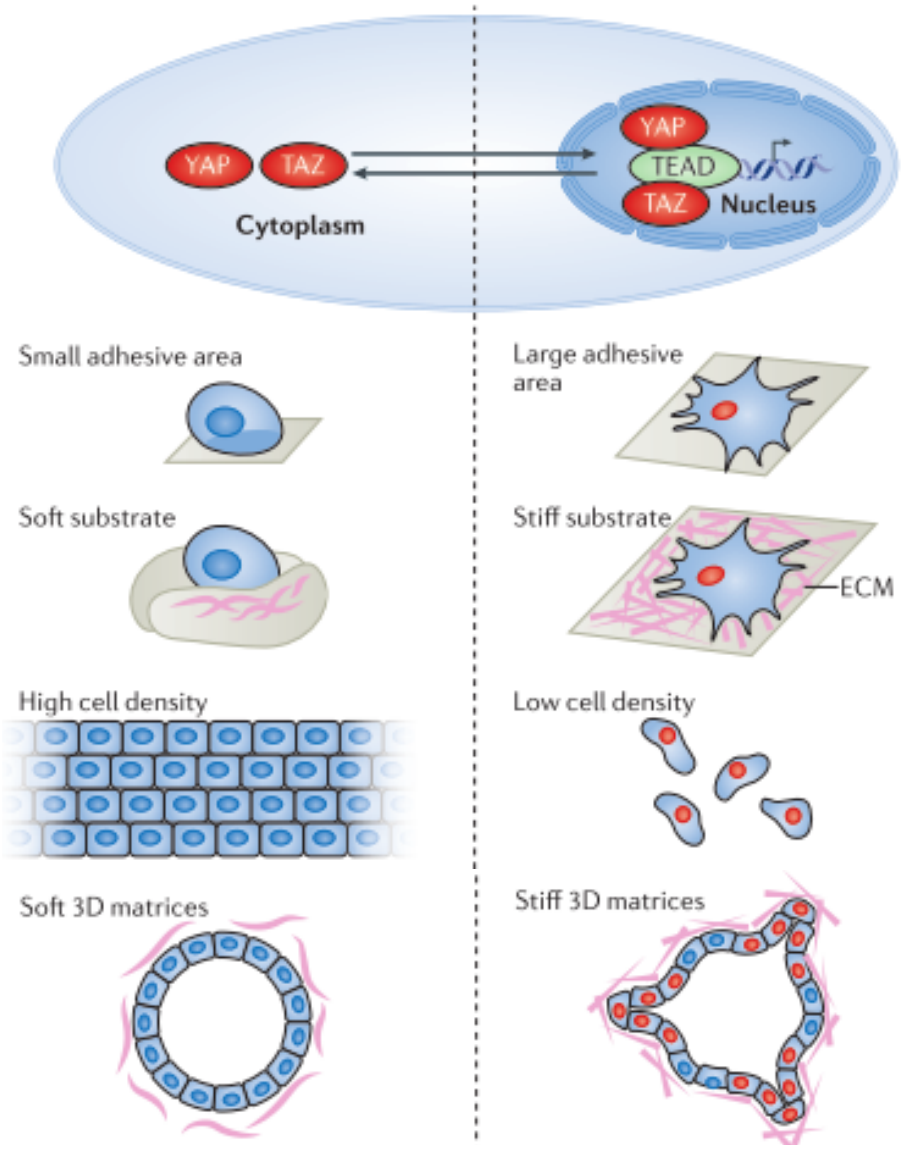

***Figure 1.16: Mechanical stimuli influencing YAP and TAZ. Top**: mechanically activation of YAP/TAZ (red), results in nuclear translocation and interaction with TEAD transcription factors. **Bottom left**: mechanical conditions where YAP/TAZ is not active. **Bottom right**: mechanical conditions that activate YAP/TAZ. Adapted from Panciera et al. 2017.*

YAP/TAZ activity is linked to their cellular localization: if they are kept outside of the nucleus, their transcription factor activity is inhibited, when they are in the nucleus they actively promote transcription. Remarkably, in cells experiencing low levels of mechanical signaling (rounded cells attached to a soft ECM or to a small adhesive area), YAP/TAZ remain in the cytoplasm, while in cells perceiving high levels of mechanical signaling (rigid substrates, cytoskeletal tension or deformation) YAP/TAZ are situated in the nucleus. They remain evenly distributed at more intermediate levels of mechanical signals[160]. Notably, no direct link between FAK and YAP/TAZ activation has been reported, but FAK activation in mandatory for YAP/TAZ activation in response to mechanical stimuli[163].

In conclusion, considering the above-mentioned complexity of integrin-, focal adhesions- and mechanotransduction-related phenomena, is not surprising how alterations in integrin activation, focal adhesion signaling or YAP/TAZ expression results in genetic diseases or in uncontrolled alterations of cell fate and ultimately in cancer[153,160,164,165].

1.2.3 ECM role in stemness

As reported above, ECM and ECM-cell relationships have great influence on cell function and cell fate. Therefore, lot of effort has been made to understand the ECM role in maintenance and differentiation of stem cells. Although ECM influence in embryogenesis and on embryonic stem cells pluripotency may be difficult to study due to technical accessibility and dynamic evolution of the embryo, another kind of stem cells is available in every tissue of the body: the adult stem cells (ASC). Indeed, ECM and cell-ECM interactions have great influence on both adult stem cells and pluripotent stem cells maintenance and differentiation.

1.2.3.1 Adult Stem Cells niche

Some tissues of the human body are constantly renovating their cell population (e.g. skin, blood, gut) in a process called tissue homeostasis,

where old or damaged cells are substituted by new cells. Other tissues (muscles, liver and brain) have lower turnover, but require fresh tissue-specific cells for tissue growth, regeneration and damage repairing. The cells source for this continuous turnover are the adult stem cells resident in the tissue itself. ASC are stem cells with low levels of potency (multi-, oligo-, unipotent or progenitors) that can differentiate only in the few cell types required for the relative tissue[166,167]. Notably, ASC pool reside in the tissue in a quiescent state, with low levels of self-renewal[168] and, upon stimulation, start to proliferate asymmetrically, giving rise to one stem cell and one differentiated cell[169]. With asymmetric proliferation, the ASC pool is maintained virtually along the whole lifespan. It is evident that ASCs represent a precious cell pool for the tissue and in fact, they are protected in a specialized microenvironment named the stem cell niche, that provides to ASC the correct balancing between quiescence, self-renew and differentiation[170]. The niche composed by the combination of ASCs, supporting stromal cells and specific ECM molecules. Niches have specific anatomical localization in the tissue and are both vascularized and innervated to be connected with the tissue itself and other tissues in the organism. The ECM composition of the niche offers biochemical and mechanical cues to direct ASC quiescence or proliferation. Of course, also ASC have a deep influence on the niche, secreting growth factors, ECM components or remodeling it.

Thanks to the combinatorial potential of integrin subunits, every cell-niche relationship is characterized by a specific set of ECM molecules-integrin interactions, with few common players. Among those, β1 integrin is essential to control the balance between symmetric and asymmetric divisions by controlling mitotic spindle orientation[171].

Moreover, the ECM provides to the cells a reservoir of growth factors embedded in the matrix. This ability of the ECM to seize growth factors is essential to regulate spatially and temporally growth factors availability to cells[172]. For example: fibronectin, vitronectin, collagens and proteoglycans can bind FGFs, HGFs, VEGFs, BMPs and TGF-β. In this scenario, the

secretion of metalloproteases or their release from ECM seizure can remodel the matrix and regulate growth factors availability to cells.

Beside the biochemical interactions, the niche provides also fundamental mechanical information on the tissue state. In the niche, the forces acting on ASC are due both to the ECM stiffness and to the surrounding cells. Therefore, an overcrowded niche will exert high pressure on the cells and will block cell proliferation, while a reduction in cell population will stimulate cell proliferation to re-establish pressure homeostasis, in a mechanism known as contact inhibition of proliferation, which is deregulated in tumors[162,173]. Similarly, an increase or decrease in ECM stiffening will induce a different ASC differentiation. For example, mesenchymal stem cell (MSC) differentiation is directed by the physical features of the cell micro- environment rather than by soluble signals: on stiff substrate MSCs follow an osteogenic fate, whereas they turn into adipocytes at low mechanical stresses, with involvement of YAP/TAZ regulation[160,174]. Another example is liver fibrosis, where tissue damage triggers YAP nuclear translocation and activation of hepatic stellate cells, with consequent increase in collagen deposition and stellate cell differentiation in myofibroblasts, resulting in liver fibrosis[175].

In conclusion, the extracellular matrix is a key player for stem cell fate, and therefore studying ECM in adult stem cell niche is therefore important not only to gain a better understanding of pathologies such as cancer or fibrosis, but also to elicit correct tissue regeneration for regenerative medicine approaches[176].

1.2.3.2 ECM in pluripotency maintenance

At first, human primed pluripotent stem cell lines have been established in vitro using medium containing animal serum in co-culture with a feeder layer of mitotically inactive mouse embryonic fibroblasts (MEF). These culture conditions are unfortunately undefined and carry along potentially xenogenic allergens derived from raw animal materials, therefore not applicable for industrial or clinical purposes. Moreover, co-

culture with feeder cells require time-consuming passaging procedures and represents a potential risk of cell contamination and scarce results reproducibility[15,177]. In recent years, many efforts have been spent to develop chemically defined, xeno-free and feeder-free systems to sustain human primed PSC proliferation and differentiation. At first MEF were substituted with MEF-conditioned medium[17], then chemically defined media have been developed both for hESC derivation[178] and for iPSC reprogramming[179]. Remarkably, chemically defined culture media have been followed by the development of more and more specific and minimal MEF surrogates, taking into account that pluripotent stem cells are adhesion-dependent and are not able to attach to tissue-culture plastic. At first, an already available product, commercially known as Matrigel[180–182] has been applied. Matrigel is a crude extract from gelatinous protein mixture secreted by Engelbreth-Holm-Swarm (EHS) mouse sarcoma cells, therefore it is an undefined mixture of laminin, entactin, collagens and heparin sulfate proteoglycan, plus several growth factors. Matrigel can sustain attachment and growth of several cell lines, and a special Matrigel reduced factor (MRF) version has been obtained by depleting growth factors to allow specifically pluripotent stem cells undifferentiated growth. Unfortunately, being Matrigel an undefined extract, it is subjected to batch-to-batch differences and variable experimental results. Moreover, it is not suitable for clinically applications because of the potential risks deriving from animal compounds. Next, by analyzing Matrigel composition, the single ECM protein contribution to maintain pluripotency has been investigated. Between laminin, collagen IV, and fibronectin coatings, laminin has proved to sustain long-term feeder free human primed PSC culture and among the different laminin isoforms, laminin-511 and -521 showed the best performances[183,184]. Recently, recombinant E8 fragments of laminin-511 (LM-E8s), which were the minimum fragments conferring integrin-binding activity, were developed as coatings for chemically defined human primed PSC culture[185]. Besides laminin, other ECM proteins have been proved to sustain long-term human primed PSC undifferentiated self-renewal, such as vitronectin

(VTN), a glycoprotein commonly found in bones and serum[18]. A truncated version of VTN, lacking the N-terminal (VTN-N) has proven better that wild type protein to support attachment and survival and is now widely used[179]. Other ECM proteins, such as fibronectin and collagen I are not as efficient at maintaining undifferentiated proliferation of human primed PSC[17]. Besides natural and recombinant compounds, also fully synthetic materials have been developed for human primed PSC culture, such as peptide-acrylate surfaces[186], PMEDSAH[187] or hydrogels with tunable elasticity[188]. In all cases, synthetic materials need an additional coating with RGD or KGGPQVTRGDVFTMP (vitronectin) peptides to allow primed PSC adhesion and proliferation. Some studies reported that also the use of decellularized ECM from hESC can sustain undifferentiated proliferation of human primed PSC[189].

The development of the above-mentioned coatings to support human primed PSC culture followed mainly empirical and combinatorial approaches, but the current knowledge on the endogenous production of ECM proteins by PSC and the intracellular signaling pathways needed to maintain pluripotency are still largely unknown. Some studies have demonstrated that laminin-511 and collagen IV are the most abundant endogenous proteins produced by human primed PSC, but their physiological role is unknown[184,190]. In particular, laminin chain α5 is important for pluripotency and disruption of endogenous α5 laminin subunit expression dramatically impaired self-renewal and increased apoptosis, with reduction of OCT4 and SOX2 expression, while culturing cells on exogenous laminin-521 restored self-renewal and survival[191]. Indeed, during differentiation, the expression pattern of different laminin isoforms in human primed PSCs changes dramatically[192].

Taken together these data demonstrate that specific cell-ECM interaction pathways are active in human primed PSC and change during differentiation in concert with the better-studied gastrulation and organogenesis gene networks. In particular, some integrin isoforms have been demonstrated to have a prominent role in pluripotency maintenance, in

correlation with the specific coating protein applied: laminin coating is correlated with high expression of α6β1 integrin, moderate levels of α2, and low levels of α1, α3 and β4 integrin subunits[17], while vitronectin coating requires αVβ5 integrin[18,193]. Another highly expressed integrin in human primed PSC is α5β1, specific for fibronectin binding, even if fibronectin coating is not used for primed PSCs expansion[193]. Importantly, the knockdown of integrin α6 in hESC led to a reduction in NANOG, OCT4, and SOX2 levels, suggesting that integrin signaling may be crucial for maintaining PSC self-renewal and the expression of pluripotency transcription factors in human primed PSC[194]. Notably, integrin subunit β1 is fundamental for the adhesion and proliferation of primed PSC on laminin or fibronectin and targeting it with a blocking antibody prevents cell attachment and growth. This phenotype can indeed be reverted by αVβ5 integrin activation by vitronectin[18]. Other possible integrin dimers with monomers that have been detected in human primed PSCs are α2β1 (binding collagen and laminin), α3β1 (binding nidogen, laminin, collagen I, and fibronectin) and α11β1 (binding collagen), bur the role of these or other integrins has not been sufficiently investigated yet[18].

As reported in paragraph 1.2.2, integrin-ECM binding activates the recruitment of a plethora of intracellular proteins. In human primed PSC, integrin signaling has been reported to converge on AKT pathway activation, which is fundamental to promote self-renewal and survival of primed PSCs. In these cells, AKT pathway requires FGF2-mediated activation of PI3K pathway and integrin β1-mediated activation of integrin-linked kinases[195,196]. Ultimately, FAK transduces integrin activation to activate AKT pathway to promote adhesion and prevent cell death by anoikis[197]. Surprisingly, recent works show that integrin-FAK signaling pathway is not active in undifferentiated human primed PSCs. Indeed, recent works report that in primed PSC, FAK is not phosphorylated at Y397, first auto phosphorylation site required for FAK activation, and it is localized in the nuclei of primed PSCs, interacting with OCT4 and SOX2 instead of being localized in focal adhesions[194,197,198]. Notably, both the nuclear localization signal and nuclear

export signal sequences of FAK have been identified in its NT domain. This interaction was demonstrated by co-immunoprecipitation studies[194]. This study suggests that integrin α6 is required to maintain FAK nuclear and dephosphorylated. In fact, during differentiation integrin α6 levels diminish, and FAK Y397 becomes phosphorylated, while during reprogramming, integrin α6 is not expressed in parental fibroblasts, but become expressed few days after reprogramming factors induction and consequently FAK loses the Y397 phosphorylation[194]. Taken together, these findings suggested that the integrin-ILK signaling pathway is active in order to maintain hPSC self-renewal and survival through the activation of AKT signaling pathways while integrin-FAK signaling pathway is not active. However, how can cells grown on vitronectin maintain FAK nuclear localization since no α6β1 integrin is involved in vitronectin binding? To clarify this point, endogenous laminin production by primed PSC was investigated and indeed these cells are able to remodel the substrate in which they are growing by secreting and depositing their own α5 laminin[194]. A useful tool to activate integrins is incubation with Mn^{2+}, which results in β1 activation, formation of focal adhesions, phosphorylation of FAK, and notably, in reduction in Oct4 expression. These data suggest that in undifferentiated primed PSCs the majority of integrins are in an inactive state, but are poised to be activated. When integrins are active, Oct4 expression is reduced; however, the knockdown of integrin α6 also induced the reduction of NANOG, OCT4, and SOX2. This suggests that in primed PSCs, integrin α6 may be pro-pluripotency by inhibiting the ability of integrin β1 to phosphorylate FAK at Y397 and with it preventing the repression of pluripotency transcription factors[194]. A similar mechanism of α6-mediated β1 inhibition was demonstrated to prevent FAK phosphorylation in myoblasts[199]. FAK has been reported to shuffle from focal adhesions to the nucleus where it acts as a scaffold for other proteins such as p53, p21 and GATA4 to promote cell proliferation and survival in stress conditions such as oxidative stress and detachment from the substratum[200,201]. FAK non-canonical activity in primed PSC has been summarized in fig. 1.17.

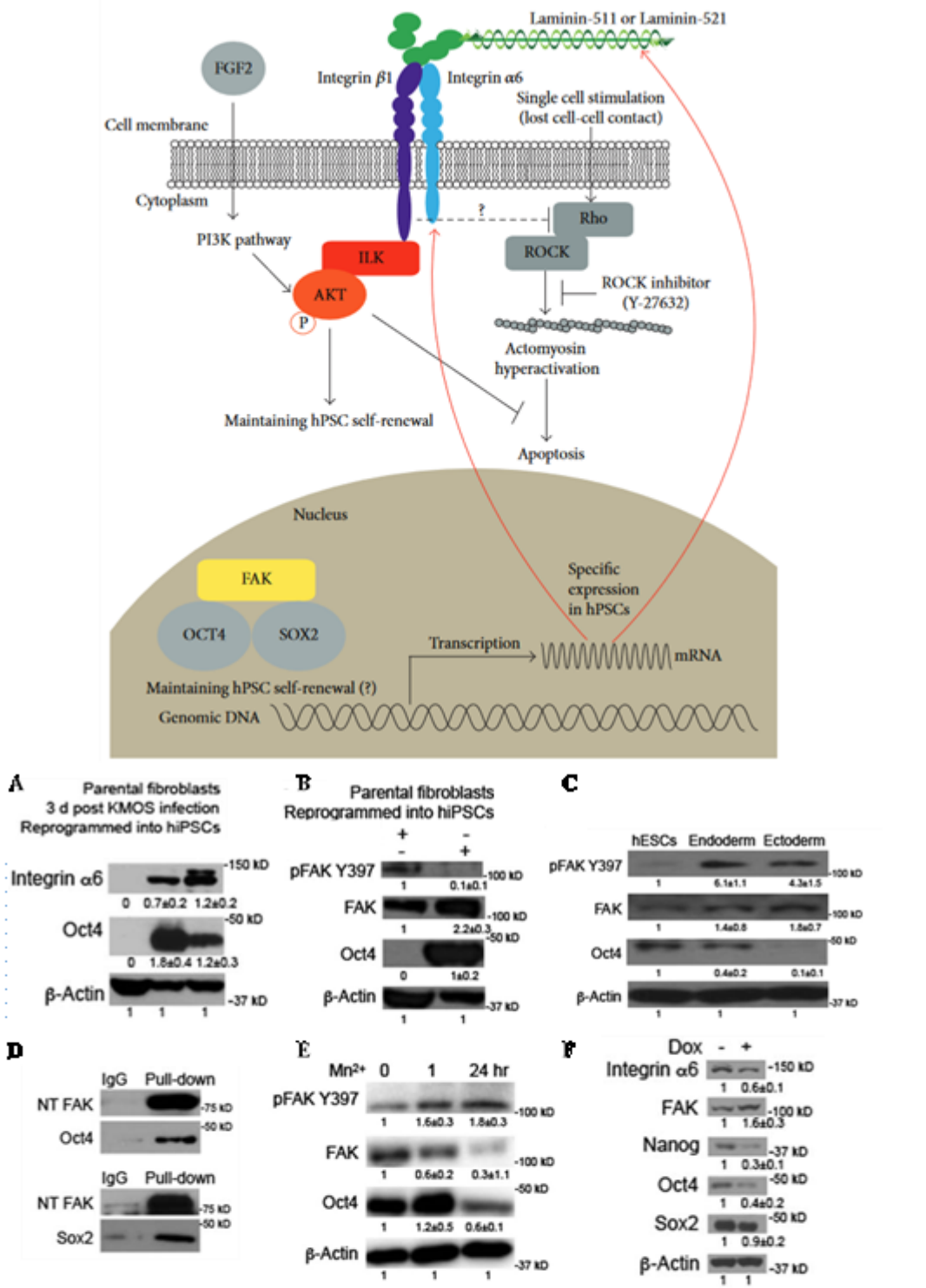

Figure 1.17: FAK non-canonical activity in primed PSC. Top: in primed PSC, FAK is localized in the nucleus and interact with OCT4 and SOX2, inducing integrin α6 and laminin-511 or -521 expression. Bottom: Western blot quantifications that confirm FAK inactivity and nuclear localization in primed PSC. (A) Upregulation of OCT4 and integrin α6 in fibroblasts 72 hours post reprogramming induction (middle lane) and in resulting fully reprogram hiPSCs (right lane), compared to protein lysate of parental fibroblasts (left lane) (B) Downregulation of FAK Y397 phosphorylation from parental fibroblasts (OCT4-) and resulting iPSCs. (C) Upregulation of FAK Y397 phosphorylation in differentiated cells (endoderm and ectoderm) comparing to pluripotent state (OCT4). (D) Co-immunoprecipitation assay showing interaction between FAK OCT4 and SOX2. (E) Mn^{2+} administration increases FAK Y397 phosphorylation, which resulted in reduction in Oct4 levels. (F) Downregulation of integrin α6, OCT4, NANOG, and SOX2 after Dox-shRNA inhibition of integrin α6. Adapted from Villa-Diaz et al. 2016[194].

Another important ECM-cell interaction for pluripotency maintenance is the modulation of RHO-myosin pathway, which is related to laminin α5 subunit and therefore to integrin α6. In fact, disruption of endogenous α5 laminin production led PSC to apoptosis and that the treatment with Rho-associated kinase (ROCK) inhibitor partially restored their self-renewal and diminished apoptosis, suggesting a strong relationship between laminin α5, integrin α6 and RHO-myosin pathway in preserving pluripotency and survival[202–204]. Indeed, in a study, human primed PSC single-cell suspension treated with laminin-511 in solution recovered from single-cell passaging without addition of ROCK inhibitor molecules[190]. Moreover, in the same study it was shown that by blocking integrin α6 in primed PSC, colony aggregation was inhibited, while by blocking integrin β1, colony attachment and proliferation was almost completely prevented. These findings could explain the low survival rate of human primed PSC after single cell passaging in absence of ROCK inhibition.

Notably, all the above-mentioned observations on ECM-related preservation of pluripotency have been made in primed PSC. As human naïve PSCs are concerned, no study has assessed the naïve endogenous ECM protein production, nor the integrin pathways operating in naïve PSC. Some speculations may be made by comparing human primed PSC features with mouse ESC, which represents the mouse counterpart of human naïve PSC. In mESC, collagen I and gelatin are suitable to maintain mESC self-renewal, while laminin or fibronectin induced the differentiated epiblast-like PSC state, the counterpart of human primed PSC. Therefore collagen I and gelatin may be more suitable for naïve state, while laminin may be more suitable for the primed one[205]. A study on FAK nuclear localization in human primed PSC showed how inhibition of FAK signaling that results in FAK nuclear localization, promotes a shift in cell behavior: from matrix-cell adhesion and a more flat phenotype, to cell-cell adhesion with a more 3D, dome-shaped morphology typical of naïve PSC[197]. Unfortunately, this study does not investigate any naïve pluripotency marker expression to validate a similar correlation.

Another demonstration of the peculiar functionality of focal adhesions in human primed PSC is linked to the overall low adhesion strength that characterizes these colonies[206] and to the organization of actin cytoskeleton in primed PSC colonies[207]. The low adhesion strength is related to the switch in integrin expression that occurs during reprogramming: in fibroblast the most expressed integrin is α5β1, while in iPSC is α6β1. This switch is required for completing reprogramming and in fact, cell-ECM interactions rearrangements and expression of integrin α6 is a major barrier toward reprogramming[208]. Indeed, reprogrammed pluripotent cells exhibit significantly lower adhesion strength, on different substrates (fibronectin, laminin, Matrigel) than parental fibroblasts and this correlated to the number of focal adhesions spotted in the two stages. Moreover, partially reprogrammed cells showed an intermediate strength, with more focal adhesions that iPSC and less than parental cells[206]. Low adhesion strength is correlated to a different actin cytoskeleton between differentiated cells and human primed PSC[207,209], as shown in fig.1.18. In fact, fibroblasts have multiple thin actin fibers aligned along the long axis of the cell and connected to focal adhesions at their distant edges, while PSC show thick actin stress fibers parallel to the colony edge, anchored to focal adhesions at the cornerstones of the colonies[207]. These thick fibers act as a fence that surrounds the colony at the bottom plane and play an active role in colony tight packaging. In colonies composed by more cells, the strength produced by the single actin fiber decreases and therefore, bigger colonies have thinner actin fibers, and higher colony density. Indeed, disruption of the actin fence (by blebbstatin, latrunculin-A or ROCK inhibitor treatment) results in reduction of SOX2 expression, cell spreading and differentiation[207]. These data suggest that also mechanical cues play a major role in primed PSC cell fate and pluripotency maintenance. In fact, Rho signaling, which is involved in mechano-sensing as above described, is involved in human primed PSC self-renewal and survival through its downstream effector YAP/TAZ[210]. In primed pluripotent stem cells, YAP/TAZ are nuclear when cells are grown on stiff substrates and relocate

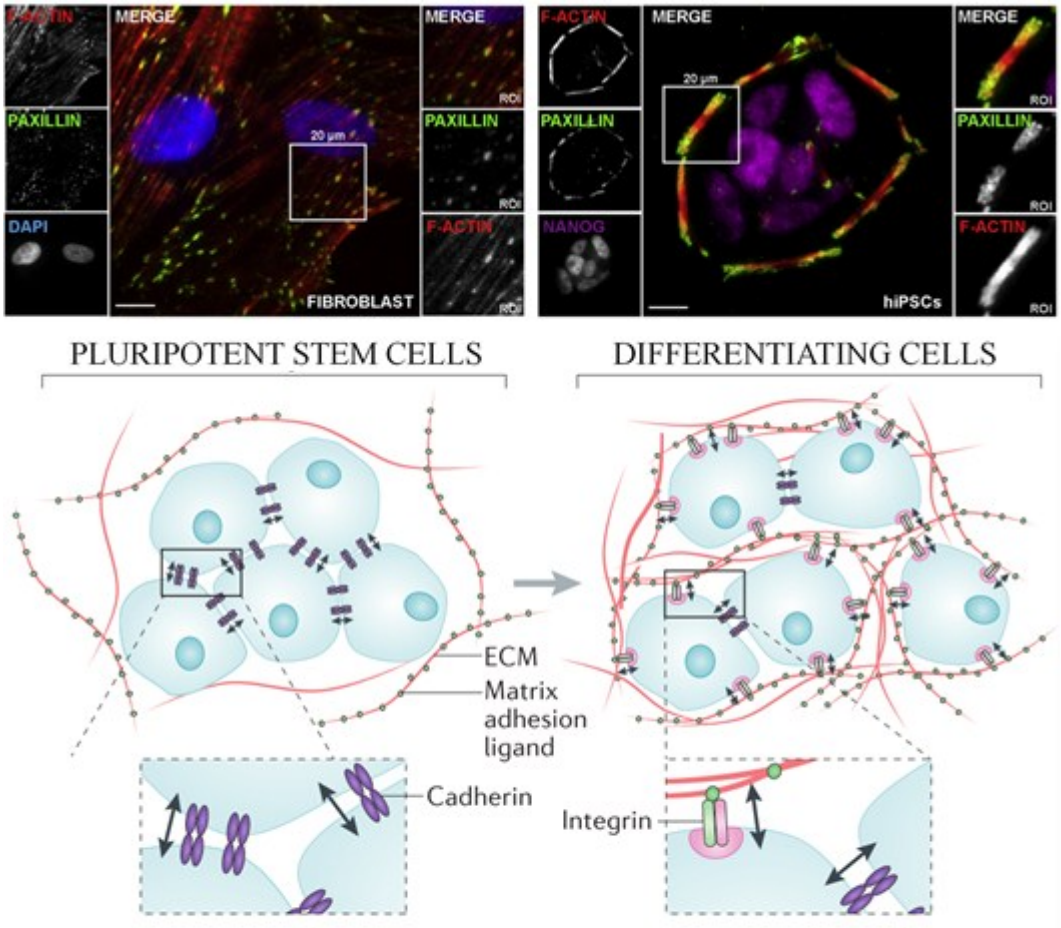

***Figure 1.18: Different organization of focal adhesions and stress fibers in fibroblasts and PSCs. Top**: in fibroblasts dorsal stress fibers cross the cell, while in hiPSCs thick actin ring surround the primea colony. . Adapted from Närvä et al. 2017. Scale bar 10µm. **Bottom**: Schematic representation of actin organization after pluripotency loss. As development progresses, intrinsic forces exerted by cells switch from prevalently cell–cell to more cell–extracellular matrix, and the actin fence is lost. Adapted from Vining et al. 2017.*

in the cytoplasm when cells are forced to adopt a round shape because of lack of mechanical stress[160]. Moreover, YAP/TAZ activation is responsible for the morula cells commitment in trophoblast cells, while cells of the inner cell mass have cytoplasmic, inactive YAP/TAZ.

As human naïve PSC are concerned, up to now, the gold standard substrate for expansion of these cells are mitotically inactivated mouse embryonic fibroblasts (MEF), only one study reports growth of feeder free human naïve PSC on Matrigel and laminin 511, but no information on maintenance of ground state pluripotency features in feeder-free conditions is reported. About the correlations between ECM features and pluripotency maintenance, some speculations may be done by looking at mouse ground

state PSC, where focal adhesion signaling pathway is strongly downregulated comparing to the differentiated counterparts[211,212]. In mouse PSC, reduction of ECM-integrin interaction by low adhesion strength results in pluripotency maintenance, while Mn^{2+} integrin activation leads to FAK phosphorylation and overall reduction of pluripotency markers expression. In 2iLIF conditions (the same conditions used to culture human naïve PSC), mouse PSC show downregulation of pathways related to integrins, FAK phosphorylation, focal adhesions and actin cytoskeleton[211,212]. These data suggest a role for low cell-ECM adhesions in the maintenance of ground state pluripotency similar to the one analyzed above for human primed PSC. A recent work on human primed PSCs demonstrated that if PSC are grown on low-adhesion substrate (low-adhesion gelatin nanofibers), two PSC subtypes with different morphologies arise. In particular, about 90% of the cells maintained a flat morphology, while about 10% of the cells acquired a dome-shaped 3D morphology[213]. A gene ontology analysis on differentially expressed genes between these two morphologies showed that the main differences were related to adhesion genes. Moreover, dome-shaped cells had higher proliferation rate, resistance to single-cell passaging and formed bigger teratomas. The characterization of the dome-shaped cells obtained in this study is not sufficient to state that the isolated population is composed by naïve PSC, but a higher expression of NANOG and KLF4 (naïve marker) is reported. Some in-depth analysis on serum response factor (SRF) suggest that it may be involved in the switch between the two morphologies. SRF is a transcription factors that regulates cell cytoskeleton structure, cell adhesion, motility and fate decision. SRF requires the binding with megakaryocytic acute leukemia (MAL), which is sensitive to variations of actin un-polymerized monomers (G-actin). When cells are exposed to low tensile and adhesive forces, actin cytoskeleton is largely un-polymerized and the monomeric G-actin prevails over the polymerized F-actin form. In the nucleus, G-actin binds to MAL, preventing it to bind with SRF, suppressing SRF signaling. Instead, if cells are subjected to stronger adhesion forces, G-actin is polymerized in F-actin, MAL interacts with SRF

and SRF signaling is active, resulting in cell differentiation[214,215]. Indeed, in cells with flat morphology F-actin prevailed over G-actin, resulting in SRF activation and downregulation of NANOG and KLF4, while in dome-like cells G-actin prevailed and no SRF activation was reported.

Another work suggests a possible role of YAP/TAZ in the conversion of human primed PSC into naïve PSC[216]. In this work, overexpression of YAP in human ESC promoted conversion of these cells into naïve-like cells, with simil-3D morphology and higher resistance to single-cell passaging comparing to the control. However, this study has some controversies: first, the 3D morphology obtained is flatter than other human naïve PSC studies; then the naïve marker characterization provided is quite poor. Therefore, more data are needed to understand YAP/TAZ role in naïve pluripotency.

1.3. MICROFLUIDIC DEVICES CREATE CONFINED ENVIRONMENT FOR CELL GROWTH

Conventionally, cell culture is performed in plastic platform with large cell-adhesive area, such as multiwell, petri dishes, cell flasks and so on. All of those systems are characterized by the need of large volumes of medium covering the cell culture. In these systems, cells are surmounted by several millimeters of medium, which correspond to about 100 times the height of the cell itself. By thinking to a tissue *in vivo*, where cells are tightly packed and nutrients are delivered to the cells by tiny capillaries and by diffusion in the few micrometers interstitial space, it is easily understood how conventional cell culture devices are not an accurate reproduction of a physiological environment. Moreover, the wider the cell-adhesive surface, the greater will be the costs.

To overcome this limitations, a new kind of cell culture devices, based on microfluidic technology has been developed.

1.3.1. Characteristics and advantages of uF devices

The field of microfluidics is characterized by the study and manipulation of fluids at the submillimeter length scale. The fluid phenomena that dominate liquids at this length scale are different from those that dominate at the macroscale[217] (Fig.1.19):

- Laminar versus turbulent flow: for microfluidic systems, flow is almost always in the laminar flow regime, allowing for highly predictable fluid dynamics. Molecular transport also changes dramatically at this scale because convective mixing does not occur, enabling predictable diffusion kinetics.
- Surface and interfacial tension: these forces play more dominant roles on the microscale compared to gravity, which is much more dominant on the macroscale.

- Capillary forces: at the microscale, capillary action is a more dominant force, allowing fluids to advance in opposition to gravity.

Certain derived properties of this peculiar flow dynamic, have made them attractive candidates to replace traditional experimental approaches, especially in the biological and medical field. By simply miniaturizing macroscopic systems and taking advantage of the possibility of massive parallel processing, some microfluidic chips enable high-throughput biological experiments. Specific effects of laminar flow at the micron-scale also enable spatial control of liquid composition at subcellular resolution, fast media and temperature changes, and single cell handling and analysis. Microfluidic technology enables studies of cell behavior from single- to multi-cellular organism level with precise and localized application of experimental conditions unreachable using macroscopic tools[218].

Moreover, microfluidic cell culture devices allow a precise control of cell microenvironment, by allowing both fine control of gradients and factors delivery at the cell level, and enhanced accumulation of paracrine factors produced by the cell itself. The concentration of a specific signaling molecule in the medium is controlled in these systems at a scale comparable to cell size (few micrometers), unlike in conventional culture systems where only bulk concentration is defined. Traditional macroscopic culture methods such as Petri dish poorly mimics in vivo conditions such as growth factor concentration, chemical and mechanical stimuli (Fig.1.19). In addition, large-scale experiments, which consist of doing a large number of experiments at the same time in different conditions, are often not feasible. Finally, the miniaturization of volumes, reagents and cell number allows a consistent reduction of experimental costs, and the possibility to automate the system reduces the manual work and the contamination risk (Fig.1.19)[219,220].

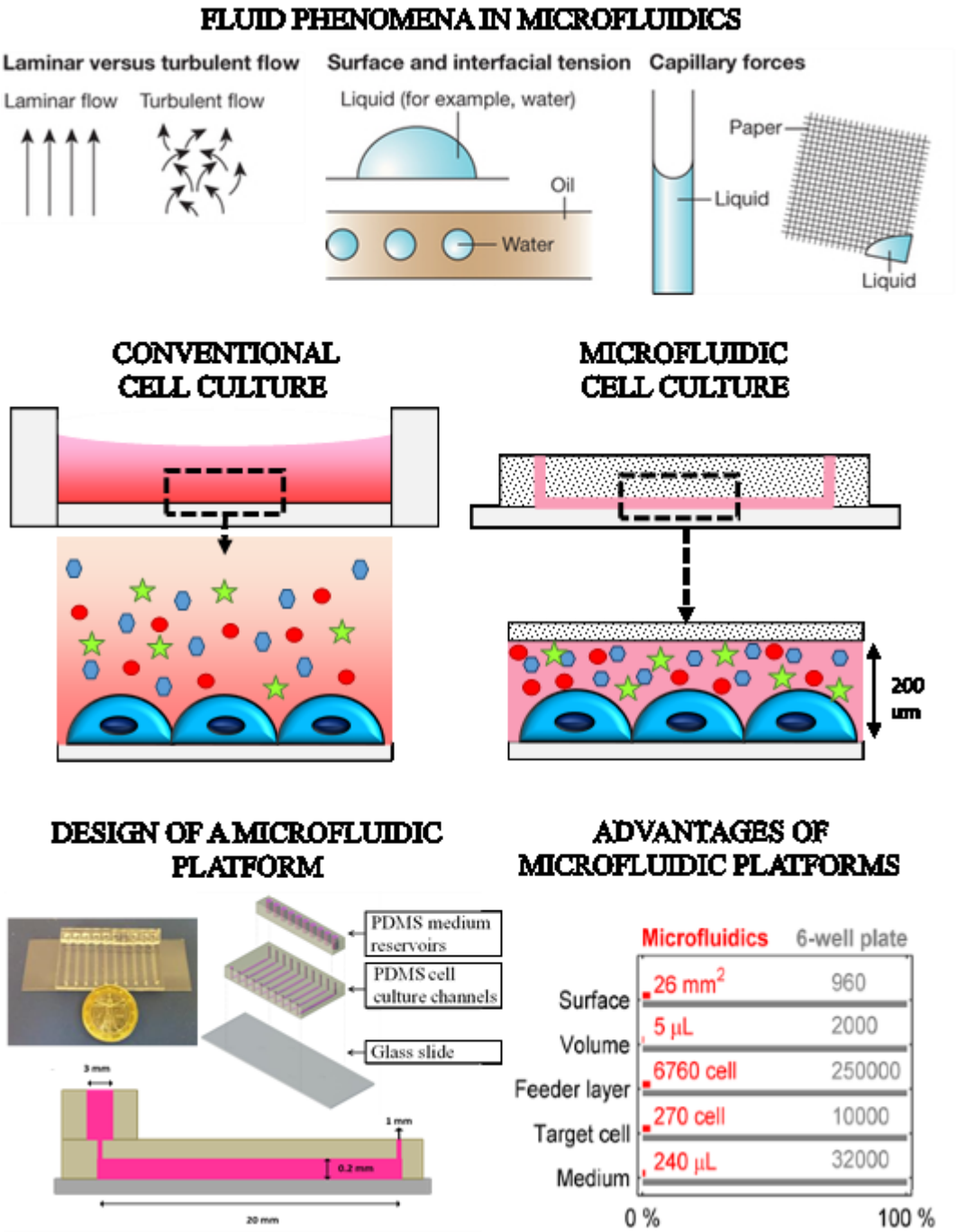

Figure 1.19: Microfluidic cell culture devices. ***Top***: *fluid phenomena at the microfluidic scale comparing to standard macroscale devices.* ***Middle***: *microfluidic devices allow concentration of cell-secreted factors and prevent dilution of paracrine signaling.* ***Bottom left***: *dimensions and component of a microfluidic platform.* ***Bottom right***: *microfluidic devices guarantee reduction of costs by downscaling volumes of reagents and cell numbers needed to perform experiments (compared to standard 6-well multiwell).*

1.3.2. Microfluidic devices enhance paracrine signaling and extracellular factors accumulation

In vitro, cells interact with extracellular environment by up taking and releasing molecules through cellular membrane into the medium. This interchange produces a gradient of factor concentration in the immediate surroundings of the cell surface. Thus, the soluble culture environment is characterized by spatially heterogeneous and dynamically changing composition. In conventional culture devices, the large amount of medium over the cells represents an essentially unlimited source of molecules for cell uptake but also strongly dilutes the concentration of factors released by the cells. In microfluidic devices instead, the few microliters of medium surrounding the cells allow any exchange of molecules between cells and soluble environment to strongly affect factors concentration. Thus, microfluidic discontinuous perfusion, where cell culture medium is changed several times a day depending on cell type and growth rate, but, between one medium change and the other, the medium is static over the cells, is an optimal strategy to grant endogenous factor local accumulation and availability of fresh growth factors. This peculiar feature of microfluidic devices has been applied to optimal maintenance of multiple cell types. In particular pluripotent stem cells, both ESC and iPSC have been demonstrate to take advantage of controlled confined microenvironment[221–224]. These studies demonstrated how optimal maintenance of pluripotent stem cell morphology and pluripotency markers required a specific frequency of medium change to maintain high and uniform expression of pluripotency markers and pluripotency morphology, as shown in fig.1.20. In particular, Guild et al. demonstrated that mouse embryonic stem cells (mESCs) inside microfluidic chambers formed colonies and expressed markers of pluripotency in the absence of feeders or pluripotency-inducing signals such as leukemia inhibitory factor (LIF), while mESCs in standard cultureware differentiated rapidly. These differences in cell response are due to endogenous production of LIF and other growth factors brought upon by cultivation in confined environment. With a different technique, but with a similar approach, Warmflash et al. cultured and differentiated hESC on

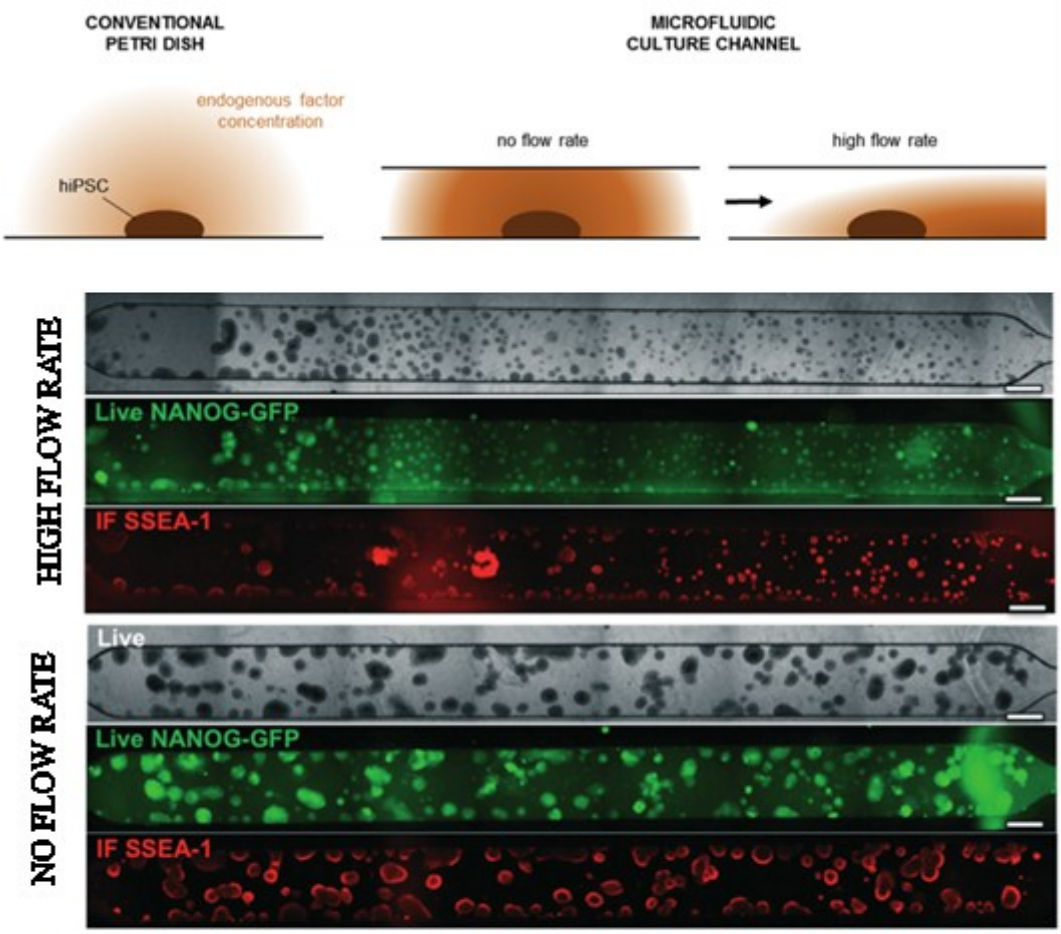

Figure 1.20: Microfluidic environment effect on cell culture. ***Top****: Confined environment promotes endogenous factor concentration and prevents dispersion, but constant liquid flow can wash out cell factors.* ***Bottom****: hiPSC culture in microfluidics under different frequency of medium change. Constant and high flow rate promote endogenous factors wash out and loss of pluripotency markers NANOG ana SSEA-1, while static flow with 2 media change per day (every 12 hours) promote hiPSC colony growth and maintenance of pluripotency markers NANOG and SSEA-1. Scale bar 600 µm. Adapted from Giulitti et al. 2013*[224] *and from Gagliano et al. 2016*[220]*.*

micropatterned surfaces that constrained the colonies in a delimited area. On these surfaces, colonies were able to self-organize in developmental patterns with precise spatial resolution[225]. This work demonstrated the importance of local gradients in embryonic self-organization during development.

In a recent work, Hu et al. analyzed the secretome of human BJ fibroblasts cultivated in microfluidic chips and in conventional platforms with SILAC-MS technique and demonstrated for the first time that the microfluidic environment can boost secretome proteins production and accumulation[288]. In this experiment, conditioned medium was collected from the two platforms during cell growth, balancing channels and wells in order to collect, for each day, the same volume of conditioned medium from the two platforms. In the devices,

the cells were seeded at the same density on the same area, heavy-labeled cells were seeded in microfluidics and light-labeled cells in wells. It is possible to notice how in microfluidics more proteins are detected compared to well system (22 proteins in µF and 14 in well) (Fig.1.21). Among those, only 28.6% of the total proteins are overlapping, 21.4% are expressed only in well and 50% of the total are expressed only in microfluidics. Furthermore, a Gene Ontology (GO) enrichment analysis was performed on this list of proteins and the most abundant protein set is the one correlated with extracellular matrix (ECM). This category is highly represented in the subset of proteins that are expressed only in microfluidic devices, suggesting a positive influence of confined environment on the deposition and remodeling of ECM[288].

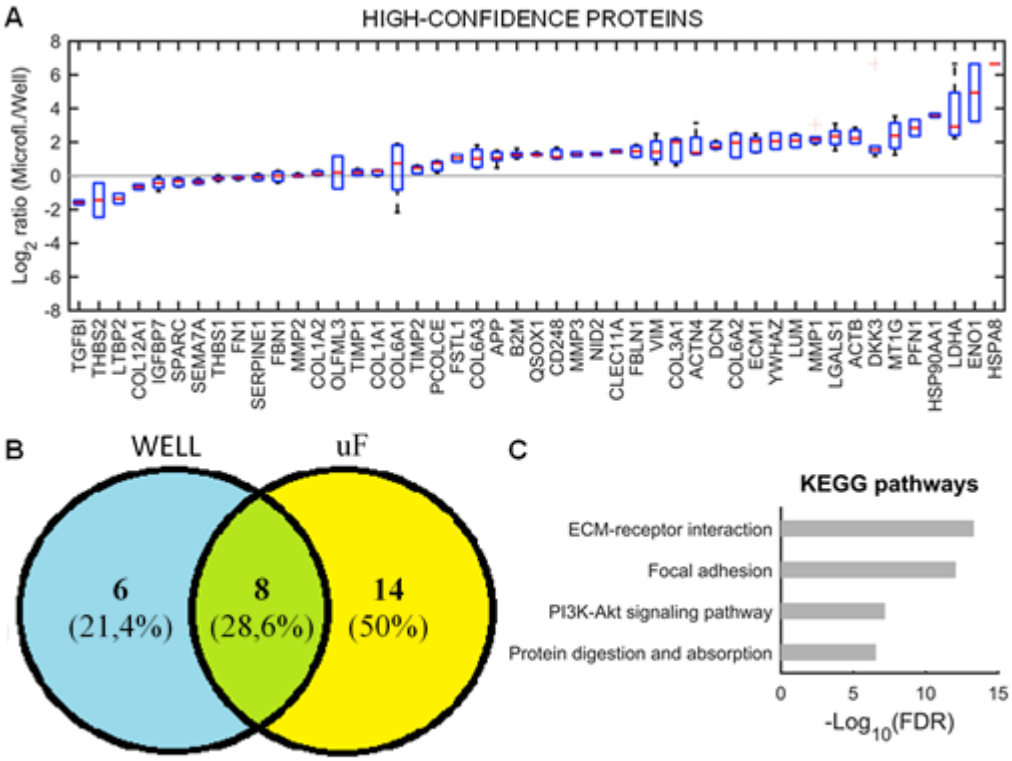

Figure 1.21 : Fibroblast SILAC secretome analysis. A) proteins upregulated in microfluidic platforms are those with Log_2 ratio>0, those upregulated in well are those with Log_2 ratio<0. B)Venn diagram of protein detected in well or in microfluidics. C) Upregulated KEGG pathways in microfluidics. Adapted form Hu et al. 2018[288].

1.3.3. High efficiency reprogramming in microfluidic devices

A groundbreaking work published by Luni et al. developed a novel protocol for high efficiency cell reprogramming in microfluidic cell culture[226].

In this work, BJ fibroblasts (a model cell line widely used for cell reprogramming) have been reprogrammed to hiPSC in microfluidic devices with a cocktail of modified mRNA (mmRNA) coding for six reprogramming factors (OCT4, SOX2, KLF4, C-MYC, LIN28 and NANOG). The mmRNA cocktail was previously validated by Warren et al[227,228].

This protocol was optimized in xeno-free, feeder-free, chemically defined conditions, in order to guarantee maximum safety and robustness to the protocol, and it consumes only ~200 μL of medium during a 14 days reprogramming. The downscaling of reprogramming conditions to a few microliters, caused a ten-fold reduction in the ratio of medium volume to cell surface area compared to that of a well plate and allowed extrinsic autocrine and paracrine factors released by the cells to concentrate rapidly. In agreement with the advantages of microfluidic devices on pluripotent stem cell culture, also cell reprogramming was deeply influenced by the confined environment. In fact, downscaling mmRNA reprogramming to microliter volumes generates a favorable environment for the acquisition of pluripotency, achieving an average efficiency of 120% (120 hiPSC colonies per 100 seeded cells) with a 50-fold increase in micro-scale compared to a multi-well plate (2.1 % ± 0.7). In this work, microfluidics allowed to achieve the highest reprogramming efficiency ever reported in the literature. Moreover, this was obtained with a 60-fold reduction of the overall amount of mmRNA per cell compared with conventional multiwells. Thus, not only microfluidics boosts cell reprogramming, but allows also a conspicuous saving in experimental costs by a 100-fold reduction of raw material compared to a standard multiwell.

Recently, this protocol has been further improved by switching from modified mRNAs to non-modified mRNA and by shortening the RNA transfections. In this case the RNA mix includes three components: non-modified mRNA of the four Yamanaka factors (OCT4, SOX2, KLF4, C-MYC),

NANOG, and LIN28; mRNA encoding for E3, K3, and B18R for evasion of the immune response, and double-stranded microRNAs (miRNAs) from the 302/367 cluster[229,230]. Further increase in reprogramming efficiency can be achieved by adding sodium butyrate, PS48 and TGF-β RI Kinase Inhibitor IV during reprogramming.

Having a system that boosts reprogramming efficiency is very important for generating hiPSC from recalcitrant cell types such as slowly proliferating and early senescent primary cells or from heterogeneous population such as cells extracted from tumor masses that contain cancer stem cells.

Nevertheless, the specific molecular mechanism or pathway responsible for this increase in reprogramming efficiency has not been uncovered yet and further analysis are needed to characterize the system.

1.4. DISSECTING CELL HETEROGENEITY AT SINGLE-CELL LEVEL

As it is widely known, the gene expression profile of a cell defines its function in a specific period of time and in a specific spatial localization. All cells of a human organism share the same DNA and therefore the same set of about 20000 genes. However, different cells transcribe into RNA a different portions of the total genome, leading to cell-cell difference in gene expression profiles. Therefore, only by analyzing the RNA expression profile of cells it is possible to have insight on the cell function.

In decades, different approaches have been developed to inquire RNA expression in cell populations. At first only targeted analysis such as PCR or qPCR were available, strongly limiting knowledge possibilities to hypothesis-driven experiments. Later whole transcriptome analysis such as RNA-sequencing (RNA-seq) have become available to study the whole RNA expression in a cell population. With the introduction of transcriptomic approaches, experimental strategies have changed from being gene-focused or pathway-focused to modern holistic views. In fact, with pre-omic approaches, only specific targets were interrogated in each analysis, with the risk of losing the complete picture of the phenomena-of-interest. Thanks to RNA-seq, instead, it is possible to snap a comprehensive portrait of cell activity in specific experimental conditions. In this way, new and previously unexplored correlations can be found, enhancing total knowledge.

However, until less than 10 years ago, RNA-seq has been limited to the analysis of pooled populations of cells, which was necessary to obtain sufficient RNA for analysis. For example, to obtain the transcriptomic profile of a specific tissue, the whole tissue was processed as a whole. In this way, RNA amount was not a limiting factor anymore, but any information of cell heterogeneity was completely lost. Therefore, it was possible to distinguish the expression profile of brain tissue from muscle tissue for instance, or of a tumor mass from a healthy tissue, but it was impossible to distinguish rare cell populations such as the adult

stem cell pool from the differentiated cell or the cancer stem cells from the main tumor mass. This kind of RNA-seq approach is defined bulk RNA-seq and focuses on the analysis of pooled cell populations, which does not enable the identification of different cell types that express different genes but instead provides a virtual average of the multiple cellular components, which may well say very little about any specific cell type present. Besides tissue anatomy and tumor organization, cell heterogeneity is also a main feature of embryogenesis, where progenitor cells that are often histologically indistinguishable undergo diverse differentiation decisions to become specific cell types. Analysis of the gene expression of pooled populations of progenitor cells does not enable distinction of the signals that drive a progenitor down a particular differentiation pathway. For example, with bulk RNA-seq analysis of a morula-stage embryo it would be impossible to distinguish morula cells that will become the trophoblast from those that will become the inner cell mass.

For these reasons, in the past decade new approaches to enable gene expression analysis at much higher resolution than previously possible have been developed. The currently available techniques, known as single-cell RNA sequencing (scRNA-seq), allow depicting the expression level of every gene, even in a single cell. Such analysis provides much more meaningful insights into cell behaviour than analysis of pooled cells[231–234].

From 2009, when the first scRNA-seq was published by Tang et al.[235], single cell techniques have been extensively applied to complex tissues to enable identification of new, previously unknown cell types[236–241], to study tumor composition and evolution[242–245] or to study embryonic development, pluripotency acquisition and stem cell heterogeneity[70,246–252].

1.4.1. scRNA-seq strategies

scRNA-seq techniques have evolved rapidly in the past decade, improving sequencing quality, depth and throughput, passing from tens of cells up to hundreds of thousands of single cells per study in few years[232]. However, the different techniques all share the same basic principles and pipelines: scRNA-seq starts with single cell isolation, cell lysis, mRNA isolaton and

reverse transcription in cDNA. The obtained cDNA can be amplified by PCR to build a cDNA library suitable for the most diffused sequencing systems. The sequenced reads are then re-aligned on a reference genome to decipher the expressed genes. According to the relative reads abundance, differential expressed genes are then identified. Cells with similar expression profiles can be clustered together in principal component analysis (PCA) or by hierarchical clustering.

Of course, performing this pipeline at single-cell level has numerous limitations, first of all successful single-cell isolation must be achieved to avoid fake expression profiles linked to the analysis of multiple cells instead of a single cell. Then, for successful signal detection with RNA-seq, on the order of 0.1–1.0 μg of total RNA is needed, but a single cell only hosts from 1–50 pg of RNA depending on cell type[232]. One way to overcome this problem is to amplify the total cDNA before library construction, but this need universal primer and has to prevent amplification biases that may mask relative transcript abundance.

In general, when approaching a scRNA-seq experiment, the nature of the research question plays an important role in determining which scRNA-seq protocol and platform should be employed. To date, about 20 different scRNA-seq protocols have been published to date, but the key difference among these methods is that some provide high quality, full-length transcript data, whereas others specifically count only the 3'-ends of the transcripts, giving only a superficial overview of the cell population. Indeed, significant variation was revealed in the sensitivity of each protocol[232,234,253]. On the other hand, high-resolution methods require time-consuming cell isolation and library preparation protocols and high sequencing costs per cell and therefore only a limited amount of cells, from tens to few hundreds, can be analyzed per experiment. Low-resolution strategies instead usually employ microfluidic-based or other high-throughput devices to isolate and process hundreds of thousands of cells per experiment, thus lowering overall costs per cell. A comparison between the two strategies is shown in fig.1.22.

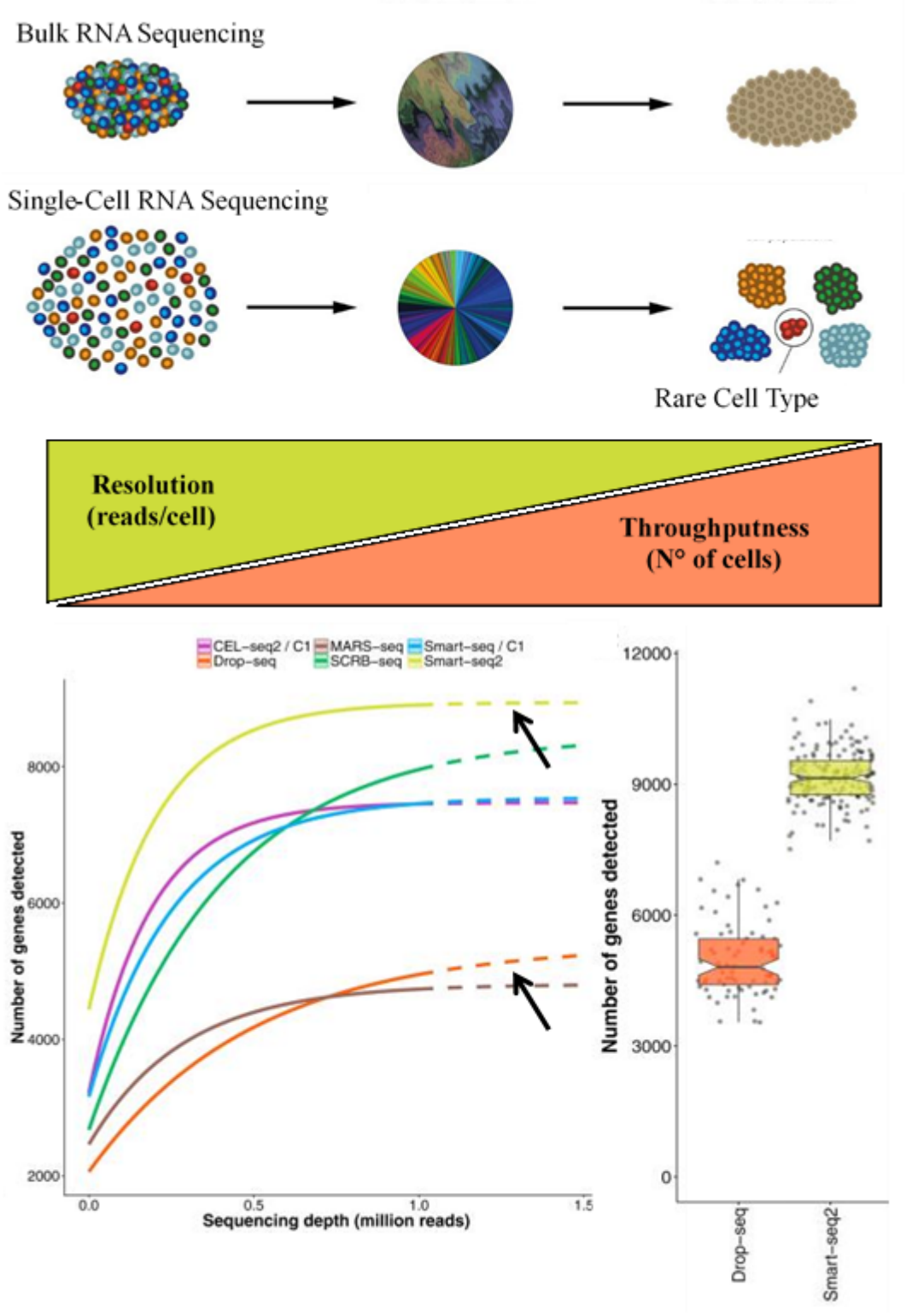

***Figure 1.22: scRNA-seq strategies**. **Top**: with scRNA-seq it is possible to detect rare cell types. **Middle**: two possible approaches for designing scRNA-seq experiments. **Bottom**: comparison between Smart-seq high-resolution – low-throughput method and Drop-seq low-resolution – high-throughput method. Adapted from Ziegenhain et al. 2017.*

For example, if analyzing a well characterized biological model, low-resolution – high-throughput methods are to be preferred since a superficial information is per se sufficient to recognize the relative cell population. As well, if info on alternative splicing or on base mutations is not required, but the aim of the study is to count mRNA molecule copy number to deduce relative expression in the target cell population, low-resolution – high-throughput methods can give information on a higher number of cells per run, thus delineating better the biological landscape. If the aim of the experiment instead is more specific (e.g. detect splicing variants or gaining a deep knowledge on a poorly characterized cell model) then high-resolution – low-throughput methods shall be used[233,253].

1.4.1.1. Smart-seq scRNA-seq

The most used techniques that provides high resolution data but low throughput information is Smart-seq (from version 2 to version 4)[254]. This method requires a manual cell separation step that can be performed with a FACS sorter, by manual pipetting or by serial dilution. Since every cell is considered as a sample itself, it has to be processed separately from the others, therefore analyzing hundreds of cells at the same time can be very time consuming. Due to the complexity and low throughput of the technique, the costs per cell are very high, about 200 €/cell. The technique is represented in fig.1.23.

1.4.1.2. Drop-seq scRNA-seq

A major breakthrough in single-cell screenings derived from the introduction of droplet microfluidics technology, coupled with transcriptome barcoding. The methods based on this approach are characterized by a general low-resolution in data depth, but allow the pooling of thousands of cells in a single-tube pipeline, thus reducing processing operation, timings and costs. Many techniques available apply this approach, here Drop-seq scRNA-seq[238] will be described as an example, since it represents a method that can be set up in any laboratory at an affordable cost and is brand independent. A representation of this technique is shown in fig.1.24.

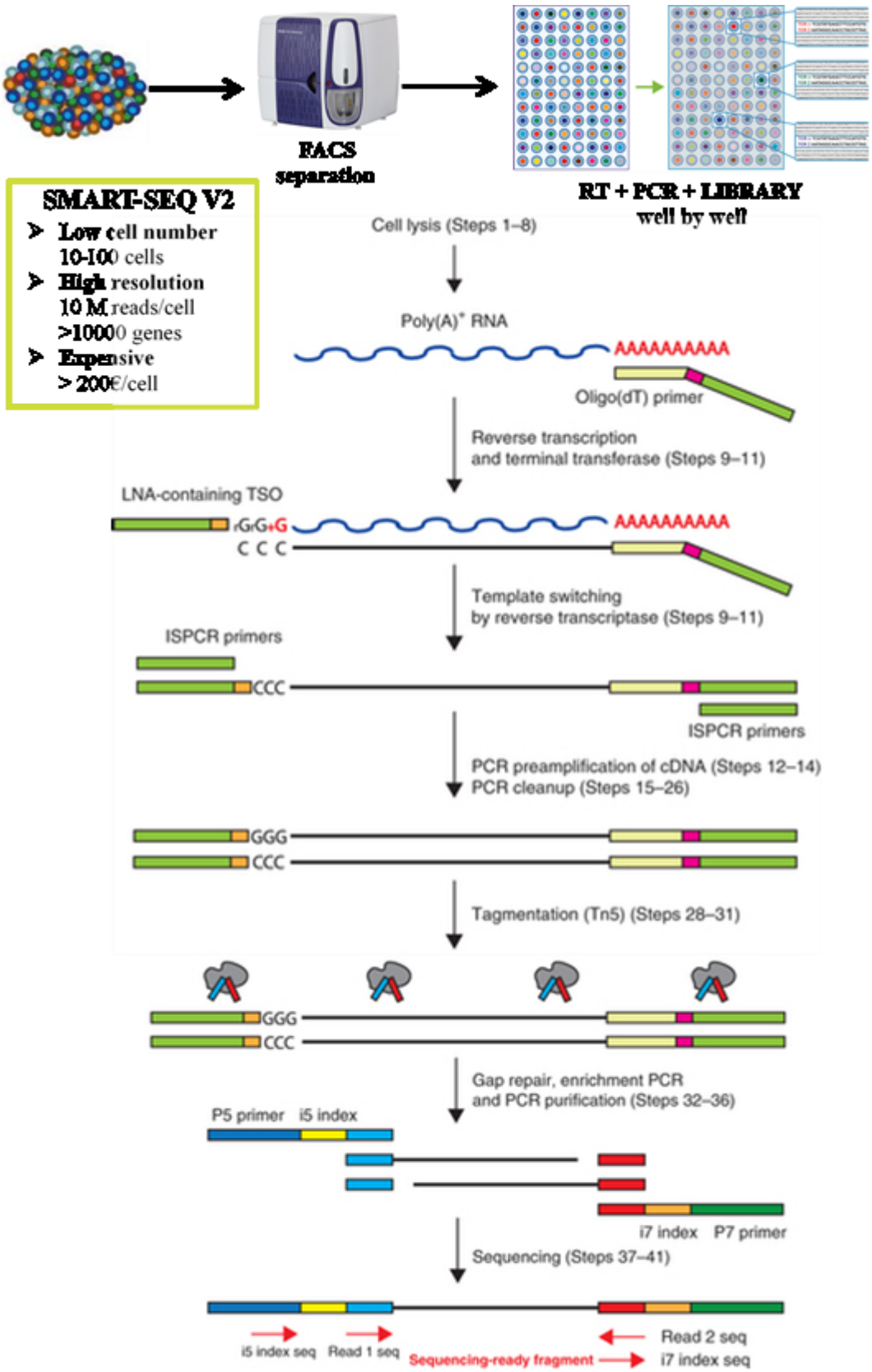

Figure 1.23: Smart-seq v2 pipeline *Single cells are isolated in separate tubes by FACS sorting or manual sorting. After cell lysis mRNA is reverse transcribed with a Oligo(dT) primer and Template-Switch Oligo approach, which allows to attach a PCR primer at 5'-end. In this way, only full-length transcripts will be amplified by PCR. Library for Illumina sequencing is produced by Tagmentation and indexing. Adapted from Picelli et al. 2014[254].*

The microfluidic platform developed of Drop-seq scRNA-seq is composed by three inlets: one for cell solution, one for barcoded beads and lysis buffer solution and one for the droplet-forming oil. Cells and beads combine simultaneously with the oil flux and form droplets of water-soluble solution in oil. The average dimension of the droplets is 80 μm and all fluxes are optimized to guarantee that droplets contain one cell and one barcoded bead per droplet. The barcoded beads are about 40 μm and are functionalized by mRNA-capturing oligos. Those sequences contain a PCR primer, a cell-specific barcode that identifies the captured cell uniquely, an unique molecule identifier (UMI) sequence that tags the specific mRNA molecule and a oligo(dT) to capture mRNA. When the cell solution encounters the bead lysis solution inside the droplet, the cell is lysed, the mRNA is released in solution and can be captured by the barcoded bead. Beads are then reverse-transcribed with template-switch oligo approach in order to attach a universal PCR primer at 3'-end of mRNA sequence. After PCR amplification, the whole transcriptome of single cells is uniquely tagged with a cell-specific barcode and, within the same barcode, single-molecules are tagged with a molecule-specific UMI, which allows calculating the relative abundance of single mRNA molecules in the related cell. Thanks to the barcode-UMI technique, which is shared by all high-throughput scRNA-seq methods[249,255,256], it is possible to process all the beads together, thus reducing dramatically experimental time, reagents and general costs. After PCR amplification, cDNA is tagmented for Illumina library preparation and only 5'-end with the barcode is recovered and sequenced. In this way, the information of the complete mRNA sequence is lost, but it is still possible to count the relative mRNA expression in different cells and therefore taking a wide picture on the heterogeneity of cell landscape. Drop-seq pipeline is described in fig.1.24. Starting from this work, many companies created commercial products for high-throughput scRNA-seq, such as 10x Genomics' "Chromium Single Cell Gene Expression Solution".

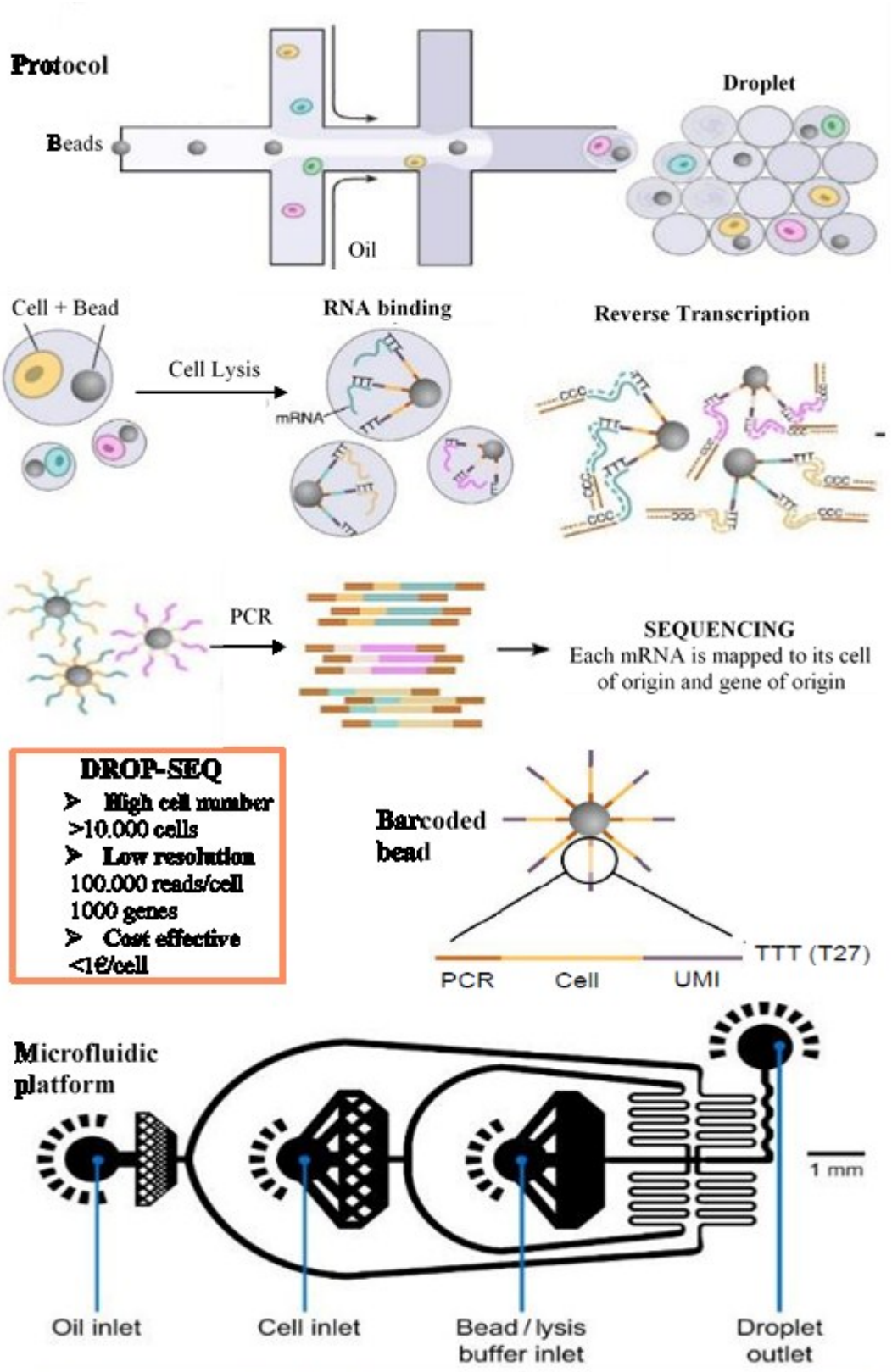

Figure 1.24: Drop-seq pipeline. Top: Drop-seq protocol from single-cell isolation to sequencing. Middle: representation of barcoded beads. Bottom: Microfluidic platform designed for Drop-seq. Adapted from Macosko et al. 2015.

CHAPTER 2: AIM

Pluripotency state is a dynamic contest with high degrees of complexity, where cell-specific gene expression program is constantly in crosstalk with extracellular cues provided by the surrounding cells or by the environment. Embryonic development can be considered the most perfect example of cells self-assembly represent an example of the great ability of cells to shape their environment by creating their own extracellular matrix. However, the current knowledge on cell-extracellular matrix relations in pluripotent stem cells is still limited and the commonly used simplistic *in vitro* cell culture conditions provided by conventional cell culture systems are not able to recapitulate the *in vivo* complexity.

In the recent years, new systems based on microfluidic technology have been applied to cell cultures. Microfluidics provides a confined environment for cell culture, with limited volume of medium surrounding the cells. A confined environment influences the cell under several points of view: chemical signaling, mechanotransduction, gene and protein expression are all influenced by this system. In particular, secreted factors are allowed to accumulate around the cells thanks to the physical constrains provided by the microfluidic channels and therefore paracrine signaling pathways are boosted. This provides a useful tool to mimic the *in vivo* extracellular environment, one step forward for recreating a synthetic microenvironment to study pluripotent stem cells. Moreover, microfluidics proved to extremely enhance reprogramming efficiency, but no explanation for this behavior has been exhaustive so far.

In this scenario, the aim of this thesis is to analyze the influence of confined microfluidic environment on pluripotency acquisition and maintenance, with a focus on the role of extracellular matrix.

To achieve this goal, naïve and primed pluripotent stem cells, together with differentiated fibroblasts and cells undergoing reprogramming have been cultured in conventional wells and in microfluidic platforms and the features of their extracellular matrix network have been analyzed. To cope with the high complexity of the biological question, conventional hypothesis-driven and targeted analysis techniques such as immunofluorescence staining and western blot have been coupled with global, high-throughput, multi-omics approaches such as RNA sequencing and mass spectrometry. Moreover, single-cell approaches have been used to take into account the different expression profiles of the single cells.

By applying microfluidic confinement to pluripotent stem cell culture with the resulting enhancement of accumulation of paracrine signals, this work aims not only at characterizing the main features of extracellular matrix network in different developmental stages, but also to begin to uncover the contribution of extracellular matrix and single cell-specific signals for maintenance and acquisition of pluripotency.

In addition, a second aim this thesis is the analysis of the contributions of the serin-protease inhibitor SERPINB3 and of its related gene network to the process of cell reprogramming, in the context of using cell reprogramming for the epigenetic rewriting of tumors with high expression of SERPINB3.

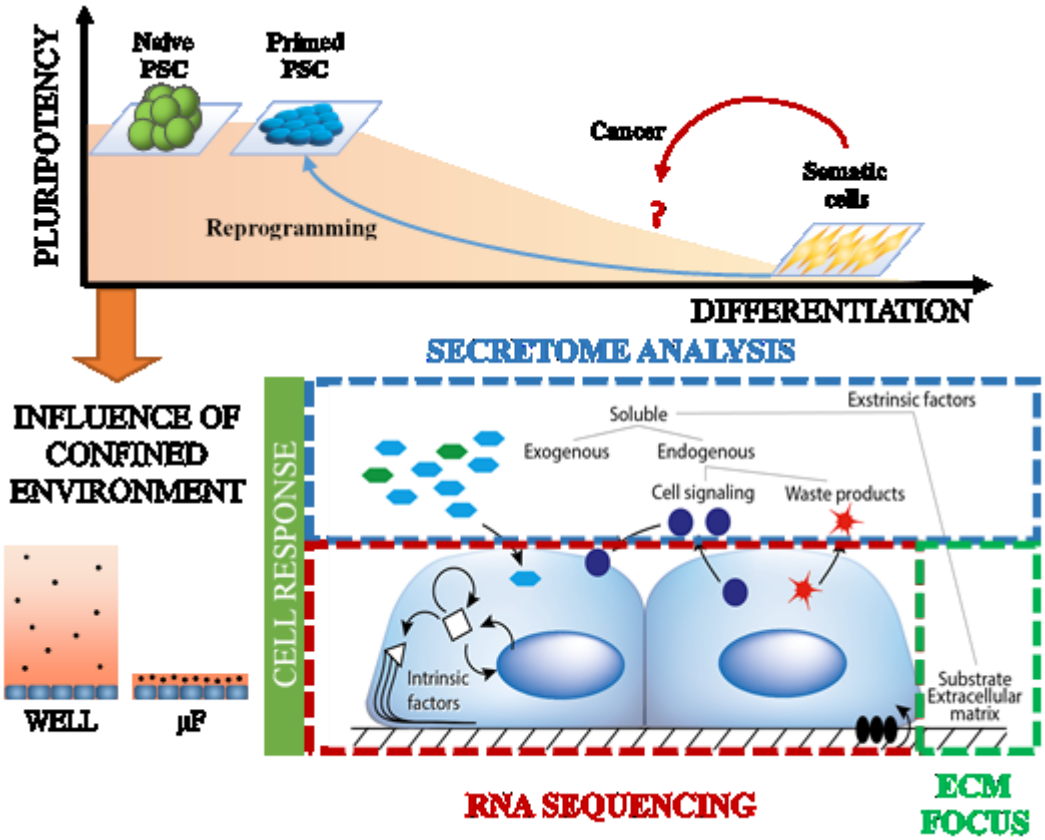

***Figure 1.1: Graphical abstract**. Analysis of the influence of confined microfluidic environment on pluripotency acquisition and maintenance, with a focus on the role of extracellular matrix.*

CHAPTER 3: MATERIALS AND METHODS

3.1. MICROFLUIDIC PLATFORMS

The microfluidic platform used in this work, also called microfluidic chip, is designed and fabricated in house according to standard soft-lithographic techniques and molded in polydimethylsiloxane (PDMS) as previously described[224,226]. It is composed by 10 independent microfluidic channels, each one with a surface of 27 mm^2 (18mm long, 1.5mm wide) and a height of 200 μm. The desired pattern was designed in AutoCAD and printed on acetate foil at 8,000 dpi. By soft-lithography, the pattern was then engraved on a 4-inch silicon wafer (Siegert) covered by 200-μm-thick SU-2100 photoresist (MicroChem). The wafer was coated for 1h with chlorotrimethylsilane vapors (Sigma- Aldrich) at room temperature. PDMS (Sylgard 184, 1:10 base:curing agent ratio, Dow Corning) was poured liquid over the patterned wafer and, after de-bubbling, cured for 2h at 75 °C. The PDMS mold with multiple independent channels, when solid, was extracted from the wafer, punched with 1 mm biopsy punch (Kai Medical) and bound covalently to a 75x25 mm microscope glass slide (Menzel-Glaser) by plasma treatment (Plasma Cleaner, Harrick Plasma). On one side of the microfluidic channels a second layer of PDMS reservoirs with a height of 3 mm and a diameter of 3 mm was attached with plasma treatment. The chip was washed once with isopropanol and twice with distilled water to wash uncured PDMS and check channel functionality, then autoclaved to guarantee sterility. The procedure to produce microfluidic platforms is represented in fig.3.1.

PDMS is the elastomer of choice for microfluidic platforms designed for cell culture because it is chemically inert which makes microfluidic platform biocompatible; it is homogeneous, isotropic, and optically transparent down to about 300nm, which makes possible coupling with detection analysis instruments like fluorescence microscopy. Moreover, it is highly permeable to several gases, included oxygen and carbon dioxide, allowing fast equilibration time in standard cell culture incubators. Finally, it is a durable elastomer, allowing long-term experiments to be performed[219,257].

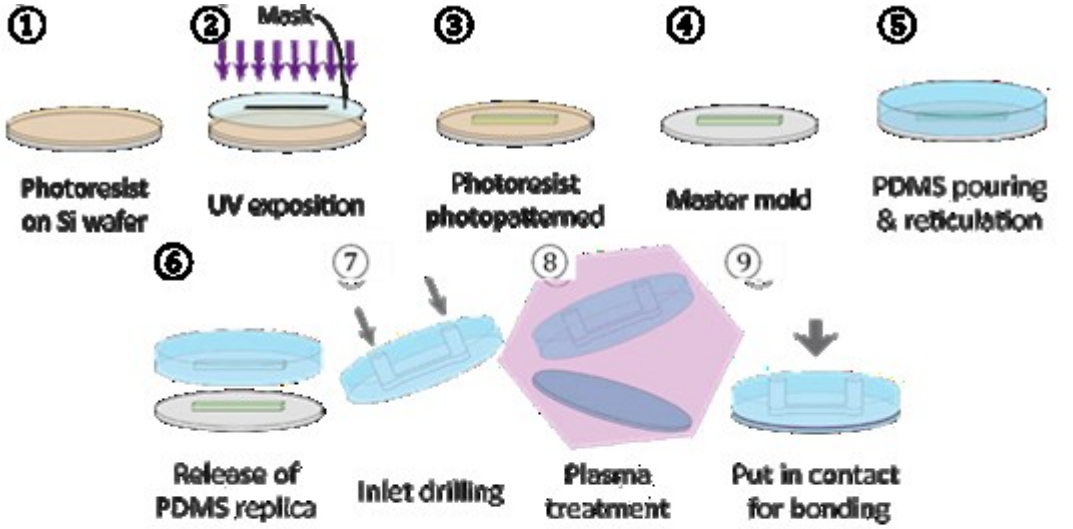

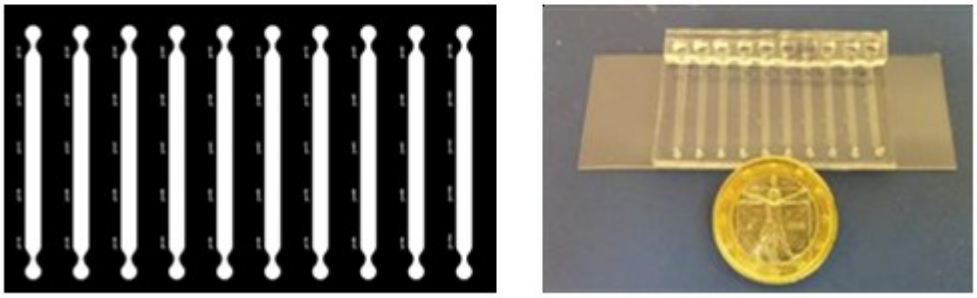

Figure 3.1: Microfluidic chip fabrication. Top: production of a microfluidic chip by replica-molding technique. Bottom: the microfluidic chip used in this work; AutoCAD design (left) and ready to use (right).

3.2. CELL LINES AND CULTURE SYSTEMS

In this work, somatic and pluripotent cell lines have been used, both in microfluidic devices and in conventional cell culture systems. All cell lines were cultured at 37 °C and 5% CO2 atmosphere. All commercially available cell lines were certified mycoplasma free. All cells used in this study have been verified for absence of mycoplasma contamination.

Notably, adaptations are required when culturing cells in microfluidic chips.

3.2.1 Cell culture in conventional devices

3.2.1.1. FIBROBLASTS

Human foreskin BJ fibroblasts (Miltenyi Biotec) and human foreskin fibroblasts HFF-1 (ATCC) were routinely cultured in High Glucose Dulbecco's modified Eagle Medium (DMEM, ThermoFisher Scientific) supplemented with 10% Fetal Bovine Serum (FBS, ThermoFisher Scientific) on tissue culture treated 100 mm petri dish (Falcon) with medium change every second day. When confluent, fibroblasts were washed with phosphate buffer without Ca^{2+}/Mg^{2+} ($PBS^{-/-}$, ThermoFisher Scientific) and incubated with Trypsin-EDTA 0.25% (ThermoFisher Scientific) for 5' at 37 °C. Growth medium with FBS was added to inactivate trypsin; cells were centrifuged at 300 g for 5' and seeded in the reported medium. BJ fibroblasts were used for reprogramming only up to passage 12. Cells were frozen in FBS supplemented with 10% DMSO (Sigma-Aldrich).

3.2.1.2. NAÏVE HUMAN PLURIPOTENT STEM CELLS

In this study, Naïve HPD06: an induced pluripotent stem cell line reprogrammed from HFF fibroblasts to naïve state was used. After microfluidic naïve reprogramming (article under revision), cells were extracted from the microfluidic chip and cultured on confluent (~300 MEF per mm^2) mitotically-inactivated mouse embryonic fibroblasts (MEF, DR4 ATCC) with RSeT medium (STEMCELL Technologies) in 12-well multiwells (Falcon). MEF feeders were routinely seeded on 0.1% gelatin from porcine skin (Sigma-Aldrich) in MilliQ water at least one day before naïve passaging. For extracellular matrix-related experiments, human

vitronectin was used instead of gelatin as coating for MEF feeders. Naïve HPD06 colonies were passaged every 4-6 days, when the colony diameter reached about 100 µm. To passage naïve cells, colonies were washed with $PBS^{-/-}$ and routinely dissociated at single cell level with TrypLE™ Select Enzyme (Thermo Fischer Scientific) for 5' at room temperature, inactivated with equal volume of 0.5 mg/ml Soybean Trypsin Inhibitor (ThermoFisher Scientific) and centrifuged at 300 g for 5'. Cells were seeded routinely on MEF feeders in RSeT medium supplemented with 10 µM StemMACS Y27632 ROCK Inhibitor (Miltenyi Biotec). Other coatings have been tested in this study: Matrigel Growth Factor Reduced (MRF, Corning) diluted in KnockOut DMEM (ThermoFisher Scientific) at the concentration of 5% (5% MRF) and human vitronectin (VTN-N 0.5 µg/cm2, ThermoFisher Scientific). ROCK inhibitor was used only for 24 h after passaging. Naïve medium was changed once a day and cells were frozen in KnockOut Serum Replacement (KSR, ThermoFisher Scientific) supplemented with 10% DMSO (Sigma).

To produce mitotically-inactivated mouse embryonic fibroblasts to be used as feeder layer, DR4 MEF line (ATCC) was expanded on 0.1% gelatin from porcine skin (Sigma-Aldrich) in MilliQ water coating until confluent. Confluent MEF were mitotically-inactivated with 10 µg/ml Mitomicin-C for 2 h at 37 °C, then frozen in FBS supplemented with 10% DMSO (Sigma-Aldrich).

3.2.1.3. PRIMED HUMAN PLURIPOTENT STEM CELLS

Naïve HPD06 cell line has been converted to primed pluripotency state to have an isogenic primed PSC control. To convert naïve HPD06 to primed state, cells have been cultured in 12-well multiwell (Falcon) on MEF feeder layers in RSeT medium until ready to be splitted. The first day of transition, medium was changed to N2B27 medium: 48% DMEM/F12 (ThermoFisher Scientific), 48% Neurobasal medium (ThermoFisher Scientific), 1% B-27 Supplement (1:100, ThermoFisher Scientific), 0.5% N-2 Supplement (50x, ThermoFisher Scientific), 1% GlutaMAX Supplement (100x, ThermoFisher Scientific), 1% MEM Non-Essential Amino Acids Solution

(100x, ThermoFisher Scientific), 0.01% 2-Mercaptoethanol (50 mM, ThermoFisher Scientific) and 0.25% Insulin (1,72 mM, Sigma-Aldrich). The second day cells were dissociated at single-cell with TrypLE™ Select Enzyme (Thermo Fischer Scientific) for 5' at room temperature, inactivated with equal volume of 0.5 mg/ml Soybean Trypsin Inhibitor (ThermoFisher Scientific) and centrifuged at 300 g for 5'. Cells were seeded on Matrigel Growth Factor Reduced (MRF, Corning) diluted in KnockOut DMEM (ThermoFisher Scientific) at the concentration of 0.5% (0.5% MRF) in N2B27 medium supplemented with 10 μM StemMACS Y27632 ROCK Inhibitor (Miltenyi Biotec). From day 3 to day 6 medium was gradually switched from N2B27 to Essential 8 (E8, ThermoFisher Scientific), with the following gradient: day 3 75% N2B27 - 25% E8; day 4 50% N2B27 - 50% E8; day 5 25% N2B27 - 75% E8 and day 6 100% E8. When colonies with primed-like, flat morphology appeared were passaged with 0.5 mM EDTA (ThermoFisher Scientific) on 6-well multiwell (Falcon) coated with 0.5% MRF and selected until stable.

Freshly derived hiPSC, reprogrammed from BJ fibroblasts with modified mRNA as described in Luni et al. 2016, have been extracted from the microfluidic device and stabilized in 6-well multiwell plates (Falcon)[226]. Stable hiPSC clones were routinely cultured on 6-well multiwell plates (Falcon) coated with human vitronectin (VTN-N 0.5 μg/cm2, ThermoFisher Scientific) or with 0.5% MRF. hiPSC medium was StemMACSTM iPS-Brew XF (Miltenyi Biotec) or Essential E8 (E8, ThermoFisher Scientific).

In all primed PSC lines used in this study, medium was changed once a day. hiPSCs were passaged with 0.5 mM EDTA (ThermoFisher Scientific) and frozen in KnockOut Serum Replacement (KSR, ThermoFisher Scientific) supplemented with 10% DMSO (Sigma).

3.2.2 Cell culture in microfluidic devices

Autoclaved microfluidic chips, produced as reported in paragraph 3.1, are kept inside 100 mm petri dishes (Falcon) with a $PBS^{-/-}$ bath to maintain sterility and controlled humidity. When dry, the $PBS^{-/-}$ bath is refilled with sterile MilliQ water to keep the salt concentration constant. Every channel has a volume of 5.4 µl, but to fill channel, inlet, outlet and reservoir, a volume of 12 µl per channel is used. Unless otherwise specified, 12 µl is the standard volume of solution per channel used. Before cell seeding, chips are washed once with $PBS^{-/-}$ to remove possible debris and then coated for one hour with the desired coating. When seeding primed PSC cells, MRF concentration is increased to 2.5%. Since wash and coating are performed when the channels are empty, to ease the inflow of protein solution and avid bubbles, the pipet tip should go precisely inside the inlet hole. At the end of the incubation period, typically 1 hour at room temperature, the coating solution is replaced with fresh medium that is left in the chamber until cell seeding. Part of the solution in the reservoir, containing a mixture of coating solution and medium is aspirated, without completely emptying the reservoir. Also during cell seeding, the tip should be placed precisely inside the inlet hole. 12-µL of well-mixed cell suspension should be injected by quick pipetting. The reservoir will be full at the end of seeding and it is possible to leave a little amount of medium at the inlet; it is convenient not to aspirate this medium, to obtain a spatially homogeneous seeding along the culture chamber.

Microfluidic platforms require two medium change per day, one every 12 hours. Only after cell seeding, usually performed in the morning, the second change is skipped to prevent cell detachment due to shear stress. During medium changes, the strategy that minimizes bubble formation consists in depositing 12 µL of medium near the inlet; because the reservoir is almost full, a droplet of medium is formed at the inlet. Then, using a 200-µL pipette some medium can be aspirated from the reservoir, in order to have all the medium at the inlet entering the chamber (it enters by capillarity). A representation of cell culturing procedures in microfluidic channels is shown in fig.3.2.

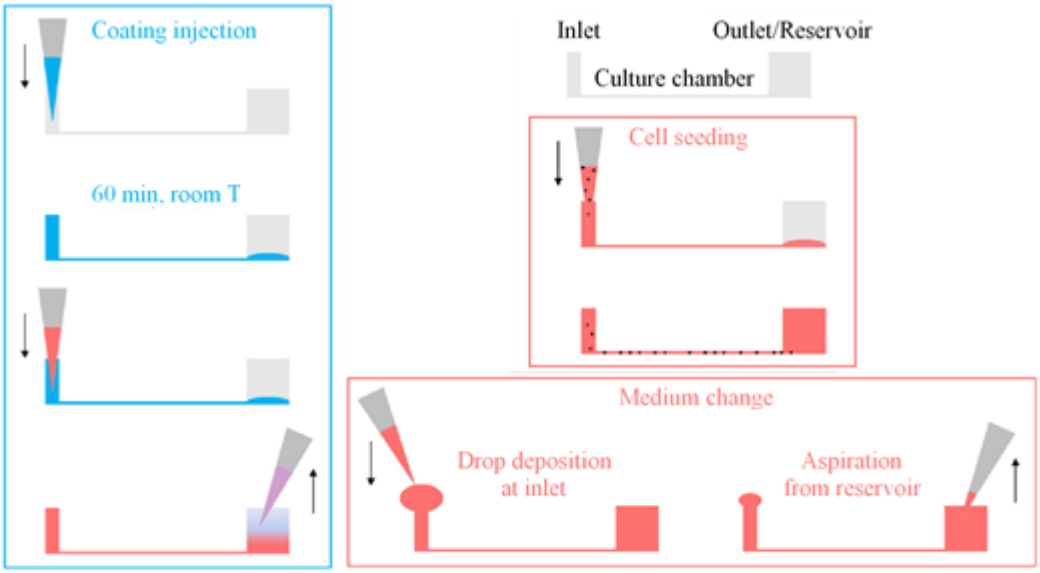

***Figure 3.2: Operating a microfluidic chip**. Left: Coating procedure. Right: cell seeding and medium change procedure.*

3.3. CELL REPROGRAMMING

3.3.1 Modified mRNA reprogramming to primed pluripotency in microfluidics

BJ human fibroblasts were reprogrammed in feeder-free, chemical defined conditions in microfluidic devices as previously described[226] using modified synthetic mRNA (mmRNA) developed by Warren et al.[227,228]. On D-3 (referred to the beginning of mmRNA transfections) cells were detached from the Petri dish with Trypsin-EDTA 0.25% (Life Technologies) for 2' at 37 °C, resuspended in High Glucose Dulbecco's modified Eagle Medium (DMEM 41965, Life Technologies) supplemented with 10% FBS (FBS, Life Technologies), counted with a Burker chamber and seeded at low density (5-10 cell/mm^2) in the microfluidic channels coated with fibronectin (Fn, 25 µg/mL, Sigma-Aldrich). The day after (D-2) medium was switched to Pluriton reprogramming medium (Stemgent), a chemically defined, TGF-β-free medium and cells were allowed 2 days to adapt to the new medium, with medium change twice a day. On D0 the mmRNA transfections were started and 12 daily transfections were performed because mmRNA transfection leads to transient production of the proteins of interest, with a peak of production

between 12 and 24 h, and complete clearance at 42 h after transfection, therefore daily transfections are needed. During transfections, medium was supplemented with B18R recombinant protein (200 ng/mL, eBioscience) to suppress single-strand RNA-induced immune response mediated by type I interferons[258]. mmRNA Reprogramming kit (Miltenyi Biotech) was used according to the manufacturer instructions: single lyophilized mmRNAs (OCT4, SOX2, KLF4, c-MYC, NANOG, LIN28 and nGFP) were first resuspended with RNAse-free water and pooled together with 3:1:1:1:1:1:1 stoichiometry. nGFP mmRNA was added to evaluate the transfection efficiency. Single use aliquots were prepared and stored at -80 °C. All RNA-related operations were performed with RNAse free consumables and all surfaces were pre-treated with RNAse-Zap (Ambion). The transfection mix was prepared according to the manual of the StemMACS mRNA Transfection Reagent (Miltenyi Biotec) pooling two solutions: the first obtained diluting 5x 100 ng μL−1 mmRNA in transfection buffer solution, and the second diluting 10× transfection reagent in transfection buffer solution. The two solutions were mixed and incubated for 20' at room temperature. The transfection mix was diluted in reprogramming medium and handled to the microfluidic channels. Cells were incubated with the transfection reagent for 4 h and then medium was replaced with fresh reprogramming medium. After 7 days of transfections cells undergo mesenchymal-to-epithelial transition and at D10-11 first colonies arise. After 12 days of transfection the medium was no longer supplemented with B18R protein and cells were cultured for 2 additional days to degrade all exogenous mmRNA. From D14 medium was switched to primed pluripotency medium such as was StemMACSTM iPS-Brew XF (Miltenyi Biotec) or Essential E8 (E8, ThermoFisher Scientific). At D14, if reprogramming efficiency needed to be established, cells were stained for pluripotency markers and the reprogramming efficiency was calculated as n° of $NANOG^+$ colonies per seeded cells per channel. If colonies needed to be extracted, reprogrammed cells were allowed to grow for additional days before extraction.

3.3.2 Non-modified mRNA reprogramming to primed pluripotency in microfluidics

This protocol is closely derived from the previous, with few modifications. The RNA mix of the reprogramming kit used in this protocol includes three components[63]: non-modified mRNA of the four Yamanaka factors (OCT4, SOX2, KLF4, C-MYC), NANOG, and LIN28; mRNA encoding for E3, K3, and B18R for evasion of the immune response, and double-stranded microRNAs (miRNAs) from the 302/367 cluster[230] (StemRNA-NM Reprogramming Kit, Stemgent). This protocol though being similar to the one applied to mmRNA, due to the higher efficiency it is shorter. On D0 (considering D1 the day of the first transfection) cells were detached from the Petri dish with Trypsin-EDTA 0.25% (ThermoFisher Scientific) for 2' at 37 °C, resuspended in High Glucose Dulbecco's modified Eagle Medium (DMEM 41965, ThermoFisher Scientific) supplemented with 10% FBS (FBS, ThermoFisher Scientific), counted with a Burker chamber and seeded at 60 cell/mm^2 in the microfluidic channels coated with vitronectin solution at 25 µg/mL in DPBS. A hypoxia incubator is used for the whole duration of the experiment (37°C, 5% CO_2, 5% O_2). The day after (D1) medium is switched to Pluriton reprogramming medium (Stemgent) and the first transfection is performed with StemMACS mRNA Transfection Kit (Miltenyi Biotec). Transfections are performed for 8 days, eventually adjusting mRNA amount to support cell growth. After 4 days of transfections cells undergo mesenchymal-to-epithelial transition and at D7-8 first colonies arise. From D9 medium is replaced with StemMACS iPSBREW XF (Miltenyi Biotec) and colonies are allowed to grow until D15. At D15 if reprogramming efficiency needed to be established, cells were stained for pluripotency markers and the reprogramming efficiency was calculated as n° of NANOG$^+$ colonies per seeded cells per channel. If colonies needed to be extracted, reprogrammed cells were allowed to grow for additional days before extraction.

3.4. IMMUNOASSAYS AND IMAGING

3.4.1. Immunofluorescence stainings

For immunofluorescence staining cells were fixed in 4% (w/v) paraformaldehyde (Sigma-Aldrich) for 7' and blocked with 10% FBS in $PBS^{-/-}$ with 0.1% (v/v) Triton-X-100 (Sigma-Aldrich) for 1 h at room temperature, then incubated overnight at +4°C with primary antibodies in $PBS^{-/-}$ with 1% (w/v) BSA (Sigma-Aldrich). The day after samples are washed 3 times with $PBS^{-/-}$ (5' per wash) and incubated with secondary antibody for 45' at 37°C. The antibodies used in this study are reported in Table 3. Hoechst 3342 (ThermoFisher Scientific) was added 1:1000 during the incubation with the secondary antibody. When phalloidin was used to stain actin filaments, phalloidin (488 nm, ThermoFisher Scientific #A12379 or 647 nm, ThermoFisher Scientific #A22287) was added 1:60 during the incubation with the secondary antibody. Large field images (whole channel mosaics) were acquired with a DMI6000B fluorescence microscope with motorized stage (Leica Microsystems), while confocal images were acquired with a TCS SP5 confocal microscope (Leica Microsystems).

3.4.2. Western Blot analysis

HFF fibroblasts, naïve and primed HPD06 were cultured for 4 days in microfluidic chips or in 24-well multiwell (Falcon) with glass coverslip. HFF fibroblasts were cultured on vitronectin coating, primed HPD06 on 2.5% MRF coating and naïve HPD06 on MEF feeders. After 4 days in culture cells were lysed by using RIPA Lysis and Extraction Buffer (ThermoFisher Scientific) additioned with 25x cOmplete protease inhibitor cocktail (Roche) following manufacturing instructions to extract total protein content. In wells, 100 µl of RIPA buffer was used and surface was scratched to recover extracellular matrix proteins. In microfluidic chips, each channel was cut open with a sterile blade and protein were extracted with 10 µl RIPA buffer, scratching the glass surface. In parallel, a vial of frozen HL-60 promyeloblast form peripheral blood (ATCC) has been thaw and cells lysed directly in 100 µl RIPA Lysis and Extraction Buffer (ThermoFisher Scientific) additioned with 25x cOmplete protease

inhibitor cocktail (Roche). Samples were quantified with BCA protein assay kit (ThermoFisher Scientific) to load 20 µg of total protein per sample. Western blot was performed under reducing conditions by sodium dodecyl sulfate polyacrylamide gel electrophoresis onto NuPAGE 4-12% Bis-Tris Protein Gels (ThermoFisher Scientific), followed by transfer to Invitrolon PVDF membrane (ThermoFisher Scientific). The antibodies used in this study are reported in Table 3.

Table 3: Antibodies used in this study.

Target	Brand, cat#	Host	IF dilution	WB dilution
Collagen 1 (COL1)	Abcam #34710	Rabbit	1:500	1:1000
Collagen 4 (COL4)	Abcam #6586	Rabbit	1:1000	1:1000
Collagen 5α1 (COL5A1)	Santa Cruz # SC-166155	Mouse	1:50	
Collagen 6 (COL6)	Fitzgerald # 70R-CR009X	Rabbit	1:50	
Collagen 23a1(COL23A1)	Santa Cruz # SC-514835	Mouse	1:50	
Fibronectin (FN)	Sigma-Aldrich #F7387	Mouse	1:200	
Focal Adhesion Kinase (FAK)	Santa Cruz #SC-558	Rabbit	1:50	
Focal Adhesion Kinase (FAK)	Thermo #AHO0502	Rabbit		1:500
Laminin (LAM)	Sigma-Aldrich #L9393	Rabbit	1:250	1:1000
YAP	Santa Cruz sc-101199	Mouse	1:50	
KLF17	Sigma-Aldrich # HPA024629	Rabbit	1:250	
NANOG	Reprocell #RCAB0004P-F	Rabbit	1:100	
OCT4	Santa Cruz #SC-5279	Mouse	1:200	

TRA-1-60	Cell Signalling #4746s	Mouse	1:250	
TFCP2L1	RnD #AF5726-SP	Goat	1:250	
TFE3	Sigma-Aldrich #HPA023881	Rabbit	1:250	
GAPDH	Cell Signaling # D16H11	Rabbit		1:1000
Donkey anti-Rabbit 488 nm	Thermo #A-21206	Donkey	1:200	
Donkey anti-Rabbit 594 nm	Thermo #A10042	Donkey	1:200	
Donkey anti-Mouse 488 nm	Thermo #A-21202	Donkey	1:200	
Donkey anti-Mouse 594 nm	Thermo #A10037	Donkey	1:200	
Donkey anti-Goat 647 nm	Thermo #A-21447	Donkey	1:200	
Goat anti-Rabbit HRP	Thermo #G-21234	Goat		1:5000
Goat anti-Mouse HRP	BioRad #1706516	Goat		1:1000

3.4.3. Second Harmonic Generation imaging

The introduction of multiphoton fluorescence microscopy enabled 3D imaging with high spatial resolution and significant depth penetration in tissues[261]. Multiphoton fluorescence microscopy can be used to excite both exogenous and endogenous fluorescence signals to image intrinsic signals using the scattering phenomena of Second Harmonic Generation (SHG). In the process of SHG light is scattered by non-centrosymmetric structures to combine two incoming photons into one outgoing photon without the loss of energy due to a Stoke's shift as seen in fluorescence. Hence the outgoing photon has the same total energy as the incoming photons, and half the incoming wavelength. The primary tissue constituent responsible for SHG is collagen[262], therefore, a two-photon fluorescence microscopy (Thorlab) was used to image extracellular matrix deposition from naïve HPD06 cells cultivated on MEF

feeders and on 5% MRF, from primed HPD06 cells cultivated on 2.5% MRF and from HFF cultivated on vitronectin coating by exciting samples at 800 nm.

3.4.4. Electron Microscopy

Naïve HPD06 colonies cultivated on MEF feeders, 5% MRF or vitronectin in 24-well multiwell on glass coverslips have been fixed in glutaraldehyde 2.5% in cacodylate buffer 0.1M pH 7.4 (both Sigma-Aldrich) at 4°C for 2 hours, then washed with cacodylate buffer and stored at +4°C. Scanning electron microscopy (SEM) and transmission electron microscopy imaging was performed by our collaborators Dott.ssa Patrizia Sabatelli and Dott. Stefano Squarzoni at "Istituto di Genetica Molecolare – Consiglio Nazionale delle Ricerche c/o Istituto Ortopedico Rizzoli Bologna (BO)".

3.5. RNA-BASED ASSAYS

3.5.1. RT-PCR and qPCR analysis

Microfluidic channels were washed with PBS, then dried and injected with iScript (Bio-Rad) for total RNA extraction. The solution was left on the channels for exactly 60 seconds. RNA (0.1 µg) was directly reverse transcribed into cDNA with High-Capacity cDNA Reverse Transcription Kit (ThermoFisher Scientific). qPCR was performed with TaqMan gene expression assay probes (ThermoFisher Scientific) according to manufacturer's instructions with TaqMan Universal PCR Master Mix (ThermoFisher Scientific). Reactions were performed on ABI Prism 7000 machine and results were analyzed with ABI Prism 7000 SDS software. GAPDH expression was used to normalize Ct values of gene expression, and data were shown as relative fold change to control cells using the ΔΔCt method. The probes used in this study are reported in Table 4.

Table 4: TaqMan qPCR probes used in this study.

Target	TaqMan Cat#
GAPDH	Hs02758991_g1
OCT4	Hs04260367_gH
NANOG	Hs04399610_g1
SOX2	Hs01053049_s1
VIMENTIN	Hs00958111_m1
E-CADHERIN	Hs01023894_m1
N-CADHERIN	Hs00983056_m1
B-CATENIN	Hs00355049_m1
TGF-β1	Hs00998133_m1
SNAI1	Hs00195591_m1

3.5.2. Transcriptomic analysis of SERPINB3-related genes

Microarray data (GSE50206) collected during human fibroblast reprogramming published in the recent paper of Takahashi et al.[263] were analyzed. In this analysis, a subset of genes related to SERPINB3 was selected from literature data and used to perform cluster analysis (Table 5). Bioinformatic analysis was performed using MATLAB R2017a software. Gene expression data were log2 transformed and normalized according to quantile normalization. For heatmap graphics data were median-centered. Hierarchical clustering was performed with average linkage and Euclidean distance. Differentially expressed genes between pairs of conditions were found using one-way ANOVA with Benjamini and Hochberg correction.

***Table 5: SERPINB3-related genes**. Literature revision (related articles indicated).*

GENE NAME	ENTREZ GENE ID	GENE NAME	ENTREZ GENE ID
SERPINB3	6317		
Downstream of SERPINB3			
Activated By SB3		Inhibited by SB3	
ACTA2[264]	59	BCL2[265]	596
ACVR2B[266]	93	BID[265]	637
AKT[266]	207	CAPN1[267]	823
ATF4[268]	468	CASP3[269,270]	836
ATF6[268]	22926	CASP9[265]	842
AXL[126]	558	CBR1[271]	873
BCL2L2[266]	599	CDH1[124,264,268,272]	999
BIRC5[126]	332	CTRB1[273]	1504
CDC25A[126]	993	CTSK[273]	1513
CDK1[266]	983	CTSL[273,274]	1514
CDK4[126]	1019	CTSS[273]	1520
COX2[118]	4513	EPCAM[268]	4072
CSF2[275]	1437	MAPK8[276]	5599
CSF3[275]	1440	MAPK13[276]	5603
CTNNB1[118,264,277,278]	1499	MAPK14[276]	1432
CXCL1[275]	2919	SHC1[279]	6464

CXCL12[266]	6387
CXCL8[275]	3576
EGFL7[266]	51162
EGFR[266]	1956
EIF2AK3[268]	9451
EPAS1[121]	2034
FN1[268]	2335
GSK3B[264]	2932
HMGA2[266]	8091
HRAS[266]	3265
IGF1R[266]	3480
IL6[269,275,280]	3569
KLF6[266]	1316
KRAS[266]	3845
LEF1[118]	51176
MCL1[266]	4170
MKI67[269]	4288
MMP16[266]	4325
MMP9[264,281]	4318
MTOR[266,279]	2475
MYC[126,282]	4609
NAE1[122,283]	8883
NPM1[126]	4869
NRAS[266]	4893
PTMA[126]	5757
PTTG1IP[266]	754
RELA[275]	5970
SMAD4[266]	4089
SNAI1[124]	6615
SUV39H1[266]	6839
TCF7[118]	6932
TGFB1[259]	7040
VEGFA[266]	7422
VIMENTIN[124,268]	7431
WNT-1[278]	7471
WNT7A[278]	7476
XBP1[268,275]	7494

YAP1[126]	10413
Upstream of SERPINB3	
Activate SB3	
EPAS1[122,283]	2034
ETV4[275]	2118
HRAS[266,275]	3265
IL13[284]	3596
IL4[284]	3565
KRAS[266,275]	3845
MAPK8[276]	5599
NRAS[266,275]	4893
PIK3CA[279]	5290
STAT3[285]	6774
STAT6[286]	6778

3.5.3. Transcriptomic analysis of fibroblasts, naïve and primed PSC datasets

The following RNA-sequencing dataset analyzed in this work were deposited in GEO (Gene Expression Omnibus) or in ENA (European Nucleotide Archive).

- GEO: HFF GSM2448850, GSM2448851 and GSM2448852 from GSE93226; BJ fibroblasts: GSM1553088, GSM1553089 and GSM1553090 from GSE63577; Naive pluripotent stem cells: GSM2218668, GSM2218669, GSM2218670 and GSM2218671 from GSE75868; Primed pluripotent stem cells GSM2218660 and GSM2218671.
- ENA: Naïve pluripotent stem cells ERS1059993, ERS1059996 and ERS1059999 from PRJEB12748, ERS537884, ERS537876 and ERS537881 from PRJEB7132; Primed pluripotent stem cells ERS537890 and ERS537878 from PRJEB7132, ERS559332, ERS559334, ERS559335 and ERS559336 from PRJEB7450

Other samples (BJ – This study, primed iPS – this study, niPS HFF uF, hiPS BJ well, hiPS BJ uF) were obtained from previous experiments of the laboratory, where uF indicates that the cells were cultured in microfluidic platforms. RNA-seq data were subjected to quantile normalization, log2-transformed and median-centered before plotting in heatmaps. Heatmap were drawn to represent the results from hierarchical clustering performed using Euclidean distance and complete linkage. The different sets of genes plotted were manually compiled from gene annotations referring to KEGG pathways gene lists. Differentially expressed genes (DEGs) were identified by ANOVA test, with post-test correction to account for multiple comparisons based on Benjamini–Hochberg method. A mixed criterion based on corrected p-value lower than 0.05 and log2-fold change higher than 1.5 was used to define a gene as differentially expressed.

3.5.4. Bulk RNA-sequencing

Samples for bulk RNA-sequencing were extracted from HFF fibroblasts, naïve and primed HPD06 cultured in microfluidic chips and in 24-well multiwell (Falcon) with glass coverslip. HFF fibroblasts were cultured on vitronectin coating, primed HPD06 on 2.5% MRF coating and naïve HPD06 on MEF feeders. After 4 days in culture, RNA was extracted with RNeasy Plus Micro Kit (Qiagen) following manufacturer instructions. In addition, 3D and 2D naïve HPD06 colonies cultured on MEF feeders were manually picked from microfluidic chips or from 24-wells multiwells and processed for RNA extraction and RNA-sequencing. At least 10 colonies have been analyzed per sample.

RNA-sequencing was performed by the Next Generation Sequencing Facility of the Telethon Institute of Genetics and Medicine (TIGEM) in Napoli (NA). Sequencing strategy was 3'-end mRNA sequencing based on QuantSeq sequencing for RNA quantification[287].

3.5.5. Single-cell RNA-sequencing of microfluidic reprogramming

BJ human fibroblasts (p5-p6) were reprogrammed in microfluidic chips with non-modified mRNA, following the protocol presented in paragraph 3.3.2.

At D1-3-5-7-9-11-13 and 15 cells were harvested from the chips and cryo-preserved for scRNA-seq. For every time point, 20-22 hours after the last transfection, at about 4 pm, cells were washed three times with $PBS^{-/-}$ and dissociated with TrypLE™ Select Enzyme (Thermo Fischer Scientific) for 10' at 37°C. Enzyme was inactivated with DMEM/F12 (ThermoFisher Scientific) supplemented with 40% KSR (ThermoFisher Scientific) and 1% RevitaCell Supplement (100X) (ThermoFisher Scientific). Cells were centrifuged at 300 g for 5' at +4°C, counted and diluted at 100000 cell/ml. 5000 cells aliquots were frozen (15% DMSO final) for scRNA-seq. For each time point, two biological replicates and at least five technical replicates were prepared. scRNA-seq was performed with 10x Genomics' "Chromium Single Cell Gene Expression Solution" by our collaborator Prof. Davide Cacchiarelli at Telethon Institute of Genetics and Medicine (TIGEM) in Napoli (NA).

3.5.6. Drop-seq scRNA-seq setup

Drop-seq scRNA-seq system was setup and tested for single-cell capturing efficiency and mRNA recovery efficiency. The microfluidic platform was prepared according to the protocol reported in paragraph 3.1, using the AutoCAD file provided by Macosko at al. 2015. Inlets and outlets were punched with a 0.75 mm biopsy punch (Kai Medical). Shortly before the Drop-seq experiment, chips were treated with Aquapel solution (Pittsburgh Glass Works) for 60 seconds to achieve maximum water-repellent behavior from the microfluidic channels. Aquapel was removed with Fluorinert FC-40 oil (Sigma-Aldrich) and air and chips were dried at 65°C for 20'.

mRNA capturing beads were purchased from Chemgenes, resuspended in ethanol and stored in TE-TW solution (10 mM Tris pH 8.9, 1 mM EDTA, both ThermoFisher Scientific, 0.01% Tween-20, Sigma-Aldrich; all solution were bought RNAse- and DNAse-free and operated under biological hood treated with RNaseZap, ThermoFisher Scientific to minimize RNase contamination). The following lots of beads were tested: 011416B and 082516. Coupled primers were also purchased from Chemgenes and sequences are reported in Table 6.

Table 6: Drop-Seq Bead sequences, where J-sequence indicates cell-specific Barcode and N-sequence indicates the UMI sequence on the beads. TSO primer is used to perform reverse-transcription and SMART PCR primer is needed for PCR amplification.

NAME	SEQUENCE
Barcoded Bead SeqB	5'–Bead–Linker--- TTTTTTTAAGCAGTGGTATCAAC GCAGAGTACJJJJJJJJJJJJNNNNNNNN TTTTTTTTTTTTTTTTTTTTTTTTTTTT---3'
Template Switch Oligo (TSO)	AAGCAGTGGTATCAACGCAGAGTGAATrGrGrG
SMART PCR Primer	AAGCAGTGGTATCAACGCAGAGT

At the moment of performing Drop-seq experiment, beads were counted and diluted at 300 beads/µl in Lysis Buffer (RNase-free water, ThermoFisher Scientific, 6% Ficoll PM-400, Sigma-Aldrich; 0.2% N-Lauroylsarcosine sodium salt solution, Sigma-Aldrich; 20 mM EDTA, ThermoFisher Scientific; 200 mM Tris-HCl ph 7.5, ThermoFisher Scientific; 50 mM DTT, Sigma-Aldrich).

Cells of two different kinds (BJ human fibroblasts and H9 hESC) were used to perform a mixed cell experiment, to estimate the mRNA capture efficiency and single-cell resolution efficiency. At the moment of performing Drop-seq experiment, cells were dissociated at single cell with TrypLE Select Enzyme (Thermo Fischer Scientific) for 5' at room temperature, then spinned at 300 g for 5' and resuspended in PBS - 0.001% BSA (Sigma-Aldrich) at the concentration of 620 cell/µl. BJ and H9 cells were mixed with 1:1 ratio.

To setup a Drop-seq experiment, first Droplet generation oil (Bio-Rad) is loaded in a 10 ml syringe (BD), and the syringe is connected to the oil inlet of the microfluidic chip via a 26G luer lock needle (BD) and a 60 cm Teflon tube (Scientific Commodities). The syringe is loaded in a syringe pump (Harvard Apparatus) and flow rate set at 12000 µl/hour. Then cell suspension is loaded in a 3 ml syringe (BD), and the syringe is connected to the cell inlet of the microfluidic chip via a 26G luer lock needle and a 60 cm Teflon tube (Scientific Commodities). A magnetic stirrer disk (Hanna Instruments) is placed inside the cell suspension and the syringe is placed on a syringe pump (Harvard

Apparatus), close to a magnetic stirrer (Hanna Instruments), in order to keep cells in homogeneous suspension. To test the viability of stirring cells during the experiment, runs without stirring disc were also performed. Finally, bead suspension is loaded in another 3 ml syringe (BD) with magnetic stirring and connected to the bead inlet of the chip analogously to the cells. Cells and beads flow rate was set at 2400 µl/hour.

Keeping the chip under a microscope to control that no clogs are formed in the microfluidic channels, the pumps are started in the following order: cells, beads and oil. After 15' of sample collection, cells and beads are consumed and the fluxes are stopped in the following order: beads, cells and oil. The sample is collected in a 50 ml tube (Falcon) and processed for droplet breakage. To control bead doublet-rate, an aliquot of droplet solution is analyzed and counted with ImageJ software (NIH). To verify cell doublet rate, cells were stained with 1 µM Calcein-AM (ThermoFisher Scientific) and fluorescent Calcein release in the droplets after cell lysis was evaluated with ImageJ software (NIH) and analyzed with using MATLAB R2017a (The Mathworks).

Droplet breakage was performed with 6x SSC (ThermoFisher Scientific) and perfluorooctanol (PFO, Sigma-Aldrich). After three 6x SSC washes, beads with captured mRNA were reverse-transcribed with the following RT mix: RNase-free water (ThermoFisher Scientific); 5x Maxima H Minus Reverse Transcriptase Buffer (ThermoFisher Scientific), 4% Ficoll PM-400 (Sigma-Aldrich), 1 mM dNTPs (Clontech), 40x RNase Inhibitor (Lucigen), 2.5 µM TSO Primer, 20x Maxima H Minus Reverse Transcriptase Enzyme (ThermoFisher Scientific). Reverse transcription was performed on a thermomixer (Eppendorf) for 30' at room temperature and 90' at 42°C with rotation. After reverse-transcription, beads with cDNA were treated wih Exoniclease I (New England Biolabs) to chew the excess of bead primers that did not capture any mRNA molecule. Recovered beads were counted and divided in 2000 µl aliquots and PCR amplification was performed for each aliquot separately. 2x Kapa HiFi Hotstart Readymix (Kapa) and 0.8 µM SMART PCR PRIMER was used to perform PCR amplification with the following PCR program:

1x 95°C 3’

4x 98°C 20’’ – 65°C 45’’ – 72°C 3’

15x 98°C 20’’ – 67°C 20’’ – 72°C 3’

1x 72°C 5’

4°C forever

PCR amplified sequences can then be processed for Illumina sequencing library preparation (Nextera XT, Illumina).

After reverse-transcription and after PCR amplification samples were analyzed by qPCR for housekeeping gene GAPDH to confirm bead capturing and processing efficiency. RNA amplified with random primers (ThermoFisher Scientific) was used as control. PCR products have also been imaged with 2% Agarose gel in TAE Buffer and SYBR Safe (all ThermoFisher Scientific).

Capturing experiment was also performed in 200 µl tubes (Eppendorf) with beads and purified mRNA (from H9 hESC), in the same conditions as reported for the Drop-seq experiment, but without cells and droplet formation. As control, mRNA reverse-transcribed with High-Capacity cDNA Reverse Transcription Kit (ThermoFisher Scientific) was used.

3.6. SILAC SECRETOME ANALYSIS

SILAC analysis of BJ fibroblasts and BJ-derived primed hiPSCs were performed by the Laboratory of Biological Engineering at SIAIS Institute, ShanghaiTech University, Shanghai (China). Results obtained in fibroblasts have been published in Hu et al. 2018[288]. Here the methods reported in the paper and applied also to primed hiPSCs analysis.

3.6.1. Cell isotopic labeling for SILAC

Human fibroblasts were cultured in DMEM medium for SILAC (ThermoFisher Scientific) supplemented with 0.8 mM light (ThermoFisher Scientific) or heavy ($^{13}C_6$, 99%; $^{15}N_2$) lysine, 0.4 mM light (ThermoFisher Scientific) or heavy ($^{13}C_6$; $^{15}N_2$, ThermoFisher Scientific) arginine, and 10% dialyzed FBS (ThermoFisher Scientific) at 37 °C and 5% CO_2. To check labeling efficiency, cells were cultured for 11 days in medium containing heavy amino acids, lysates were collected after treatment with RIPA Lysis and Extraction Buffer (ThermoFisher Scientific) with MS-SAFE Protease and Phosphatase Inhibitor (Sigma) and analyzed by LC-MS/MS daily starting from day 4. Subsequent experiments were performed with cells labeled for at least 8 days, sufficient to have a labeling of more than 98%.

3.6.2. Collection of conditioned media for secretome analysis

Conditioned media for secretome analyses were performed using the chemically-defined E8 medium, which only contains four proteins: fibroblast growth factor 2 (FGF2, Peprotech), transforming growth factor beta (TGFB, R&D), insulin (Sigma-Aldrich), holo-transferrin (Sigma-Aldrich), substituting the lysine and arginine amino acid with either heavy or light lysine (0.5 mM) and arginine (0.7 mM). For preliminary validation experiments, human heavy and light fibroblasts were seeded into standard wells at 150 cell/mm^2. Conditioned media were collected every 24 h and kept at −80 °C until use. Equal volumes of heavy and light conditioned media were mixed and processed as described below. In subsequent experiments, heavy cells and light cells were seeded into wells and microfluidic channels, or the contrary, at 150 cell/mm^2.

Conditioned media were collected every 12 h from microfluidic channels and every 24 h from wells, and kept at −80 °C until use. Equal volumes of heavy and light conditioned media were pooled together.

3.6.3. Sample preprocessing for LC-MS/MS

Heavy and light conditioned media were mixed in 1:1 volume ratio, for a total of 1 ml. Amicon® Ultra centrifugal filters (Merck/Millipore) were used for protein purification and concentration. Then, proteins were reduced in 0.1 M DTT at 95 °C for 5 min and dissolved in 8 M urea solution. Alkylation was performed for 30 min at 25 °C in the dark with 55 mM iodacetamide, followed by trypsin (Promega) digestion for 16 h. Peptides were desalted by C-18 spin column (Pierce) and dried into powder. Before MS analysis, peptides were resuspended in 30 µl of 0.1% acetic acid.

3.6.4. LC-MS/MS analysis

Thermo Fusion Mass Spectrometer coupled with Thermo Easy-nLC1000 Liquid Chromatography was used to get the peptides profiles. 170 min of LC-MS gradients were generated by mixing buffer A (0.5% acetic acid in water) with buffer B (0.5% acetic acid in 80% ACN in water) by different proportions. Using NSI as the ion source and Orbitrap as the detector, the mass scan Rang was at 300–1800 m/z, and the resolution was set to 120K. The MS/MS was isolated by Quadrupole and detected by Iontrap, whose resolution was set to 30K. The activation type was HCD. Peak list files were searched against UniProt human reference proteome (UP000005640) by Thermo Proteome Discoverer v. 2.1.

3.6.5. Bioinformatic analysis

All bioinformatic analyses were carried out using MATLAB R2017a (The Mathworks). Proteomic data were filtered to exclude proteins that were detected only in one of three replicates. Protein functional classification and over-representation analyses were performed using DAVID 6.8.

3.7. EXPERIMENTAL DESIGN: ECM DEPOSITION, ORGANIZATION AND ROLE IN PLURIPOTENCY

In chapter 4.1, 4.2, 4.3 and 4.4, results related to extracellular matrix deposition in pluripotent stem cells will be presented. Here the specific experimental design and technical methods related to these experiments are reported.

3.7.1. ECM deposition evaluation

General ECM deposition has been evaluated by SHG, SEM and TEM imaging, as reported in paragraph 3.4.3 and 3.4.4. Specific protein deposition has been tested in the following cell lines:

- Naïve HPD06 pluripotent stem cells grown on MEF feeders (which in turn have been seeded on vitronectin coating), on 5% MRF or on vitronectin coating, as described in paragraph 3.2 in microfluidic chips and 24-well multiwell or 8-chammbers chamberslides (Falcon).
- Primed HPD06 hiPSC stem cells grown on 2.5% MRF as described in paragraph 3.2 in microfluidic chips and 24-well multiwell or 8-chammbers chamberslides (Falcon).
- HFF fibroblasts grown on vitronectin as described in paragraph 3.2 in microfluidic chips and 24-well multiwell or 8-chammbers chamberslides (Falcon).
- Mitotically-inactive MEF feeder layer seeded on vitronectin as described in paragraph 3.2 in 24-well multiwell or 8-chammbers chamberslides (Falcon).

The following ECM specific proteins and pluripotency markers have been tested in these analysis: Collagen 1, Collagen 4, Collagen 6, Collagen 23, Fibronectin, Laminin, Yap, KLF17, TFE3, TFCP2L1, OCT4, NANOG, with dilutions reported in Table 3.

3.7.2. Naïve HPD06 colony picking and re-seeding

Naïve HPD06 colonies grown in RSeT medium on MEF feeders were manually picked according to their morphology. A pool of 2D or 3D colonies (at least 10 colonies per pool) was centrifuged at 300 g for 5' and dissociated at single cell level with TrypLE™ Select Enzyme (Thermo Fischer Scientific) for 5' at room temperature, inactivated with equal volume of 0.5 mg/ml Soybean Trypsin Inhibitor (ThermoFisher Scientific) and centrifuged at 300 g for 5'. Cells were seeded on MEF feeders in RSeT medium supplemented with 10 µM StemMACS Y27632 ROCK Inhibitor (Miltenyi Biotec). Re-seeded cells were allowed to grow for 4 days before PFA fixation and immunofluorescence staining. Colony height was evaluated with Leica TCS SP5 confocal microscope (Leica Microsystems). For statistical analyses, single pairwise comparisons were analyzed using Student's t-test with $P < 0.05$ (*), $P < 0.01$ (**) or $P < 0.001$ (***) indicating significance with GraphPad Prism 6 software.

3.7.3. Blocking antibody assays

The following blocking antibodies were used in the indicated dilution in RSeT naïve culture medium: anti-integrin α4 (1:50, 10 µg/ml, BD #553314) anti-integrin β1 (1:100, 10 µg/ml, Origene #BM6028P) and anti-CSPG (1:40, 5 µg/ml, Santa Cruz #SC80003). Blocking analysis was performed in microfluidic chips, seeding naïve HPD06 dissociated at single-cell over MEF feeder layer. Blocking antibody was administered either at the moment of cell seeding ("Blocking from Day 0" condition) or after 12 hours of cell attachment (Blocking from Day 1" condition). Colony number and growth was monitored daily by large field imaging acquired with DMI6000B microscope with motorized stage (Leica Microsystems). After four days, colonies were fixed with PFA for immunofluorescence staining. Colony number and diameter was measured with NIH ImageJ software. For statistical analyses, single pairwise comparisons were analyzed using Student's t-test with $P < 0.05$ (*), $P < 0.01$ (**), $P < 0.001$ (***), $P < 0.0001$ (****) indicating significance with GraphPad Prism 6 software.

3.7.4. Mn^{2+} and Latrunculin-A assays

Naïve HPD06 cells were seeded in microfluidic chips on MEF feeders on day 0. From day 1 to day 4 or from day 3 to day 4, RSeT naïve medium was supplemented with 0.5 mM $MnCl_2$ (Sigma-Aldrich) dissolved in water. Colony number and growth was monitored daily by large field imaging acquired with DMI6000B microscope with motorized stage (Leica Microsystems). After four days, colonies were fixed with PFA for immunofluorescence staining. Colony number and diameter was measured with NIH ImageJ software. For statistical analyses, single pairwise comparisons were analyzed using Student's t-test with $P < 0.05$ (*), $P < 0.01$ (**), $P < 0.001$ (***), $P < 0.0001$ (****) indicating significance with GraphPad Prism 6 software.

For cytoskeleton assembly inhibition assay, naïve HPD06 cells were seeded in microfluidic chips on MEF feeders and allowed to grow for 4 days in RSeT naïve medium. On day 4, Latrunculin-A (0.5 μM, ThermoFisher Scientific) was supplemented to RSeT medium and administered to cells for 30' at 37°C. Right after treatment, cells have been fixed with PFA for immunofluorescence staining.

3.8. STATISTICAL ANALYSIS

Data are expressed as mean ± standard deviation. When two samples are compared, statistical significance is determined by unpaired Student's t test with two-tailed p-value. When more than two samples have been compared, statistical significance is determined by repeated measures ANOVA. For all the statistical analysis, the software GraphPad Prism 6.01 was used. A p-value of less than 0.05 is considered statistically significant (ns: p-value > 0-05, *: p-value < 0.05, **: p-value < 0.01, ***: p-value <0.001, ****: p-value < 0.0001).

3.9. EXPERIMENTAL DESIGN: SERPINB3 INFLUENCE ON CELL REPROGRAMMING ANALYSIS

Several experiments to evaluate SERPINB3 influence on cell reprogramming were performed. Here described the experimental design and methods employed.

3.9.1. Recombinant SERPINB3 production

The recombinant wild-type purified protein used in this work has already been extensively characterized[259,260] and it was supplemented fresh daily to the reprogramming medium at the concentration of 200 ng/ml, a protein concentration identified biologically active in preliminary experiments (data not shown).

Plasmid construct. Total RNA was extracted using Trizol reagent (ThermoFisher Scientific) from human liver cancer tissue obtained at the time of surgical resection from patients carrying wild-type SERPINB3 (Accession No. NM_006919). The first strand of cDNA was synthesized (Superscript II reverse transcriptase, ThermoFisher Scientific) and used for SERPINB3 cDNA gene amplification by nested polymerase chain reaction (PCR). The PCR fragment of the wild-type SERPINB3 was cloned into pcDNA3.1D7V5-His-TOPO (ThermoFisher Scientific). This was propagated in Escherichia coli TOP10- competent cells (ThermoFisher Scientific) and purified using the Genopure Plasmid Maxi kit (Roche Applied Science). Sequencing was performed using an ABI 310 automated DNA sequencer (Applied Biosystems).

SERPINB3 protein purification. Wild-type SERPINB3 cDNA was cloned into pET101 (ThermoFisher Scientific). The plasmid construct was grown in BL21 Star (DE3) cells (ThermoFisher Scientific) with pET101/SCCA1 for protein expression. The soluble fractions of bacterial extracts were dialyzed against 20 mM 2-(N-morpholino) ethanesulphonic acid (MES), pH 6, and loaded on an anion exchange column (Mono Q, GE Healthcare Bio-Sciences

AB). The recovered protein fractions were dialyzed against PBS and characterized by SDS–PAGE electrophoresis.

3.9.2. SERPINB3 administration during reprogramming

To test SERPINB3 influence during cell reprogramming, reprogramming protocols, either using mmRNA or non-modified mRNA were divided in two parts: a pre- mesenchymal to epithelial transition phase (pre-MET) and a post-MET phase. SERPINB3 recombinant protein at 200 ng/ml (produced in house) was supplemented to reprogramming medium only in the pre-MET phase, only in the post-MET phase or during the entire reprogramming protocol. When mmRNA are used, the pre-MET phase is identified from D0 to D7 (condition "SERPINB3 Day 0-7"), the post-MET phase from D7 to D14 (condition "SERPINB3 Day 7-14"). Condition "SERPINB3 Day 0-14" indicates SERPINB3 administration all along the protocol. When non-modified mRNA are used, MET occurs earlier, as previously reported, therefore the pre-MET phase is identified from D0 to D4 (condition "SERPINB3 Day 0-4"), the post-MET phase from D4 to D15 (condition "SERPINB3 Day 4-15"). Condition "SERPINB3 Day 0-15" indicates SERPINB3 administration all along the protocol. At the end of the protocol, cells were stained for pluripotency markers and the reprogramming efficiency was calculated as n° of $NANOG^+$ colonies per seeded cells per channel.

3.9.3. EMT-MET marker analysis

To evaluate whether SERPINB3 administration could impair EMT-MET marker expression, such as Vimentin, E-Cadherin, β-Catenin and Snai1, BJ human fibroblasts were treated with the recombinant protein in different conditions. On one side BJ human fibroblast were grown in microfluidic chips in DMEM high glucose + 10 % FBS for 7 days with and without SERPINB3 to evaluate SERPINB3 effect on EMT-MET markers on basal culture conditions. After 7 days, mRNA was collected for qPCR analysis. On the other side the fibroblasts were reprogrammed in microfluidic chips with mmRNA and non-modified mRNA until day 7 with and without SERPINB3

administration as previously described. At day 7, mRNA was collected for qPCR analysis. For each condition, three independent channels were used.

3.9.4. Pluripotency gene expression in hiPSC treated with SERPINB3

To evaluate the possible influence of SERPINB3 administration on pluripotency gene expression, hiPSC cells were detached from 6-well multiwell with EDTA 0.5 mM and seeded on vitronectin-coated microfluidic chips at 100 cell/mm^2 in StemMACSTM iPS-Brew XF medium. After seeding, cells were allowed to grow and adapt to microfluidic conditions for 4 days. Then were treated with or without SERPINB3 for 7 days and mRNA was extracted for qPCR analysis. For each condition, three independent channels were used.

3.9.5. TGF-β1 analysis

To evaluate whether SERPINB3 administration could impair TGF-β1 expression, fundamental for cell reprogramming41, BJ human fibroblasts were grown in microfluidic chips in DMEM high glucose + 10 % FBS for 7 days with or without SERPINB3 administration. After 7 days, mRNA was collected for qPCR analysis. For each condition, three independent channels were used.

CHAPTER 4: RESULTS

4.1. ECM ORGANIZATION IN NAIVE AND PRIMED HUMAN PLURIPOTENT STEM CELLS

To understand if the expression of ECM could be related to the developmental stage of cultured cells, both ECM-related gene expression and ECM network organization has been evaluated in fibroblasts, naïve and primed pluripotent stem cells.

4.1.1. Distinct pluripotency states are characterized by different ECM genes expression profile

Expression of ECM-related genes and in particular of collagen genes has been analyzed by comparing different RNA-sequencing data available in GEO and ENA databases (access numbers in paragraph 3.5.3) or derived from previous experiments carried on in the laboratory. As shown in fig.4.1, collagen expression has been compared in fibroblasts and in pluripotent stem cells, both primed and naïve, embryo-derived or obtained by reprogramming, showing a different pattern of expression in the three groups. In particular, it is evident how the expression of collagen genes is per se sufficient to cluster separately fibroblasts, naïve and primed PSCs.

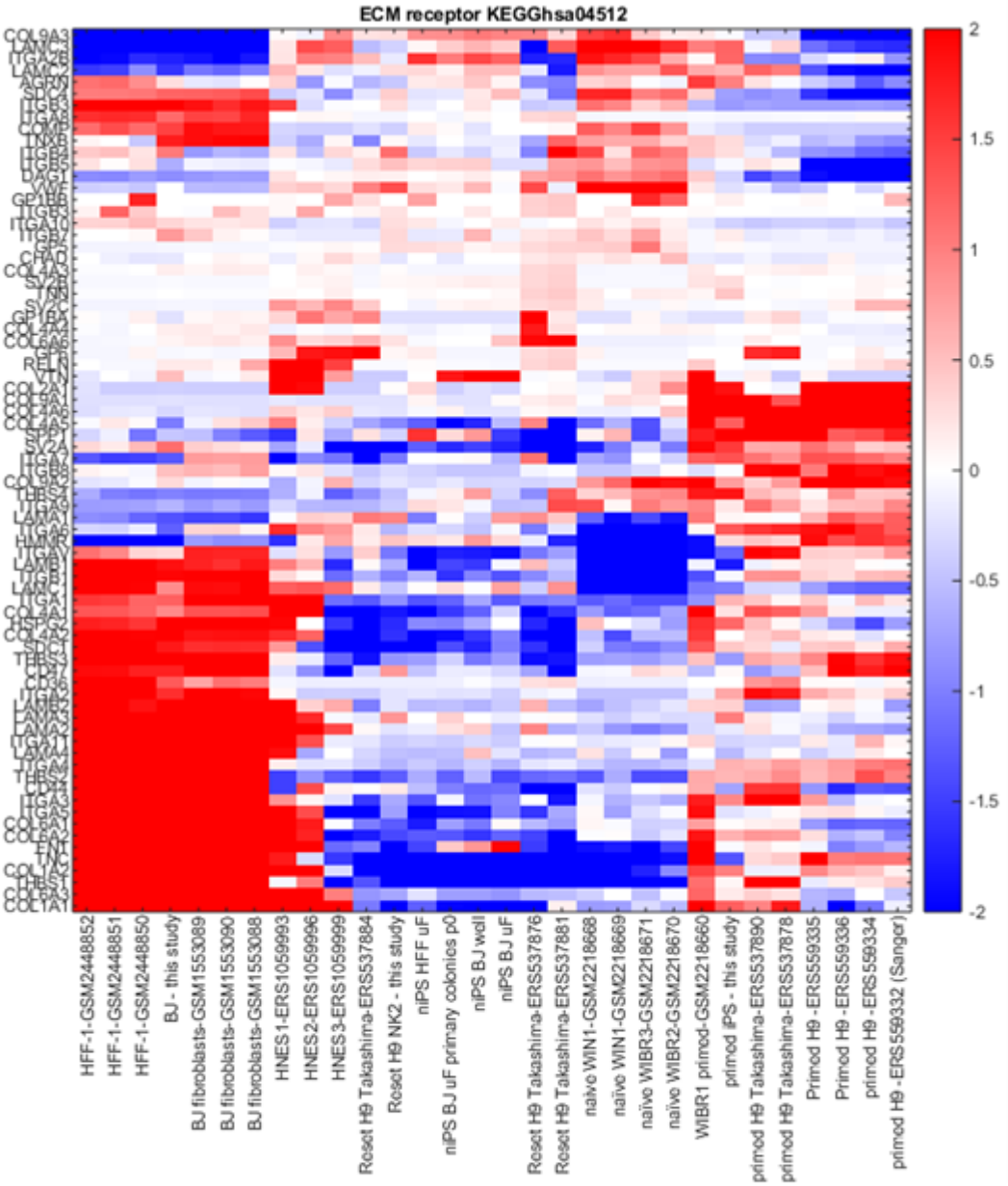

Figure 4.1: ECM-related genes transcriptomic expression. *RNA sequencing analysis of ECM protein expression in different lines of fibroblasts, naïve and primed pluripotent stem cells previously published in literature. Red indicates overexpression relative to the median gene expression of the database while blue indicates downregulation.*

4.1.2. ECM protein organization is different in Naive and Primed PSC

Therefore, we investigated whether this difference in gene expression between fibroblasts and the two pluripotent states of naïve and primed PSCs was also reflected in a different structural organization of the ECM proteins. Second harmonic generation imaging allows the visualization of ECM proteins characterized by non-centrosymmetric structures, such as collagens, which are the main responsible for SHG signal in tissues[261-262]. With this analysis it is possible

to image the general ECM network, taking into account all the contributions from the different collagens and other ECM proteins. Therefore, we performed such analysis by comparing human foreskin fibroblasts (HFF), naïve and primed PSCs derived from HFF. As it can be seen in the second harmonic generation images of fig.4.2, the general organization of ECM is remarkably different in the three samples. In particular, fibroblast ECM deposition is highly ordinated, while primed PSC ECM deposition is inhomogeneous and only few spots of ECM fibers can be appreciated. Moreover, in the naïve samples, ECM deposition depends on the substrate where the cells were cultured: MEF feeder layer or Matrigel growth factor reduced (MRF). Naïve colonies show higher ECM deposition comparing to primed colonies when cultured on MEF feeder cells and the ECM is organized in fibers. Differently, when naïve colonies are grown on MRF, the SHG signal is mostly intracellular.

To further compare naïve and primed pluripotent stem cells, scanning election microscopy (SEM) was used. With this analysis it is possible to picture the surface of the colonies, in order to understand the deposition of ECM above and around the colonies. Differently from what observed in primed PSC colonies (fig.4.3), naïve colonies on the three coatings have a marked 3D morphology, almost spherical, with few anchorage points to the surface. This observation is confirmed by the lateral view of the 3D colony reported in fig.4.8.

Moreover, the naïve colonies appear as a compact dome-shaped cluster of cells in which is impossible to distinguish the single cells from which it is composed. Rather an extracellular structure seems to cover each entire colony. Such "capsule" is visible in all the coating conditions, but it is fluffier on MEF

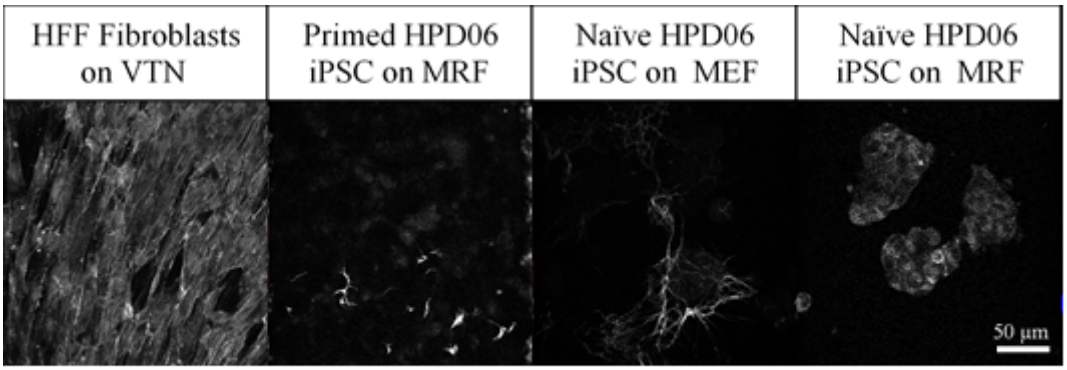

Figure 4.2: Second Harmonic Generation images of total ECM organization *in HFF fibroblasts, naïve HPD06 and primed HPD06. Scale bar 50 µm.*

feeder layers, while on VTN coating is smooth. Moreover, some spherical components emerge from the colony, suggesting the presence of cellular blebs, apoptotic bodies, single cells or part of the colony separated from the main body. In addition, and to better clarify the entity of the "capsule" revealed by SEM, TEM analysis have been performed by slicing the naïve colonies in parallel to the adhesion surface. As it is possible to appreciate in fig.4.4, an electron-light layer of non-organized ECM surrounds the colonies (panel A and B, white arrows) this data can confirm the capsule of ECM structure covering the colonies detected by SEM imaging. In panel B, the dashed line indicates a spherical component separated by the main body of the colony, as previously

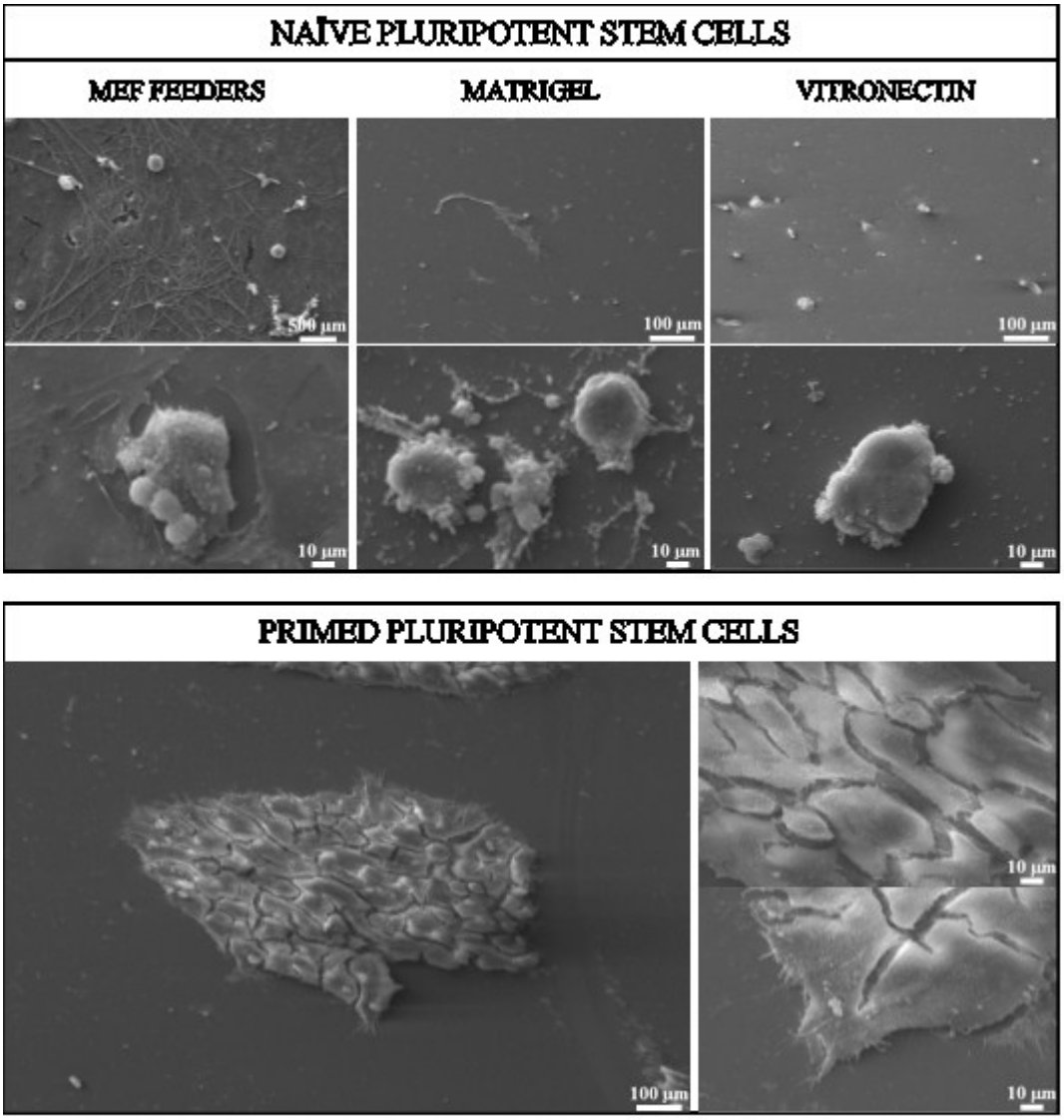

Figure 4.3: SEM analysis of naïve and primed HPD06 colonies. ***Top:*** *Naïve colonies, low and high magnification. Naïve colonies plated on MEF feeders, MRF or VTN coating.* ***Bottom****: Primed colonies seeded on MRF coating, low and high magnification.*

seen in the SEM images. Between the main colony and the detached body, some electron-dense material is accumulated. Inside the colony, numerous junctions connect cells (panel C and D magnification). Between the cells some electron-light material accumulates (white arrows, panel C and D). These data could explain matrix accumulation in spots inside the colonies that are reported also in the following immunofluorescence analysis. By analyzing primed

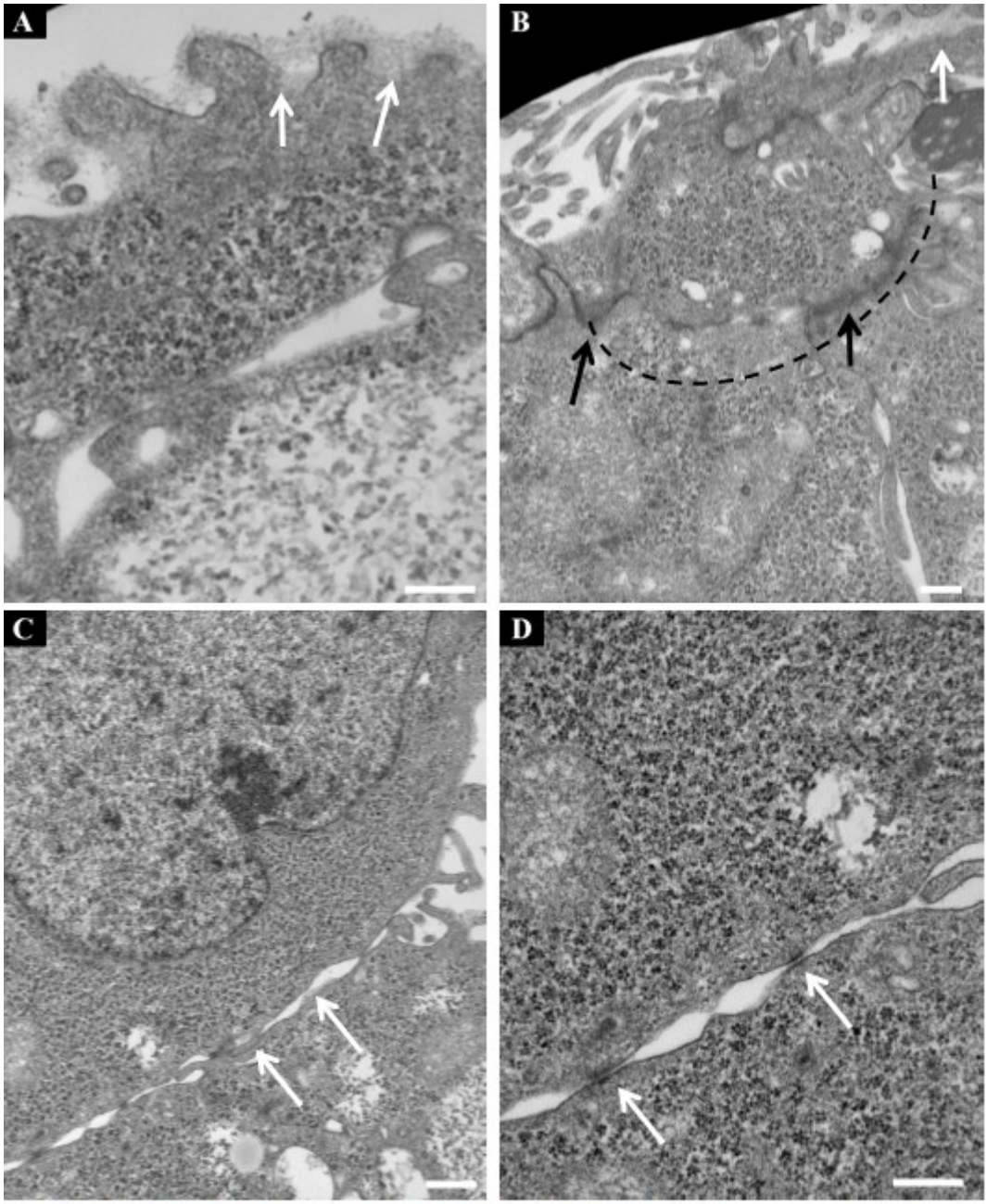

Figure 4.4: TEM analysis of naïve HPD06 colonies on MEF feeders. *A) electron-light material surrounding the colony. B) Detaching body with electron-dense material. C) cell-cell junctions with some electron-light material between different cells. D) magnification of the cell-cell junctions. Scale bar 300 µm.*

colonies with TEM microscopy, it is possible to appreciate the absence of the electron-light material surrounding the cells, as shown in fig.4.5. The main cell-cell junction visible in these cells is adherens junction (fig.4.5, black arrows) typical of epithelial-like tissues such as primed epiblast-like cells. One major cadherin involved in adherens junctions is E-cadherin, which is a main marker of primed PSCs[72,73]. Moreover, in adherens junctions, the actin cytoskeleton is organized in actin rings around the cells, as reported in fig.4.7 and as previously demonstrated[207]. This data is in agreement with the poor matrix deposition and organization revealed by immunofluorescence staining of fig.4.7.

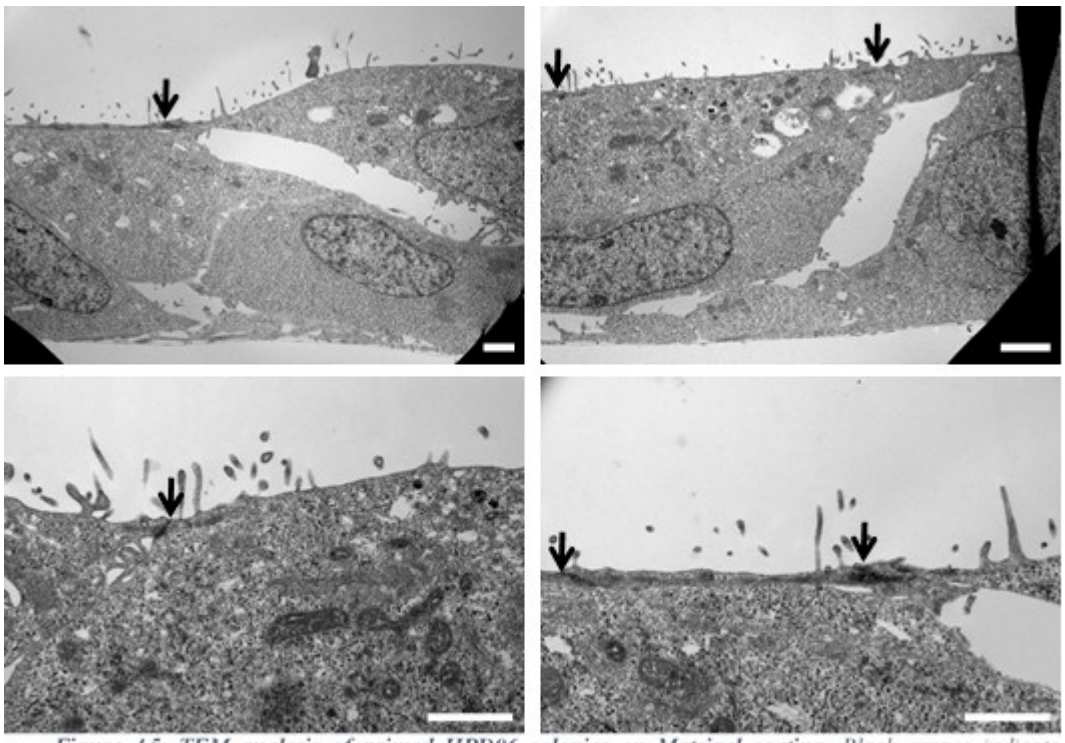

Figure 4.5: TEM analysis of primed HPD06 colonies on Matrigel coating. *Black arrows indicate adherens junctions. Scale bar 1 µm.*

Next, we investigated single ECM proteins by immunofluorescence staining and confocal microscope. The main components of the basal lamina together with the most abundant proteins find in tissues were firstly investigated[135-138,141,143,144]. In the following panels, every picture is composed by the z-stack of many confocal images taken at different heights along the z-axis. Each frame was captured at the minimal distance in z-axis allowed by the resolution of the microscope.

In fig.4.6, five ECM proteins: Collagen I, collagen IV, collagen VI, laminin and fibronectin are analyzed in HFF cells, together with actin cytoskeleton stained with phalloidin and nuclear HOECHST staining. The ECM proteins are partially secreted and organized in extracellular network, but not from all cells. Collagen I and laminin are mostly retained in the cytoplasm. Actin is organized in fibers.

In fig.4.7, the same proteins are stained in HPD06 primed PSCs grown on MRF coating. In these cells, proteins are mostly retained inside the cells or secreted but not organized in an extracellular network. This confirm the differences that can occur in ECM organization between fibroblasts and pluripotent cells.

Surprisingly, naïve HPD06 colonies show a remarkably different ECM organization comparing both to fibroblasts and to primed state, as shown in fig.4.8.

In fact, when cultured on MEF feeders, the naïve colonies are in contact with a network of extracellular collagen I and collagen VI, as if colonies were engulfed in a niche. Naïve HPD06 have high expression of collagen IV and laminin. Fig.4.8 shows also a lateral view of a naïve colony grown on MEF feeders. In this figure, it is possible to appreciate the typical 3D dome-like shape of naïve colonies and how ECM proteins such as collagen I are organized around the colonies. However, since MEF feeder layer is itself producing ECM, as reported in fig.4.9, whether the ECM found in naïve PSC cultivated on MEF feeders was produced by MEF and rearranged by naïve colonies or if naïve colonies were able to produce ECM proteins themselves was investigated.

Notably, as shown in fig.4.9, the ECM proteins produced by MEF alone are organized differently comparing to the ECM detected nearby naïve colonies as shown in fig.4.8. ECM produced by these MEF is scarce and by comparing fig.4.8 and fig.4.9.

To verify if naïve HPD06 were preserving ECM organization in absence of MEF, this line was cultured in feeder-free conditions. As feeder replacement 5% Matrigel (MRF) was used and in these conditions ECM proteins can be stained on naïve colonies as shown in fig.4.10. Differently than the staining on MEF, organized matrix could be seen only around or inside the single colonies, not between different colonies. Remarkably, since Matrigel is a complex substrate made of a cocktail of ECM proteins, these staining helped to confirm naïve cells ability to remodel ECM (see black halo around the colonies in fig.4.10) but did not confirm the ability of those cells to produce ECM protein themselves. Therefore, naïve HPD06 colonies were plated in feeder-free conditions on vitronectin coating (VTN). Since VTN is the only protein in this coating, all the stained ECM proteins shown in fig.4.11 are produced by the naïve HPD06 themselves. On VTN coating it's possible to appreciate how most proteins are retained inside the cells, only collagen VI and laminin are secreted but scarcely organized. Fibronectin does not have a net-like organization as in fibroblasts, but it is secreted in spots or retained in the cells.

Taken together these data demonstrate for the first time that naïve and primed pluripotent stem cells have different ECM protein expression, deposition and organization. Moreover, for the first time direct ECM production by naïve pluripotent stem cells without feeder cells contribution has been demonstrated.

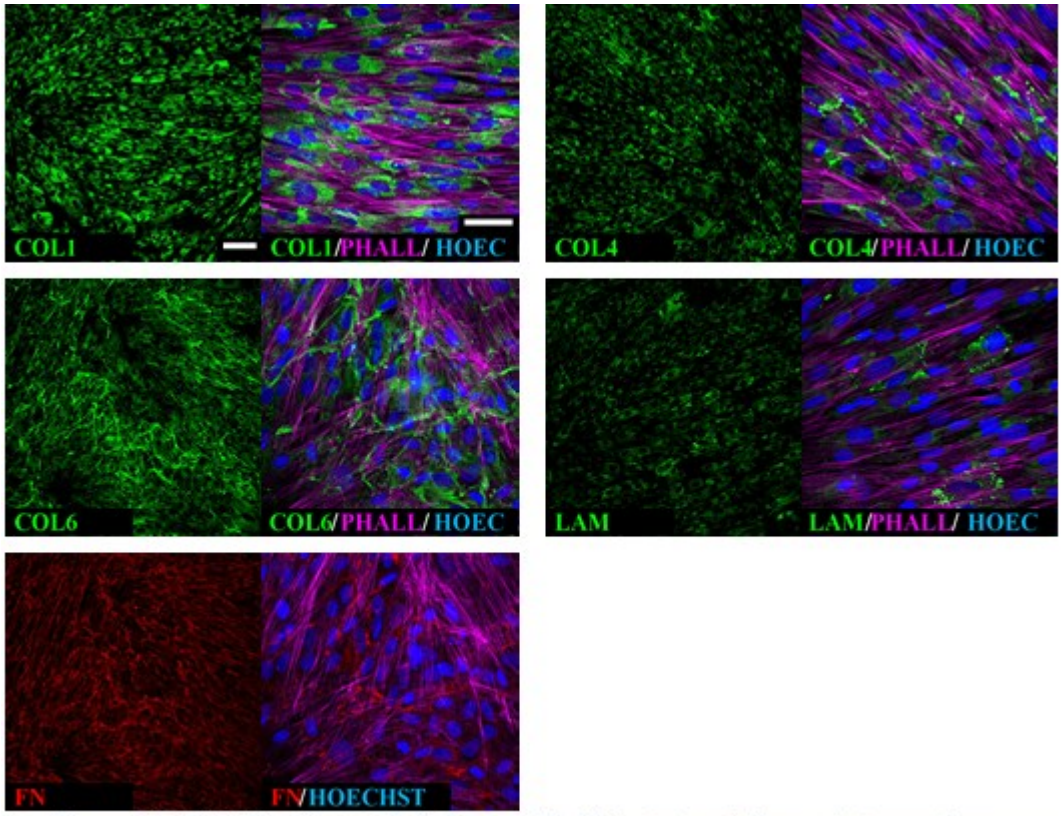

Figure 4.6: ECM fibroblasts well. *Collagen I, IV, VI, laminin and fibronectin immunofluorescence staining in HFF fibroblasts in well. Scale bar: 100 µm; magnification: 50 µm.*

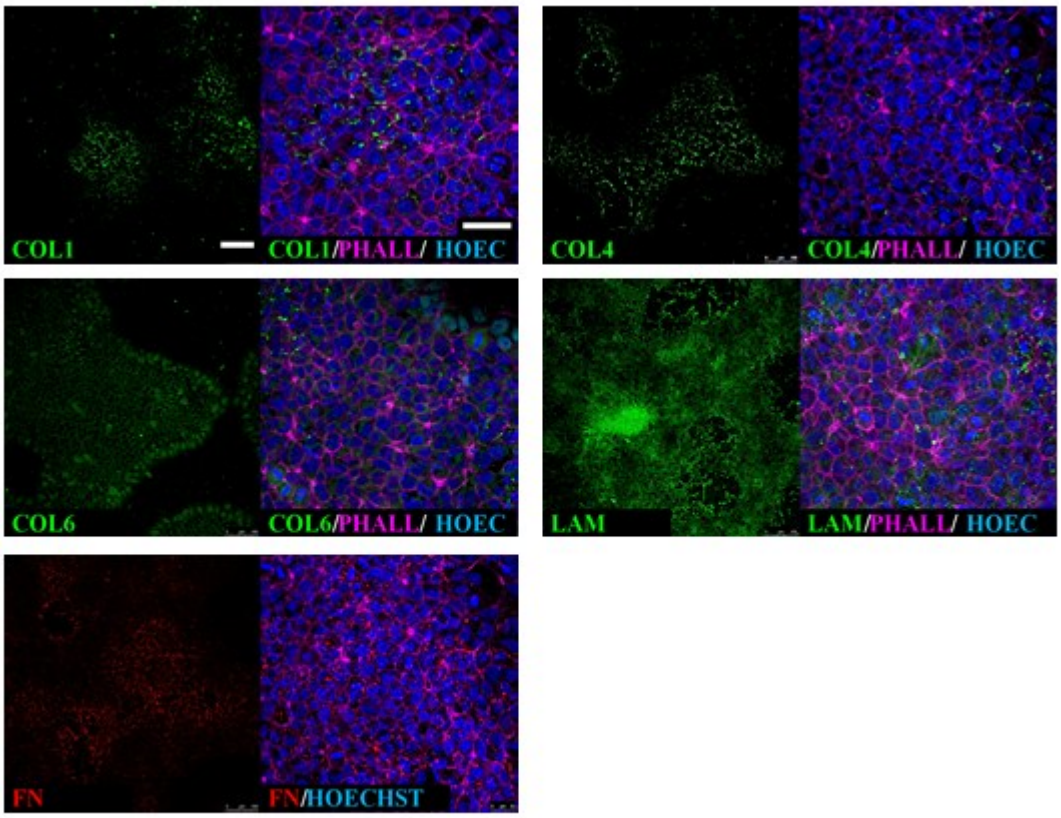

Figure 4.7: ECM primed PSC well. *Collagen I, IV, VI, laminin and fibronectin immunofluorescence staining in primed HPD06 in well. Scale bar: 100 µm; magnification: 50 µm.*

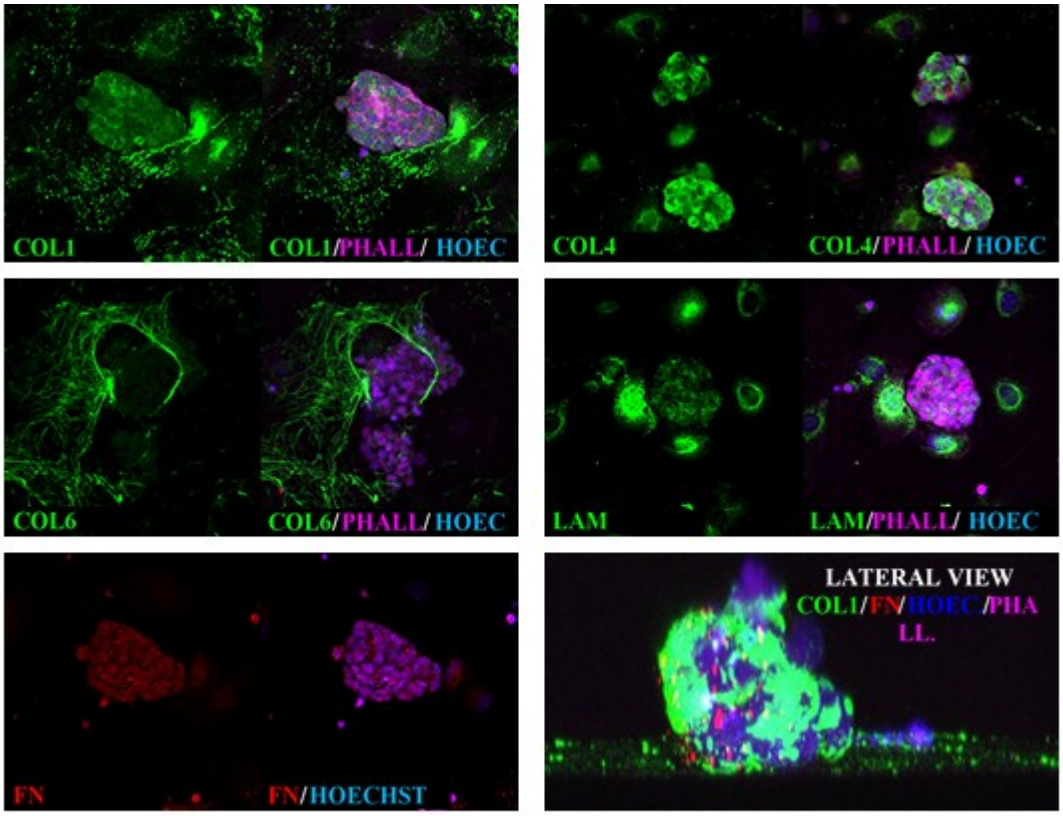

Figure 4.8: ECM naïve PSC well MEF. *Collagen I, IV, VI, laminin and fibronectin immunofluorescence staining in naïve HPD06 in well on MEF feeder layer. Bottom left: lateral view of the colony Scale bar: 56 µm.*

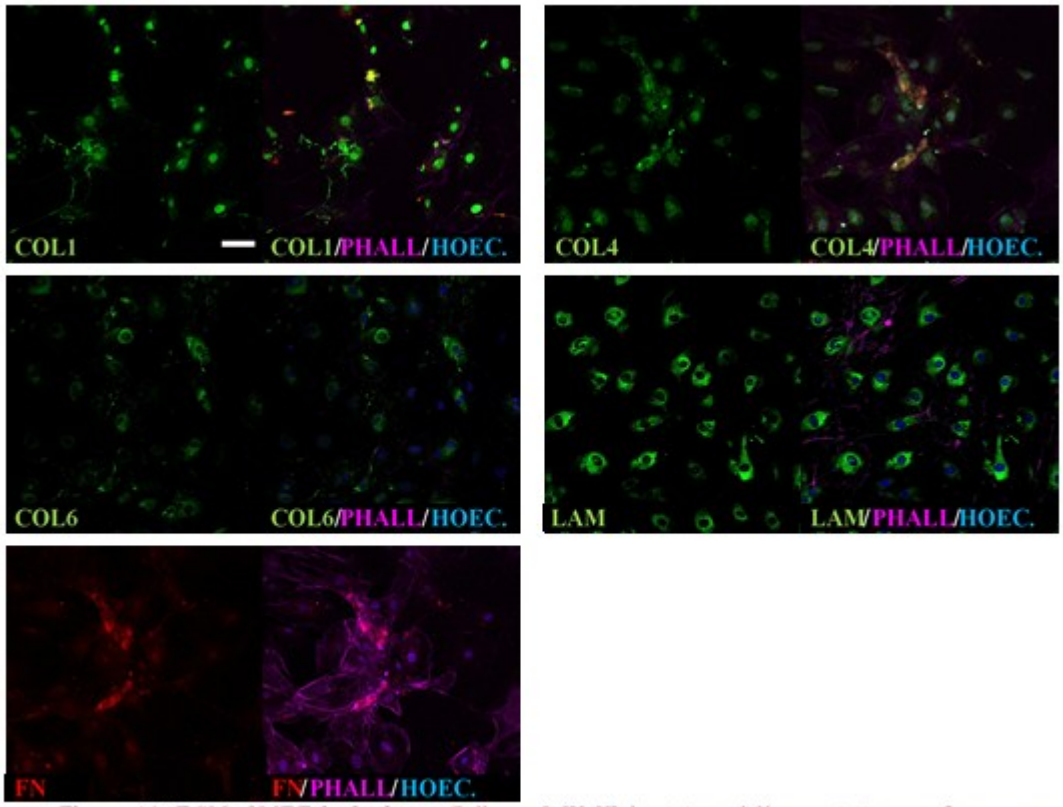

Figure 4.9: ECM of MEF feeder layer. *Collagen I, IV, VI, laminin and fibronectin immunofluorescence staining in HFF fibroblasts in well. Scale bar: 100 µm.*

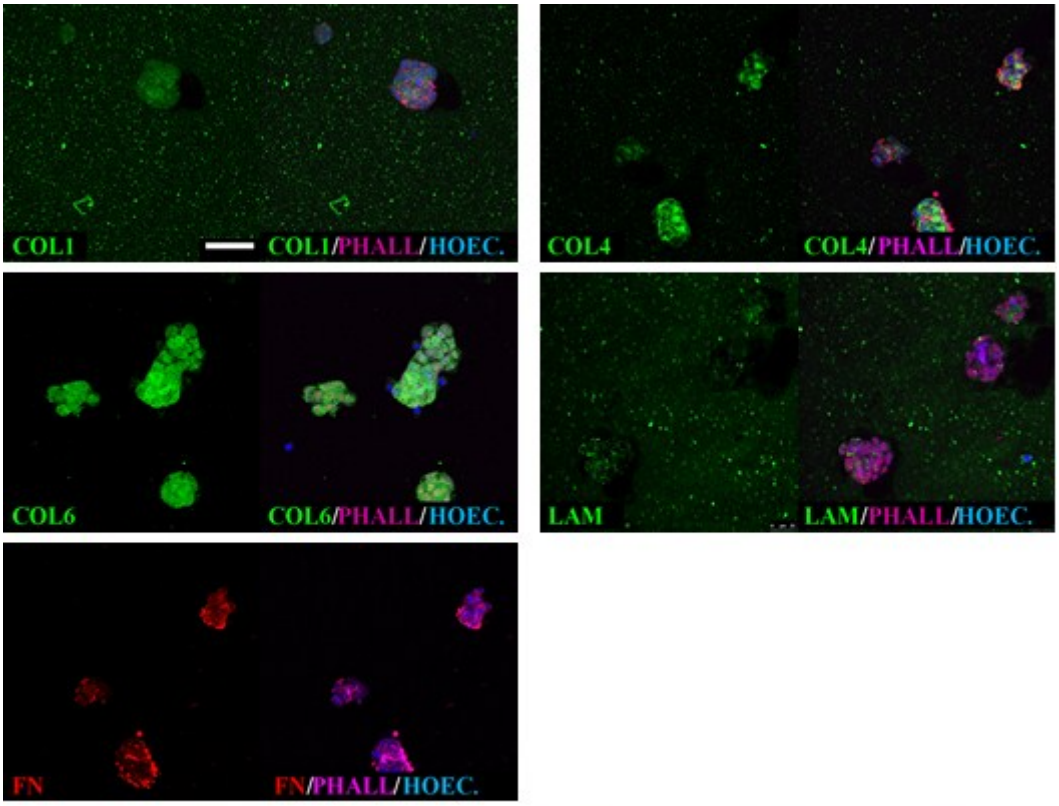

Figure 4.10: ECM naïve PSC in well on Matrigel. *Collagen I, IV, VI, laminin and fibronectin immunofluorescence staining in naïve HPD06 in well on MRF coating. Scale bar: 50 µm.*

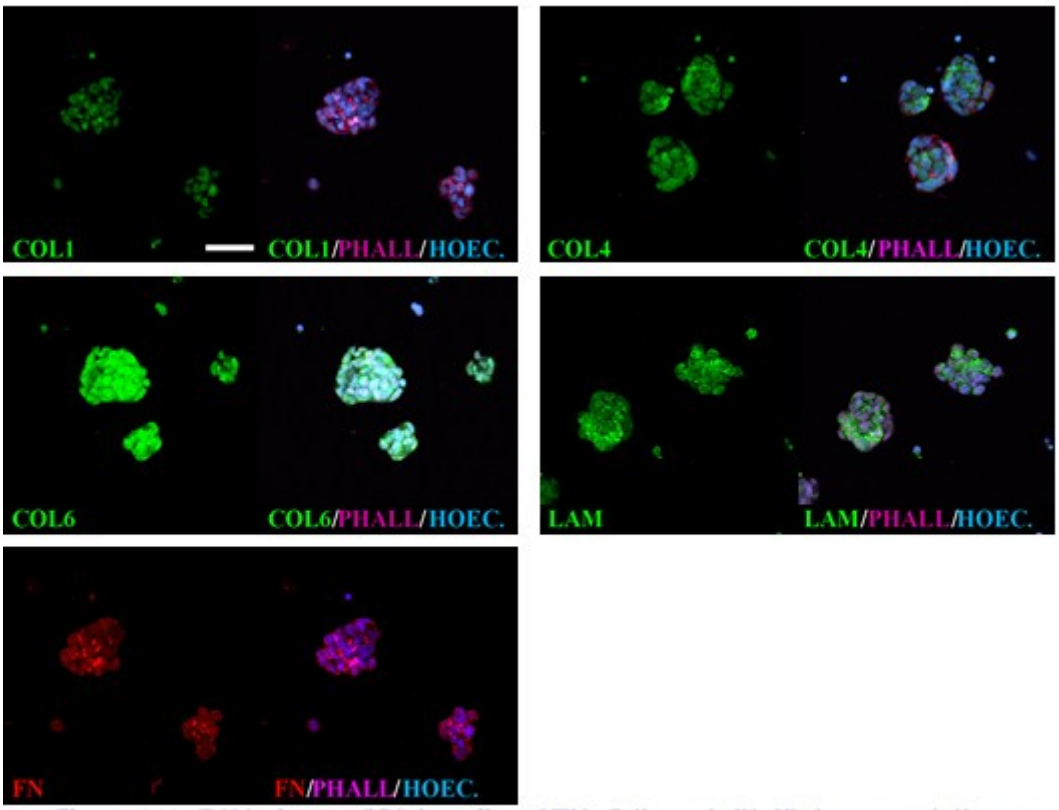

Figura 4.11: ECM of naïve PSC in well on VTN. *Collagen I, IV, VI, laminin and fibronectin immunofluorescence staining in naïve HPD06 in well on VTN coating. Scale bar: 50 µm.*

4.2. INFLUENCE OF CONFINED ENVIRONMENT ON ECM PROTEINS

After evaluating ECM deposition in conventional cell culture devices such as multiwell, HPD06 cell system was analyzed in microfluidic devices to understand if a confined environment with enhanced paracrine signaling could have influence on ECM deposition. First, the general influence of confined environment on cell secretome, which comprehends the overall production of secreted proteins, was analyzed by high throughput approaches; then the structure of ECM proteins in microfluidics was investigated.

4.2.1. Confined environment promotes accumulation of secreted proteins

To analyze secreted proteins, SILAC-MS was applied to HPD06 cell system. SILAC (stable isotope labeling by/with amino acids in cell culture) is a technique based on mass spectrometry that detects differences in protein abundance among samples using non-radioactive isotopic labeling. In a SILAC experiment, two populations of cells are cultivated in different cell culture media. One is fed with growth medium containing normal amino acids (eg. $^{12}C_6{}^{14}N_2$ L-Lysine and $^{12}C_6{}^{14}N_4$ L-arginine). The second population is fed with growth medium containing amino acids labeled with stable (non-radioactive) heavy isotopes (eg. $^{13}C_6{}^{15}N_2$ L-Lysine and $^{13}C_6{}^{15}N_4$ L-arginine). Medium collected from both cell populations can be combined and analyzed together by mass spectrometry. Pairs of chemically identical peptides of different stable-isotope composition can be differentiated in a mass spectrometer according to their mass difference. The ratio of peak intensities in the mass spectrum for such peptide pairs reflects the abundance ratio for the two proteins.

With this technique, it is possible to compare secretome (the global study of secreted proteins and secretory pathways) form cells grown in conventional well for cell culture and from cells grown in microfluidic platforms, after

appropriate volume and cell number normalization, and to discover which pathways are influenced by environmental confinement (Fig.4.12).

Similarly to the experiment performed by Hu et al.[288] described in 1.3.2, the secretome of different hiPS cell lines reprogrammed from BJ fibroblasts was analyzed (Fig4.13 and Fig.4.14). Cells were seeded on the platforms and let 2 days to adapt. In order to avoid any variability induced by the material or any contaminant from the coating solution, wells with glass bottom and coating with recombinant human vitronectin were used. Also in this case, heavy-labeled cells were seeded in microfluidics, light-labeled cells in wells. Conditioned medium was collected from the two platforms during cell growth, balancing channels and wells in order to collect, for each day, the same volume of conditioned medium from the two platforms. In the devices, the cells were seeded at the same density on the same area.

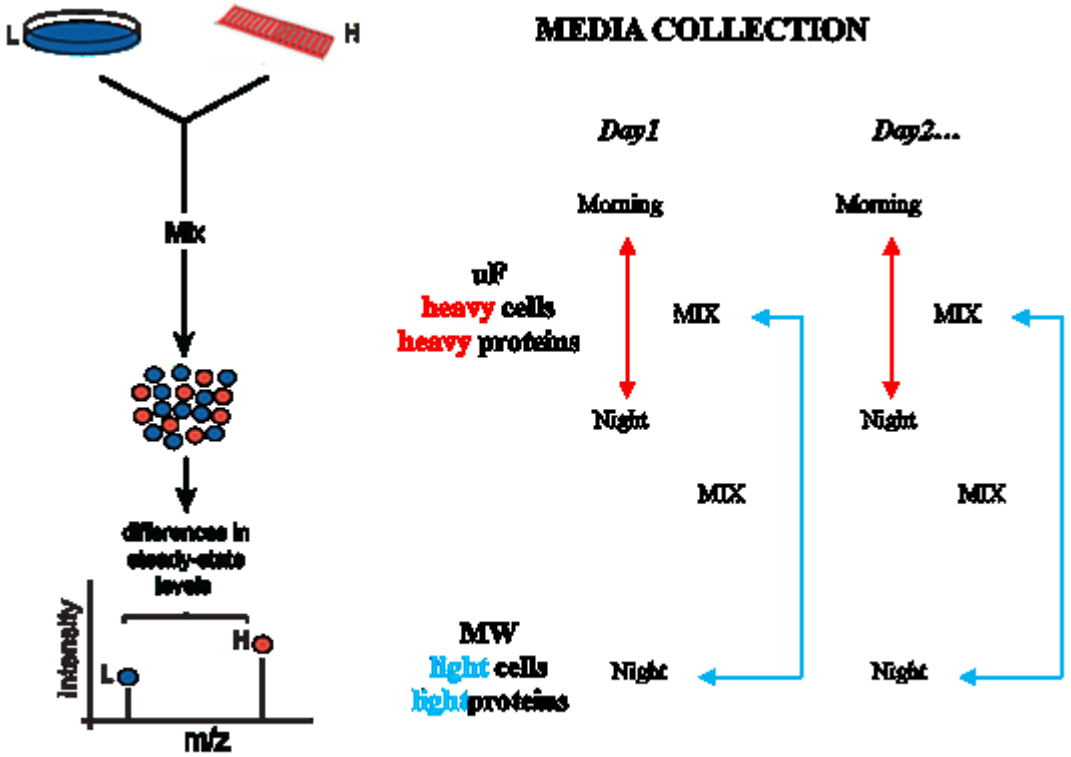

Figure 4.12: SILAC experiment design to compare well and microfluidic secretome.

In the statistical analysis on the collected data (μF and well together) the circles represent the total number of detected proteins per day and, meaning the total number of different proteins detected, not the total quantity or concentration (Fig.4.13). The increasing diameters indicate increase in number of detected proteins, and this leaves space for different interpretations: on one side, from day 2 to day 5 cells are growing in number and therefore more cells produce more secreted proteins and in the last days even less expressed proteins reach the mass spectrometry detection threshold. On the other hand, it is possible that some proteins are expressed only at a certain time point. Finally, it is possible that those proteins are due to an increment of dead cells or exosomes. The green circle represents the GO category "extracellular proteins" and, since the circle diameter is not increasing, it is possible to assume that the system sensitivity on those proteins is good already from day 2.

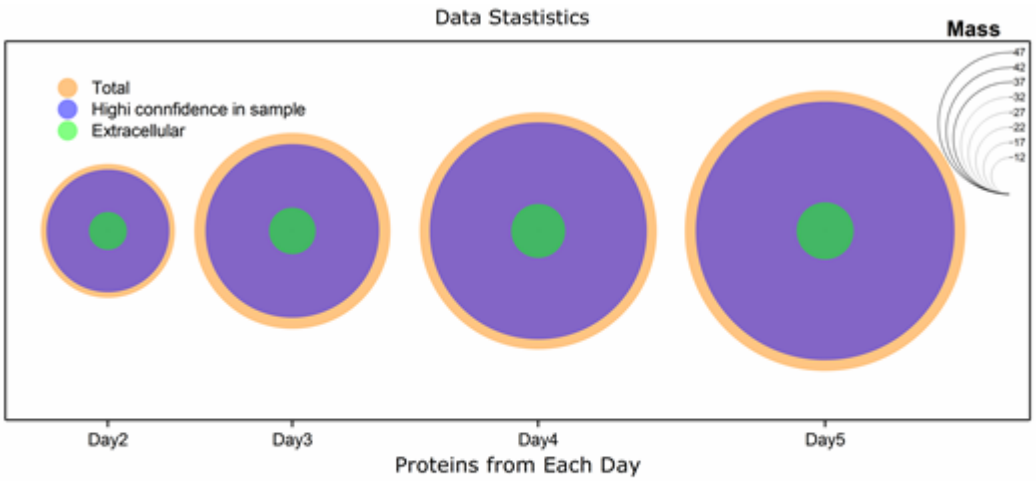

Figure 4.13: ***SILAC transcriptomic analysis of primed iPSCs secretome in well and in microfluidic devices – Statistical analysis****. Statistical analysis of detected proteins from day 1 to day 4 indicating the number of protein detected day by day.*

SILAC-MS PROTEOMIC ANALYSIS OF PRIMED iPSC IN WELL AND MICROFLUIDICS

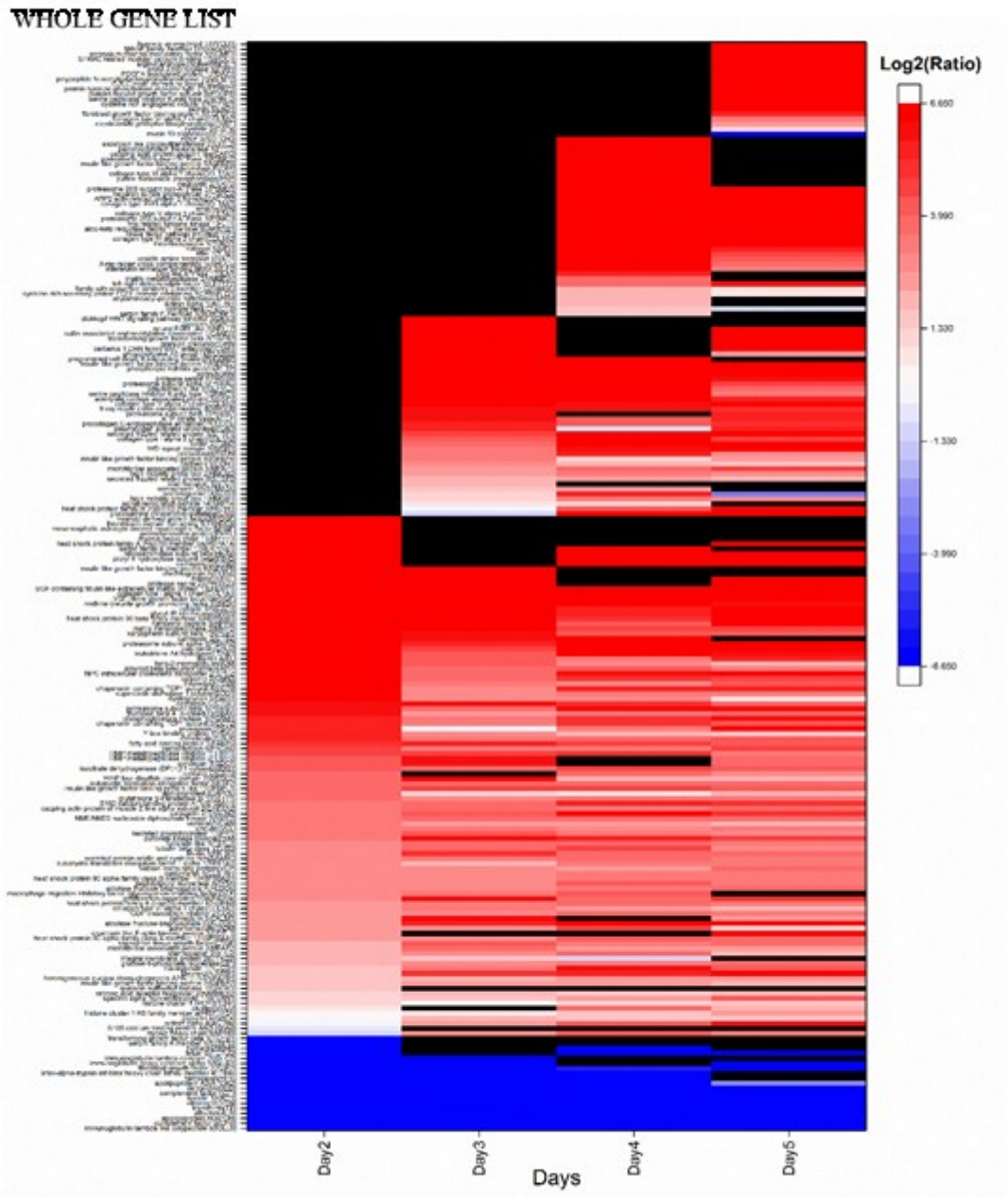

Figure 4.14: SILAC transcriptomic analysis of primed iPSCs secretome in well and in microfluidic devices. Heatmap of total detected proteins, red indicates overexpression in microfluidics, blue indicates overexpression in wells.

To further analyze the extracellular protein compound, the differential expression analysis that is represented in the middle heatmap was performed (Fig.4.13). The colors are relative to the Heavy/Light Ratio, and therefore red indicates that the given protein, at a certain time point is more expressed in microfluidics compared to well. White indicates no differences in expression between microfluidics and wells and blue indicates an overexpression in wells compared to chips. Last, proteins not detected at certain time points are labeled in black, but it is not always possible to tell if it is a problem of experimental sensitivity or a real oscillation in protein expression. For example, if a protein is detected at day 2, not detected at day 3 and then detected again at day 4 we can be sure that we are observing a real oscillation, because protein signal was already detectable with few cells. Instead, if the protein is only detected from day 4 on, it is not possible to distinguish between biologically significative oscillation and experimental sensitivity.

It's very important to notice that the great majority of extracellular proteins are overexpressed in microfluidics and that among the few proteins overexpressed in well it is possible to find all proteins coming from cell culture medium (TGF- β, FGF2, Albumin) and from the coating solution (VTN) that are obviously light-labeled. In Fig.4.15 there is a selection of all detected collagens and, also in this cell model, the confined environment enhances the production of collagens and ECM proteins. The most detected collagens in this analysis were COL1A2, COL4A2, COL 5A1, COL5A2, COL6A1, COL6A2, COL11A1 and COL18A1. In particular, COL6A1 is detected from the very first days, while the others are detected in the following days. This analysis supports the need to investigate by immunofluorescence staining the ECM organization of these collagens, as previously reported and as shown in the following results.

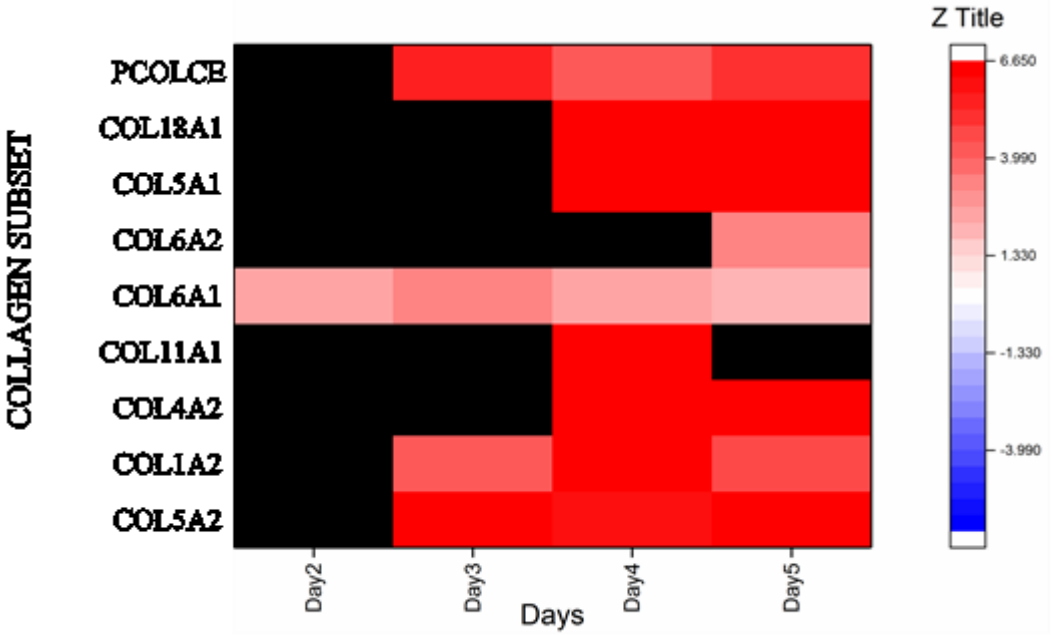

Figure 4.15: Collagen detected in hiPSCs secretome (subgroup of heatmap in fig. 4.14).

4.2.2. RNA-seq analysis of fibroblasts, naïve and primed PSCs reaveals distinct matrisome gene expression in well and microfluidic systems.

After the result obtained with hiPSC secretome analysis in well and microfluidic environment, a trascriptomic analysis was performed on the isogenic cell system introduced in paragraph 4.1.

In this system, HFF fibroblasts, naïve HPD06 pluripotent stem cells and primed HPD06 pluripotent stem cells share the same genetic background, since naïve HPD06 have been reprogrammed to naïve ground state directly from HFF fibroblasts and primed HPD06 have been differentiated to primed state from the naïve cell line. Therefore, the differences detected in RNA-sequencing analysis should be addressed to the differences in developmental stage. To perform bulk RNA-seq, cells were seeded in wells and microfluidic chips at the same density at Day 0 as reported in chapter 3. RNA was extracted at Day 1, 4 and 7 of cell proliferation after seeding and sequenced by 3'-single end RNA-seq as described in chapter 3. At Day 4, cells were fixed with PFA for immunofluorescence staining, as will be described in paragraph 4.2.3.

Moreover, at Day 4, naïve colonies with 3D or 2D morphology were manually picked from wells and from microfluidic chips and analyzed separately.

As shown in fig.4.16, an average of 15000 genes/sample was detected in fibroblasts and primed HPD06 cells. In naïve cells instead, the number of detected genes was sometimes reduced compared to other samples, even if the total amount of sequenced RNA was comparable. This may be due to the presence of MEF as feeder layer for naïve cells, whose transcripts are not aligned with the human genome and result in a decrease of total detected genes. Nevertheless, in the principal component analysis shown in fig.4.16, the three developmental stages can be well separated and clusterize well among each other, no matter the day of the experiment or the cell growth system.

In fig.4.17, a detail on HFF fibroblasts is reported. In the PCA analysis it is possible to appreciate how samples grown in microfluidic devices are separated from those coming from conventional well systems. Moreover, in microfluidics HFF fibroblasts require some time to adapt and stabilize, in fact, samples from Day 1 are separated from samples from Day 4 and 7. Nevertheless, as shown from the hierarchical clustering in fig.4.17, the main difference between the samples (first branching of the tree) is the culture system, while the culture time represents the second branching of the tree. By analyzing the differences in the reactome of HFF fibroblasts in wells and microfluidics after 7 days, it is possible to detect that in well matrix-related genes are overexpressed, while in confined environment the most upregulated pathway is related to lipids metabolism. This may sound in contrast to the data previously reported, but a possible explanation for this behavior is that in microfluidic chips cells are accumulating ECM proteins faster, from the first days, therefore there is less need for matrix-related gene transcription at Day 7. Indeed, as shown from panel C and D of fig.4.17, a confined environment has a deep influence on the expression of matrix genes and matrix-related genes. The genes selected for this analysis belong to the category of Core Matrisome and Matrisome-Associated (The Matrisome Project – MIT[297]). And it is possible to appreciate how the relative expression of these genes is completely opposite in wells compared to microfluidic chips.

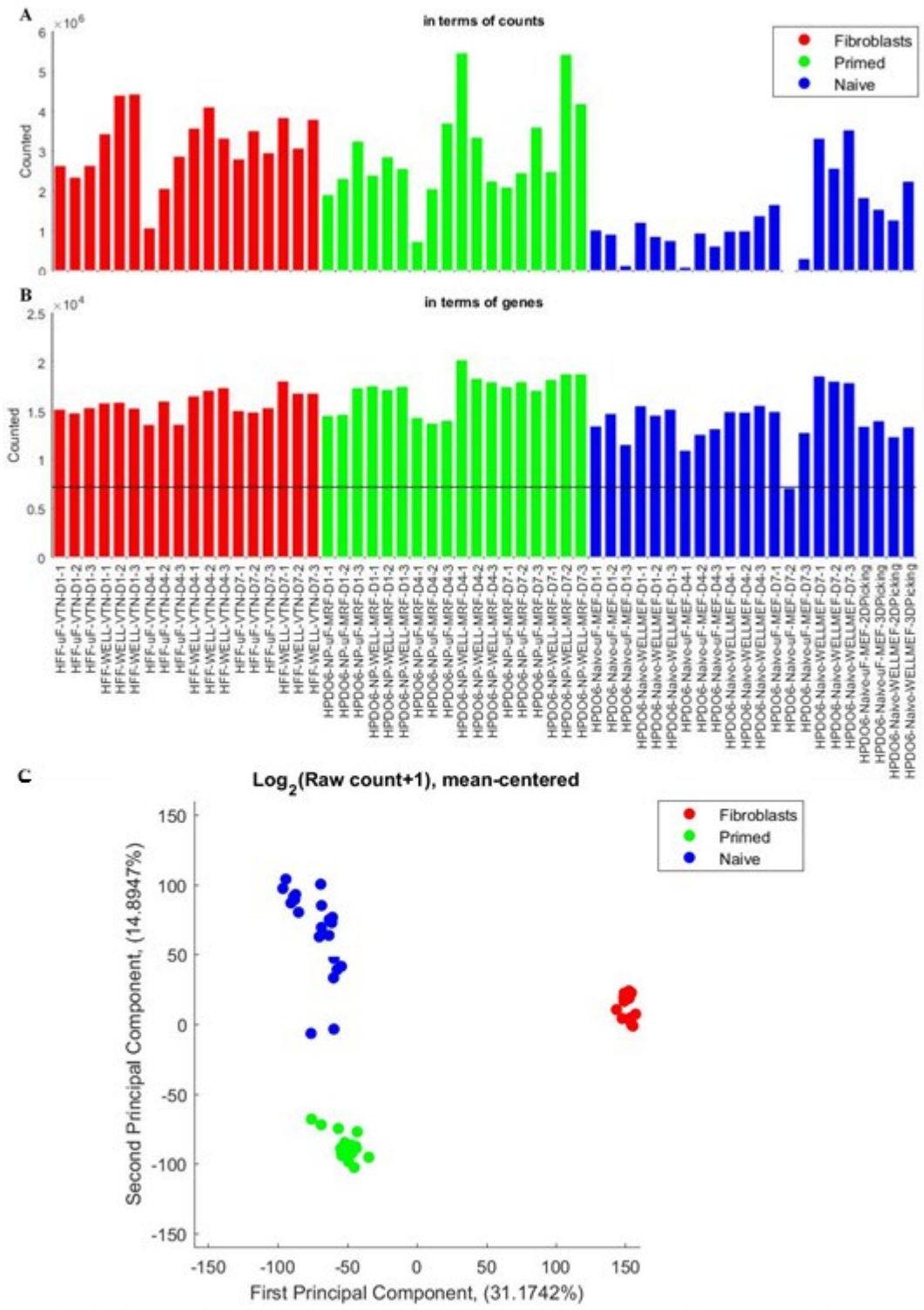

Figure 4.16: Fibroblasts, naïve and primed PSC RNA-sequencing – General overlook. (A) Read counts per sample. (B)Number of detected genes per sample. (C) PCA of general expression of fibroblasts, naïve and primed PSC.

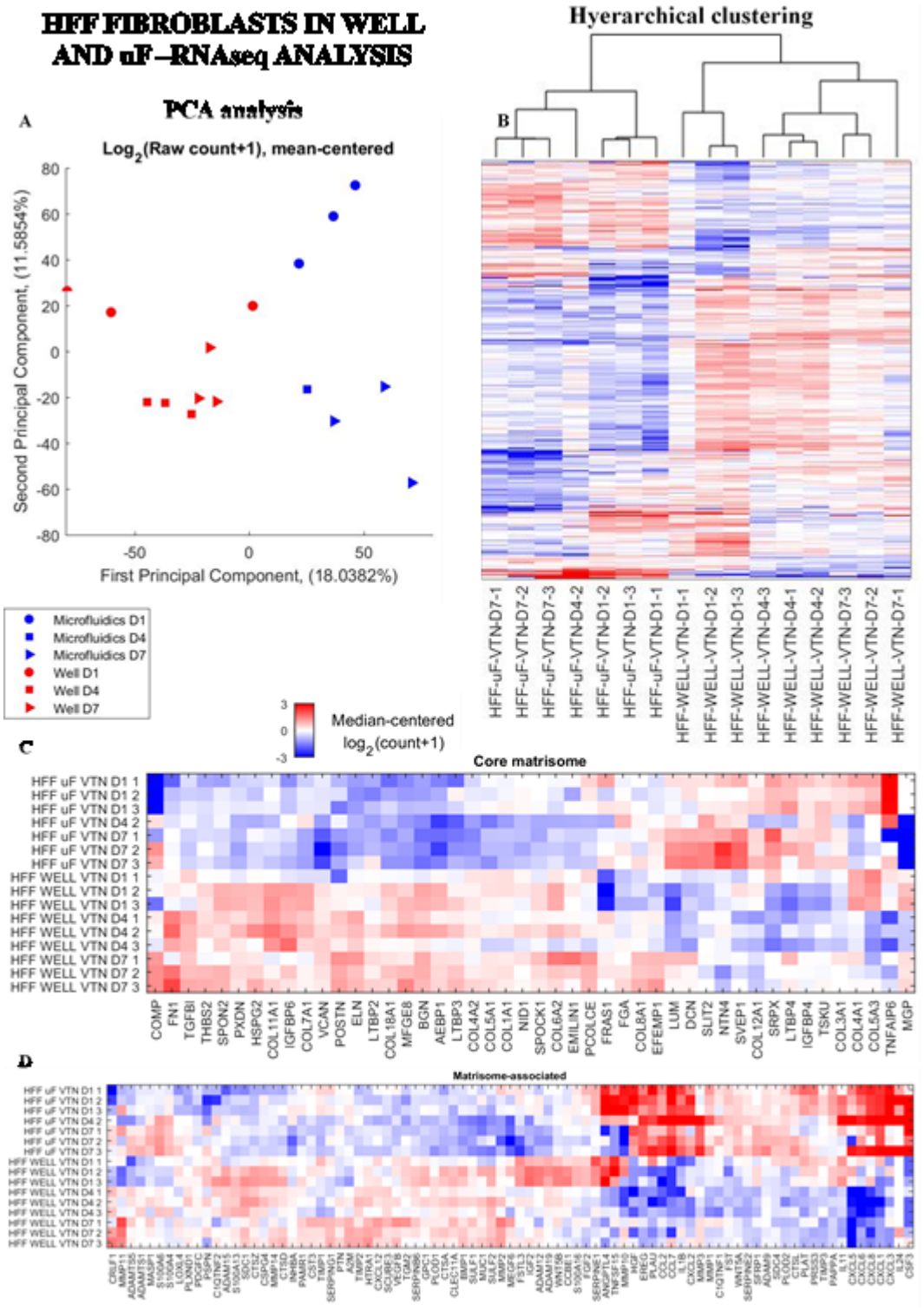

Figure 4.17: HFF Fibroblasts in well and microfluidics – RNA-seq analysis. (A) PCA analysis of samples collected from wells (in red) and samples collected from microfluidic chips (in blue) at Day 1, 4 and 7 after seeding. (B) Hierarchical clustering based on all the differential expressed genes among any couple of samples in the list. (C) Cluster analysis of matrix genes (The Matrisome Project: Core Matrisome). (D) Cluster analysis of matrix-associated genes(The Matrisome Project: Matrisome-Associated).

In fig.4.18 and 4.19 the results related to pluripotent stem cells, both naïve and primed have been described. Fig.4.18 represents the hierarchical clustering of all the pluripotent samples, including the manually picked 3D or 2D naïve colonies. It is possible to appreciate how the general expression pattern is different between primed and naïve pluripotent state. As shown from the branching of the tree, picked colonies are recognized as naïve samples, but no appreciable difference was detected between 2D and 3D colonies, both from well or microfluidic chips. Indeed, as shown in fig.4.19, the manually picked samples are very separated from the naïve samples and a possible explanation for this behavior is the picking method itself. In fact, for each sample, at least 20 colonies were manually picked and the overall operation required about one hour per sample. Therefore, these stressing conditions could have altered the cell expression program to the point of masking other differences among those four samples. For this reason, the picked samples will not be included in the following analysis.

Fig.4.20 shows a more detailed analysis of primed HPD06 samples. The PCA analysis shows how in well, gene expression is stable in these cells from Day 1 to Day 7, while the culture of these cells in confined microfluidic environment requires few days to adapt. In fact, samples from Day 1 and 4 are distant from the main cluster but converge at Day 7. This may be due to an initial adaptation shock: primed HPD06 cells are routinely cultured in conventional wells and seeded in the microfluidic platform at the starting of each experiment. Therefore, it is possible that the seeding in a confined environment from the conventional well may cause a perturbation in gene expression that is fixed after few days in culture in the confined environment. As shown from panels B and C of fig.4.20, primed HPD06 genes belonging to the core matrisome or associate to the matrisome are not as different from wells to microfluidic platforms as reported for HFF fibroblasts. Indeed, the main differences in matrix-related genes expression observed between wells and microfluidic chips appear mainly in samples collected from microfluidic chips at Day 1 and 4, while at Day 7 matrix-related gene expression is comparable to cells cultivated in wells.

PLURIPOTENT STEM CELLS – NAIVE AND PRIMED HPD06 IN WELL AND uF – RNAseq ANALYSIS HYERARCHICAL CLUSTERING

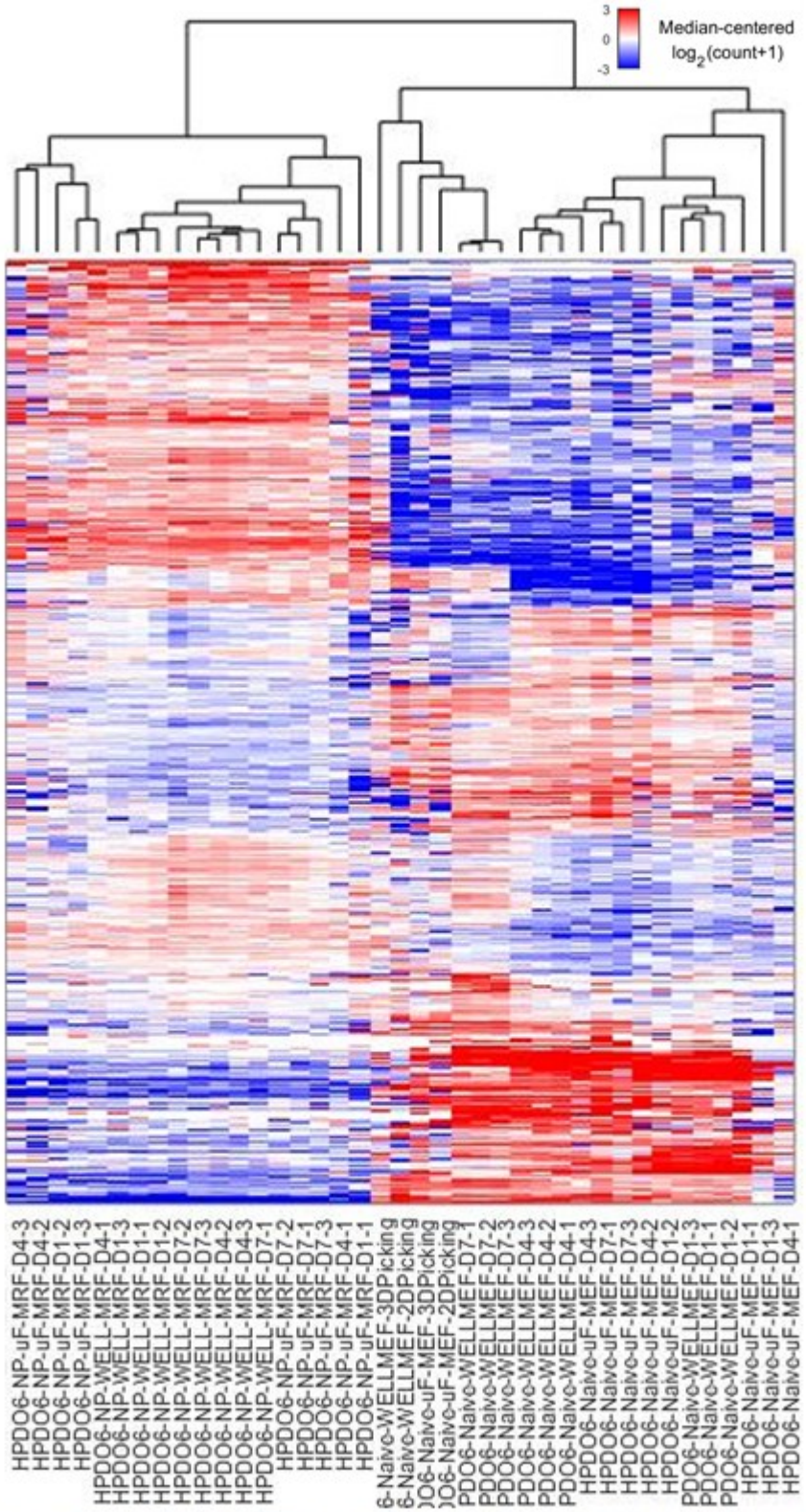

Figure 4.18: Naïve and primed HPD06 in well and microfluidics – RNA-seq analysis – Hierarchical clustering. Cluster analysis of differential expressed genes among any couple of samples. Picked naïve 2D and 3D colonies were included in this analysis.

PLURIPOTENT STEM CELLS – NAIVE AND PRIMED HPD06 IN WELL AND uF – RNAseq ANALYSIS
PCA ANALYSIS

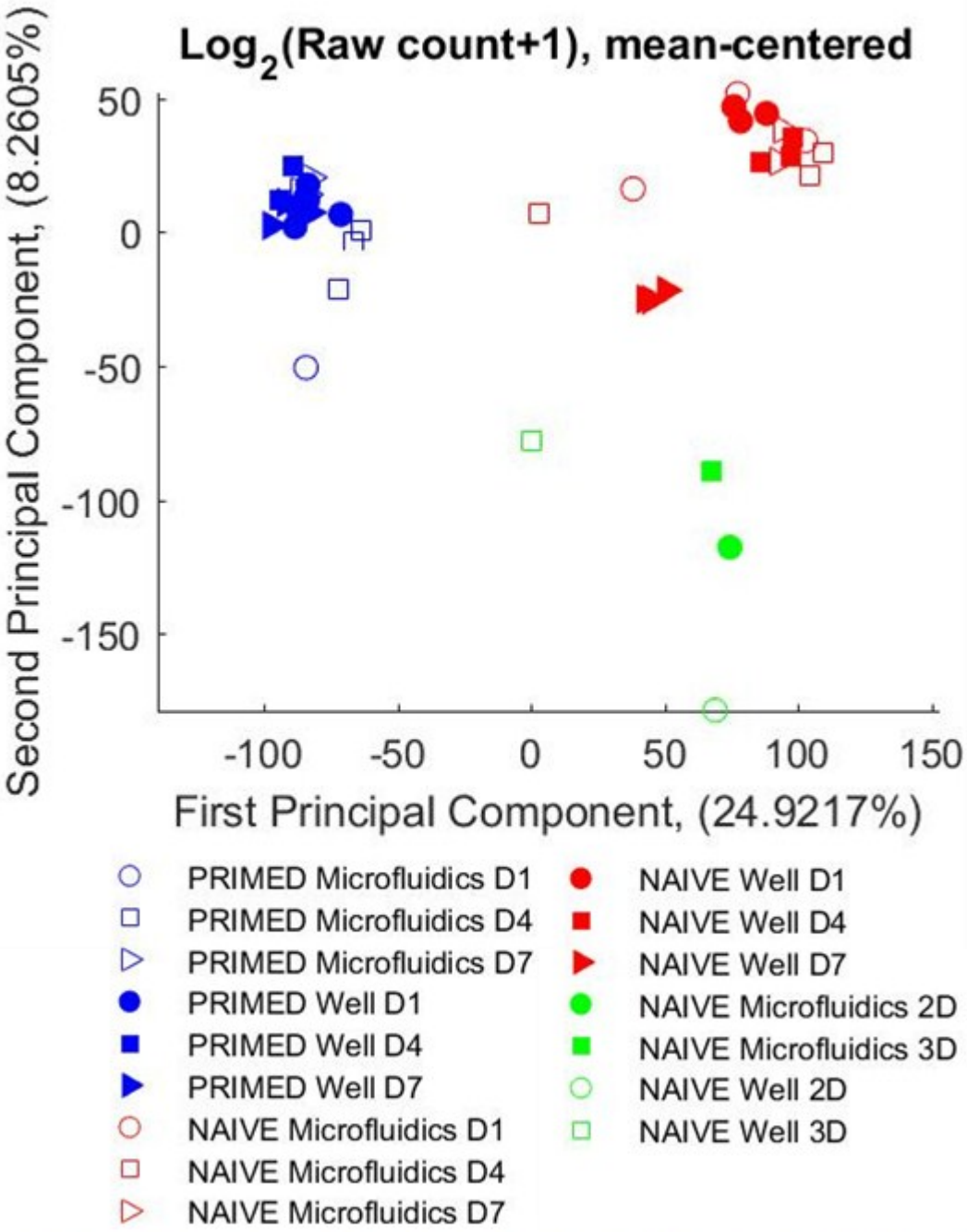

Figure 4.19: Naïve and primed HPD06 in well and microfluidics – RNA-seq analysis – PCA analysis. Picked naïve 2D and 3D colonies were included in this analysis.

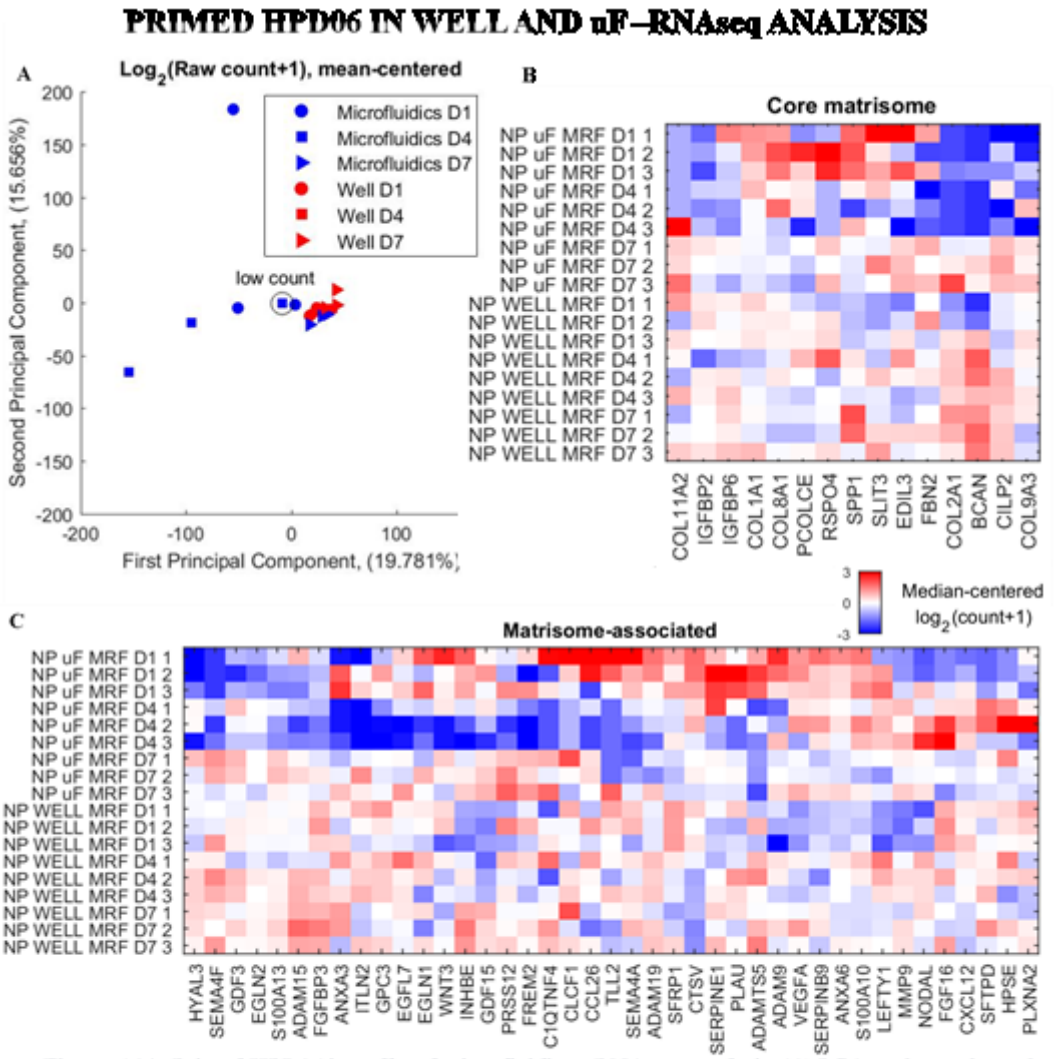

Figure 4.20: Primed HPD06 in well and microfluidics –RNA-seq analysis. (A) PCA analysis of samples collected from wells (in red) and samples collected from microfluidic chips (in blue) at Day 1, 4 and 7 after seeding. One sample is highlighted as low count, meaning that the total reads and gene count was not comparable to the other samples. (B) Hierarchical clustering based on all the differential expressed genes among any couple of samples in the list. (C) Cluster analysis of matrix genes (The Matrisome Project: Core Matrisome). (D) Cluster analysis of matrix-associated genes (The Matrisome Project: Matrisome-Associated).

In fig.4.21, a detail of gene expression of naïve HPD06 samples is reported. By comparing the PCA of fig.4.21 with the PCA of fig.4.20 it is possible to see that naïve HPD06 are more variable compared to primed HPD06. Moreover, in naïve samples, cells from Day 7 in microfluidics correspond to cells from Day 4 in wells. By looking at the matrisome detail of panels B and C it seems that there is a strong upregulation of ECM-related genes transcription in Day 1 of cell culture. Core matrisome gene expression and Matrisome-associated gene expression of naïve and primed HPD06 is summarized in fig.4.22.

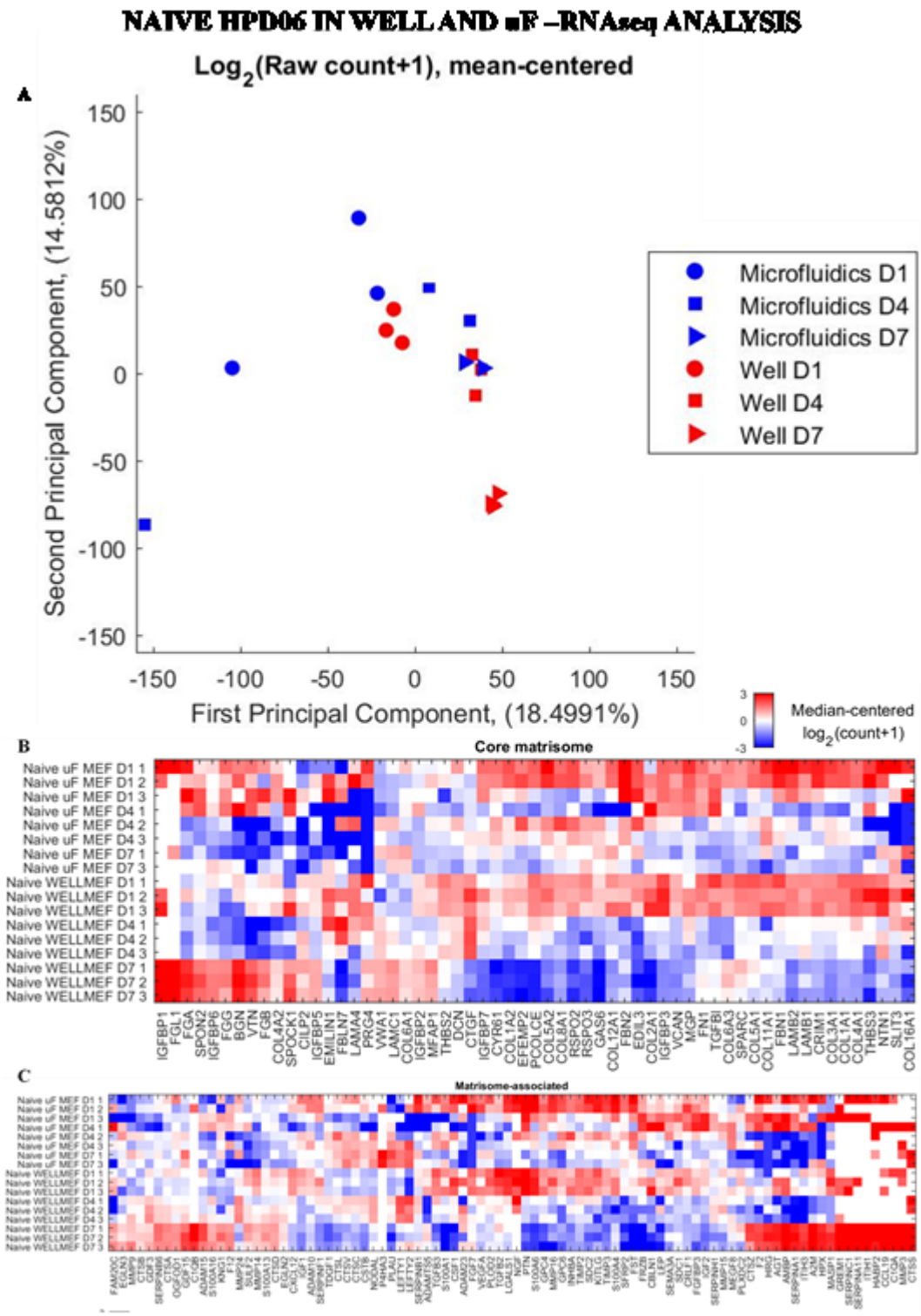

Figure 4.21: Naïve HPD06 in well and microfluidics – RNA-seq analysis. (A) PCA analysis of samples collected from wells (in red) and samples collected from microfluidic chips (in blue) at Day 1, 4 and 7 after seeding. (B) Hierarchical clustering based on all the differential expressed genes among any couple of samples in the list. (C) Cluster analysis of matrix genes (The Matrisome Project:: Core Matrisome). (D) Cluster analysis of matrix-associated genes (The Matrisome Project: Matrisome-Associated).

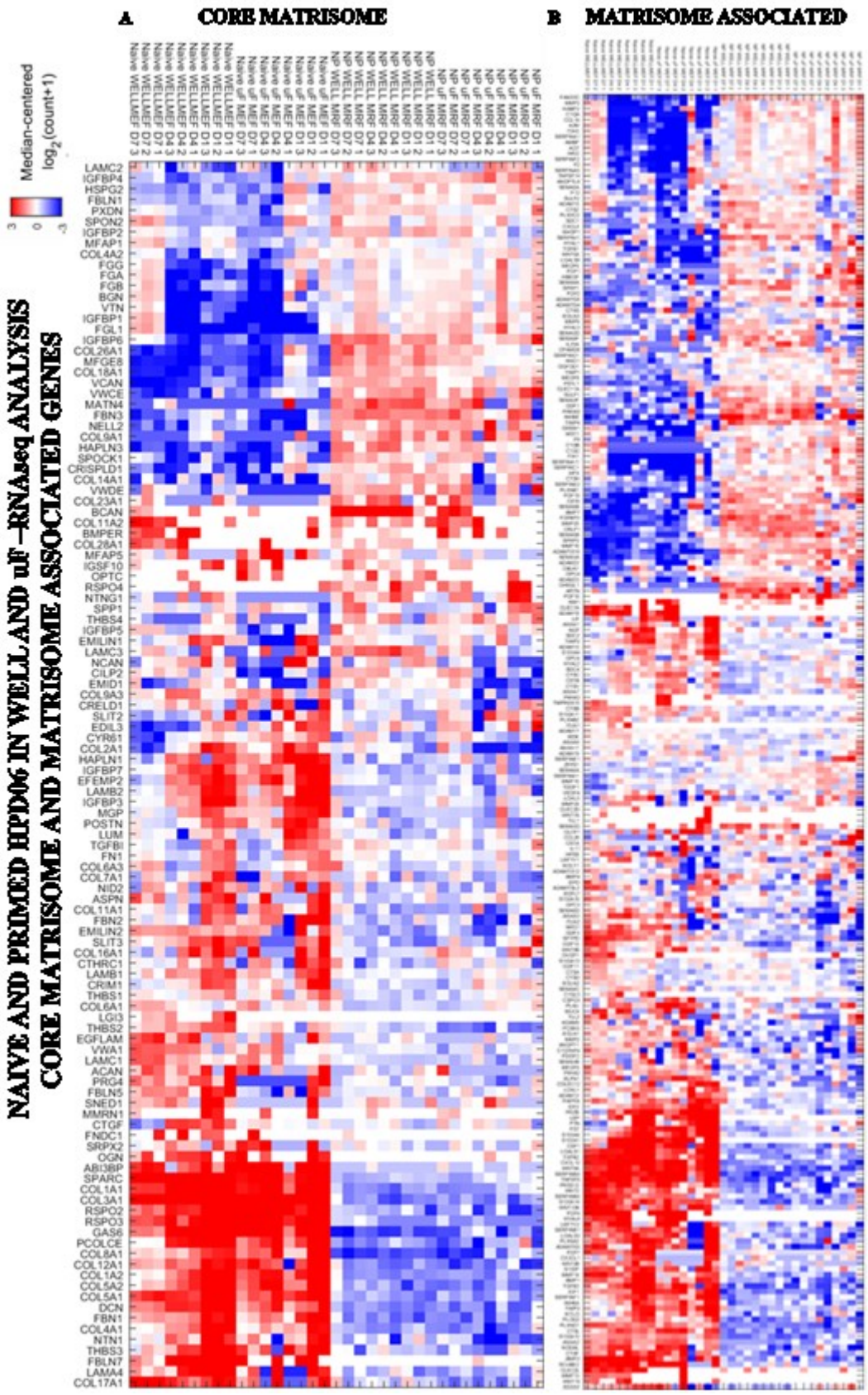

(The Matrisome Project: Matrisome-Associated).

4.2.3. Microfluidics enhances ECM deposition

Therefore, confined environment influence on specific ECM protein deposition was analyzed in HFF, primed HPD06, primed H9 and naïve HPD06 cells (fig.4.23, 4.24, 4.25 and 4.26).

In HFF fibroblasts (fig.4.23), confined environment promoted the deposition of a thicker extracellular network of collagen IV and fibronectin compared to conventional wells, while did not show increase in collagen I and collagen VI deposition.

In primed HPD06 colonies (fig.4.24), confined environment promotes accumulation of collagen I, IV, VI and fibronectin, but does not promote organized deposition of collagen I and IV in fibers. Collagen VI is produced intracellularly but not secreted and organized.

Naïve HPD06 colonies instead show a remarkable difference in ECM deposition between conventional cell culture systems and microfluidic devices. In particular, when colonies are grown in confined environment, ECM proteins are more expressed and organized around the colonies as shown in fig.4.25. This has been confirmed for all coating conditions previously tested on these cells (MEF feeder layer, MRF and VTN). For example, collagen I in microfluidics is strongly deposited around the colony, surrounding the colony

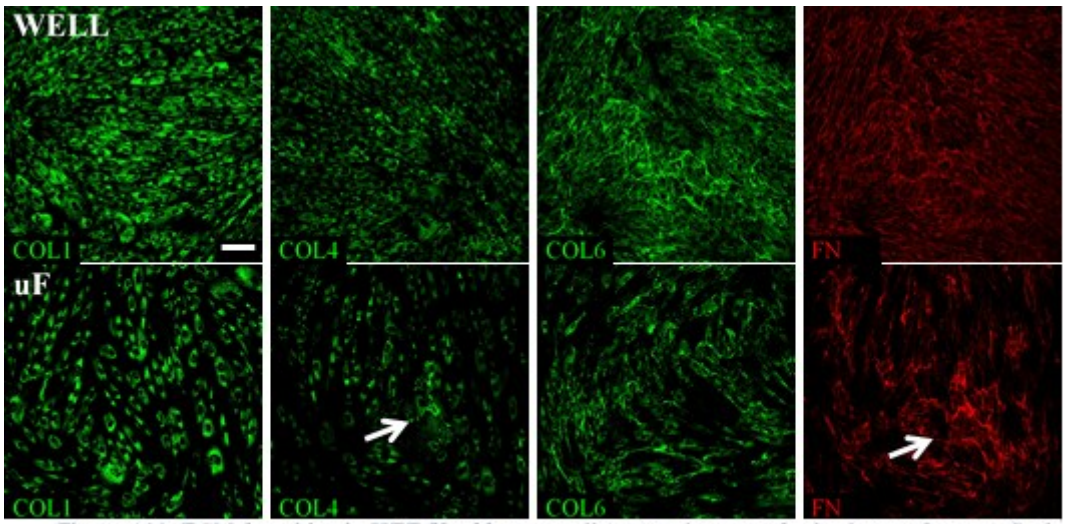

Figure 4.23: ECM deposition in HFF fibroblasts in well (top) and in microfluidic devices (bottom). Scale bar 100 µm.

as a ring or creating sectors inside the colonies. Collagen IV is highly deposited inside the colonies, creating thick sectors.Collagen VI in confined systems can be observed outside the cells, weakly organized in spots, whether in conventional devices was only retained inside the cells. Also fibronectin deposition in spots is enhanced in microfluidics.

In conclusion, confined environment granted by in microfluidic devices, promotes the secretion of proteins belonging to the gene ontology category of "extracellular proteins", among which the most abundant group belongs to the category "extracellular matrix" and to the KEGG pathway of cell-ECM interaction. Moreover, confined environment promotes a more defined ECM organization in pluripotent stem cells (naïve and primed HPD06 lines).

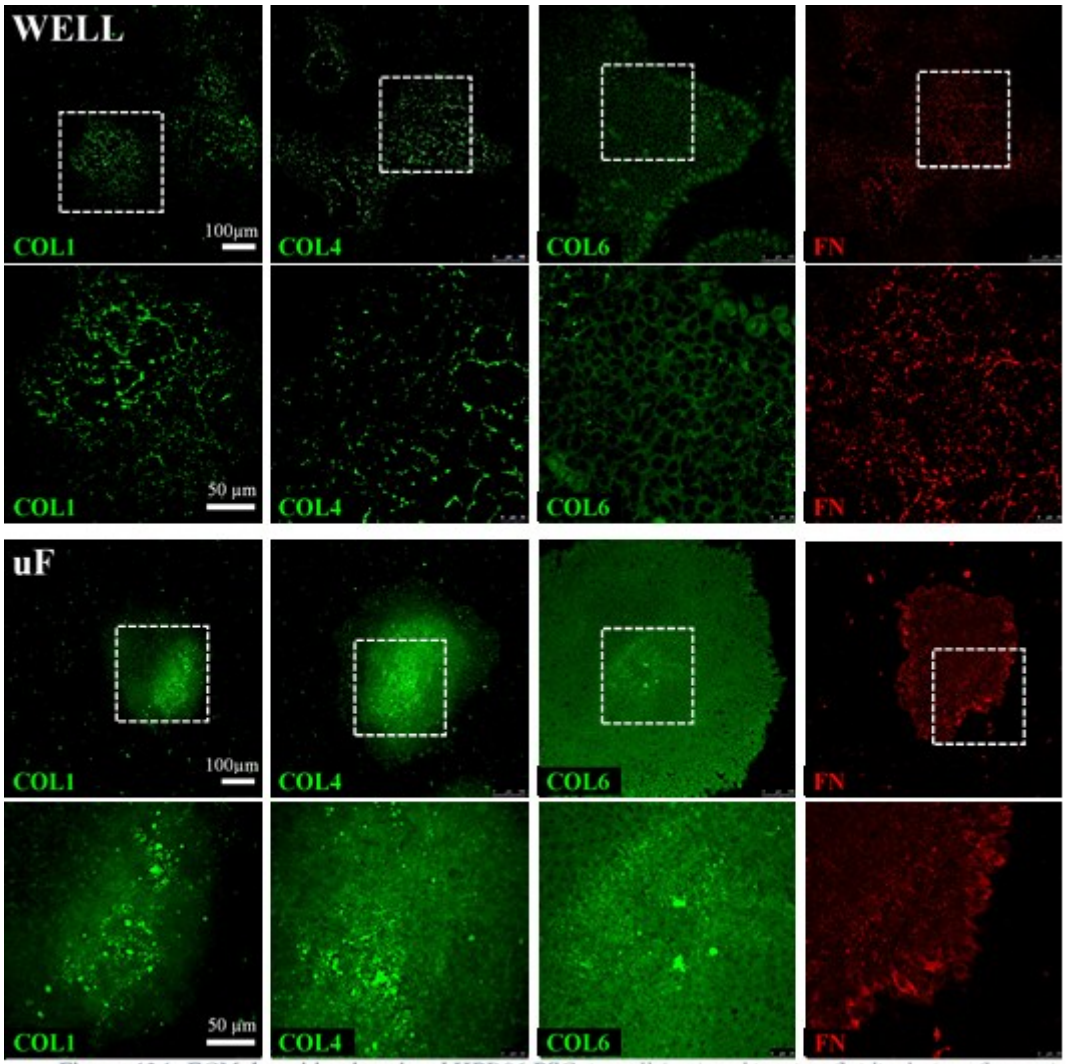

***Figure 4.24 : ECM deposition in primed HPD06 PSCs** in well (top) and in microfluidic devices (bottom). Scale bar 100 µm in the upper panel and 50 µm in the lower zoom. Dashed square indicates the zoomed area.*

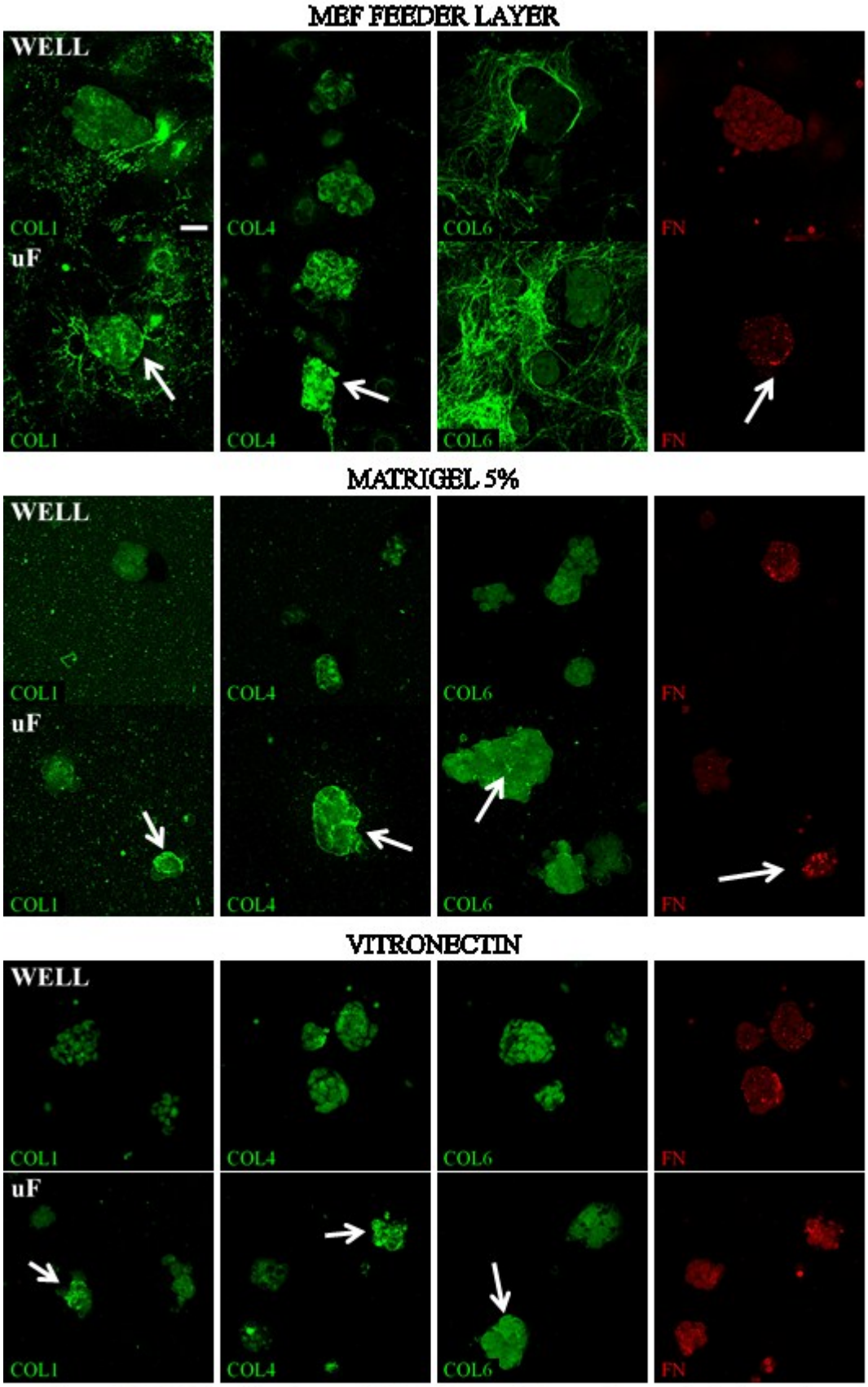

***Figure 4.25: ECM deposition in naïve HPD06 PSCs** in well (top) and in microfluidic devices (bottom) on three different coatings: MEF feeder layer, Matrigel and vitronectin. Scale bar 50 µm.*

4.3. NAÏVE COLONY 3D SHAPE, ECM AND PLURIPOTENCY MARKERS

Since the most evident difference between naïve and primed pluripotent stem cells from a morphological point of view is the 3D organization of the two pluripotent stages, a possible correlation between colony shape and pluripotency marker expression was investigated.

4.3.1. Naïve colony 3D shape is linked to ECM deposition and pluripotency markers expression

As previously reported, bona fide naïve colonies are characterized by 3D dome-shape morphology and this characteristic is considered a key feature to confirm appropriate culture conditions. Nevertheless, naïve pluripotent stem cells *in vitro* culture is a rather new achievement and it is not possible to guarantee complete stability of the culture conditions, also because, as seen in chapter 1.1, pluripotency is a continuous process *in vivo*, hard to stabilize *in vitro*. Indeed, in naïve cultures, both in conventional wells and in microfluidic platforms, two different morphologies can be identified: most of the colonies retain the typical 3D dome-like shape, but some colonies acquire a 2D flat morphology. In this chapter, data that link 3D morphology to a higher ECM deposition will be presented.

The height difference measured on the z-axis between the two phenotypes is statistically different, as represented in fig.4.19, while in fig.4.20, an example of the two morphologies is shown. When measuring the height of the two types, 3D colonies have an average height of 33.18 μm ± 2.242 μm , while 2D colonies have an average height of 16.41 μm ± 0.8047 μm. Another striking feature that distinguishes flat and 3D colonies is the actin cytoskeleton arrangement. In fact, 3D colonies are characterized by a thick actin ring that surrounds the colonies, typical feature of pluripotent cells with low adhesion to the substrate, as described in chapter 1[207].

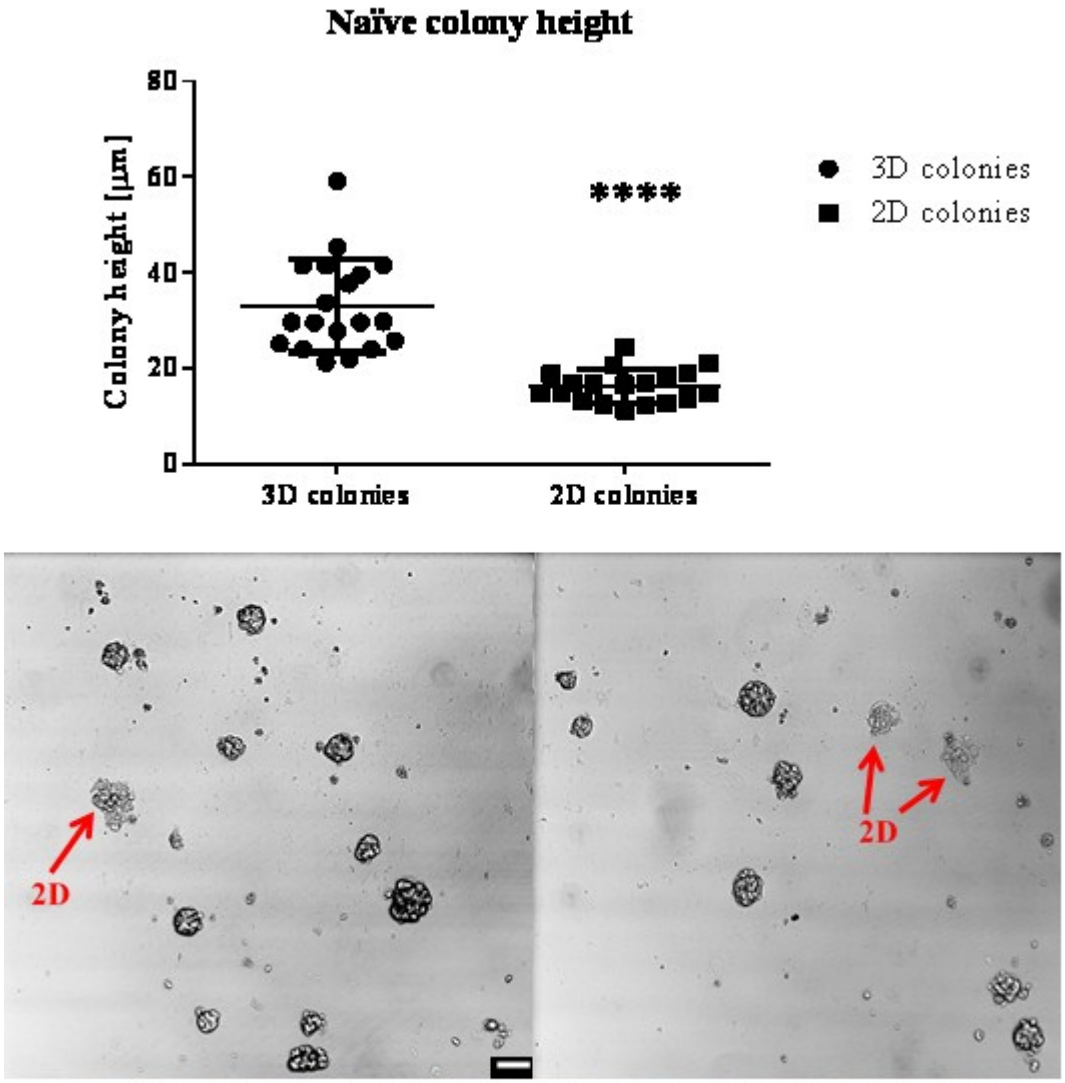

Figure 4.19: Medium height of 3D or 2D naïve HPD06 colonies. *Top: Colony height of 3D (n=19) or 2D (n=19) colonies was measured by confocal microscopy and statistical significance was measured with GraphPad Prism 6.01 software. Unpaired t-test was used to calculate significance. P-value < 0.0001. Bottom: two explicative fields of HPD06 naïve colonies on MEF feeder layer with 2D colonies (red arrow) among 3D colonies (all other colonies are 3D dome-like, as can be seen by the different bright-field contrast). Scale bar 100 µm.*

From the lateral view in fig.4.20 it is possible to see that flat colonies are composed by a single layer of cells, while the 3D colonies are composed by multiple layers of cells. Moreover, in flat colonies nuclei are flat, while in 3D colonies nuclei are vertically elongated. In fig.4.20 it is also shown a 3D reconstruction of collagen I deposition in a 2D and in a 3D colony. Collagen I is produced all around the 3D colony, confirming the shell-like deposition already shown in fig 4.8.

When looking at matrix deposition in the two types of colony, a striking difference appeared; in fact, comparing to 2D colonies where ECM proteins are not assembled or weakly organized, only 3D naïve colonies show organized ECM, as shown in fig.4.21. This panel summarizes differences in ECM deposition in 2D and 3D colonies grown on MEF feeder layer and on Matrigel coating. As shown by the green arrows, collagen I, IV, VI, laminin and fibronectin are all better organized in an extracellular network in 3D colonies or around them. Instead, as shown by the red arrows, in 2D colonies those proteins are downregulated. For example, on MEF feeders, collagen VI produced by MEF assembles only around the two 3D colonies, while the flat one is not surrounded by the thick collagen VI fibers.

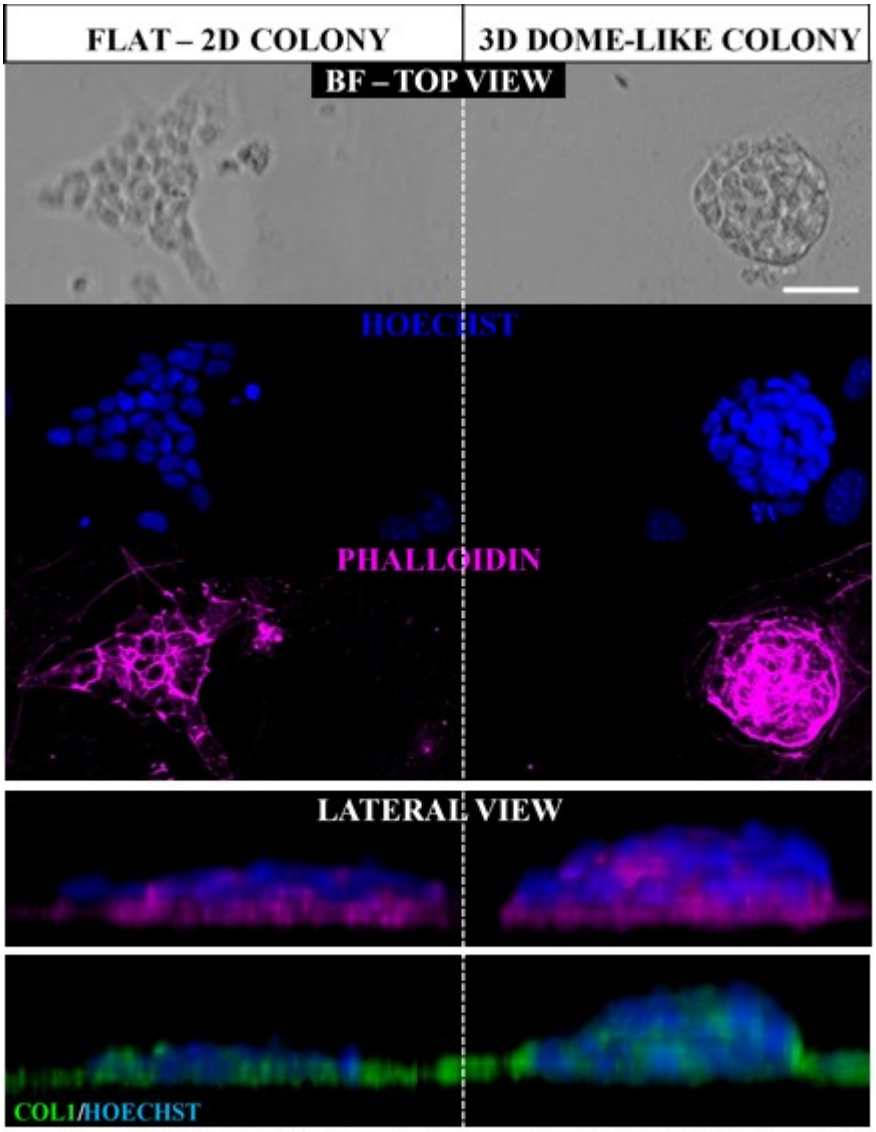

Figure 4.20: 3D and 2D naïve colonies comparison. *Naïve HPD06 cells on MEF feeder layer, staining for nuclei, COL1 and cytoskeleton. Lateral view: 3D stack reconstruction with ImageJ software.*

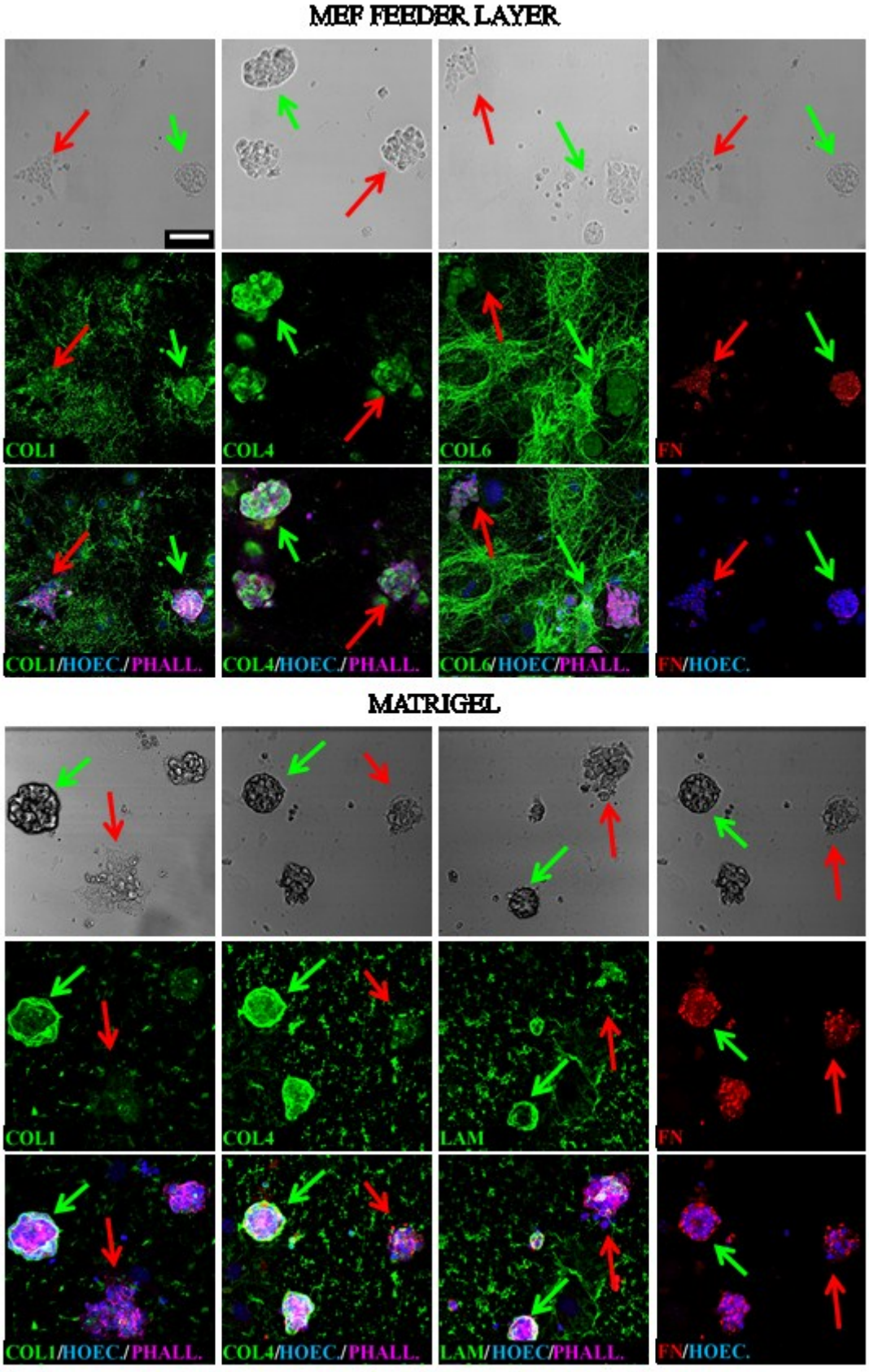

Figure 4.21: 3D naïve colonies have enhanced ECM deposition. *Green arrows indicate 3D colonies, rea arrows 2 D colonies. Naïve HPD06 colonies on MEF feeders or on Matrigel coating. Scale bar 50 µm.*

Therefore, pluripotency marker expression in 2D and 3D colonies was analyzed. Indeed, as shown in fig.4.22, 3D morphology is linked to enhanced expression of naïve pluripotency markers such as KLF17, OCT4, TFE3 and TFCP2L1, while flat morphology is linked to a downregulation of naïve pluripotency markers expression. This happens independently from the coating used to growth the cells, in fact, in the top panel cells are seeded on Matrigel, in the left one on vitronectin and on the right one on MEF feeders. The top panel of fig.4.22 shows one 2D colony and two 3D colony positively stained for collagen VI, laminin and TFCP2L1, a naïve marker. Between those two colonies, the smaller one has unorganized laminin. The flat colony instead, does not show any sign of laminin staining and is only weakly stained for collagen VI and TFCP2L1. The fact that the colony, even though with flat morphology, retains a residual TFCP2L1 expression may suggest that flat colonies are still naïve, but with a downregulated expression of naïve markers. On the left panel, the colony with 3D morphology also shows increased collagen VI deposition and OCT4 expression. In the 2D colony, collagen VI is only retained inside the cells, while in the 3D colony it is also secreted and organized. On the right panel, 3D morphology is linked to KLF17 expression, fundamental marker for naïve pluripotent stem cells recognition. As shown in this panel, KLF17 expression is nevertheless heterogeneous inside the colony itself, however, a peculiar collagen such as collagen 23 which is a transmembrane collagen (MACIT) associated with focal adhesions[139], is expressed only in cells where KLF17 expression is lower.

Next, the randomness of 3D or 2D colony morphology was evaluated by picking separately 2D or 3D colonies, dissociating them at single cell level, re-plating the cells and allowing new colonies to grow for four days. In this way, if morphology is a random choice for cells, single cell dissociation should result in random probability of 2D or 3D colony formation, while if the shape depends on the endogenous state of the cells of the colony, the original morphology should be conserved.

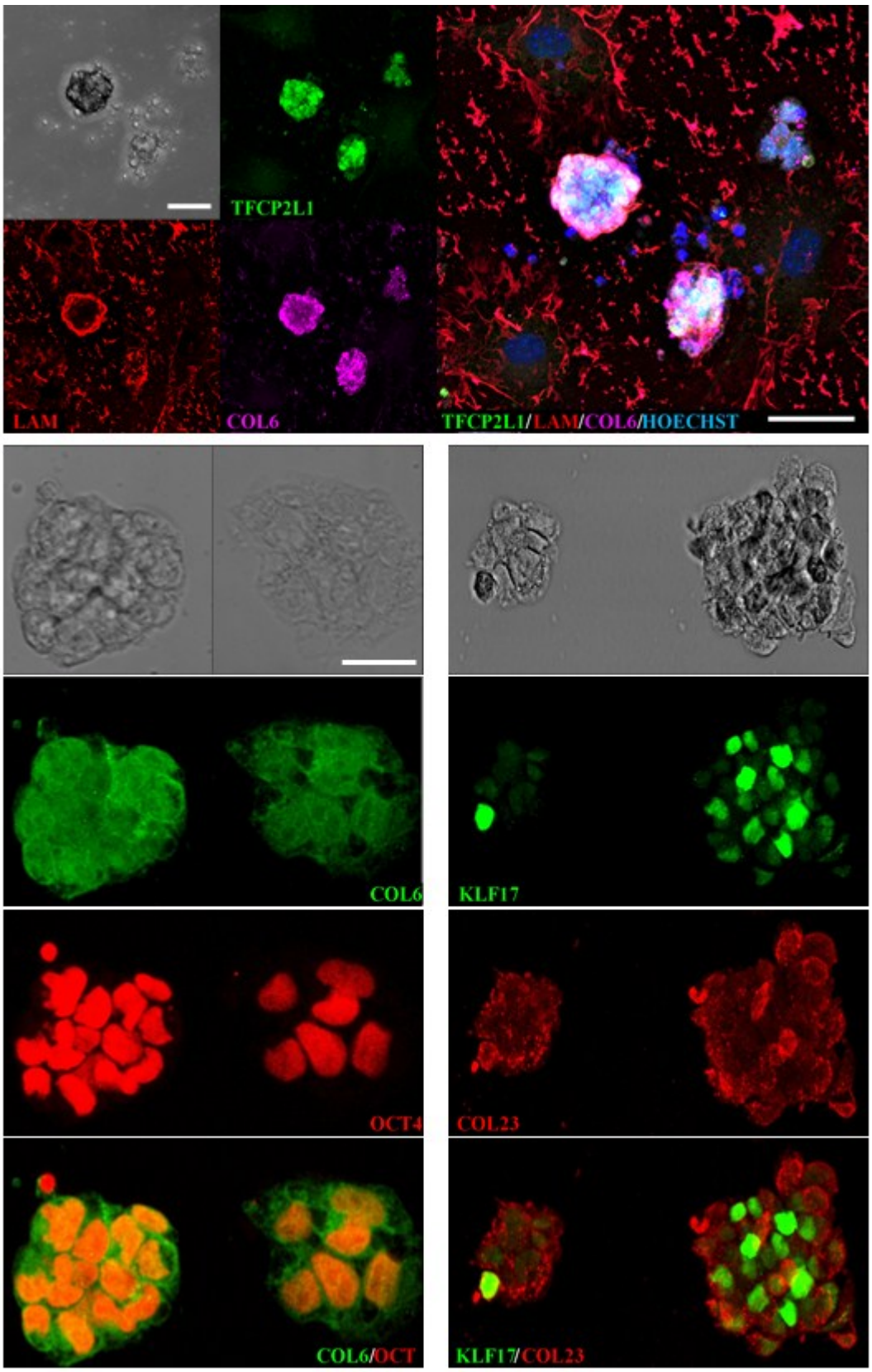

Figure 4.22: 3D shape is related to ECM proteins and naïve pluripotency markers. *Naïve HPD06 colonies seeded on Matrigel (Top panel), on VTN (Left panel) and on MEF feeders (Right panel) with flat 2D or 3D morphology. Scale bar 50 µm.*

The experiment has been performed in well and in microfluidic chip. Four days after colony picking and re-seeding, colonies have been analyzed for laminin and OCT4 expression and, as shown in fig.4.23, 3D colonies derived from 3D picked colonies are more compact, surrounded by a ring of laminin and have uniform expression of OCT4. 2D colonies derived from 2D picked colonies have a generally weaker and more heterogeneous expression of OCT4 and are not surrounded by the laminin ring. Average colony height obtained by picking and re-plating 3D colonies was 27,75 μm ± 2,323 μm (N=4) and all colonies had the typical 3D dome shape, while the average colony height obtained by picking and re-plating 2D colonies was 21,00 μm ± 0,7071 μm (N=4) and the colony had a less compact morphology. Despite additional experiments need to be done, this preliminary data suggests a link between cell-specific pluripotency state and flat or 3D shape of the resulting colony. However, the experiment should be repeated to increase sample size and confirm the result.

Bulk RNA samples have been collected from naïve HPD06 (on MEF, Matrigel and VTN), primed HPD06 and HFF, grown for one, four or seven days in microfluidic platforms or conventional wells. Moreover, whole 3D or 2D colonies from microfluidic platforms or conventional wells have been picked and lysed to recover RNA. These samples have been send to TIGEM institute (Naples) for bulk RNA-sequencing. When available, results will be presented discussed.

To organize themselves in space, cells need not only to secrete ECM proteins and to rearrange the cytoskeleton, but also to remodel the extracellular environment. In fact, the difference in ECM organization between primed and naïve colonies can be explained both by a different ECM transcripts expression profiles, as reported in fig.4.1, but also by a different production of ECM remodeling enzymes. Indeed, as reported in fig.4.24, also metalloproteases and other ECM remodeling protein expression have a distinct expression profile in fibroblasts, naïve and prime pluripotent stem cells.

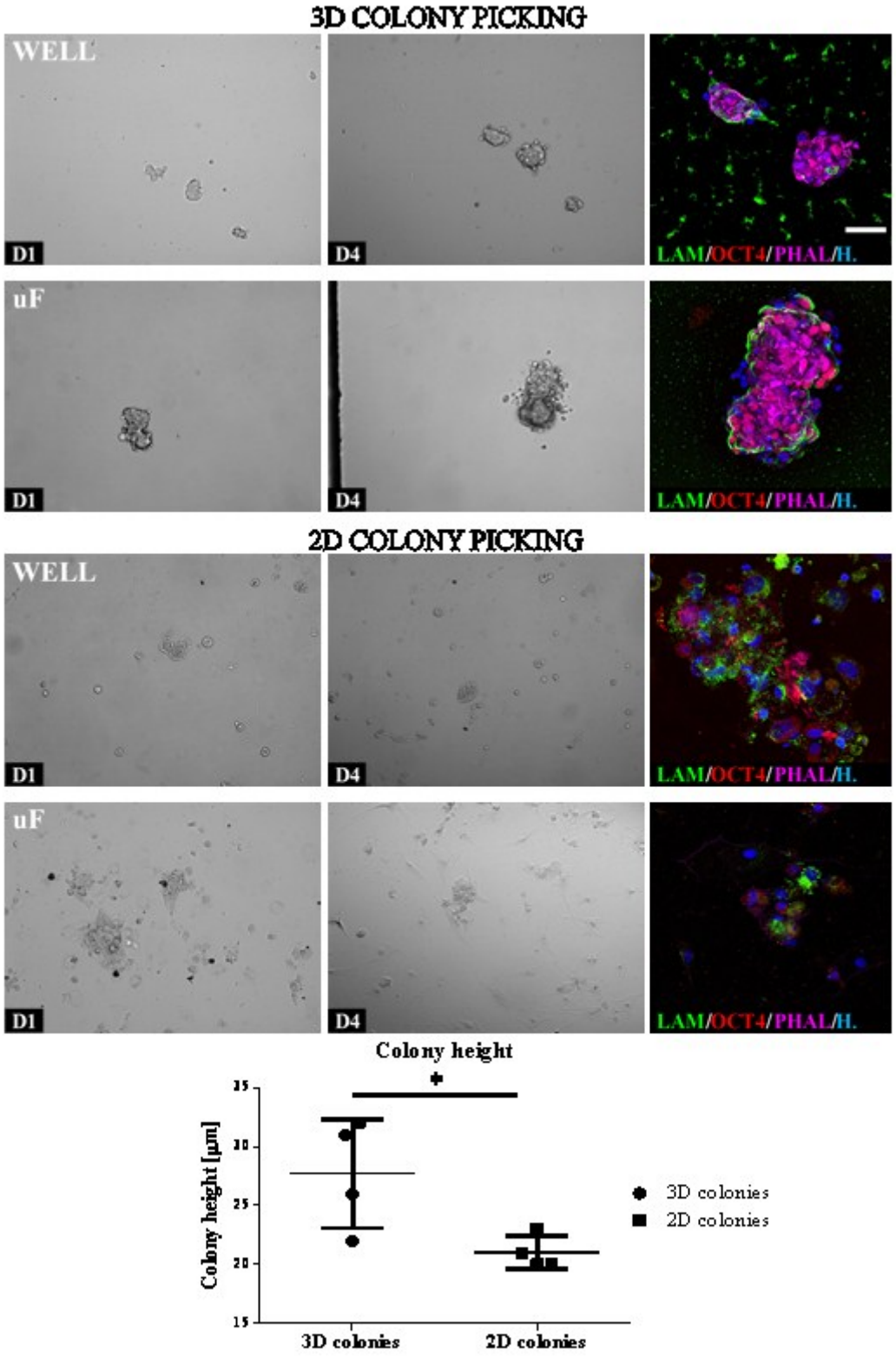

***Figure 4.23: 3D and 2D colony picking. Top**: 3D colonies derive from 3D picked colonies, both in microfluidic devices and in wells. **Middle**: 2D colonies derive from 2D picked colonies, both in microfluidic devices and in wells. Scale bar 50 µm. **Bottom**: average colony height after picking. Colony height measured 4 days after picking and re-seeding. 3D colonies: 27,75 µm ± 2,323 µm (N=4); 2D colonies: 21,00 µm ± 0,7071 µm (N=4). p-value: 0.032.*

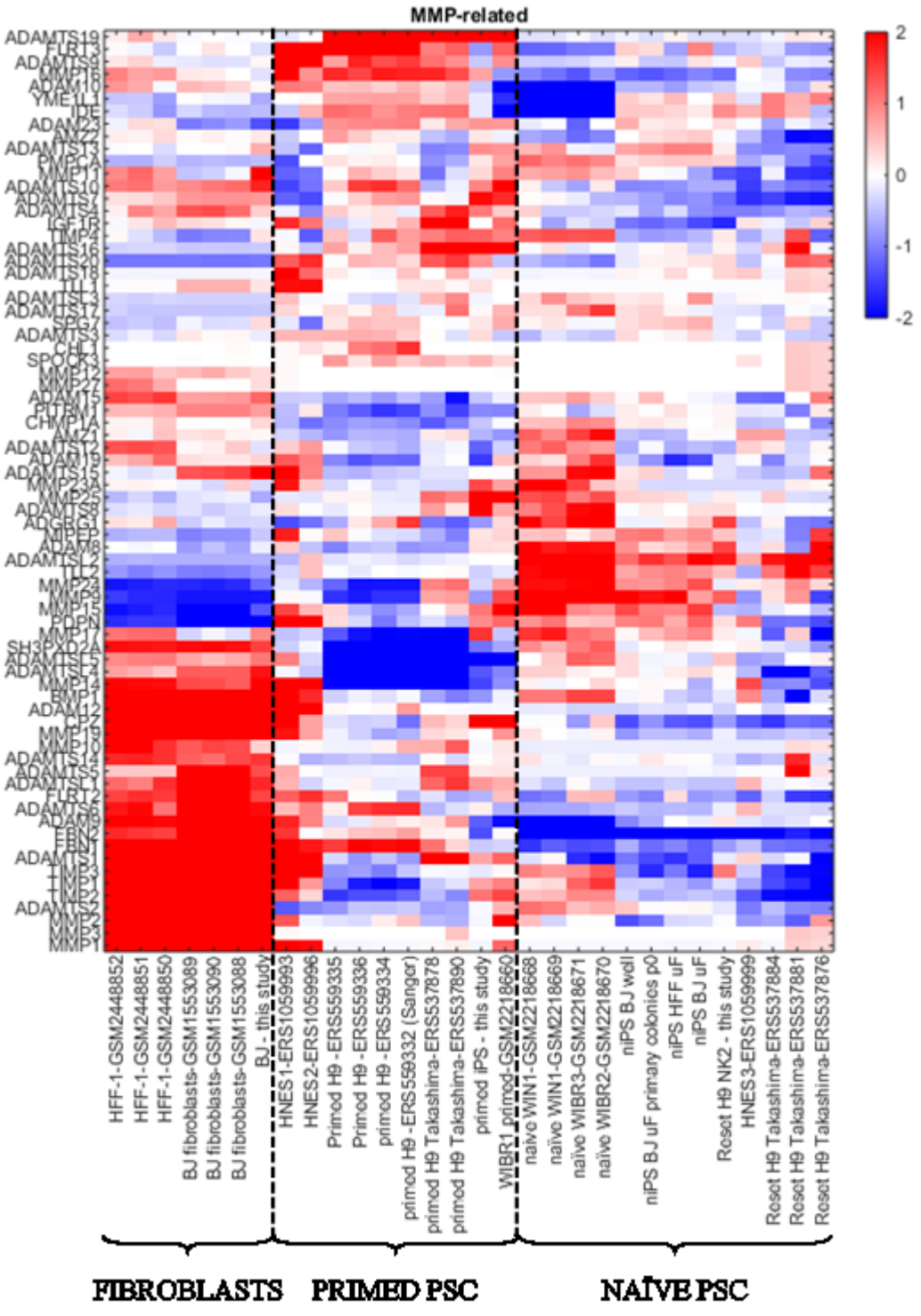

Figure 4.24: MMP-related protein gene expression in fibroblasts, naïve or primed PSC. RNA-sequencing database analysis of KEGG pathway: MMP-related proteins.

4.3.2. Insight into cell-ECM interaction in naïve pluripotent stem cells

Since naïve and primed pluripotent stem cells have such a remarkable difference in ECM gene expression and protein deposition, components of the cell-ECM adhesion pathways have been investigated, with particular focus on integrin expressions, which are the first proteins involved in cell-ECM engagement and on proteoglycans expression. As shown in fig.4.25, fibroblasts, naïve and primed PSC have different expression profiles when compared

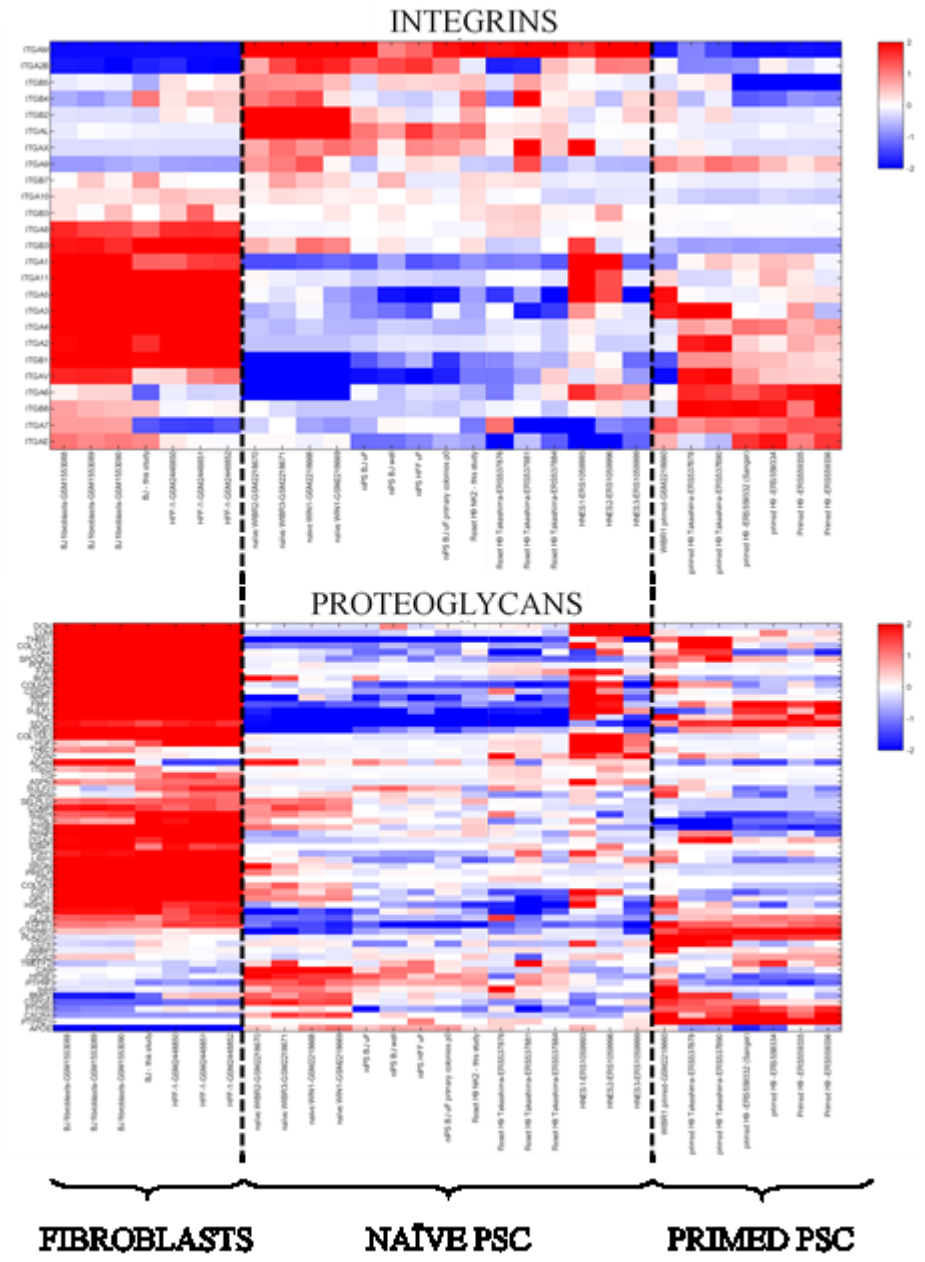

Figure 4.25: Integrins and proteoglycans gene expression in fibroblasts, naïve or primed PSC. RNA-sequencing database analysis of KEGG cathegory: proteoglycans and of human integrins.

among integrins or proteoglycans expressions. The most upregulated integrins in naïve samples are integrin αM, α2B, αL, αX, α9, β2, β4 and β5, of which only α9, β4 and β5 have been previously related with stemness, as discussed below. Since the role of those integrins has never been deeply investigated, few tools and assays (such as blocking antibodies or molecules designed to bind to the active site) are available to study these proteins. Gene silencing or molecular antagonism experiments are needed to study the role of these integrin. As a preliminary approach, this work started with the analysis of more well-characterized integrins such as integrin α4 and β1, which are among the most studied integrins for pluripotency maintenance and for binding the ECM proteins analyzed in previous results of this work. However, the role of this integrins has never been analyzed in naïve pluripotent stem cells. In addition, it is important to notice that, even if α4, α6, αV, β1 and other integrins well known to be important for embryogenesis are downregulated in naïve cells compared to the other samples of the database, this does not imply that naïve cells do not express them at all.

Therefore, blocking antibodies against the extracellular portion of integrin α4 and β1 have been used to disturb integrin attachment with ECM components. In this experiment, naïve HPD06 cells have been seeded as single cells in microfluidic channels on MEF feeder layer and have been treated with anti-α4 blocking antibody, anti-β1 blocking antibody or with a combination of both. Two different conditions have been setup: in the first one the treatment has been started at day 0, when cells were still in suspension, in the second at day 1, after cells had adhered to the MEF layer. With this approach, the difference between the role of this integrins in cell-adhesion process has been discerned from the role of the integrins in colony maintenance. In particular, in the first case (named “Blocking from Day 0 in fig.4.26), Naïve HPD06 colonies have been dissociated at single-cell level and seeded in the microfluidic channels in presence of anti-α4 blocking antibody, anti-β1 blocking antibody or with a combination of both. Instead, in the second case (named “Blocking from Day 1 in fig.4.26), naïve HPD06 colonies have been dissociated at single-cell level and seeded without blocking antibodies in the microfluidic channels. The

following day, when cells were already attached, medium was supplemented with anti-α4 blocking antibody, anti-β1 blocking antibody or with a combination of both. Both conditions were kept in medium with blocking antibodies for four days. After four days colony number has been calculated and colony diameter has been measured. As shown in fig.4.26, blocking α4 integrin interaction with matrix proteins reduced colony number inside the microfluidic channel and overall colony diameter, thus demonstrating an anti-proliferative effect on naïve pluripotent stem cells. Blocking β1 integrin instead did not have a significative influence on colony number or on colony diameter, demonstrating the inactivation of this integrin in naïve cells. However, the treatment with blocking antibodies had a visible effect on MEF morphology: on treated channels, MEF cells looked shrunk, leaving large empty areas in the feeder layer. As shown in fig.4.26, blocking α4 and β1 integrin gave also an effect on colony morphology: in samples treated from Day 0, in control channels, the 3D dome-shape morphology prevailed, while channels treated with anti-α4 blocking antibody, flat colonies were more frequent than in the controls. This data was calculated as 2D colony number on total colonies counted in the channel. In samples treated from Day 1 instead, the increase in 2D colonies fraction is increased in all conditions where blocking antibodies were administered. However, the overall fraction of 2D colonies in these samples is lower comparing to the samples treated from Day 0. Nevertheless, the results reported are preliminary data, which need to be repeated to increase sample numerosity and statistical significance.

Since blocking β1 integrin had only a mild effect on naïve stem cells growth, an opposite approach has been applied. Naïve HPD06 colonies have been treated with Mn^{2+}, which aspecifically activates integrins. Naïve HPD06 colonies have been seeded on MEF feeders after single cell dissociation and treated with Mn^{2+} from day 1 to day 4 to understand Mn^{2+} effect on forming colonies, or just from day 3 to day 4 to dissect Mn^{2+} effect on already formed 3D colonies (fig.4.27).

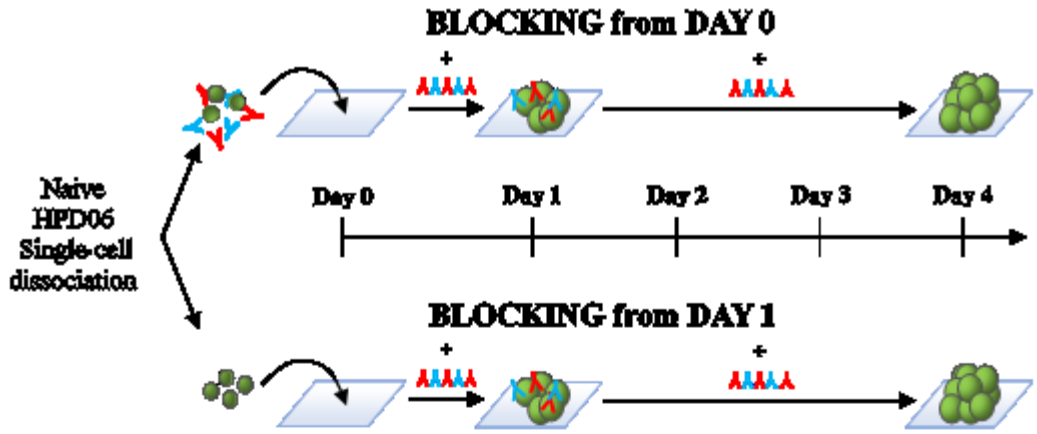
BLOCKING from DAY 0
Naive
HPD06
Single-cell
dissociation
Day 0
Day 1
Day 2
Day 3
Day 4
BLOCKING from DAY 1

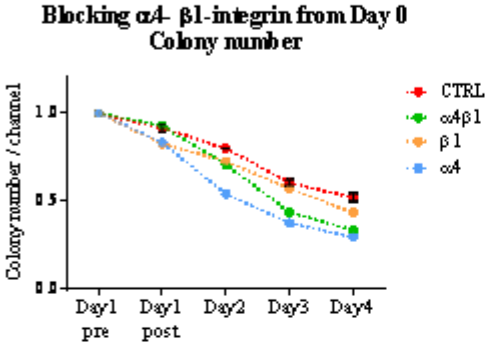
Blocking α4- β1-integrin from Day 0
Colony number
Colony number / channel
CTRL
α4β1
β1
α4
Day1 pre
Day1 post
Day2
Day3
Day4

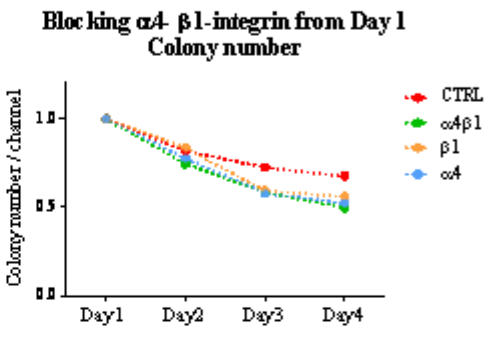
Blocking α4- β1-integrin from Day 1
Colony number
Colony number / channel
CTRL
α4β1
β1
α4
Day1
Day2
Day3
Day4

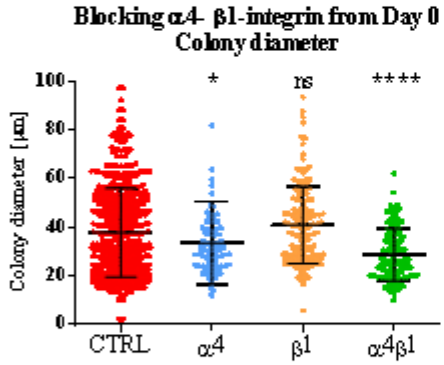
Blocking α4- β1-integrin from Day 0
Colony diameter
Colony diameter [µm]
*
ns
****
CTRL
α4
β1
α4β1

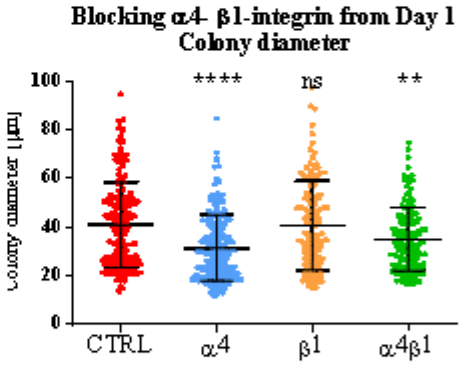
Blocking α4- β1-integrin from Day 1
Colony diameter
Colony diameter [µm]
****
ns
**
CTRL
α4
β1
α4β1

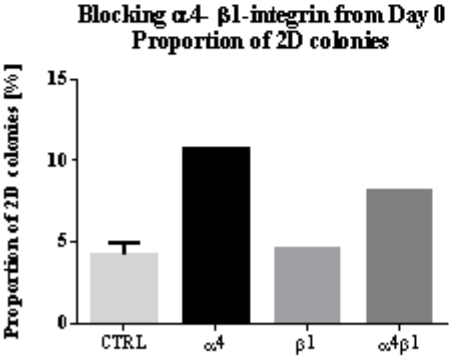
Blocking α4- β1-integrin from Day 0
Proportion of 2D colonies
Proportion of 2D colonies [%]
CTRL
α4
β1
α4β1

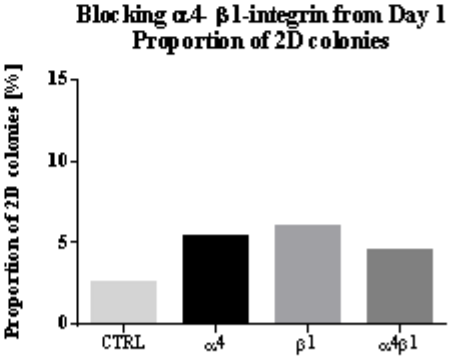
Blocking α4- β1-integrin from Day 1
Proportion of 2D colonies
Proportion of 2D colonies [%]
CTRL
α4
β1
α4β1

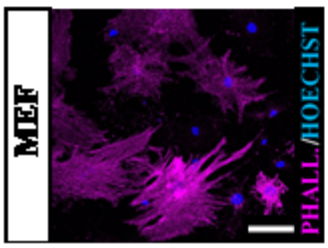
MEF
PHALL./HOECHST

As reported in fig4.27, integrin activation did not have significative effect on colony number if given from day 1, when naïve cells are at single-cell state, while it results in colony detachment if given at day 3 when colonies are grown. On contrary, Mn^{2+} treatment reduces overall colony diameter if given from day 1, while it has no significative effect on colony diameter if administered from day 3. Taken together these data indicates that integrin aspecific activation when cells are at single-cell state does influence the maintenance of colony number after. Instead, integrin activation on grown colonies induces cell detachment. However, more experiments should be performed to investigate long-term effect of Mn^{2+} treatment on naïve pluripotent stem cells.

As previously seen in fig.4.25, also proteoglycans show a different pattern of gene expression between fibroblasts, naïve and primed pluripotent stem cells. To investigate whether blocking proteoglycan attachment with matrix proteins could have an effect on naïve cells, a blocking antibody against chondroitin

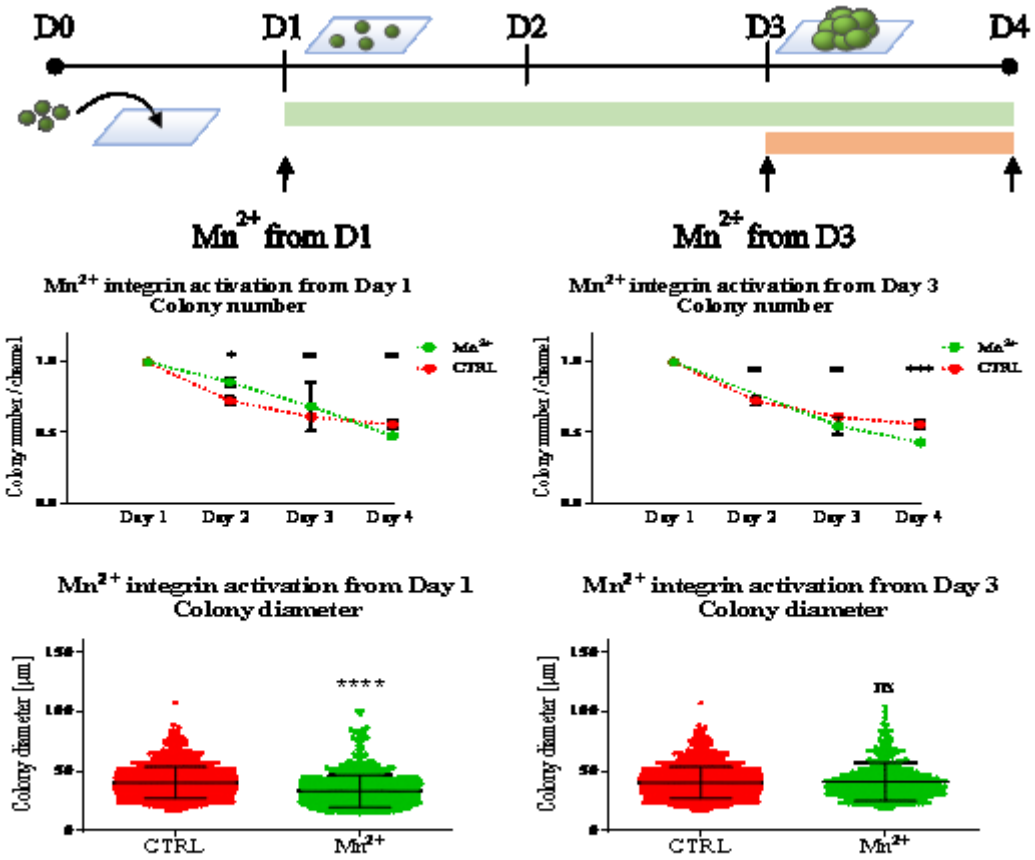

Figure 4.27: Integrin aspecific activation by Mn^{2+}treatment. Top: experiment design. Middle: colony number variation normalized on starting cell number. Bottom: colony diameter after four days of treatment.

sulfate proteoglycans (CSPG) domain was administered to naïve HPD06 colonies. This target was shown because CSPG family proteoglycans, such as CSPG5 are upregulated in naïve colonies, as reported in fig.4.25. Therefore, the same experimental plan designed for integrin α4 and β1 blocking assay was applied and, as shown in fig. 4.28, CSPG blocking for four days resulted in colony number and colony diameter decrease. Moreover, CSPG blocking from Day 0 promoted an increase in 2D colonies proportion, while its blocking from Day 1 did not have a significative effect on 2D colony number. However, data should be repeated to increase sample size and significance.

4.3.3. Naive and Primed PSC have different FAK and YAP protein localization

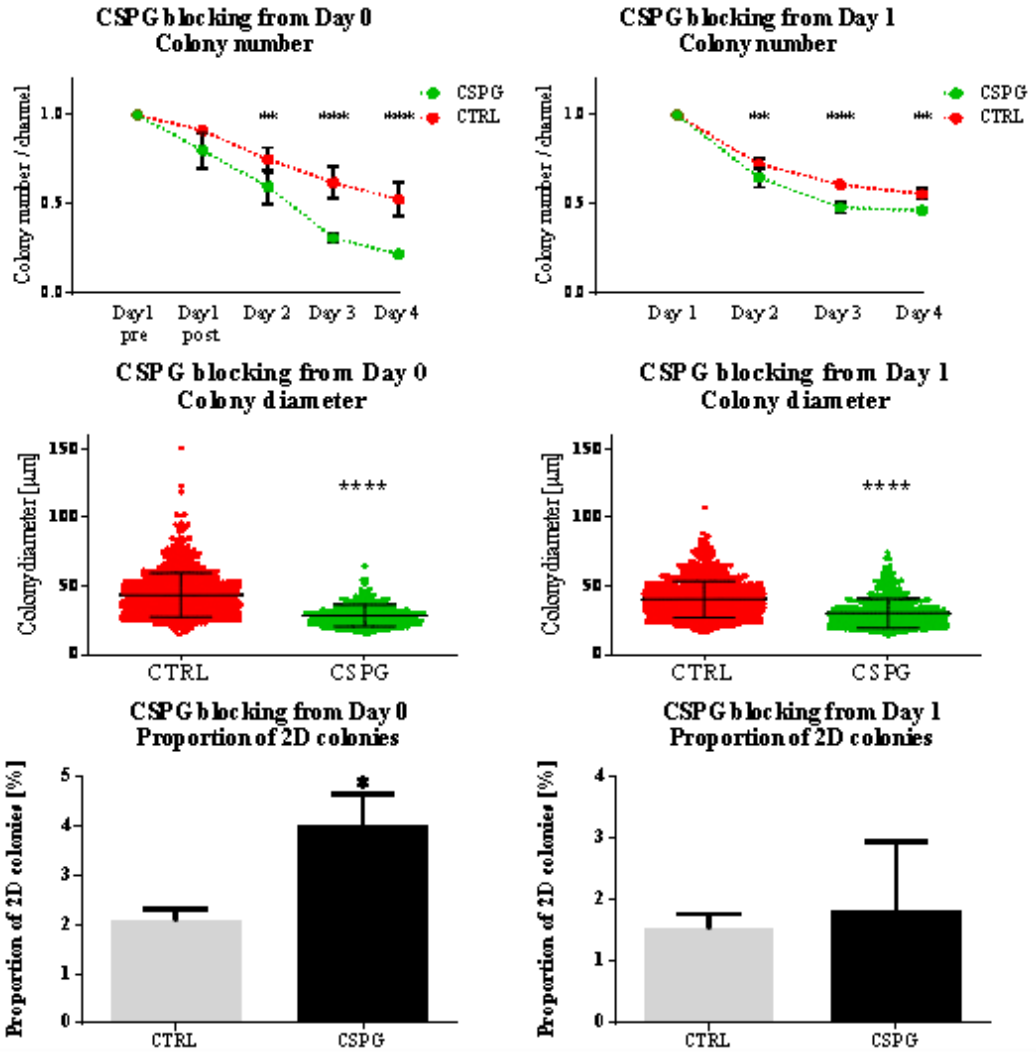

*Figure 4.28: Blocking CSPG proteoglycan assay. **Top**: colony number variation. **Middle**: colony diameter after four days of treatment. CTRL n=730 colonies, CSPG n=242 colonies). **Bottom**: percentage of 2D colonies after CSPG blocking treatment.*

It has extensively been described in paragraph 1.2.3 how extracellular matrix influences also the stiffness of the environment in which cells are embedded. Therefore, the ECM compartment can send mechanic stimuli to the cell through a complex of signaling cascades known as mechanotransduction. Thus, next, mechanotransduction and signaling pathways that connect cell to the nucleus have been investigated in naïve and primed PSC. In fact In fig. 4.28 it is possible to appreciate how focal adhesion-related proteins and Hippo pathway (pathway involved in mechanotransduction that exploits YAP/TAZ as effector)-related proteins have different expression signatures in fibroblasts, naïve or primed pluripotent stem cells. In fig.4.29, fibroblasts samples are grouped on the left, primed PSCs samples in the middle and naïve PSCs on the right. These evidences point out a different role of these pathways in pluripotent cells comparing to differentiated cells, but also a different activation in primed comparing to naïve PSCs. Besides a different gene expression of focal adhesions-related genes and of Hippo pathway-related genes, it has been reported in literature that a fundamental protein such as FAK assumes a different localization in pluripotent or differentiated cells[194,197,198]. Moreover it has been demonstrated that YAP activity is related to its nuclear or cytoplasmic localization[161,162]. Therefore, FAK and YAP localization have been analyzed in naïve and primed pluripotent stem cells.

As shown in fig.4.30, in 3D dome-shape naïve colonies, FAK has a diffused localization, inside the cells, and clearly, it is not concentrated in focal adhesions. If the bottom and the top part of the 3D colonies are analyzed separately, it is possible to notice that FAK is more expressed at the bottom and at the edge of the colony, where the deposition of the ECM network is higher. In 2D flat colonies instead, FAK is more concentrated in focal adhesions, and, in fact, instead of a diffused fluorescence signal, 2D colonies are scattered of bright FAK positive spots. As it is possible to see by looking at cytoskeleton organization stained with phalloidin, where actin ring surrounds the colonies as in 3D colonies, indicating absence of punctual focal adhesions, FAK is disengaged and diffused between nucleus and cytoplasm.

Instead, when actin ring is disassembled and stress fibers are formed as in 2D colonies, FAK is engaged in focal adhesions.

In primed pluripotent stem cells colonies, as shown in fig.4.31, FAK has a different localization in the center of the colony comparing to the edge of the colony. It has been demonstrated by traction force microscopy that in primed colonies, cells at the edge of the colony have stronger mechanical interactions with the extracellular matrix than those at the center of the colony[296]. Indeed, in the center, where cells have lower contacts with the ECM network and less mechanical stimuli, FAK has a diffused localization, similar to the one reported for naïve colonies. At the edge of the colony instead, cells have a stronger interaction with the matrix and FAK shows a total nuclear localization. Total FAK protein expression has been analyzed by Western blot (fig.4.30) in HFF, naïve and primed PSC. HL-60, a line of promyeloblast from peripheral blood was used as control, since circulating cells do not have active focal adhesions. This analysis shows similar amount of FAK in the two pluripotent stages, but as demonstrated by immunofluorescence stainings (fig.4.30 and fig.4.31) with different cellular localization. Moreover, total FAK amount is higher than in differentiated HFF, highlighting once more the importance of this protein for pluripotency. As control of naïve and primed pluripotency, OCT4 is expressed both in primed and naïve pluripotent stem cells, while KLF17 only in naïve cells.

Taken together, these data confirm FAK non-canonical activation in primed and naïve pluripotent stem cells, even though more experiments are needed to evaluate the biological functionality of this non-canonical pathway in these cells.

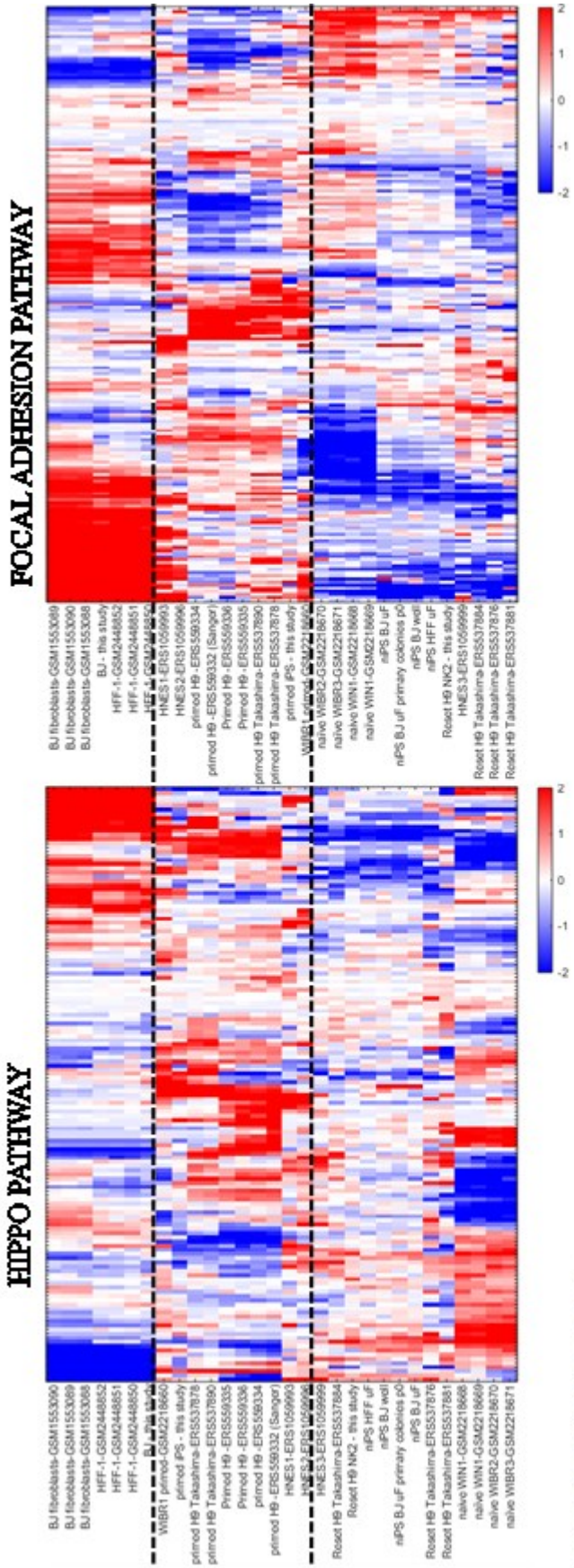

Figure 4.29: Focal adhesion pathway and Hippo pathway gene expression in fibroblasts, naïve or primed PSC. *RNA-sequencing database analysis of KEGG category: human focal adhesion and human Hippo pathway.*

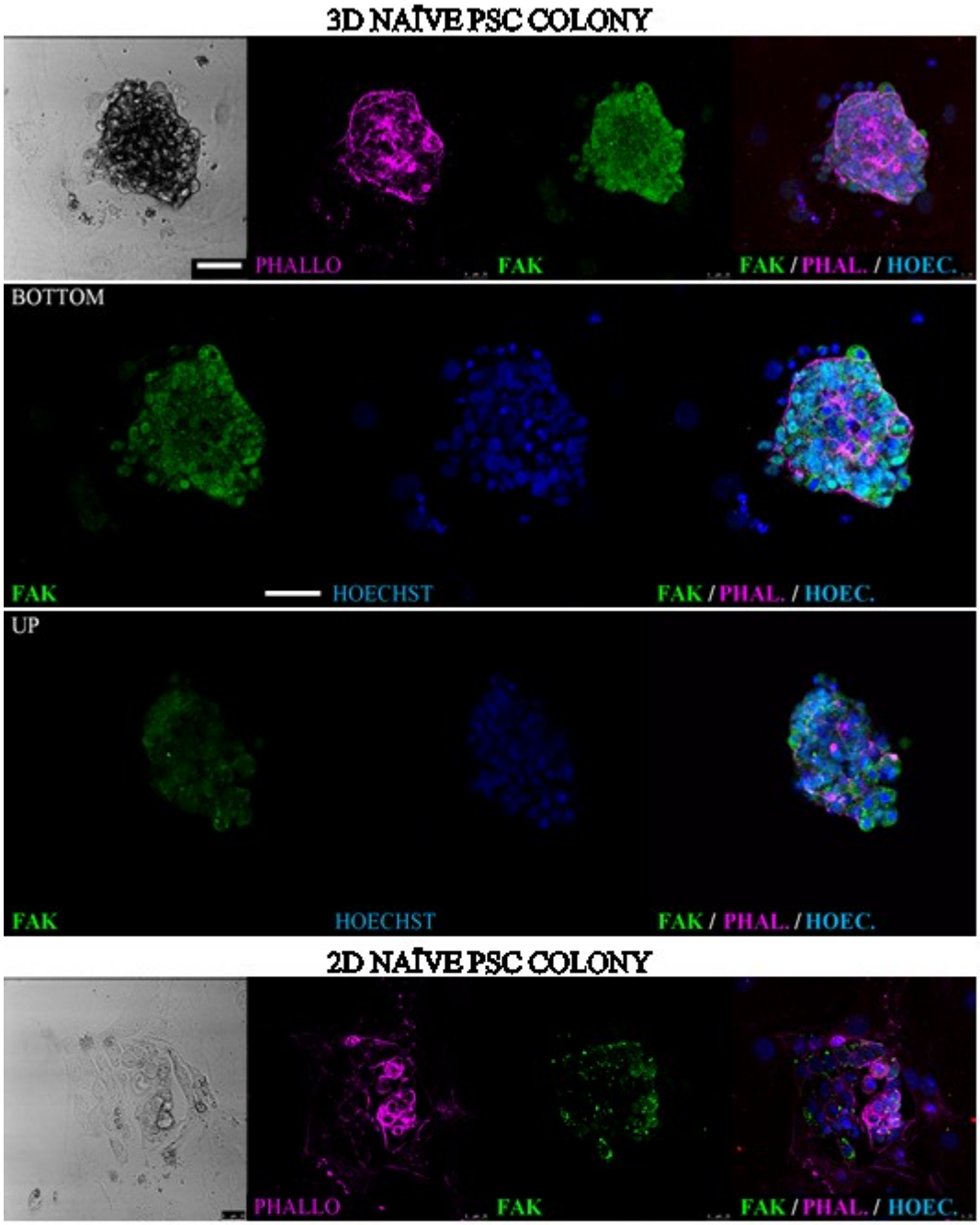

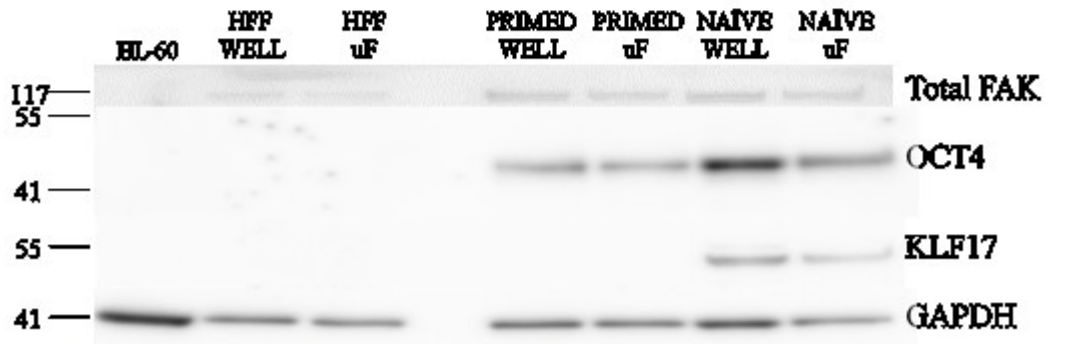

Figure 4.30: FAK localization in 2D or 3D naïve HPD06 colonies. *Scale bar 50 µm. In 3D colonies, the first row of figures is composed by stacks of images in the z-axis, while the magnifications are composed by a single confocal image.* ***Wester blot****: protein expression of FAK, OCT4 and KLF17 in HFF, naïve and primed HPD06 and in HL-60 promyeloblast line.*

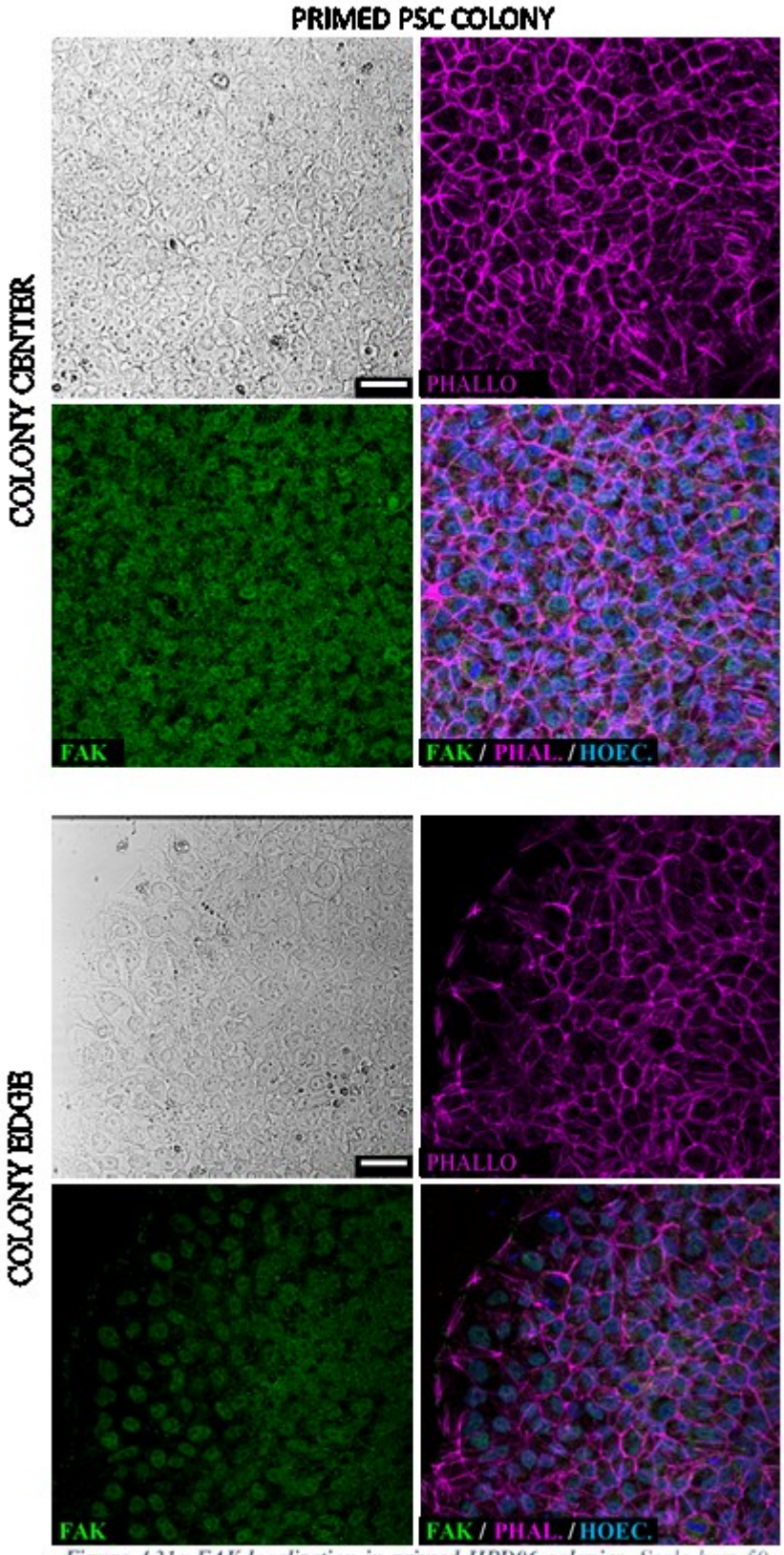

Figure 4.31 : FAK localization in primed HPD06 colonies. *Scale bar: 50 µm. Top: imaging of the center of the colony. Bottom: edge of the colony.*

Afterwards, YAP expression and localization was analyzed in correlation with FAK localization in naïve and primed HPD06 pluripotent stem cells (fig. 4.32 and 4.33). As shown in fig. 4.32, in 3D naïve HPD06 also YAP has a diffused localization, meaning that YAP-mediated transcription is not fully active. It is possible to appreciate that some cells at the bottom and at the edge of the colony have more nuclear YAP localization, while in cells at the top of the colony YAP is diffused both in the cytoplasm and in the nucleus. It is important to notice that neither at the bottom or at the top of the colony YAP is excluded from the nucleus, meaning that YAP-mediated transcription of downstream genes is always at least partially active in naïve 3D colonies. In 2D colonies instead, YAP has a more defined nuclear localization.

In primed HPD06 colonies, as shown in fig.4.33, YAP expression pattern changes from the center to the edge of the colony. In fact, in the center of the colony YAP has is diffused both in the cytoplasm and in the nucleus of the cells, even if some nuclei have a more intense and defined YAP signal. At the edge of the colony, instead, YAP has a well-defined nuclear localization.

To investigate FAK-YAP relationship in naïve pluripotent stem cells, Latrunculin-A, a chemical compound that interferes with actin cytoskeleton polymerization, was administered to naïve PSCs colonies for 30 minutes. In previous works od differentiated cells[161], Latrunculin-A treatment provoked the exclusion of YAP form the nucleus. As shown in fig.4.34, after Latrunculin-A treatment, the smooth surface of naïve HPD06 colonies becomes irregular and full of blebs and the actin ring is completely disassembled. FAK and YAP response is shown in fig.4.35: differently from what was reported in differentiated cells, after Latrinculin-A treatment, both YAP and FAK localize in the nucleus of the cells, independently whether considering the bottom or the top of the naïve colony.

This results indicates once more the relationship between FAK, the actin cytoskeleton and YAP, also in naïve pluripotent stem cells and that those players have a singular role in pluripotency.

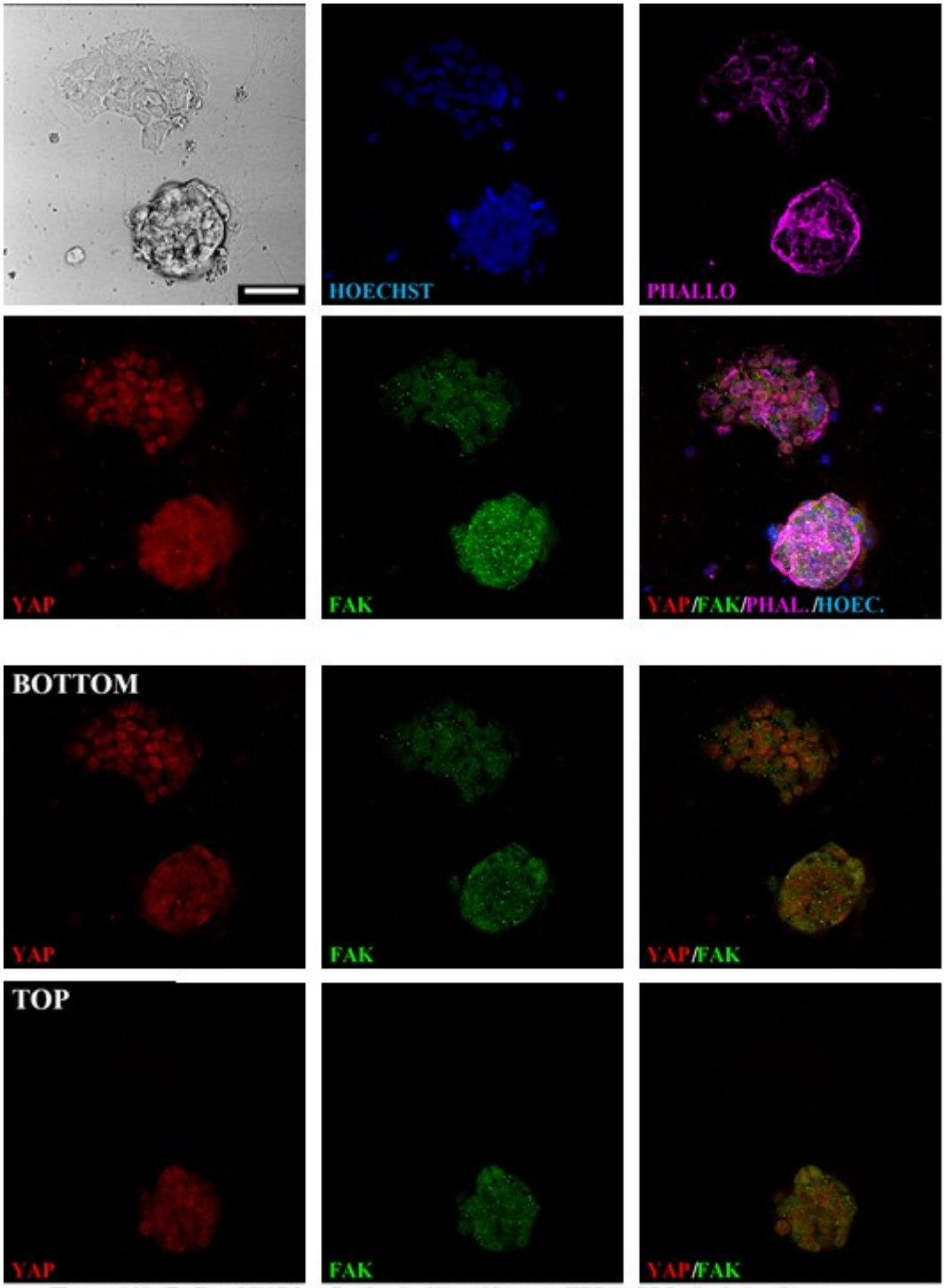

Figure 4.32: FAK and YAP localization in 3D or 2D naïve HPD06 PSCs. Scale bar 50 µm.

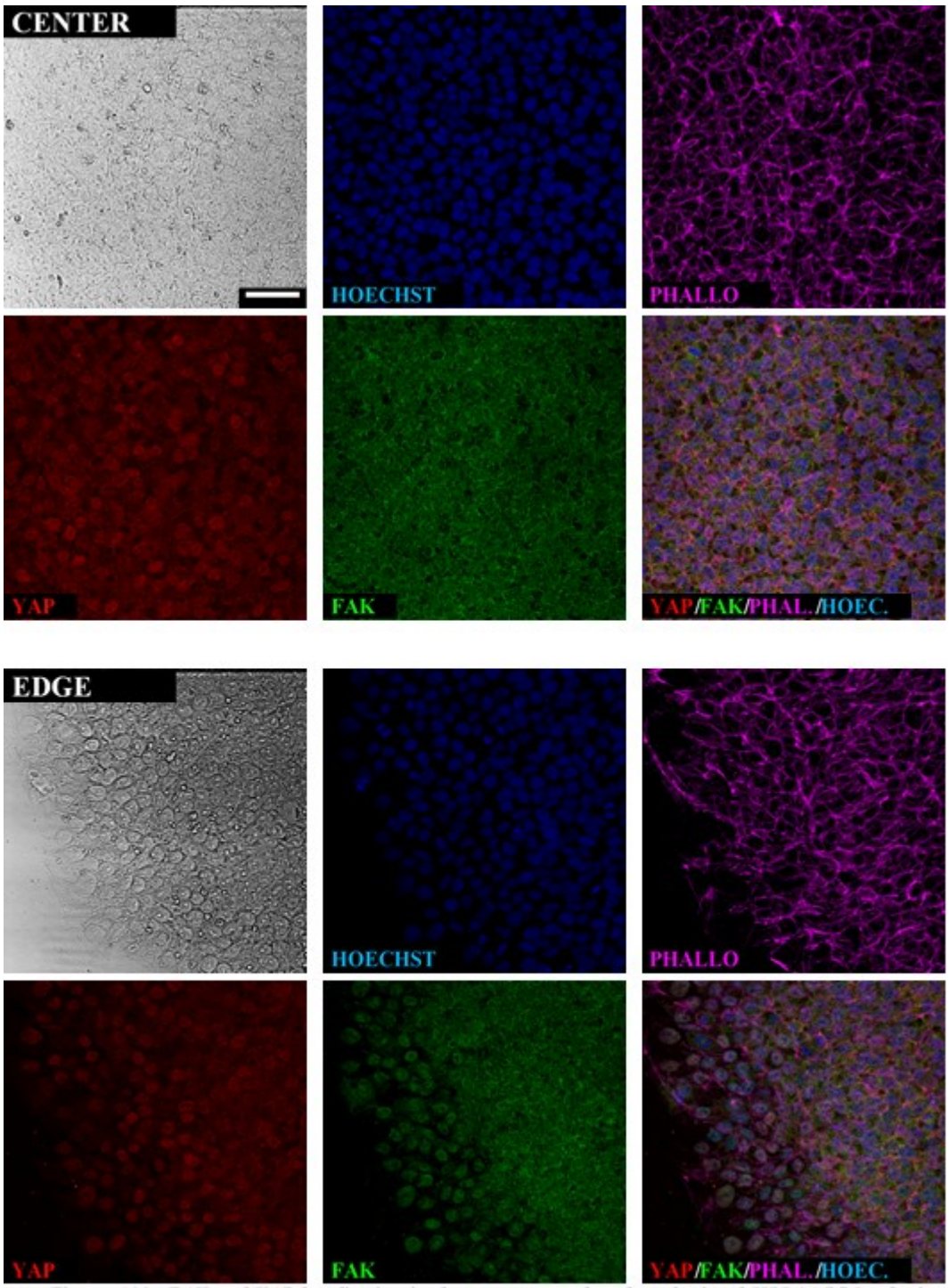

Figure 433: FAK and YAP localization in the center or at the edge of primed HPD06 PSC colonies. Scale bar 50 µm.

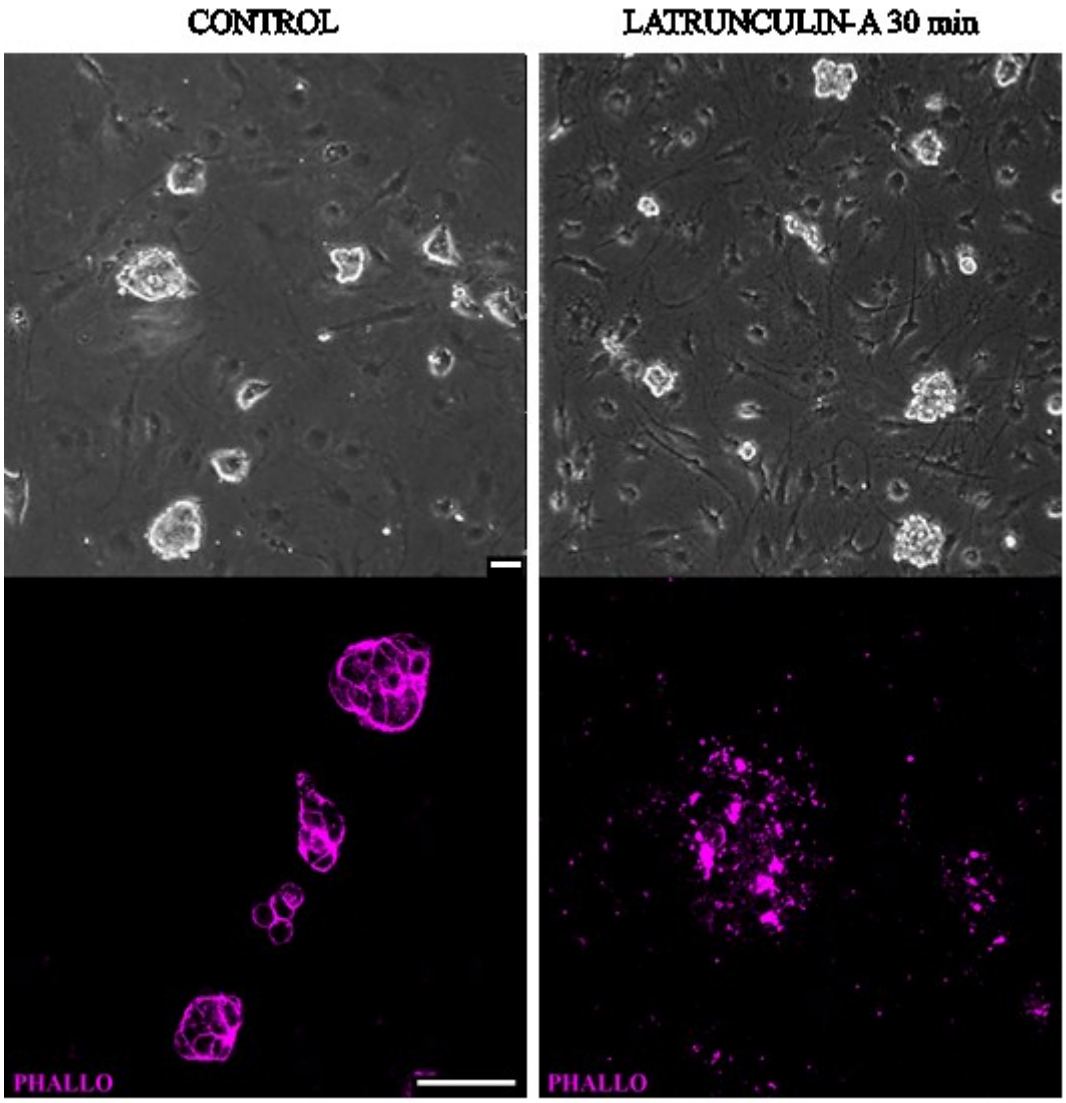

Figure 4.34: Latrunculin-A treatment on naïve HPD06 colonies shape. *Disassembled actin cytoskeleton. Scale bar 50 µm.*

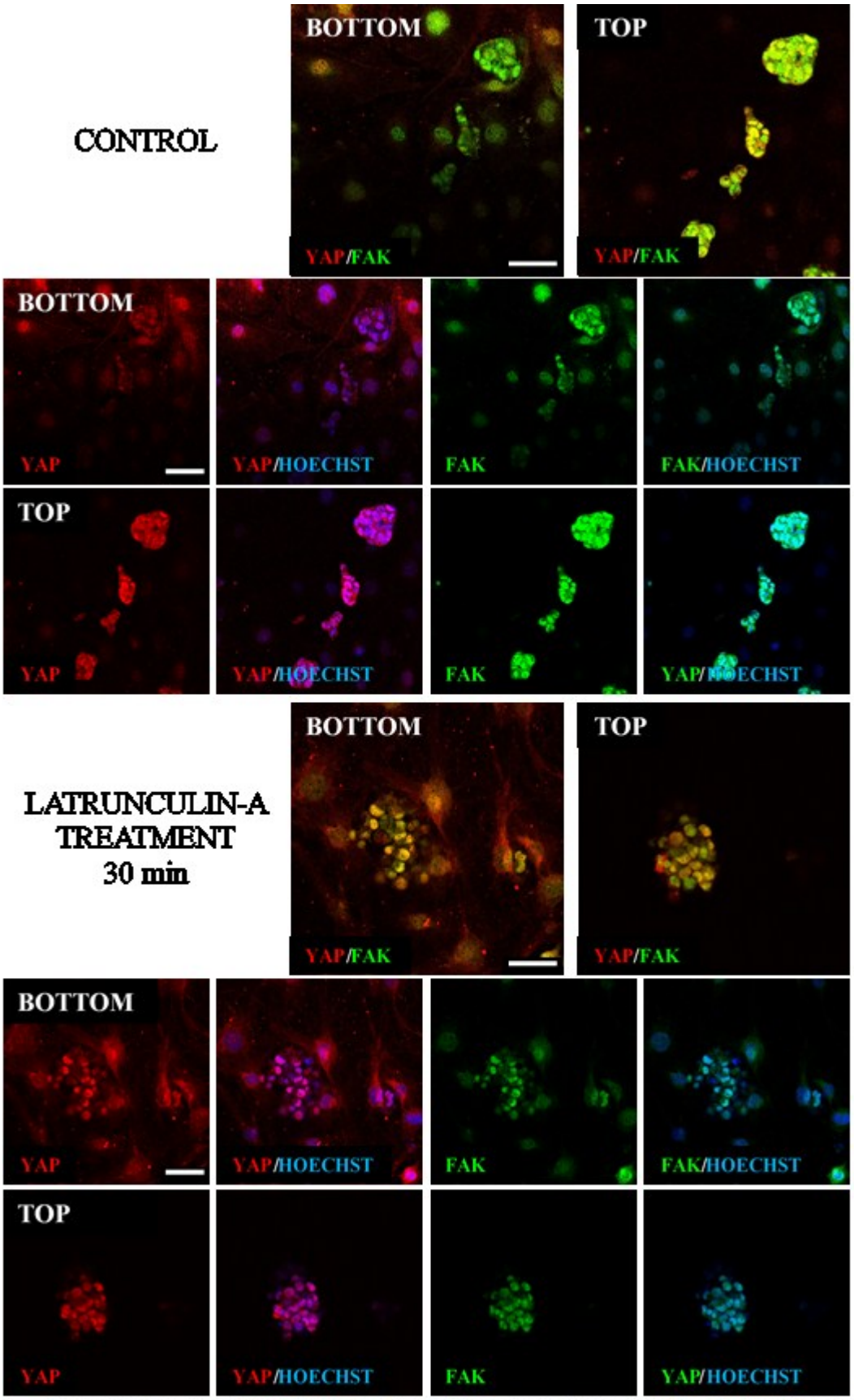

Figure 4.35: Latrunculin-A treatment on naïve HPD06 colonies. FAK and YAP localization. Scale bar 50 μm.

4.4. ANALYSIS OF ECM AFTER REPROGRAMMING IN CONVENTIONAL AND CONFINED ENVIRONMENT

It has been demonstrated that microfluidic environment promotes high efficiency cell reprogramming, with substantial increase in reprogramming efficiency compared to other methods already available that exploit conventional cell culture devices[207]. In Luni et al. 2016, an increase in TGF-β1 endogenous pattern activation is reported as partial explanation for this result, but only with a high throughput approach it will be possible to identify all the players involved in this stunning increase in reprogramming efficiency. With SILAC-mass spectrometry technique, the secretome of human fibroblasts (which represent the starting point of cell reprogramming) and of hiPSCs (which are the end point of the process) have been analyzed, as already reported in chapter 4.2. These data point out how microfluidic environment promotes extracellular proteins secretion and accumulation and Gene Ontology analysis identify extracellular matrix components as the first category represented in proteins overexpressed in microfluidics. Therefore, ECM deposition was analyzed at the end of reprogramming process in microfluidics and in conventional cell culture devices.

4.4.1. ECM deposition is enhanced around and over the newborn iPSC colonies in microfluidics

At the end of a typical cell reprogramming experiment, some of the fibroblasts that underwent the process will give rise to iPSC colonies, which can be identified among the un-reprogrammed fibroblasts as a compact mass of small cells with high nucleus to cytoplasm ratio. The non-reprogrammed fibroblasts will generally arrange around the colony providing support as feeder cells. To verify the organization of ECM network in reprogrammed colonies and in non-reprogrammed fibroblasts, immunofluorescence staining was performed. In fig.4.36 and fig.4.37, the staining of extracellular matrix proteins (collagen I, IV, VI, laminin and fibronectin) on cells at the end of reprogramming process highlights clear differences in ECM deposition and

organization between non-reprogrammed fibroblasts and newborn hiPSC colonies.

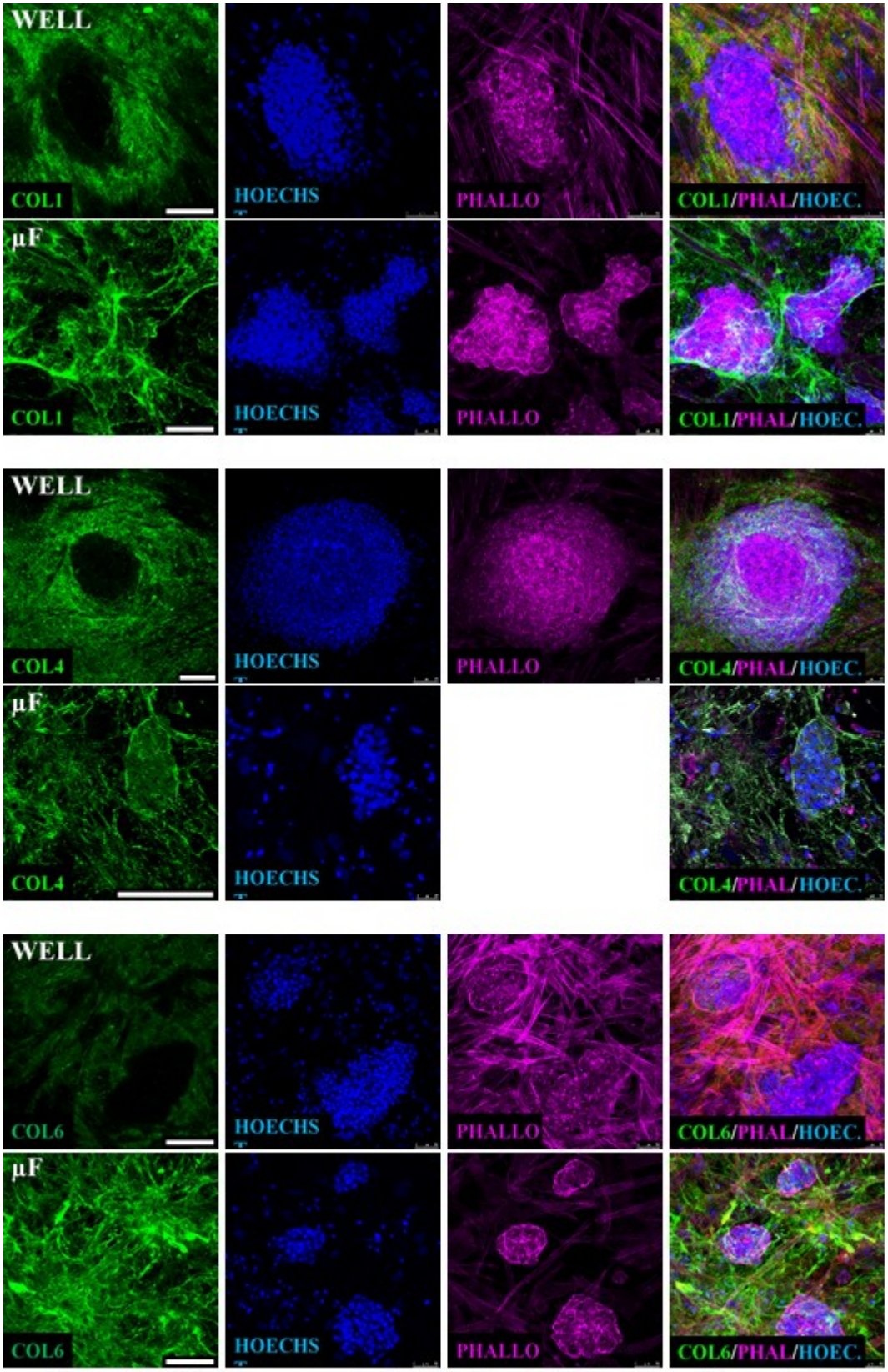

Figure 4.3 6: ECM after reprogramming in well and in microfluidic platforms (first part). Scale bar: 100 µm.

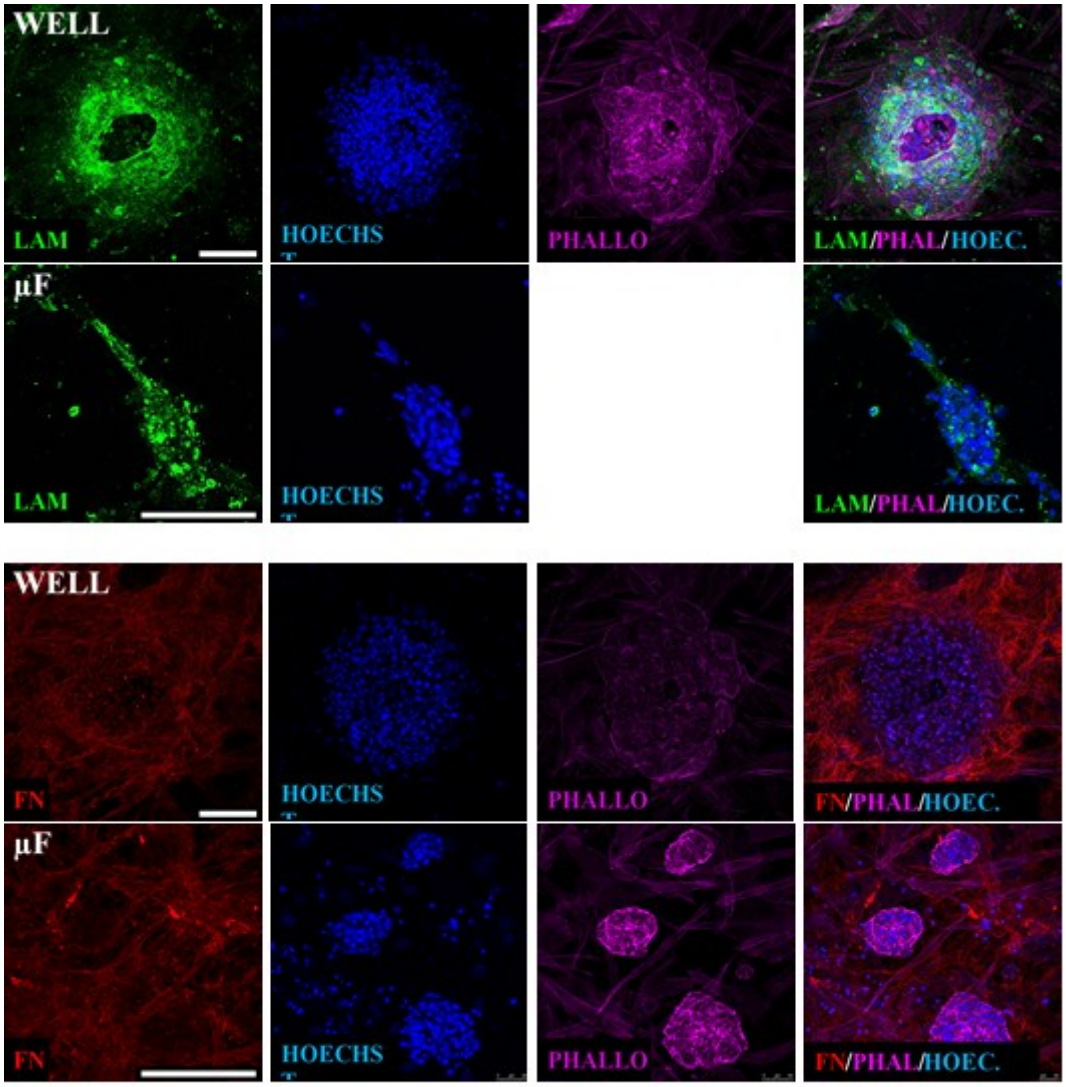

*Figure 4.37: **ECM after reprogramming in well and in microfluidic platforms (second part).** Scale bar: 100 µm.*

At the end of reprogramming protocol, both in well and in microfluidics, the ECM proteins produced have a different arrangement in correspondence to fibroblasts or to hiPSC colonies. By analyzing the differences between well and microfluidic ECM deposition after reprogramming, it is possible to observe that in well the colony is surrounded by the ECM network produced by the non-reprogrammed fibroblasts, leaving an empty space in the ECM networks. In confined environment instead, ECM proteins coat the colonies as a shell, or surround and innervate the colonies with thick fibers such as those made of collagen I. This observation is really striking for collagen I, IV, VI and laminin. Moreover, in microfluidics, a thicker and more defined actin ring, as shown by phalloidin staining, is observed at the edges of the colonies.

As a demonstration that in conventional reprogramming performed in well, fibroblasts and hiPSC matrices are not interconnected, a simple experiment was performed: with a pair of tweezer, the non-reprogrammed fibroblast layer was mechanically removed and it detached without altering hiPSC colonies position. In Fig. 4.38 it is possible to observe the detached floating fibroblast layer and the hole left in the layer by the colonies that remained attached to the plastic surface of the well instead.

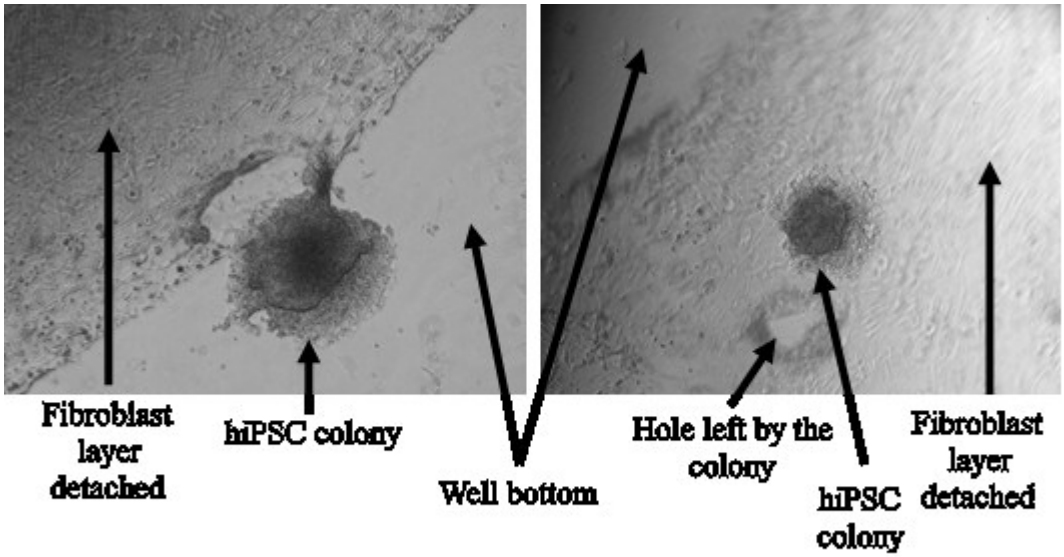

Figure 4.38: Fibroblasts and hiPSC colony ECM are not interconnected

The observation that ECM deposition after cell reprogramming is different in microfluidics comparing to conventional cell culture devices could help to understand why in microfluidics cell reprogramming is more efficient than in other supports.

To increase the understanding of microfluidic high-efficiency cell reprogramming, single-cell RNA-sequencing of different time-points along the reprogramming protocol has been performed. Today, all experimental samples have been collected and sent to sequencing at TIGEM institute (Naples). Sequencing data will be analyzed and commented when available.

4.5. SERPINB3 ADMINISTRATION INFLUENCE ON CELL REPROGRAMMIG

To elucidate the effect of SERPINB3 on cell reprogramming genetic alteration typical of cancer cells, the well-established high-efficient model of cell reprogramming based on BJ human fibroblast reprogramming in microfluidic platforms was coupled with SERPINB3 administration.

4.5.1. SERPINB3 inhibits cell reprogramming

In order to evaluate SERPINB3 effect to cell reprogramming, BJ human fibroblasts were reprogrammed with mmRNA technology couopled with exogenous SERPINB3 administration at different time points of the reprogramming process, following the experimental strategy reported in paragraph 3.8. Coherently with previous data[1], BJ fibroblasts reprogrammed following the standard protocol (CTRL condition) underwent high efficiency cell reprogramming (108.7%) as reported in fig.4.39. In this condition, after about seven mmRNA transfections (Day7), BJ fibroblast started to change morphology, losing the typical fibroblast elongated, mesenchymal shape and becoming more round and compact, with large nuclei. Moreover, cell clusters started to appear. These morphological changes represent the Mesenchymal-to-Epithelial Transition (MET) that is required for successful cell reprogramming. As expected, after 14 days of protocol hiPSC colonies were fully formed (fig.4.39, dashed lines) and abundant along the microfluidic channel. When SERPINB3 was administered from day 0 to day 7 during reprogramming, cells showed a delayed MET, with many elongated cells still present at day 7. This delay determined a 72.15% reduction of reprogramming efficiency. A similar behavior was observed when SERPINB3 was administered during the whole reprogramming protocol, from day 0 to day 14. In this condition the reprogramming inhibition was even more drastic, since a 80.44% drop of the reprogramming efficiency was observed, with values that were about 5.5 times less than CTRL.

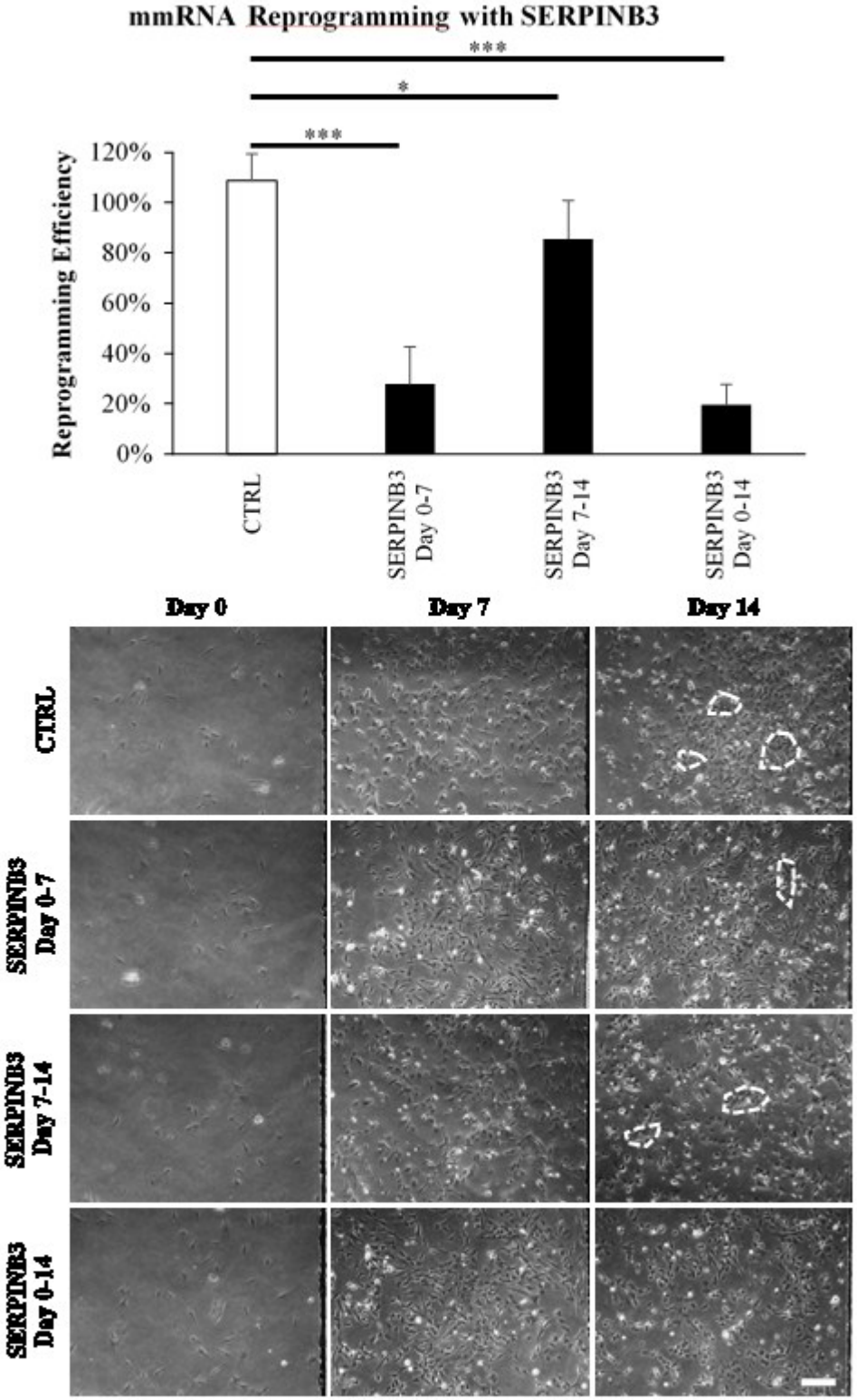

Figure 4.39: SERPINB3 administration inhibits cell reprogramming. ***Top****: reprogramming efficiency in BJ human fibroblasts reprogrammed in microfluidic devices with SERPINB3 administration at different time points.* ***Bottom****: Cell reprogramming progression. At D0 cell density and morphology is the same in all conditions. At D7 cells in CTRL and SERPINB3 Day 8-14 conditions show regular MET with round cells and first cell clusters, while SERPINB3 Day 0-7 and Day 0-14 conditions have a more elongated morphology. At D14 hiPSC colonies appear (dashed white lines). Scale bar: 200 µm.*

Also in this condition a delayed MET was observed. On the contrary, when SERPINB3 was administered just after MET, from day 7 to day 14 of the reprogramming protocol, only 14.44% reduction of the reprogramming efficiency was observed. These data demonstrate that in our model SERPINB3 administration during cell reprogramming considerably inhibits reprogramming efficiency, but the effect is more drastic if the protein is given before the MET.

4.5.2. SERPINB3 does not affect pluripotency factors

We analyzed whether cell reprogramming inhibition was due to SERPINB3 interaction with pluripotency genes, since it has been demonstrated that SERPINB3 expression is correlated with undifferentiated tumors with stem proprieties[2–4]. Stabilized hiPSC have been seeded in microfluidic chips and cultured for 7 days with and without SERPINB3 administration. Main pluripotency genes expression (OCT4, NANOG and SOX2) has been evaluated by qPCR analysis and no significant alteration was detected (fig.4.40). Cell morphology was similar in the two conditions, with compact colonies and cells with high nuclear-cytoplasmic ratio (fig.4.40).

4.5.3. SERPINB3 impairs EMT-MET markers expression

We then focused on SERPINB3 effect on the first days of the reprogramming protocol, since our data indicate that the first seven days, before MET, are crucial for a correct and efficient cell reprogramming. From previous data SERPINB3 has been reported to promote Epithelial-to-Mesenchymal transition (EMT) in tumor progression, leading to cell detachment, invasiveness and metastasis formation[5]. Since EMT is the opposite transition of MET, required for cell reprogramming, we analyzed SERPINB3 effect on EMT-MET markers. BJ human fibroblast were cultured in microfluidic chips for 7 days in standard culture medium (DMEM high glucose + 10% FBS) with or without SERPINB3 administration. These conditions were compared to BJ human fibroblasts undergoing reprogramming protocol for 7 days, with or without SERPINB3 administration.

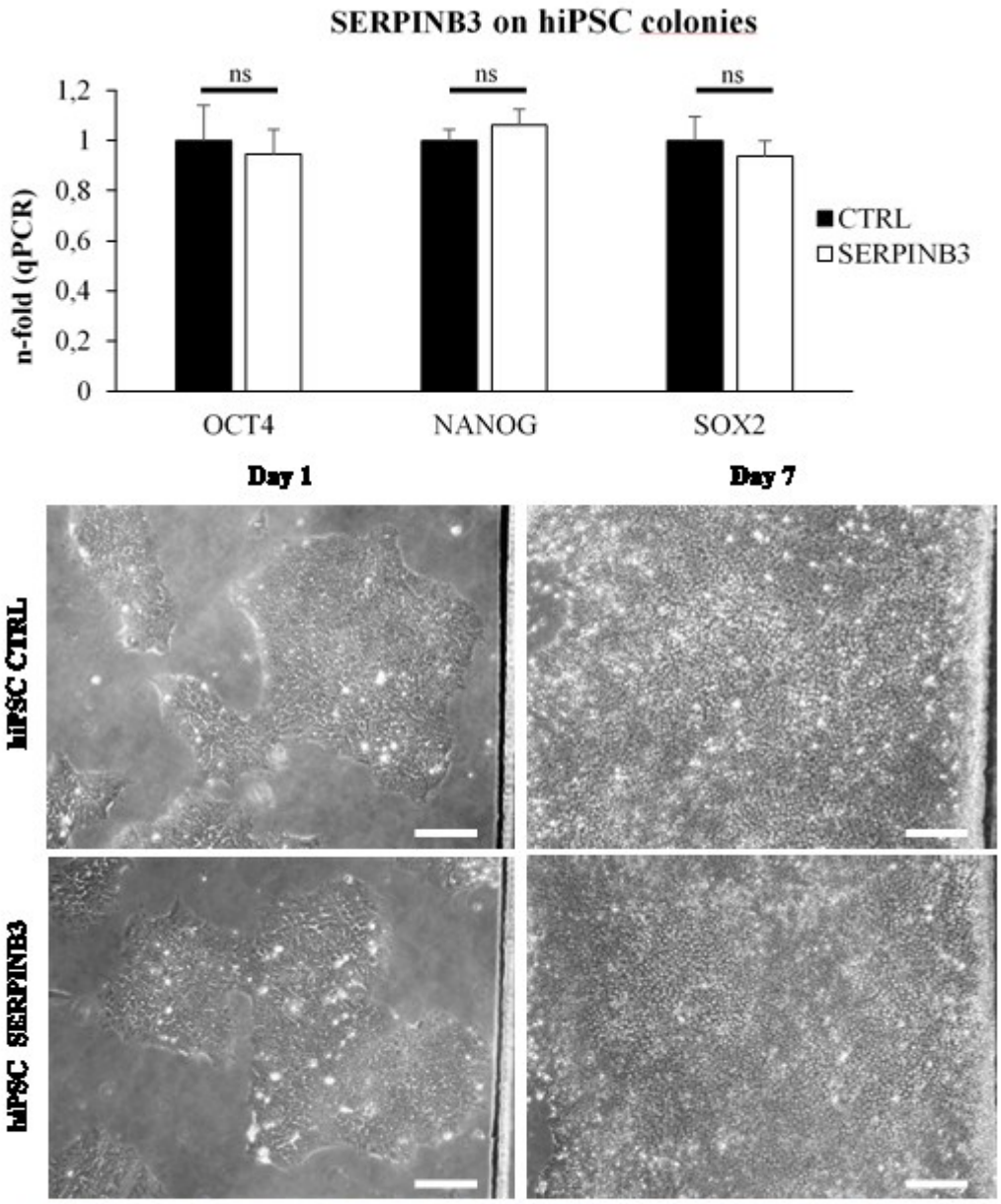

*Figure 4.40: SERPINB3 does not affect pluripotency genes expression. Top: SERPINB3 administered for 7 days to hiPSC cells grown in microfluidic device does not have significant effect on the expression of OCT4, NANOG and SOX2, compared to control (hiPSC cells without SERPINB3 administration). **Bottom**: SERPINB3 administration does not cause morphological alterations in hiPSC colonies from D0 to D7. Scale bar: 200 µm.*

The experiment was stopped when full MET was observed in the untreated reprogrammed cells and well established EMT-MET markers were analyzed by qPCR. All the analyzed markers (VIMENTIN, E-CADHERIN, β-CATENIN, SNAI1) were impaired by the administration of SERPINB3, and in particular E-Cadherin expression was greatly de-regulated during cell reprogramming with SERPINB3 (fig.4.41).

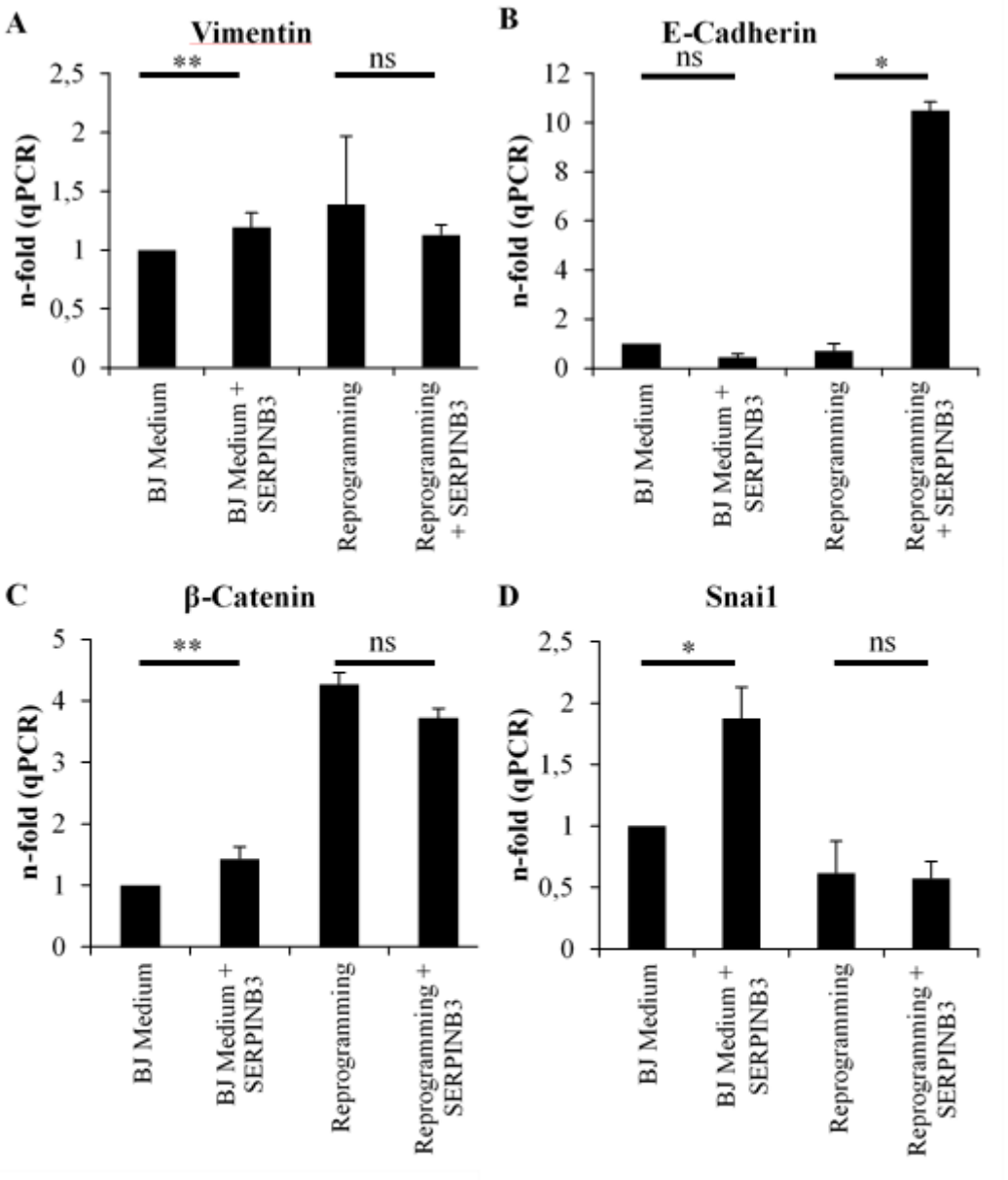

Figure 4.41: SERPINB3 effect on EMT-MET markers VIMENTIN, E-CADHERIN, β-CATENIN, SNAI1. *BJ Medium = BJ human fibroblasts grown in microfluidic chips with standard growth medium DMEM high glucose + 10% FBS for 7 days, with or without SERPINB3 exogenous administration. Reprogramming = BJ human fibroblasts undergoing cell reprogramming in microfluidic devices for 7 days, with or without SERPINB3 administration. (A) SERPINB3 upregulates VIMENTIN expression in BJ Medium but gives an opposite trend during reprogramming (non-significant data). (B) SERPINB3 upregulates E-CADHERIN during cell reprogramming. (C) SERPINB3 upregulates β-CATENIN expression in BJ Medium but gives an opposite trend during reprogramming (non-significative data). (D) SERPINB3 upregulates SNAIL expression in BJ Medium.*

4.5.4. SERPINB3 disrupts TGF-β1 expression

The effect of SERPINB3 administration on TGF-β1 expression was then analyzed, since it has been demonstrated that this cytokine is essential for cell reprogramming. BJ human fibroblasts, cultivated in microfluidic chips in standard culture medium, showed 73.82% reduction of TGF-β1 expression in presence of SERPINB3 (fig.4.42).

4.5.5. Transcriptomic analysis of SERPINB3-related genes during reprogramming

Transcriptomic microarray data of human dermal fibroblasts (HDF) reprogrammed with retroviral vectors[6] were analyzed. This particular reprogramming protocol lasts 49 days and MET occurs around day 15-20. mRNA samples were collected from starting HDF, from reprogramming at day 3-7-11-15-20-28-35-42 and 49, from freshly derived hiPSC and from human embryonic stem cells (hESC) as control. In our analysis we evaluated if SERPINB3 and SERPINB3-related genes (Table 6) were significantly differentially expressed in this database, indicating that those genes played a significant role in cell reprogramming.

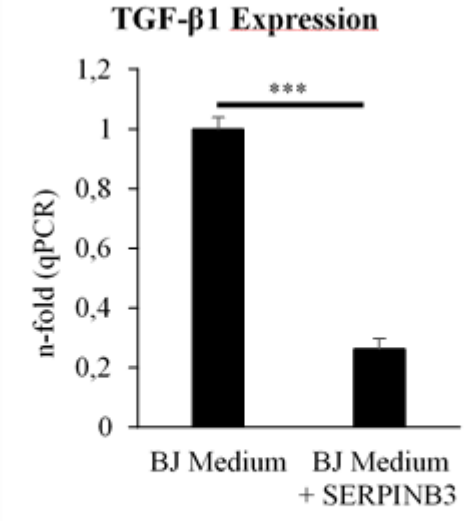

Figure 4.42: SERPINB3 inhibits TGF-β1 expression. BJ Medium = BJ human fibroblasts grown in microfluidic chips with standard growth medium DMEM high glucose + 10% FBS for 7 days, with or without SERPINB3 exogenous administration.

First of all the whole database was analyzed by principal component analysis (PCA). PCA plot shown in fig.4.43 shows how cells undergoing reprogramming (human dermal fibroblasts, HDF) evolve (indicated by arrows) from fibroblasts, to an intermediate state and to their final pluripotency state. The main shift is linked to the completion of MET, spanning from day 7 to day 15 in this protocol. The PCA loading plot instead indicates the contribution of all the genes in the database to the shifts reported in the main PCA analysis. Genes at the center of the plot have low influence on the shift and are therefore of limited importance for reprogramming process. Genes on the edge of the plot have instead great influence on the shift and represent the fundamental genes for cell reprogramming. Highlighted in red and blue, SERPINB3-related genes, in blue the genes downregulated by SERPINB3, in red those upregulated by SERPINB3. Many SERPINB3-related genes are located at the edge of the plot, indicating high contribution to reprogramming process.

Next, SERPINB3-related genes expression during reprogramming was analyzed. Coherently with SERPINB3 role in directing cell fate, SERPINB3-related genes delineated a temporal order of reprogramming stages in this unsupervised cluster analysis (fig.4.44).

In this analysis, 3 main clusters could be identified: on the left of the heatmap (red tree) gene expression of HDF cells clusters together with samples collected at the very beginning of reprogramming process (day 3); in the middle (blue tree), data from day 7, 11 and 15 cluster together representing gene expression in the pre-MET phase; finally on the right (green tree), all samples from day 20 to day 49 cluster together with hiPSC and hESC samples, indicating similar expression of SERPINB3 and SERPINB3-related genes after MET. Taking a closer look to SERPINB3 differential expression during the reprogramming transition, the expression of this molecule was found downregulated compared to the median gene expression, until the very late phases of reprogramming (day 35, 49 and hiPSC samples).

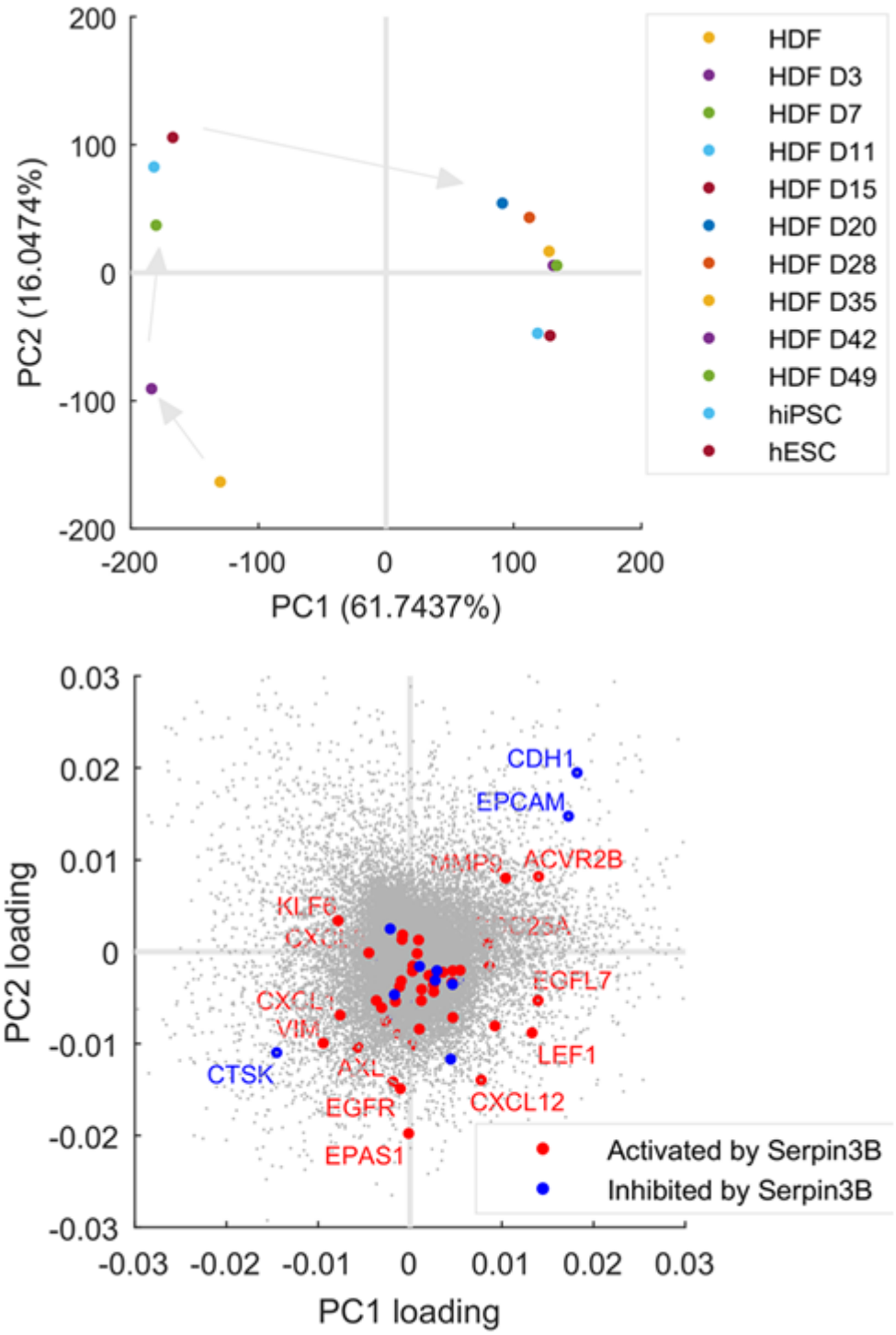

Figure 4.43. Analysis of microarray gene expression analysis during cell reprogramming. Top: PCA analysis of the total database. Bottom: PCA loadings related to top plot.

Next SERPINB3-related genes were divided into 3 subgroups according to literature data (Table 6): Subgroup 1 identifies all genes that in literature are reported to be downregulated by SERPINB3, Subgroup 2 represents all genes upregulated by SERPINB3 and Subgroup 3 classifies all genes upstream of

SERPINB3, that activate the expression of this serpin. The cluster hierarchy is maintained as in fig.4.44, where pre-reprogramming samples cluster together on the left, pre-MET samples on the middle and post-MET samples on the right. As shown in fig.4.45, during unperturbed cell reprogramming, most genes belonging to Subgroup 1 are upregulated after MET (cluster on the right), and appear in red shades in the heatmap. Therefore, administering SERPINB3 after MET (Condition Day 7-14) induces downregulation of genes that are supposed to be upregulated in regular cell reprogramming. This can explain loss of reprogramming efficiency due to SERPINB3 administration after MET (Condition Day 7-14). Similarly, genes in Subgroup 2 that in literature are reported to be upregulated by SERPINB3, during regular reprogramming are mostly downregulated before MET (middle cluster). Therefore, SERPINB3 administration before MET (Condition Day 0-7 and Day 0-14) induces a general upregulation of these genes that should be downregulated for successful reprogramming. Moreover, Subgroup 2 also collects some mesenchymal genes, typical markers of EMT-MET, such as FN1, VIM, ACTA2. These genes are strongly upregulated in fibroblasts (left cluster), but in regular reprogramming they become downregulated when reprogramming starts (middle-right cluster). This boost in mesenchymal genes expression has previously been reported to be fundamental for successful reprogramming[1,7]. When reprogramming factors administration starts, these genes gets downregulated to allow MET and the acquisition of epithelial-like phenotype typical of iPSC. Exogenous administration of SERPINB3 before MET doesn't allow the downregulation of these genes and therefore doesn't allow a correct MET, as already shown in fig.4.41. No significant trend was observed in genes belonging to Subgroup 3. Finally, about 35% of SERPINB3-related genes are significantly differentially expressed along reprogramming with a corrected p-value less than 0.0001 (Figure 7). These genes are the most important for fibroblast reprogramming and include SERPINB3 itself (Figure 7, purple arrow), indicating once more how much this serpin is involved in regulating cell fate. Among the genes in this group, 25% are SERPINB3-downregulated genes (fig.4.46, yellow dots), 67.5% SERPINB3-upregulated genes (fig.4.46,

green dots) and 0.7% genes that activate SERPINB3 (fig.4.46, blue dots). This handful of genes (41 in total) is sufficient to cluster different stages of cell reprogramming and identify MET transition with high significance.

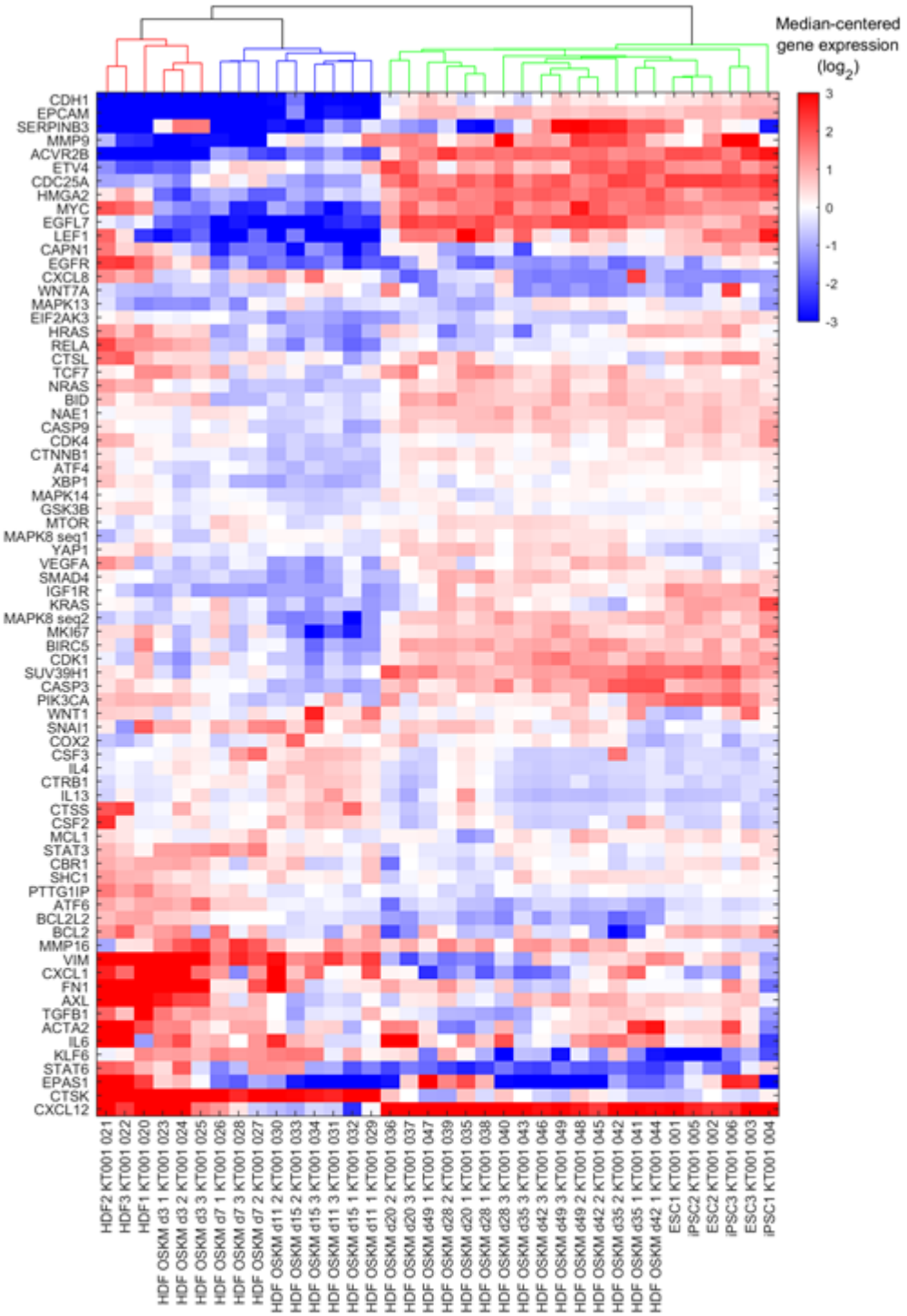

Figure 4.44: Transcriptomic analysis of SERPINB3-related genes during cell reprogramming. *SERPINB3-related genes identify 3 clusters in this reprogramming microarray dataset. The cluster on the left (red tree) groups together human dermal fibroblasts (HDF) and HDF after 3 days of reprogramming. The cluster in the middle (blue tree) groups together timepoints before MET, while the cluster on the right (green tree) groups together timepoints after MET, hiPSC samples and hESC.*

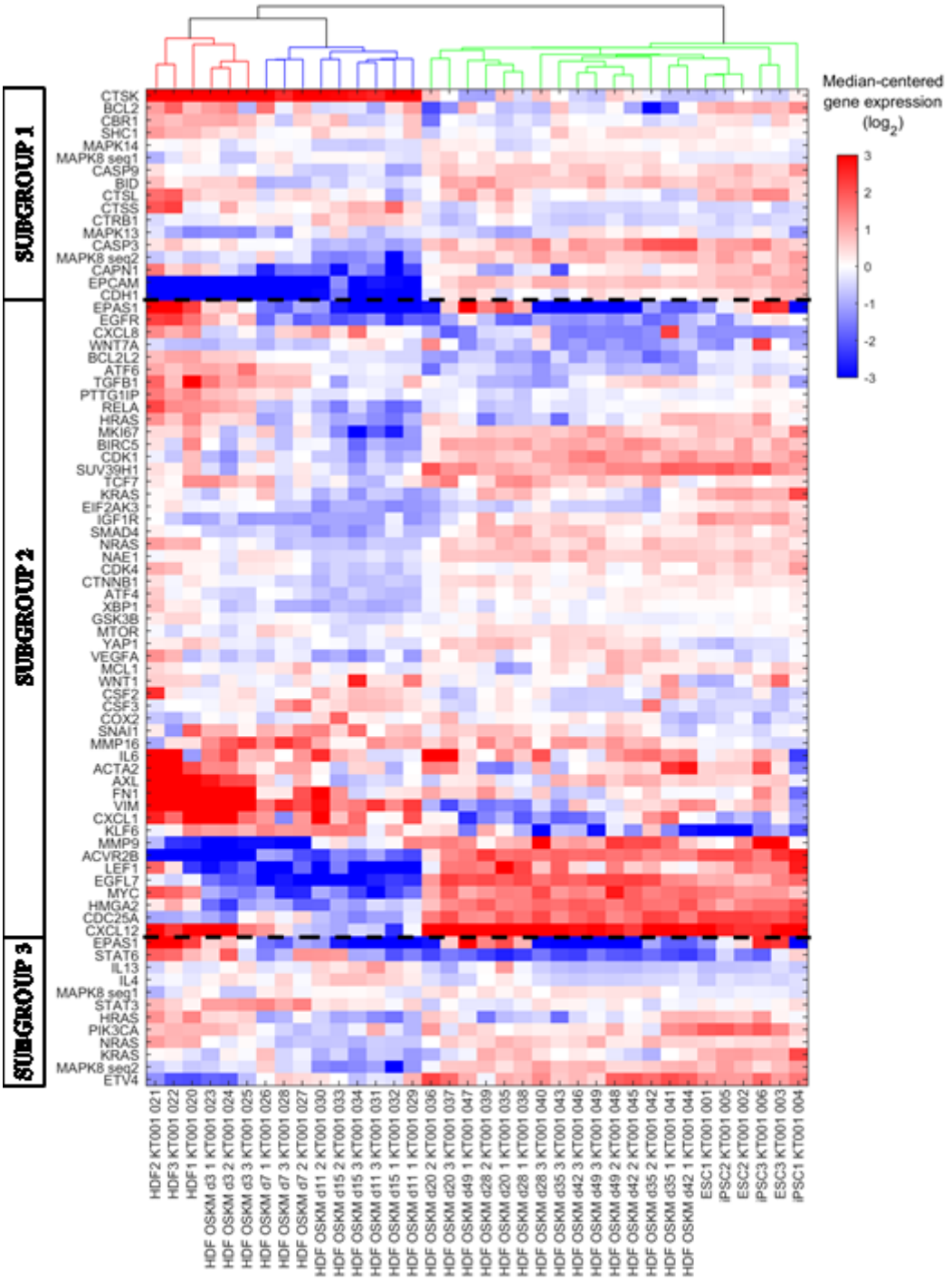

***Figure 4.45: SERPINB3-related genes can be divided into 3 subgroups**: Subgroup 1: genes downregulated by SERPINB3. Subgroup 2: genes upregulated by SERPINB3. Subgroup 3: genes upstream of SERPINB3, that upregulate this serpin. In regular reprogramming, genes in Subgroup 1 are mostly upregulated after MET. Genes in Subgroup 2, excluding mesenchymal state markers, are downregulated before MET. This trend is altered by SERPINB3 administration, leading to disruption of reprogramming dynamics and drop of reprogramming efficiency.*

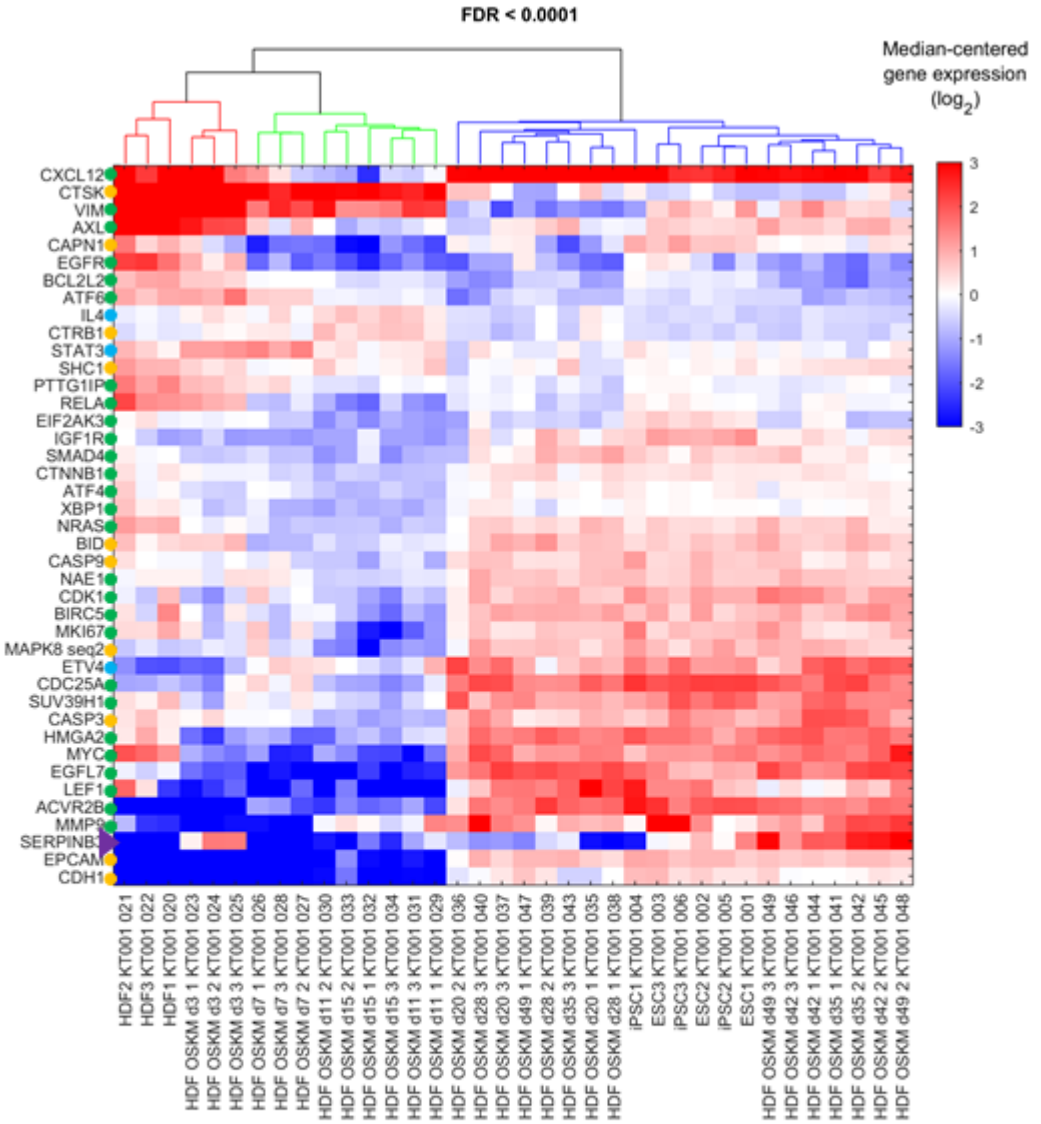

Figure 4.46: SERPINB3-related genes differentially expressed during reprogramming with high significance. *41 (35%) SERPINB3-related genes are significantly differentially expressed along reprogramming with a corrected p-value less than 0.0001. 25% are SERPINB3-inhibited genes (yellow dots), 67.5% SERPINB3-activated genes (green dots) and 0.7% genes that activate SERPINB3 (blue dots). SERPINB3 is indicated by the purple arrow. The clusters identified by those genes are the same as in Figure 4.44 and 4.45, therefore these genes are sufficient to determine significant stages during cell reprogramming.*

4.6. DROP-SEQ SETUP

Drop-Seq scRNA-seq system was setup as shown in fig.4.47. Syringe pumps and magnetic stirrers were correctly positioned and set up. After preliminary optimization experiments (data not shown), the optimal flow rates were set at 12000 µl/hour for oil and 2400 µl/hour for cells and beads, in order to obtain uniform, stable droplets with an average diameter in the range of 100-120 µm, as recommended in Macosko et al. 2015. At this flow rates the zone in the microfluidic platform where the three fluxes are mixes, called the triangle zone, is stable as indicated in fig.4.47 with the red arrow. The blurred flux downstream the triangle indicates the formation of droplets. A diameter of 107.3 ± 3.46 µm was achieved as shown in fig.4.47. This diameter is optimal to maximize cell and beads capturing efficiency and to minimize droplet volume, so that, when a cell is lysed inside the droplet, the chances for mRNA capturing on the bead are increased.

After flow rate optimization, bead encapsulation efficiency was estimated. Among the different bead concentrations tested, the best compromise between high bead encapsulation efficiency and chip clogging risk was 300 beads/µl. At this concentration, bead encapsulation efficiency is 5.47 ± 0.41%, calculated as droplets containing beads over total droplets sampled as shown in fig.4.47. This data is higher than the efficiency obtained in Macosko et al. 2015. The probability of having two beads in the same droplet is only 0.2 ± 0.04% and the one of having more than two beads in the same droplet is statistically irrelevant (0.002%).

Next, optimal cell concentration has been evaluated. Before dissociation, cells have been loaded with Calcein-AM, a cell-permeant dye that can be used to determine cell viability. In live cells the nonfluorescent calcein AM, whose fluorescence is quenched by acetoxymethyl ester group, is converted to a green-fluorescent calcein after acetoxymethyl ester hydrolysis by intracellular esterases. Dead or damaged cells are not able to perform this conversion. Therefore, live cells will be stained with green-fluorescent dye and after cell lysis inside the droplet the dye will be released in the droplet volume, where the amount of fluorescence will be proportional to the number of encapsulated cells, as shown

in fig.4.48. By fluorescence signal deconvolution it was possible to distinguish the fluorescence provoked by the lysis of one cell (first peak), two cells (second peak) and so on. Beads are auto-fluorescent if excited at 470-490 nm, and are clearly distinguishable inside the droplets, even if coupled with cells fluorescence. By counting cells and beads it was possible to estimate the number of the favorable events where only one cell and one bead are captured in the same droplet. This single-cell single-bead efficiency was 0.49 ± 0.07%, once again higher than the one reported in Macosko et al. 2015. Moreover it was possible to calculate the probability of unfortunate events where more than one cell or more than one bead are captured in the same droplet. Taking into account that having one cell with two beads results in a dilution of the phenotype, which can be corrected after sequencing by bioinformatic analysis, while having two cells with one bead results in a chimeric mixed phenotype that can alter the analysis, creating fake phenotypes. Therefore, the first case is less problematic than the second one and in the graph in fig.4.48 are represented in yellow and red respectively.

With the setup recommended in Macosko et al. 2015, cell recovery (calculated as the ratio between the number of cells loaded in the syringe and the number of cells recovered in the chip) was about 10.2%, therefore 90% of the cells were lost in the tubings or in the syringe, probably because of cell settling in the syringe. An additional stirring was then added to the cell syringe, to keep cells in suspension. To evaluate cell mortality related to the stirring (absolutely to be prevented to avoid RNA release in solution that can dirt the result), cells were loaded with Calcein-AM and kept in the syringe with or without stirring. Fluorescent dye released in solution from dead cells was measured and, as shown in fig.4.48, there is no difference in dye release, therefore cells are not disrupted by stirring. Moreover, stirring increased cell recovery rate to 48.95%.

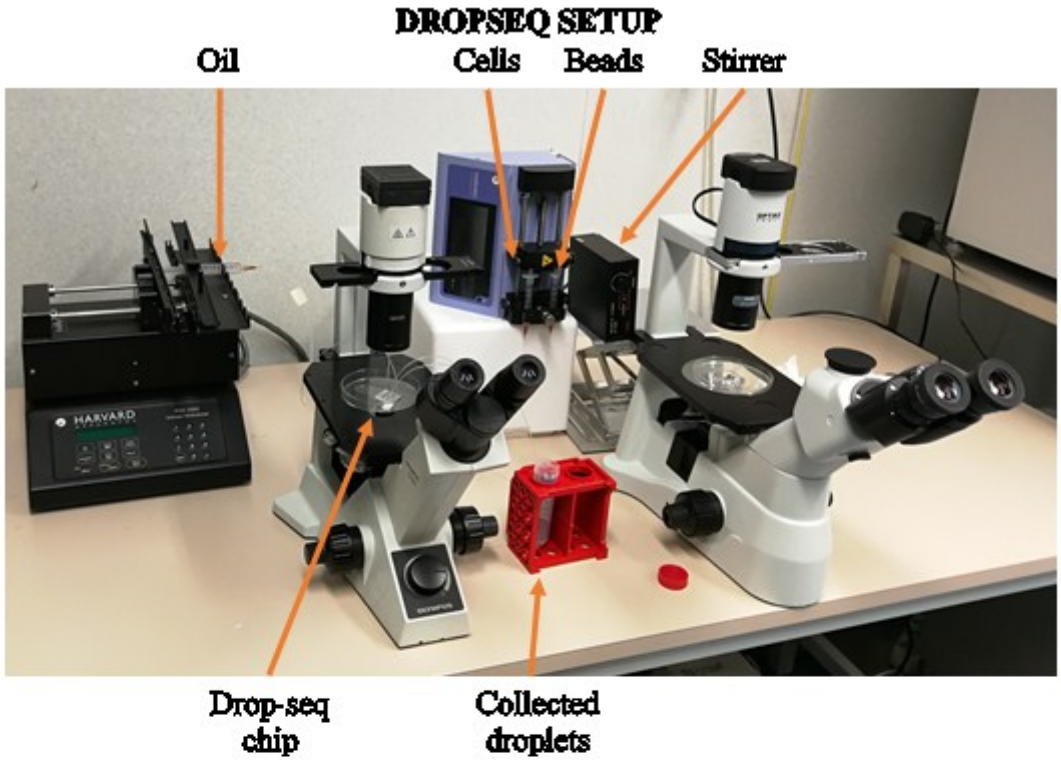

*Figure 4.47: Drop-Seq setup and bead encapsulation efficiency. **Top**: picture of Drop-Seq setup. **Middle-left**: microfluidic triangle when droplet formation. **Middle-right**: uniform droplets with beads. **Bottom-left**: average droplet diameter. **Bottom-right**: bead encapsulation efficiency. Scale bar 200 µm.*

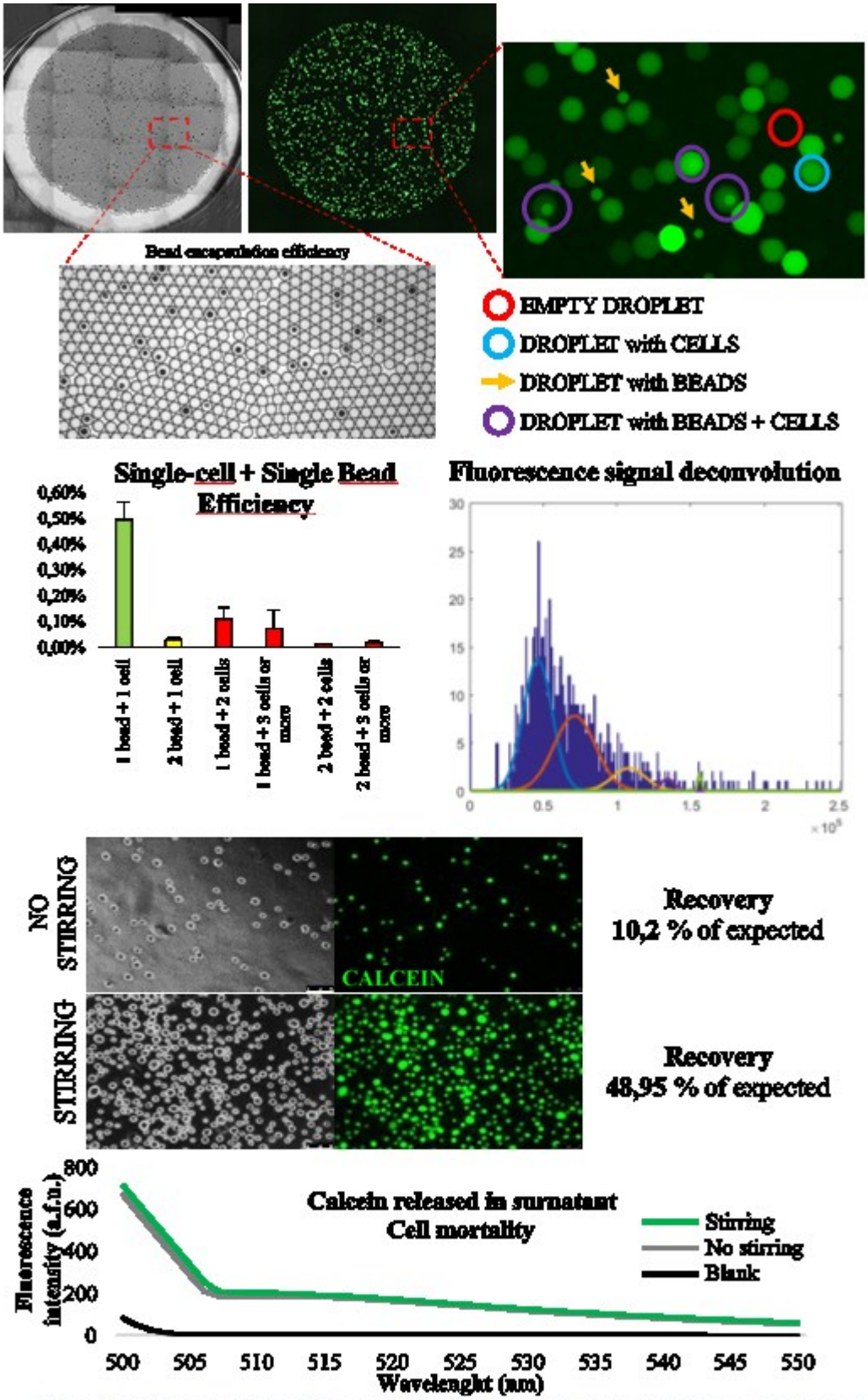

*Figure 4.48: Cell encapsulation efficiency in Drop-Seq. **Top**: cells stained with Calcein-AM encapsulated with beads. **Middle**: fluorescence deconvolution and evaluation of different scenarios probability. In green: the optimal single-cell and single-bead event. In yellow single -cell and two beads and in red the unfortunate scenarios with more than one cell. **Bottom**: effect of cell stirring on cell viability and recovery efficiency.*

Once optimized cell and bead encapsulation, mRNA recovery and amplification efficiency was tested, following strictly the procedure published by Macosko et al. In a mixed-cell type experiment, with 1:1 mix of BJ fibroblasts and H9 hESC, reverse-transcription, exonuclease I treatment and PCR amplification was performed and an aliquot of beads with cDNA and of PCR product was analyzed by qPCR on the housekeeping gene GAPDH and on type-specific genes such as NANOG and VIMENTIN. PCR products were also analyzed by agarose gel electrophoresis and Agilent BioAnalyzer capillary electrophoresis. Unfortunately, even if cDNA was present on the beads, as shown in fig.4.49, no PCR product was detectable, neither by qPCR (data not shown) nor by electrophoresis. mRNA reverse-transcribed by random primers with two different RT kit and amplified by PCR like the samples was used as control. Therefore, some problems in mRNA capturing or in PCR amplification to detach cDNA from the beads had occurred.

To test this hypothesis, in tube capturing tests were performed. For these experiments, the number of droplets that could fit 10 µl volume was calculated. A corresponding amount of beads was incubated in 10 µl total volume with the mRNA quantity expected from the same amount of cells as the beads. In this way, in the same confined volume as inside the droplet, beads were in contact with the same amount of mRNA as if one cell was lysed inside the droplet. Purified mRNA from H9 hESC cells was used. Binding time was calculated on the duration of an average Drop-Seq experiment, from droplet formation to breakage. Washes were performed as in standard Drop-Seq protocol. At each passage, surnatant was collected to calculate the fraction of mRNA that did not bind to the beads or was washed away. After 3 washes mRNA was eluted from the beads to check capturing efficiency. As control mRNA reverse-transcribed with random primers and diluted in the same solutions used in the experiment was used. Capturing efficiency was measured by qPCR on the housekeeping GAPDH gene. As shown in fig.4.50, even if the capturing is successful, only a small amount of the starting mRNA was captured by the beads and eluate from the beads after the washes. Most of the mRNA was probably lost in the washes or in inefficient bead capturing or TSO strategy is not sufficient to reverse-transcribe full length mRNA and attach PCR primer at 5'-end. However, more tests are needed to confirm this data and to obtain good library amplification.

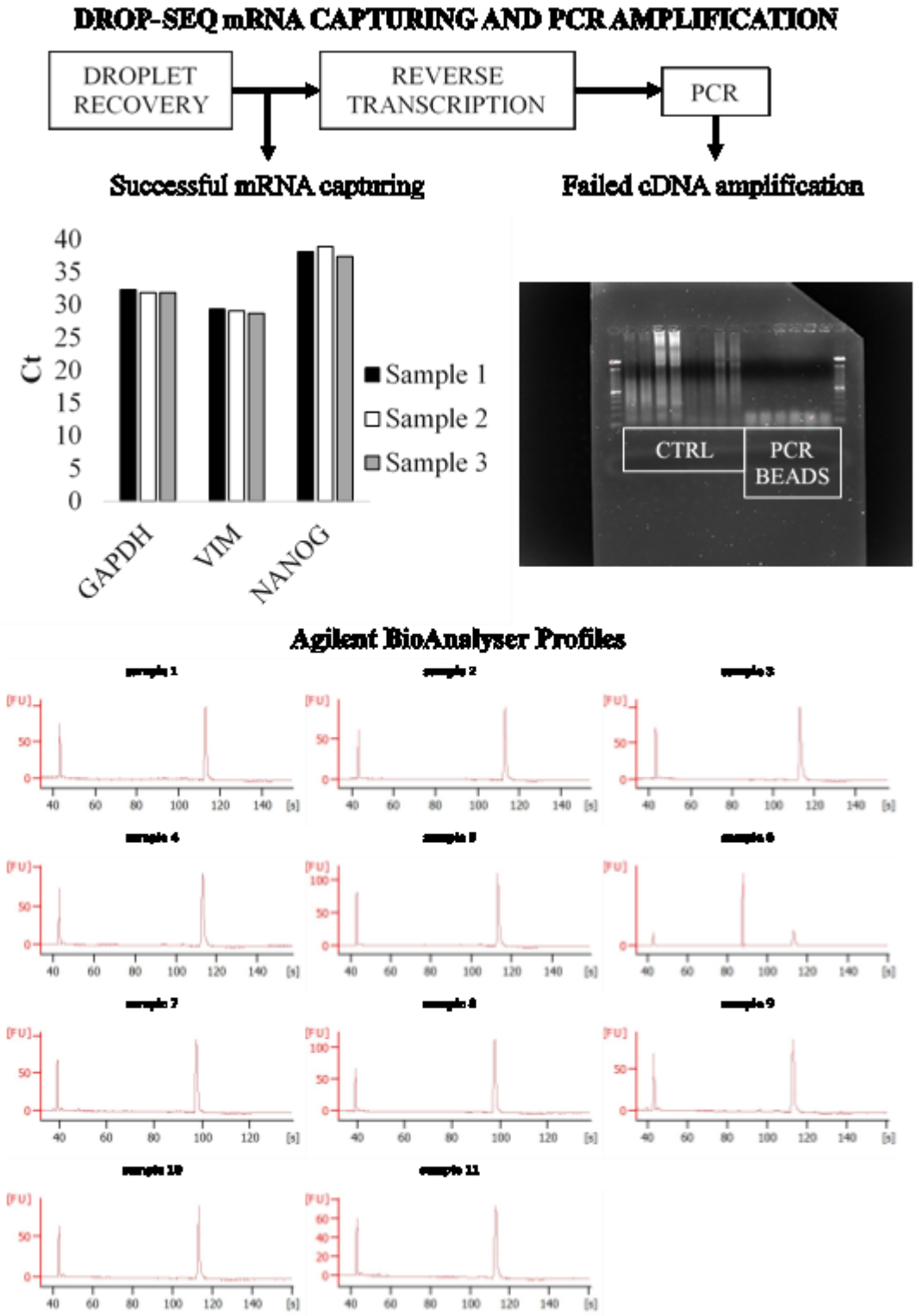

***Figure 4.49:Drop-Seq mRNA capturing and PCR amplification Top**: Drop-Seq pipeline where indicated the samples collected for qPCR analysis. **Middle left**: qPCR analysis of mRNA captured by beads. Data expressed as Threshold Cycle (Ct). **Middle right**: agarose gel electrophoresis of PCR products and controls. PCR products: three samples of a Drop-Seq experiment (2 replicates each) amplified by PCR according to Drop-Seq protocol; Controls (2 replicates each): mRNA reverse-transcribed with High Capacity cDNA kit (line 1 and 2) and amplified by PCR (line 3 and 4) or reverse-transcribed with Drop-Seq RT mix and random primers (line 5 and 6) and amplified by PCR (line 7-8). **Bottom**: Agilent BioAnalyzer capillary PCR results. The two peaks visible in every plot are control ladder peaks.*

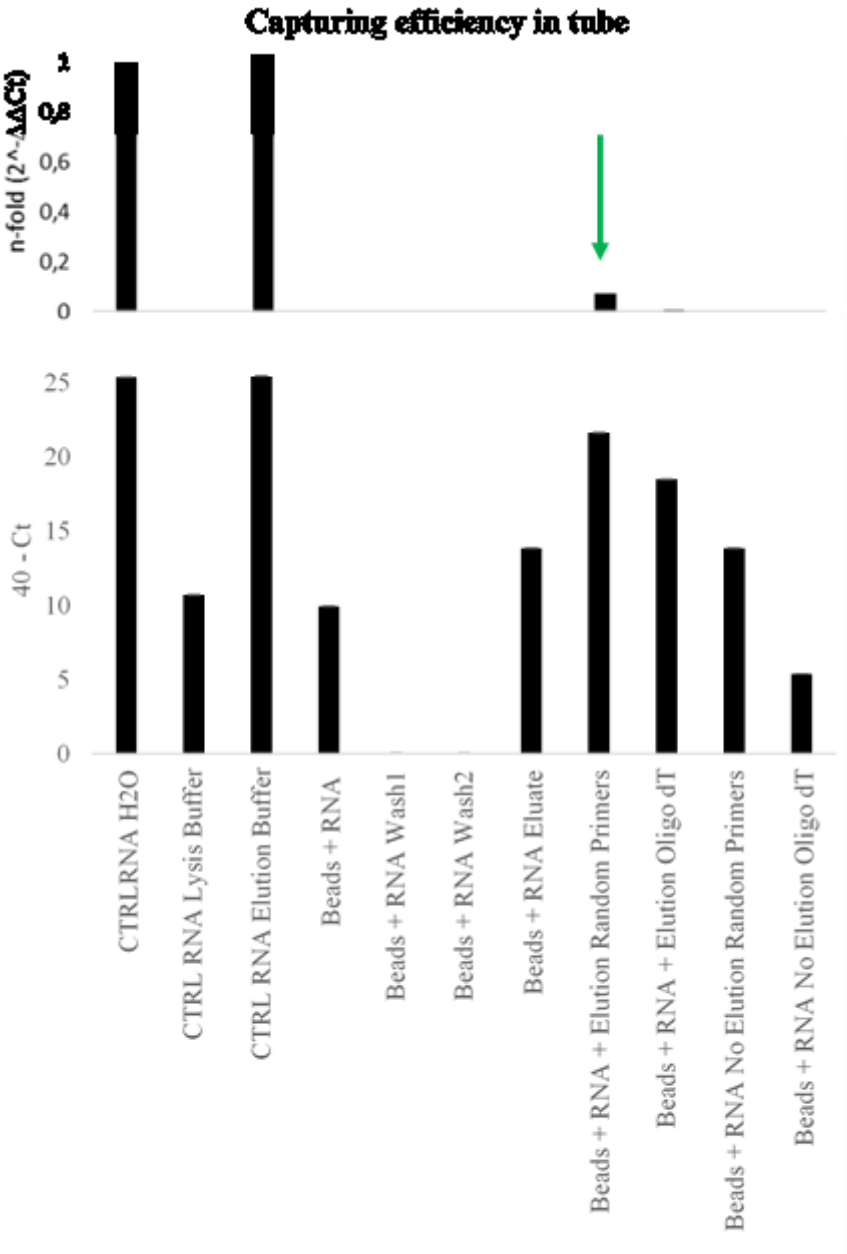

Figure 4.50: In tube capturing efficiency. *Control samples: mRNA diluted in water or lysis buffer (binding buffer) or in elution buffer. Data indicated as 40-Ct or normalizea ratio with ΔΔCt method. Green arrow: mRNA eluted from the beads, expected result is similar to control.*

Taken together, these data show good results in the microfluidic platform optimization, with excellent droplet size, cell and bead capturing efficiency. However, library construction is still not optimized and more experiments are needed to complete the setup of Drop-Seq scRNA-seq.

CHAPTER 5: DISCUSSION AND CONCLUSIONS

5.1. DIFFERENT DEVELOPMENTAL STAGES ARE CHARACTERIZED BY DIFFERENT ECM ORGANIZATION

According to data shown in paragraph 4.1, it has been demonstrated how different developmental stages, are characterized by different expression of extracellular matrix-related genes and of ECM deposition and organization. In particular, by analyzing RNA-seq data of various samples of fibroblasts, naïve and primed PSC, it is possible to appreciate how the sole expression of collagen genes is per se sufficient to identify the three main clusters of fibroblasts, naïve PSC and primed PSC (fig.4.1). These data indicate that the extracellular matrix has a specific formulation that is differentially expressed in the three cell states. Even if it could be expected that fibroblast have different ECM expression compared to PSC, as it has been extensively reported in literature, surprisingly naïve and primed PSC show a remarkably different ECM-related genes expression that is reported in this work for the first time.

Second harmonic generation imaging and electron microscopy confirm from macroscopic point of view that the differences in gene expression observed on the RNA-sequencing analysis. In fact, SHG imaging highlights the overall structure of the extracellular matrix in the sample analyzed (fig.4.2) confirming different general organization of ECM in the three developmental stage. SEM imaging

(fig.4.3) renders the outer appearance of naïve and primed PSC colonies, showing how naïve colonies appear to be surrounded by an ECM capsule, in according with the collagen I shell reported in fig.4.8. Finally TEM images (fig.4.4 and 4.5) confirm outer ECM deposition, even if with scarce organization, in naïve PSC colonies which is not observed in primed PSC colonies.

When focusing on the most common ECM proteins, such as collagen I, which is the most important fibrillar collagen[135], collagen IV, which together with laminin form the basal lamina[137], collagen VI, important for adult stem cells maintenance[138], and fibronectin, the difference between the three developmental stages is once more confirmed. As expected, ECM produced by fibroblasts is different from the one produced by pluripotent cells, but differences between naïve and primed ECM were shown. Moreover, endogenous production of ECM by naïve PSC colonies was confirmed in our feeder-free culture conditions. Endogenous production of laminin was previously reported in primed PSC[191], but no data is currently available on naïve PSC endogenous ECM production. The ability of naïve PSC to rearrange ECM proteins can be hypnotized by looking at the black halos surrounding naïve colonies on Matrigel coating. Finally, naïve HPD06 have high expression of collagen IV and laminin, two components of basal lamina, in accordance with published data which report laminin expression in pluripotent stem cells[17,183,184,185,190]. Moreover, low fibronectin expression was reported in pluripotent cells, compatible with published data, which report downregulation of fibronectin production[17].

Taken together these data demonstrate for the first time that naïve and primed pluripotent stem cells have different ECM protein expression, deposition and organization and that naïve PSC are able to produce their own ECM proteins and to rearrange ECM proteins from the environment.

5.2. CONFINED ENVIRONMENT PROMOTES ECM PROTEINS SECRETION AND DEPOSITION

From SILAC analysis reported in fig.4.13 and 4.14, it is clear how cultivating cells in a confined environment granted by microfluidic cell culture devices, promotes an increased secretion of proteins compared to conventional cell culture platforms such as multiwells. This trend has been demonstrated both with human fibroblasts and with human primed PSC. In particular, data related to human fibroblasts have been published in Hu et al, 2018. Moreover, from the bioinformatics analysis, it is clear that microfluidic environment has a deep influence on the types of secreted proteins. In fact, the most abundant category of proteins detected are related to ECM proteins and to ECM-cell interaction.

Following proteomic analysis, the deposition of ECM proteins has been investigated by bulk RNA-sequencing and by immunofluorescence staining. For transcriptomic analysis, samples of the cell model used in this study (characterized by three isogenic cell lines in three different developmental stages: HFF fibroblasts, naïve and primed HPD06) were cultured in well and microfluidic platforms and total RNA was extracted at Day 1, 4 and 7 after seeding. The samples collected for RNA-seq were cultivated as reported in other experiments: HFF fibroblasts were seeded on glass with VTN coating, naïve HPD06 were seeded on glass with VTN coating, on top of which a MEF feeder layer was seeded one day before naïve cells were seeded while primed HPD06 where seeded on glass and MRF coating. Moreover, 2D and 3D naïve HPD06 colonies were manually picked and sequenced separately but these samples were not included in the analysis because the general gene expression pattern may have been altered by the stress induced by the picking protocol itself. The results of this transcriptomic analysis are reported in fig.4.16-4.22. Referring to The Matrisome Project (MIT)[297], the matrix-associated genes were selected to perform a specific analysis. Following the classification proposed by Narba et al, matrix-related genes were divided in Core Matrisome (Collagens, ECM Glycoproteins and Proteoglycans) and Matrisome-Associated (ECM-affiliated proteins, ECM regulators and Secreted Factors). Core Matrisome and Matrisome-Associated

gene expression was analyzed in HFF fibroblasts, primed and naïve HPD06. Moreover, by analyzing the reactome, additional info on cell metabolism and stress state were collected.

Fibroblasts and pluripotent stem cells are deeply influenced by the culture environment and the confined environment influences the general gene expression pattern in all the three cell lines. From the data collected it emerges that microfluidic system require an initial adaptation time, probably due to the shock cells experience when passed from conventional wells where are routinely cultured to microfluidic platforms. This adaptation time is visible in PCA analysis of fibroblasts (fig.4.17), primed PSCs (fig.4.20) and naïve PSCs (fig.4.21), where microfluidic platforms are less similar to well samples in Day 1 and Day 4 but converge at Day 7. By analyzing the differences in the reactome of HFF fibroblasts in wells and microfluidics after 7 days in culture, it is possible to detect that in well matrix-related genes are overexpressed, while in confined environment the most upregulated pathway is related to lipids metabolism. This may sound in contrast to the data previously reported, but a possible explanation for this behavior is that in microfluidic chips cells are accumulating ECM proteins faster, from the first days, therefore there is less need for matrix-related gene transcription at Day 7. Indeed, as shown from panel C and D of fig.4.17, a confined environment has a deep influence on the expression of matrix genes and matrix-related genes. And it is possible to appreciate how the relative expression of these genes is completely opposite in wells compared to microfluidic chips.

Among pluripotent stem cells, primed and naïve HPD06 have a radical different gene expression pattern as represented from hierarchical clustering of fig.4.18 and PCA analysis of fig.4.19, and these differences may mask the differences induced by the microenvironment in this analysis, therefore in this clustering three samples from well and from microfluidics are mixed. By looking at them separately, instead differences between open or confined environment are more clear. Primed HPD06 (fig.4.20) require an adaptation time before converging with the well samples and in this period primed cells express more matrix-related genes in microfluidics compared to conventional wells. This behavior stresses out the connection between cell fate and matrix state.

Naïve HPD06 (fig.4.21) cultivated in microfluidic environment are more variable compared to colonies cultivated in wells. Moreover, in naïve samples, cells from Day 7 in microfluidics correspond to cells from Day 4 in wells. This means that cells in microfluidics are stabilized by the confined environment: in fact, routinely naïve colonies are splitted and passed every 4 days to prevent cell senescence. These cells can be cultivated up to 7 days without passaging, but the rate of colony detachment and cell senescence increases. In this RNA-seq analysis indeed, naïve cells at Day 7 cultivated in wells are separated from other naïve samples (fig.4.19 and 4.21 PCA panel), while samples from microfluidic chips, even after 7 days clusterize perfectly with samples of Day 4, suggesting a protective mechanism provided by the confined environment. From a reactome analysis it emerges that in microfluidics cell-cycle, protein translation and metabolic pathways are upregulated, while in wells RNA-degradation, stress, senescence and apoptosis pathways are upregulated, supporting a positive influence of the confined environment on naïve cells. Notably, from the matrisome analysis, it emerges a strong transcription of ECM-related genes in the first days in culture, both in well and in microfluidics.

One of the most striking results of this analysis is the fact that naïve HPD06 cells express more ECM-related genes compared to primed HPD06, as reported from the number of genes detected in fig.4.20 and fig.4.21 and from the comparative analysis of fig.4.22. This result confirm the differences developmenta stage-related ECM deposition reported in paragraph 4.1.

Following this results, ECM deposition in HFF fibroblasts, naïve and primed HPD06 grown in well or microfluidic chips has been analyzed by immunofluorescence staining. With this technique, an increased ECM production with a more organized deposition has been demonstrated in fibroblasts, naïve and primed PSCs (fig.4.23-4.25), even if the most striking results have been obtained in naïve PSCs. If primed PSC are concerned, primed HPD06 line, which is isogenic to the naïve line used in this study, shows a remarkably increased ECM deposition in confined environment.

The accumulation of endogenous proteins in confined environment was previously deduced by analysis of optimal discontinuous perfusion strategies[221,223,224]. In those studies, cell survival and pluripotency maintenance was achieved only with discontinuous cell medium change, letting the cell-secreted factors to accumulate for several hours before medium change. Instead, if continuous medium flow was applied and factors were not allowed to accumulate in the surrounding environment, cell phenotype and survival was lost in few days. Nevertheless, the experiments reported in this thesis and published in Hu et al, 2018 are the first example of secretome analysis applied to microfluidic cell culture. Indeed, it is fundamental to study cell secretome in a more physiological cell culture system that mimics the *in vivo* microenvironmental conditions such as the interstitial spaces within tissues and the results highlight once more the pivotal role of ECM in cell behavior.

Taken together these data demonstrate that exposing cells to the confined environment granted by microfluidic devices guarantees endogenous protein accumulation in the limited surrounding space. Moreover, these data report for the first time that extracellular matrix deposition is enhanced in confined environment, both in primed and in naïve pluripotent stem cells. Indeed, in microfluidic devices, not only the different collagens can be detected in higher amount, but also, the extracellular network of such proteins is better organized.

5.3. COLONY SHAPE AND MATRIX DEPOSITION ARE LINKED TO PLURIPOTENCY IN NAÏVE PLURIPOTENT STEM CELLS

As extensively described, the most striking difference between naïve and primed PSC, from a morphological point of view is the 3D organization of the cells in the colony. In fact, in primed colonies the cells spread in a bidimensional monolayer, while naïve colonies are arranged in 3D compact domes, with multiple layers of cells. Interestingly, when culturing naïve cells, seldom colonies lost the typical 3D shape for a flatter monolayer-like organization. Therefore the link between colony shape, ECM deposition and pluripotency was investigated in naïve colonies.

Indeed, only 3D naïve colonies rearrange and organize ECM in thick rings around the colonies, while flat colonies are not surrounded by ECM. Moreover, 3D naïve colonies show a higher staining for pluripotency markers such as OCT4, TFCP2L1, TFE3 and KLF17 comparing to bidimensional colonies. Finally, in naïve 3D colonies higher expression of both ECM proteins and of pluripotency markers has been reported. These data are in agreement with a previous work that analyzed the correlation between colony morphology and pluripotency in primed colonies[213]. In this work, Yu et al. cultivated primed iPSCs on low adhesive substrates, obtaining two different colony morphology: about 90% of the colonies retained the conventional flat primed morphology, while a 10% acquired a 3D dome shape, similar to the one observed in naïve colonies. Indeed, this feature was intrinsic in the cells expression program, since in following passages 3D and 2D colonies maintained the respective shape. When the authors analyzed the transcriptome of the two populations, in the 3D compartment a higher expression of NANOG and KLF4, which are typical naïve markers, has been highlighted. Unfortunately the authors did not verify any other feature typical of naïve cells. Indeed, this work underlines once more how cell populations are characterized by intrinsic heterogeneity that can only be uncovered at single-cell level.

With the quest to determine whether also naïve colonies were able to maintain 3D or 2D morphology with passaging or if the appearance of flat colonies was a random feature, the picking experiment described in fig.4.30 was performed. Indeed, 3D colonies dissociated at single cell level resulted in 3D colonies, while cells originated from flat colony picking and dissociation gave rise to flat colonies. Even if these data should be confirmed with a higher number of picked colonies, they confirm that 3D or 2D morphology is not randomly acquired but it is maintained along passages, confirming the observations of Yu et al.

As shown in fig.4.31, fibroblasts, naïve and primed PSC are also characterized by a different expression of matrix remodeling enzymes such as MMP-, TIMP-, ADAM- and ADAMTS-family proteins. Among the genes overexpressed in naïve cells, MMP9 is fundamental to remodel collagen IV and laminin and it has been associated with cancer invasion[133], while MMP14 is involved in embryo development. Nevertheless, most of the genes overexpressed in this cluster have not been exhaustively studied and their role may have to be uncovered yet, suggesting an uncovered role for ECM remodeling in naïve PSC.

Proceeding in the analysis of naïve cells-environment interactions, the whole panel of integrin expression has been analyzed in naïve and primed PSC and in fibroblasts. Also in this case, a clear clusterization has been observes, indicating a differential role of integrins in the three developmental stages. In particular, most of the integrins known in literature to be important for primed PSC maintenance, such as integrin α4, α6, αV and β1, which are overexpressed in primed samples, in naïve samples are strongly downregulated, suggesting an alternative pathway of cell-ECM adhesion in naïve colonies. Among the upregulated integrins in naïve samples, only integrin β4[289], β5[290] and α9[291] have been previously related with adult stem cells or with cancer stem cells. The role of those proteins has never been investigated in naïve or embryonic PSC and therefore few tools and assays are available to study this group of integrins. For this reason, more well-characterized integrins have been analyzed in this thesis. However, it is important to notice that, even if α4, α6, αV, β1 and other integrins well known to be important for embryogenesis are downregulated in naïve cells compared to the

other samples of the database, this does not imply that naïve cells do not express them at all.

As shown in fig.4.33, blocking α4 integrin interaction with matrix proteins reduced colony number and overall colony diameter, demonstrating a destabilizing effect on naïve pluripotent stem cells, even if more experiments are needed to validate if reduction in colony number or diameter is due to cell death, colony detachment or altered proliferation. Blocking β1 integrin instead did not have a significative influence on colony number or on colony diameter, demonstrating the inactivation of this integrin in naïve cells. In fact, as reported in chapter 1.2.3.2, in human embryonic stem cells β1 integrin is kept inactive by integrin α6, and activation of β1 integrin results in exit from pluripotency[194]. Therefore, it is acceptable that blocking β1 integrin did not have significant effect, even if more trials are needed to confirm these results. The treatment with blocking antibodies had a visible effect also on MEF morphology: on treated channels, MEF cells looked shrunk, leaving large empty areas in the feeder layer. As shown in fig.4.33, blocking α4 and β1 integrin gave also an effect on colony morphology: in control channels, the 3D dome-shape morphology prevailed, while treated channels flat colonies were more frequent than in the controls.

By applying a strategy that has been already used in literature to induce exit from ground state pluripotency in mouse embryonic stem cells[211], naïve HPD06 colonies have been treated with Mn^{2+}, which activates integrins aspecifically. As shown in fig.4.34, Mn^{2+} administration did not induce colony detachment when colonies are treated from after single-cell dissociation and seeding, even if the growth was impaired, but had a significant effect on well grown colonies, where a significative reduction in colony number was reported, indicating an involvement of integrins in well grown colonies.

As shown in fig.4.32, naïve colonies are characterized also by a peculiar expression of proteoglycans and in particular, CSPG family proteoglycans, which have been reported to be important for embryonic development[292], such as CSPG5 are upregulated in naïve colonies. By inhibiting the interaction between naïve cells and CSPG motif, a significant colony detachment and reduction in colony

diameter was observed, suggesting a possible role for proteoglycans of the CSPG family in naïve pluripotency maintenance that has never been reported before.

As described in chapter 1.2.3 and as reported in chapter 4.1, not only pluripotent stem cell are characterized by a peculiar ECM organization, but also signaling pathways linking matrix and nucleus as well as mechanotransduction pathways are different from differentiated cells. These evidences point out a different role of these pathways in pluripotent cells compared to differentiated cells, but also a different activation in primed when compared to naïve PSCs. Moreover, as discussed in chapter 1.2.3.2, in primed pluripotent stem cells the focal adhesion kinase protein (FAK) is regulated according to a non-canonical mechanism[194,197,198].

Therefore, total FAK localization has been evaluated by immunofluorescence staining in naïve and primed HPD06 colonies (Fig.4.37 and Fig.4.38). FAK, which in differentiated cells is a key component of focal adhesions, responsible for transducing the intracellular signaling cascade initiated by integrin-extracellular matrix contact, in pluripotent stem cells has a nuclear localization and interacts physically with the core pluripotency network (OCT4, SOX2 and NANOG)[194,198,201]. Upon integrin α6 downregulation, FAK is phosphorylated at Y397 and moves from the nucleus to the membrane, where it participates to focal adhesions. Indeed, in 3D naïve colonies FAK in not localized in focal adhesion, but has a diffused signal inside the cell, while in flat naïve colonies the expression of this protein is focused in bright spots corresponding to focal adhesions. FAK expression has a similar localization in the bottom and at the top of the colony, but some cells at the bottom exiting from the main body of the colony and protruding with a flatter morphology (shown in fig. 4.37) have a completely nuclear localization. These data indicate the possible activation of FAK non-canonical pathway already recognized in pluripotent cells. Also in primed colonies FAK has a diffused localization and no foci of FAK in focal adhesions have been identified. Interestingly, cells at the edge of the colony have a more marked nuclear localization of FAK. Taking into account that the cells at the edge of the colony are the most subjected to mechanical stresses and also the more protrudent, with lamellopodia[296], this shared feature between naïve and

primed PSC may suggest and involvement in FAK nuclear localization with pluripotent cells response to mechanical stimuli.

Among the possible targets of non-canonical FAK pathway there is YAP signaling activation[163], even if the precise correlation between FAK and YAP has not been found yet. Moreover, only one work analyses YAP role in naïve PSCs and concludes that YAP activates naïve pluripotency[216]. This is in agreement with the transcriptomic analysis in fig.4.36 that shows the different YAP-correlated Hippo pathway expression in naïve and primed PSCs. By analyzing together data shown in fig.4.38, 4.39 and 4.40, many similarities can be noticed in YAP and FAK localization patterns. Indeed, after cytoskeleton disruption in naïve colonies following Latrunculin-A treatment, both YAP and FAK acquired a fully nuclear localization, both responding quickly to mechanic stimuli. This may indicate a relationship between these two proteins that has previously been reported in literature, but it is still not fully understood and never reported for naïve PSCs [106,163,210,293].

In conclusion, the data presented in this paragraph indicate a strong relationship among colony shape, ECM deposition or remodeling and naïve pluripotency marker expression, which has never been previously reported. Moreover, FAK non-canonical localization has been shown to be present in both naïve and primed PSCs, at least by identifying FAK nuclear localization with immunofluorescence staining. It was also shown that YAP-mediated transcription is active in naïve and primed pluripotent stem cells, with marked nuclear localization at the bottom and at the edge of naïve PSC colonies and at the edge of primed PSC colonies. Finally, FAK and YAP localization dependence on actin cytoskeleton integrity has been reported in naïve pluripotent stem cells.

5.4. MICROFLUIDIC HIGH EFFICIENCY CELL REPROGRAMMING IS LINKED TO ECM DEPOSITION

It has been demonstrated that microfluidic environment promotes high efficiency cell reprogramming, with substantial increase in reprogramming efficiency compared to other methods already available that exploit conventional cell culture devices[226]. In Luni et al. 2016, an increase in TGF-β1 endogenous pattern activation is reported as partial explanation for this result, but only with a high throughput approach it will be possible to identify all the players involved in this stunning increase in reprogramming efficiency. With SILAC-mass spectrometry technique, the secretome of human fibroblasts (which represent the starting point of cell reprogramming) and of hiPSCs (which are the end point of the process) have been analyzed, as already reported in chapter 4.2. These data point out how microfluidic environment promotes extracellular proteins secretion and accumulation and Gene Ontology analysis identify extracellular matrix components as the first category represented in proteins overexpressed in microfluidics. Indeed, as discussed before, ECM remodeling has been recognized as a fundamental point of cell reprogramming, mandatory for the correct conversion of fibroblasts in iPSCs[208]. Therefore, ECM deposition was analyzed at the end of reprogramming process in microfluidics and in conventional cell culture devices.

As reported in fig4.36, 4.37 and 4.38, in well the newborn colonies are not embedded with ECM network, but are only surrounded by ECM proteins in correspondence to the fibroblast layer surrounding the colonies. Instead in confined environment the colonies are permeated as if innervated by ECM, in some cases are surrounded by thick fibers of ECM proteins such as collagen I and also the actin ring is thicker, as expected in pluripotent cells[207]. Some ECM proteins, such as laminin and collagen IV cover the colony as a shell in confined environment, but not in conventional wells.

More high-throughput and multi-omics analysis are needed to establish the origin of high efficiency cell reprogramming in confined environment, but these data already indicate a significant difference in ECM organization around newborn colonies in the two environments. Keeping into account the deep connection between ECM and stemness, these data may contribute to explain high efficiency cell reprogramming in microfluidics.

5.5. EXOGENOUS ADMINISTRATION OF RECOMBINANT SERPINB3 INHIBITS CELL REPROGRAMMING

As described in paragraph 1.1.4, cancer onset is characterized by a dysregulated cell expression program, with reacquisition of stem cell-specific features, such as unlimited proliferation and motility. Therefore, cancer reprogramming has been proposed as a novel approach for a better understanding of cancer biology and to discover new targets for clinical practice. Unfortunately, reprogramming cancers can be challenging due to the genetic and epigenetic aberrations characteristic of cancer cells[104-114]. Therefore, the identification of molecules that can affect cancer cell reprogramming might be helpful to better define this new therapeutic strategy. For this reason, the administration to a well-established reprogramming model of the protease inhibitor SERPINB3 has been tested to create a model of cancer reprogramming. This model was based on BJ human fibroblasts treated with exogenous administration of SERPINB3 protein, a molecule found overexpressed in tumors with poor prognosis as reported in paragraph 1.1.4.3[115-128]. Presented data have demonstrated that this treatment inhibits cell reprogramming in a time-dependent fashion. In particular, the inhibition was more drastic when the protein was administered before the Mesenchymal-to-Epithelial Transition, not because of an impairment in the expression of the pluripotency genes, but because of the impairment of TGF-β1 expression and the conflict between Epithelial-to-Mesenchymal Transition promoted by SERPINB3 and the Mesenchymal-to-Epithelial Transition promoted by cell reprogramming.

As previous data reported, SERPINB3 in tumors has both an endogenous and a paracrine signaling role[124,128], in which this serpin is secreted by the cancer cells and promotes dedifferentiation and invasiveness in the neighbor cells. Tumor environment is therefore conditioned by SERPINB3 overexpression at the point that, for example, in patients with liver cancer, high levels in serum of SERPINB3 linked to IgM are considered a marker of poor prognosis and undifferentiated

tumor[294,295]. In this scenario, the importance of SERPINB3 paracrine effect is once again confirmed and the demonstration that its exogenous administration can inhibit cell reprogramming is a further evidence of SERPINB3 role in controlling cell fate. To further validate our findings, it is important to consider that the microfluidic environment reproduces the in vivo environment in a more physiological way, since paracrine signaling is enhanced, due to the reduced amount of cell culture medium surrounding the cells. Therefore, simulating cell environment in microfluidics with SERPINB3 exogenous administration gives a better representation of the tumor microenvironment comparing to other cell culture devices.

As a support to our results, data analysis on microarray databases have shown that in regular fibroblast reprogramming, SERPINB3 is downregulated until the very last phases of reprogramming process. Moreover, the analysis on SERPINB3-related genes confirms how the overexpression of this protein with the wrong timing could disrupt a delicate process as cell reprogramming is. Nevertheless, SERPINB3 related genes are crucial for cell reprogramming and their expression can cluster with high significance the different stages of cell reprogramming.

Cancer reprogramming is an emerging field that is providing promising results in those cases where the tumorigenic potential is lost following cancer cell reprogramming and differentiation. Unfortunately many cases are reported where cancer reprogramming has failed due to unknown reasons that have been correlated to aberrant genetic or epigenetic regulation in cancer cells. The data presented provides evidence that SERPINB3 profoundly affects the cell fate and inhibition of its expression or of its biological activity might be of paramount importance when considering reprogramming strategies for malignant tumors with high expression of this serpin.

5.6. CONCLUSIONS

The data presented in this work give an important contribution to the field of cell biology, especially for the fresh field of naïve pluripotent stem cells.

For the first time, the production and organization of extracellular matrix from naïve pluripotent stem cells has been investigated, confirming that those cells produce and rearrange ECM proteins. In fact, it has been reported how the matrix produced by those cells has a peculiar organization, different not only from differentiated cells, but also from primed pluripotent stem cells. It has also been shown for the first time how the confined environment, created to better simulate the physiological cell environment thanks to microfluidic technology, promotes protein secretion and ECM proteins deposition. Furthermore, it has been reported how cell-ECM interaction and colony shape is important for the maintenance of naïve pluripotency, with new implications on the role of FAK and YAP in naïve and primed pluripotency. Moreover, a peculiar ECM organization after high efficiency cell reprogramming in microfluidics has been described. This results will open the way to a full understanding of the role of confined environment on pluripotency acquisition. In addition, a model for microfluidic cancer cell reprogramming has been proposed by analyzing the pivotal role of SERPINB3 and SERPINB3-related gene network on cell reprogramming. Finally, a microfluidic-based system for single-cell RNA-sequencing has been setup to study system heterogeneity.

In conclusion, extracellular matrix deposition has a specific organization according to cell developmental stage and confined environments can boost ECM production and the signaling feedback loops triggered by cell-ECM and cell-secreted molecules interactions. Therefore, microfluidic-based confined environment can play a fundamental role on pluripotency maintenance and acquisition.

BIBLIOGRAPHY

1. Smith, A. A glossary for stem-cell biology. Nature 441, 1060–1060 (2006).
2. Hanna, J. H., Saha, K. & Jaenisch, R. Pluripotency and cellular reprogramming: facts, hypotheses, unresolved issues. Cell 143, 508–25 (2010).
3. Gilbert, S. F. Developmental biology. (Sinauer Associates, 2000).
4. Trounson, A. & DeWitt, N. D. Pluripotent stem cells progressing to the clinic. Nat. Rev. Mol. Cell Biol. 17, 194–200 (2016).
5. Goldberg, A. D., Allis, C. D. & Bernstein, E. Epigenetics: A Landscape Takes Shape. Cell 128, 635–638 (2007).
6. Xue, Z. et al. Genetic programs in human and mouse early embryos revealed by single-cell RNA sequencing. Nature 500, 593–597 (2013).
7. Xu, Q. & Xie, W. Epigenome in Early Mammalian Development: Inheritance, Reprogramming and Establishment. Trends Cell Biol. 28, 237–253 (2018).
8. Tanaka, S., Kunath, T., Hadjantonakis, A. K., Nagy, A. & Rossant, J. Promotion of trophoblast stem cell proliferation by FGF4. Science 282, 2072–5 (1998).
9. Nishioka, N. et al. The Hippo signaling pathway components Lats and Yap pattern Tead4 activity to distinguish mouse trophectoderm from inner cell mass. Dev. Cell 16, 398–410 (2009).
10. Schrode, N., Saiz, N., Di Talia, S. & Hadjantonakis, A.-K. GATA6 Levels Modulate Primitive Endoderm Cell Fate Choice and Timing in the Mouse Blastocyst. Dev. Cell 29, 454–467 (2014).
11. Li, P. et al. Morphogen gradient reconstitution reveals Hedgehog pathway design principles. Science 360, 543–548 (2018).
12. Sagner, A. & Briscoe, J. Morphogen interpretation: concentration, time, competence, and signaling dynamics. Wiley Interdiscip. Rev. Dev. Biol. 6, e271 (2017).
13. Hogan, B. L. Changes in the behaviour of teratocarcinoma cells cultivated in vitro. Nature 263, 136–7 (1976).
14. Evans, M. J. & Kaufman, M. H. Establishment in culture of pluripotential cells from mouse embryos. Nature 292, 154–6 (1981).
15. James A. Thomson, Joseph Itskovitz-Eldor, S. S. S., Michelle A. Waknitz, Jennifer J. Swiergiel, V. S. M. & Jones, J. M. Embryonic Stem Cell Lines Derived from Human Blastocysts. Science (80-.). 282, 1145–1147 (1998).
16. Nichols, J. & Smith, A. Pluripotency in the embryo and in culture. Cold Spring Harb. Perspect. Biol. 4, a008128 (2012).
17. Xu, C. et al. Feeder-free growth of undifferentiated human embryonic stem cells. Nat. Biotechnol. 19, 971–974 (2001).

18. Braam, S. R. et al. Recombinant Vitronectin Is a Functionally Defined Substrate That Supports Human Embryonic Stem Cell Self-Renewal via αVβ5 Integrin. Stem Cells 26, 2257–2265 (2008).

19. Chia, N.-Y. et al. A genome-wide RNAi screen reveals determinants of human embryonic stem cell identity. Nature 468, 316–320 (2010).

20. Theunissen, T. W. et al. Molecular Criteria for Defining the Naive Human Pluripotent State. Cell Stem Cell 19, 502–515 (2016).

21. Watanabe, K. et al. A ROCK inhibitor permits survival of dissociated human embryonic stem cells. Nat. Biotechnol. 25, 681–686 (2007).

22. Gafni, O. et al. Derivation of novel human ground state naive pluripotent stem cells. Nature 520, 710–710 (2013).

23. Tesar, P. J. et al. New cell lines from mouse epiblast share defining features with human embryonic stem cells. Nature 448, 196–199 (2007).

24. Meissner, A. et al. Genome-scale DNA methylation maps of pluripotent and differentiated cells. Nature 454, 766–770 (2008).

25. Brons, I. G. M. et al. Derivation of pluripotent epiblast stem cells from mammalian embryos. Nature 448, 191–195 (2007).

26. Nichols, J. & Smith, A. Naive and Primed Pluripotent States. Cell Stem Cell 4, 487–492 (2009).

27. Hanna, J. et al. Metastable Pluripotent States in NOD-Mouse-Derived ESCs. Cell Stem Cell 4, 513–524 (2009).

28. Hanna, J. et al. Human embryonic stem cells with biological and epigenetic characteristics similar to those of mouse ESCs. Proc. Natl. Acad. Sci. U. S. A. 107, 9222–7 (2010).

29. Guo, G. et al. Naive Pluripotent Stem Cells Derived Directly from Isolated Cells of the Human Inner Cell Mass. Stem Cell Reports 6, 437–446 (2016).

30. Marks, H. et al. The transcriptional and epigenomic foundations of ground state pluripotency. Cell 149, 590–604 (2012).

31. Betschinger, J. et al. Exit from pluripotency is gated by intracellular redistribution of the bHLH transcription factor Tfe3. Cell 153, 335–47 (2013).

32. Collier, A. J. et al. Comprehensive Cell Surface Protein Profiling Identifies Specific Markers of Human Naive and Primed Pluripotent States. Cell Stem Cell 20, 874–890.e7 (2017).

33. Tang, W. W. C. et al. A unique gene regulatory network resets the human germline epigenome for development. Cell 161, 1453–1467 (2015).

34. Shakiba, N. et al. CD24 tracks divergent pluripotent states in mouse and human cells. Nat. Commun. 6, 7329 (2015).

35. Kilens, S. et al. Parallel derivation of isogenic human primed and naive induced pluripotent stem cells. Nat. Commun. 9, 360 (2018).

36. Gu, W. et al. Glycolytic Metabolism Plays a Functional Role in Regulating Human Pluripotent Stem Cell State. Cell Stem Cell 19, 476–490 (2016).

37. Lengner, C. J. et al. Derivation of pre-X inactivation human embryonic stem cells under physiological oxygen concentrations. Cell 141, 872–83 (2010).

38. Sahakyan, A. et al. Human Naive Pluripotent Stem Cells Model X Chromosome Dampening and X Inactivation. Cell Stem Cell 20, 87–101 (2017).

39. Nishihara, S. Glycans define the stemness of naïve and primed pluripotent stem cells. Glycoconj. J. 34, 737–747 (2017).

40. Weinberger, L., Ayyash, M., Novershtern, N. & Hanna, J. H. Dynamic stem cell states: naive to primed pluripotency in rodents and humans. Nat. Rev. 17, 155–169 (2016).

41. Weismann, A. The Germ-plasm: a theory of heredity. Translated by W. Newton Parker and Harriet Rönnfeldt. (Scribner, 1893). doi:10.5962/bhl.title.25196

42. Gurdon, J. B. The Developmental Capacity of Nuclei taken from Intestinal Epithelium Cells of Feeding Tadpoles. Development 10, (1962).

43. GURDON, J. B., ELSDALE, T. R. & FISCHBERG, M. Sexually Mature Individuals of Xenopus laevis from the Transplantation of Single Somatic Nuclei. Nature 182, 64–65 (1958).

44. Campbell, K. H. S., McWhir, J., Ritchie, W. A. & Wilmut, I. Sheep cloned by nuclear transfer from a cultured cell line. Nature 380, 64–66 (1996).

45. Tada, M., Takahama, Y., Abe, K., Nakatsuji, N. & Tada, T. Nuclear reprogramming of somatic cells by in vitro hybridization with ES cells. Curr. Biol. 11, 1553–8 (2001).

46. Cowan, C. A. Nuclear Reprogramming of Somatic Cells After Fusion with Human Embryonic Stem Cells. Science (80-.). 309, 1369–1373 (2005).

47. Davis, R. L., Weintraub, H. & Lassar, A. B. Expression of a single transfected cDNA converts fibroblasts to myoblasts. Cell 51, 987–1000 (1987).

48. Takahashi, K. & Yamanaka, S. Induction of Pluripotent Stem Cells from Mouse Embryonic and Adult Fibroblast Cultures by Defined Factors. Cell 126, 663–676 (2006).

49. Takahashi, K. et al. Induction of Pluripotent Stem Cells from Adult Human Fibroblasts by Defined Factors. Cell 131, 861–872 (2007).

50. Yu, J. et al. Induced Pluripotent Stem Cell Lines Derived from Human Somatic Cells. Science (80-.). 318, (2007).

51. Silva, J. et al. Nanog Is the Gateway to the Pluripotent Ground State. Cell 138, 722–737 (2009).

52. Newman, M. A., Thomson, J. M. & Hammond, S. M. Lin-28 interaction with the Let-7 precursor loop mediates regulated microRNA processing. RNA 14, 1539–1549 (2008).

53. Li, M. & Belmonte, J. C. I. Deconstructing the pluripotency gene regulatory network. Nat. Cell Biol. 2018 204 20, 382 (2018).

54. Shi, Y., Inoue, H., Wu, J. C. & Yamanaka, S. Induced pluripotent stem cell technology: A decade of progress. Nature Reviews Drug Discovery 16, 115–130 (2017).

55. Zhou, T. et al. Generation of human induced pluripotent stem cells from urine samples. Nat. Protoc. 7, 2080–2090 (2012).

56. Haase, A. et al. Generation of Induced Pluripotent Stem Cells from Human Cord Blood. Cell Stem Cell 5, 434–441 (2009).

57. Robinton, D. A. & Daley, G. Q. The promise of induced pluripotent stem cells in research and therapy. Nature 481, 295–305 (2012).

58. Guhr, A. et al. Recent Trends in Research with Human Pluripotent Stem Cells: Impact of Research and Use of Cell Lines in Experimental Research and Clinical Trials. Stem cell reports 0, (2018).

59. Merkle, F. T. et al. Human pluripotent stem cells recurrently acquire and expand dominant negative P53 mutations. Nature 545, 229–233 (2017).

60. Stevens, K. R. & Murry, C. E. Human Pluripotent Stem Cell-Derived Engineered Tissues: Clinical Considerations. Cell Stem Cell 22, 294–297 (2018).

61. Diecke, S., Jung, S. M., Lee, J. & Ju, J. H. Recent technological updates and clinical applications of induced pluripotent stem cells. Korean J. Intern. Med. 29, 547 (2014).

62. Malik, N. & Rao, M. S. A review of the methods for human iPSC derivation. in Methods in Molecular Biology 997, 23–33 (Humana Press, Totowa, NJ, 2013).

63. Poleganov, M. A. et al. Efficient Reprogramming of Human Fibroblasts and Blood-Derived Endothelial Progenitor Cells Using Nonmodified RNA for Reprogramming and Immune Evasion. Hum. Gene Ther. 26, 751–766 (2015).

64. Yamanaka, S. Elite and stochastic models for induced pluripotent stem cell generation. Nature 460, 49–52 (2009).

65. Rais, Y. et al. Deterministic direct reprogramming of somatic cells to pluripotency. Nature 502, 65–70 (2013).

66. Hochedlinger, K. & Jaenisch, R. Induced Pluripotency and Epigenetic Reprogramming. Cold Spring Harb. Perspect. Biol. 7, a019448 (2015).

67. Hanna, J. et al. Direct cell reprogramming is a stochastic process amenable to acceleration. Nature 462, 595–601 (2009).

68. Bar-Nur, O. et al. Small molecules facilitate rapid and synchronous iPSC generation. Nat. Methods 11, 1170–1176 (2014).

69. Vidal, S. E., Amlani, B., Chen, T., Tsirigos, A. & Stadtfeld, M. Combinatorial Modulation of Signaling Pathways Reveals Cell-Type-Specific Requirements for Highly Efficient and Synchronous iPSC Reprogramming. Stem Cell Reports 3, 574–584 (2014).

70. Cacchiarelli, D. et al. Integrative Analyses of Human Reprogramming Reveal Dynamic Nature of Induced Pluripotency. Cell 162, 412–424 (2015).

71. Stadtfeld, M., Maherali, N., Breault, D. T. & Hochedlinger, K. Defining Molecular Cornerstones during Fibroblast to iPS Cell Reprogramming in Mouse. Cell Stem Cell 2, 230–240 (2008).

72. Li, R. et al. A mesenchymal-to-Epithelial transition initiates and is required for the nuclear reprogramming of mouse fibroblasts. Cell Stem Cell 7, 51–63 (2010).

73. Samavarchi-Tehrani, P. et al. Functional Genomics Reveals a BMP-Driven Mesenchymal-to-Epithelial Transition in the Initiation of Somatic Cell Reprogramming. Cell Stem Cell 7, 64–77 (2010).

74. Liu, X. et al. Sequential introduction of reprogramming factors reveals a time-sensitive requirement for individual factors and a sequential EMT-MET mechanism for optimal reprogramming. Nat. Cell Biol. 15, 829–838 (2013).

75. Mikkelsen, T. S. et al. Dissecting direct reprogramming through integrative genomic analysis. Nature 454, 49–55 (2008).

76. Maherali, N. et al. Directly reprogrammed fibroblasts show global epigenetic remodeling and widespread tissue contribution. Cell Stem Cell 1, 55–70 (2007).

77. Li, D. et al. Chromatin Accessibility Dynamics during iPSC Reprogramming. Cell Stem Cell 21, 819–833.e6 (2017).

78. Liu, X. et al. Comprehensive characterization of distinct states of human naive pluripotency generated by reprogramming. Nat. Methods 14, 1055–1062 (2017).

79. Takashima, Y. et al. Resetting transcription factor control circuitry toward ground-state pluripotency in human. Cell 158, 1254–1269 (2014).

80. Chan, Y. S. et al. Induction of a human pluripotent state with distinct regulatory circuitry that resembles preimplantation epiblast. Cell Stem Cell 13, 663–675 (2013).

81. Theunissen, T. W. et al. Systematic Identification of Culture Conditions for Induction and Maintenance of Naive Human Pluripotency. Cell Stem Cell 15, 471–487 (2014).

82. Warrier, S. et al. Direct comparison of distinct naive pluripotent states in human embryonic stem cells. Nat. Commun. 8, (2017).

83. Goding, C. R., Pei, D. & Lu, X. Cancer: pathological nuclear reprogramming? Nat. Rev. Cancer 14, 568–573 (2014).

84. Brabletz, T., Kalluri, R., Nieto, M. A. & Weinberg, R. A. EMT in cancer. Nat. Rev. Cancer 18, 128–134 (2018).

85. Toh, T. B., Lim, J. J. & Chow, E. K.-H. Epigenetics in cancer stem cells. Mol. Cancer 16, 29 (2017).

86. Bonnet, D. & Dick, J. E. Human acute myeloid leukemia is organized as a hierarchy that originates from a primitive hematopoietic cell. Nat. Med. 3, 730–737 (1997).

87. Al-Hajj, M., Wicha, M. S., Benito-Hernandez, A., Morrison, S. J. & Clarke, M. F. Prospective identification of tumorigenic breast cancer cells. Proc. Natl. Acad. Sci. 100, 3983–3988 (2003).

88. Annett, S. & Robson, T. Targeting cancer stem cells in the clinic: Current status and perspectives. Pharmacol. Ther. 187, 13–30 (2018).

89. Islam, F., Qiao, B., Smith, R. A., Gopalan, V. & Lam, A. K.-Y. Cancer stem cell: Fundamental experimental pathological concepts and updates. Exp. Mol. Pathol. 98, 184–191 (2015).

90. Nguyen, L. V., Vanner, R., Dirks, P. & Eaves, C. J. Cancer stem cells: an evolving concept. Nat. Rev. Cancer 12, 133 (2012).

91. Yamashita, T. et al. EpCAM-Positive Hepatocellular Carcinoma Cells Are Tumor-Initiating Cells With Stem/Progenitor Cell Features. Gastroenterology 136, (2009).

92. Thorgeirsson, S. S. & Grisham, J. W. Molecular pathogenesis of human hepatocellular carcinoma. Nature Genetics 31, 339–346 (2002).

93. Kelly, P. N., Dakic, A., Adams, J. M., Nutt, S. L. & Strasser, A. Tumor growth need not be driven by rare cancer stem cells. Science 317, 337 (2007).

94. Magee, J. A., Piskounova, E. & Morrison, S. J. Cancer Stem Cells: Impact, Heterogeneity, and Uncertainty. Cancer Cell 21, 283–296 (2012).

95. Clarke, M. F. et al. Cancer Stem Cells—Perspectives on Current Status and Future Directions: AACR Workshop on Cancer Stem Cells. Cancer Res. 66, 9339–9344 (2006).

96. Lee, H. E. et al. An increase in cancer stem cell population after primary systemic therapy is a poor prognostic factor in breast cancer. Br. J. Cancer 104, 1730–1738 (2011).

97. Visvader, J. E. Cells of origin in cancer. Nature 469, 314–322 (2011).

98. Ben-Porath, I. et al. An embryonic stem cell–like gene expression signature in poorly differentiated aggressive human tumors. Nat. Genet. 40, 499–507 (2008).

99. Kreso, A. et al. Variable clonal repopulation dynamics influence chemotherapy response in colorectal cancer. Science (80-.). 339, 543–548 (2013).

100. Friedmann-Morvinski, D. & Verma, I. M. Dedifferentiation and reprogramming: origins of cancer stem cells. EMBO Rep. 15, 244–253 (2014).

101. Vermeulen, L. et al. Wnt activity defines colon cancer stem cells and is regulated by the microenvironment. Nat. Cell Biol. 12, 468–476 (2010).

102. Batlle, E. & Clevers, H. Cancer stem cells revisited. Nat. Med. 23, 1124–1134 (2017).

103. Pardal, R., Clarke, M. F. & Morrison, S. J. Applying the principles of stem-cell biology to cancer. Nat. Rev. Cancer 3, 895–902 (2003).

104. Lim, K. L. et al. Reprogramming cancer cells: overview & current progress. Expert Opin. Biol. Ther. 16, 941–951 (2016).

105. Czerwińska, P., Mazurek, S. & Wiznerowicz, M. Application of induced pluripotency in cancer studies. Reports Pract. Oncol. Radiother. 23, 207–214 (2018).

106. Kim, J. et al. An iPSC line from human pancreatic ductal adenocarcinoma undergoes early to invasive stages of pancreatic cancer progression. Cell Rep. 3, 2088–99 (2013).

107. Nishi, M. et al. Induction of cells with cancer stem cell properties from nontumorigenic human mammary epithelial cells by defined reprogramming factors. Oncogene 33614, 643–652 (2014).

108. Zhang, X., Cruz, F. D., Terry, M., Remotti, F. & Matushansky, I. Terminal differentiation and loss of tumorigenicity of human cancers via pluripotency-based reprogramming. Oncogene 32, 2249–2260 (2013).

109. Suvà, M. L. et al. Reconstructing and reprogramming the tumor-propagating potential of glioblastoma stem-like cells. Cell 157, 580–594 (2014).

110. Stricker, S. H. et al. Widespread resetting of DNA methylation in glioblastoma-initiating cells suppresses malignant cellular behavior in a lineage-dependent manner. Genes Dev. 27, 654–669 (2013).

111. Pan, X. Y. et al. Application of Cancer Cell Reprogramming Technology to Human Cancer Research. Anticancer Res. 37, 3367–3377 (2017).

112. Zhou, S. et al. Reprogramming Malignant Cancer Cells toward a Benign Phenotype following Exposure to Human Embryonic Stem Cell Microenvironment. PLoS One 12, e0169899 (2017).

113. Stricker, S. & Pollard, S. Reprogramming cancer cells to pluripotency. Epigenetics 9, 798–802 (2014).

114. Mahalingam, D. et al. Reversal of Aberrant Cancer Methylome and Transcriptome upon Direct Reprogramming of Lung Cancer Cells. Sci. Rep. 2, 592 (2012).

115. Turato, C. et al. Over-expression of SERPINB3 in hepatoblastoma: A possible insight into the genesis of this tumour? Eur. J. Cancer 48, 1219–1226 (2012).

116. Turato, C. et al. SERPINB3 is associated with TGF-β1 and cytoplasmic β-catenin expression in hepatocellular carcinomas with poor prognosis. Br. J. Cancer 110, (2014).

117. Fassan, M. et al. Squamous cell carcinoma antigen (SCCA) is up-regulated during Barrett's carcinogenesis and predicts esophageal adenocarcinoma resistance to neoadjuvant chemotherapy. Oncotarget 8, 24372–24379 (2017).

118. Terrin, L. et al. SerpinB3 upregulates the Cyclooxygenase-2 / β-Catenin positive loop in colorectal cancer. Oncotarget 8, 15732–15743 (2017).

119. Vidalino, L. et al. SERPINB3, apoptosis and autoimmunity. Autoimmunity Reviews 9, 108–112 (2009).

120. Ciscato, F. et al. SERPINB3 protects from oxidative damage by chemotherapeutics through inhibition of mitochondrial respiratory complex I. Oncotarget 5, 2418–2427 (2014).

121. Cannito, S. et al. Hypoxia up-regulates SERPINB3 through HIF-2α in human liver cancer cells. Oncotarget 6, 2206–2221 (2015).

122. Morello, E. et al. Positive correlation of HIF2α and SERPINB3 in human hepatocellular carcinoma: selectivity and prognostic implications. Dig. Liver Dis. 47, e41–e42 (2015).

123. Pollutri, D. et al. MiR-122 targets SerpinB3 and is involved in Sorafenib resistance in hepatocellular carcinoma. Dig. Liver Dis. 49, e28 (2017).

124. Quarta, S. et al. SERPINB3 induces epithelial-mesenchymal transition. J. Pathol. 221, 343–356 (2010).

125. Novo, E. et al. SerpinB3 promotes pro-fibrogenic responses in activated hepatic stellate cells. Sci. Rep. 7, 3420 (2017).

126. Turato, C. et al. SerpinB3 and Yap Interplay Increases Myc Oncogenic Activity. Sci. Rep. 5, (2015).

127. Raggi, C. et al. The protease-inhibitor SerpinB3 outlines a stem-like subset in human cholangiocarcinoma. Dig. Liver Dis. 50, 47–48 (2018).

128. Catanzaro, J. M., Sheshadri, N. & Zong, W. X. SerpinB3/B4: Mediators of ras-driven inflammation and oncogenesis. Cell Cycle 13, 3155–3156 (2014).

129. Frantz, C., Stewart, K. M. & Weaver, V. M. The extracellular matrix at a glance. J. Cell Sci. 123, 4195–200 (2010).

130. Bissell, M. J., Hall, H. G. & Parry, G. How does the extracellular matrix direct gene expression? J. Theor. Biol. 99, 31–68 (1982).

131. Iozzo, R. V. & Gubbiotti, M. A. Extracellular matrix: The driving force of mammalian diseases. Matrix Biol. (2018). doi:10.1016/j.matbio.2018.03.023

132. Bonnans, C., Chou, J. & Werb, Z. Remodelling the extracellular matrix in development and disease. Nat. Rev. 15, 786–801 (2014).

133. Apte, S. S. & Parks, W. C. Metalloproteinases: A parade of functions in matrix biology and an outlook for the future. (2015). doi:10.1016/j.matbio.2015.04.005

134. Gordon, M. K. & Hahn, R. A. Collagens. Cell Tissue Res. 339, 247–257 (2010).

135. Mouw, J. K., Ou, G. & Weaver, V. M. Extracellular matrix assembly: a multiscale deconstruction. Nat. Rev. Mol. Cell Biol. 15, 771–785 (2014).

136. Olsen, B. R. in Principles of Tissue Engineering 189–208 (Elsevier, 2014). doi:10.1016/B978-0-12-398358-9.00010-0

137. Yurchenco, P. D. Basement Membranes: Cell Scaffoldings and Signaling Platforms. Cold Spring Harb. Perspect. Biol. 3, a004911–a004911 (2011).

138. Cescon, M., Gattazzo, F., Chen, P. & Bonaldo, P. Collagen VI at a glance. J. Cell Sci. 128, 3525–31 (2015).

139. Franzke, C.-W., Bruckner, P. & Bruckner-Tuderman, L. Collagenous transmembrane proteins: recent insights into biology and pathology. J. Biol. Chem. 280, 4005–8 (2005).

140. Banyard, J., Bao, L. & Zetter, B. R. Type XXIII collagen, a new transmembrane collagen identified in metastatic tumor cells. J. Biol. Chem. 278, 20989–94 (2003).

141. Pankov, R. & Yamada, K. M. Fibronectin at a glance. J. Cell Sci. 115, 3861–3 (2002).

142. Zollinger, A. J. & Smith, M. L. Fibronectin, the extracellular glue. Matrix Biol. 60–61, 27–37 (2017).

143. Durbeej, M. Laminins. Cell Tissue Res. 339, 259–268 (2010).

144. Domogatskaya, A. & Rodin, S. in 59–82 (Humana Press, Cham, 2018). doi:10.1007/978-3-319-77023-9_3

145. Pomin, V. & Mulloy, B. Glycosaminoglycans and Proteoglycans. Pharmaceuticals 11, 27 (2018).

146. Schaefer, L. & Schaefer, R. M. Proteoglycans: from structural compounds to signaling molecules. Cell Tissue Res. 339, 237–246 (2010).

147. Nikitovic, D. et al. Proteoglycans—Biomarkers and Targets in Cancer Therapy. Front. Endocrinol. (Lausanne). 9, 69 (2018).

148. Van der Flier, A. & Sonnenberg, A. Function and interactions of integrins. Cell and Tissue Research 305, 285–298 (2001).

149. Petreaca, M. & Martins-Green, M. The Dynamics of Cell-ECM Interactions, with Implications for Tissue Engineering. Princ. Tissue Eng. 161–187 (2014). doi:10.1016/B978-0-12-398358-9.00009-4

150. Shattil, S. J., Kim, C. & Ginsberg, M. H. The final steps of integrin activation: the end game. Nat. Rev. Mol. Cell Biol. 11, 288–300 (2010).

151. Takagi, J., Petre, B. M., Walz, T. & Springer, T. A. Global conformational rearrangements in integrin extracellular domains in outside-in and inside-out signaling. Cell 110, 599–11 (2002).

152. Kanchanawong, P. et al. Nanoscale architecture of integrin-based cell adhesions. Nature 468, 580–584 (2010).

153. Winograd-Katz, S. E., Fässler, R., Geiger, B. & Legate, K. R. The integrin adhesome: from genes and proteins to human disease. Nat. Rev. Mol. Cell Biol. 15, 273–288 (2014).

154. Horton, E. R. et al. Definition of a consensus integrin adhesome and its dynamics during adhesion complex assembly and disassembly. Nat. Cell Biol. 17, 1577–1587 (2015).

155. Sun, Z., Guo, S. S. & Fässler, R. Integrin-mediated mechanotransduction. J. Cell Biol. 215, 445–456 (2016).

156. Zhao, X. & Guan, J.-L. Focal adhesion kinase and its signaling pathways in cell migration and angiogenesis. Adv. Drug Deliv. Rev. 63, 610–615 (2011).

157. Goñi, G. M. et al. Phosphatidylinositol 4,5-bisphosphate triggers activation of focal adhesion kinase by inducing clustering and conformational changes. doi:10.1073/pnas.1317022111

158. Elosegui-Artola, A., Trepat, X. & Roca-Cusachs, P. Control of Mechanotransduction by Molecular Clutch Dynamics. Trends in Cell Biology 28, 356–367 (2018).

159. Martino, F., Perestrelo, A. R., Vinarský, V., Pagliari, S. & Forte, G. Cellular Mechanotransduction: From Tension to Function. Front. Physiol. 9, 824 (2018).

160. Panciera, T., Azzolin, L., Cordenonsi, M. & Piccolo, S. Mechanobiology of YAP and TAZ in physiology and disease. Nat. Rev. Mol. Cell Biol. 18, 758–770 (2017).

161. Dupont, S. et al. Role of YAP/TAZ in mechanotransduction. Nature 474, 179–183 (2011).

162. Aragona, M. et al. A Mechanical Checkpoint Controls Multicellular Growth through YAP/TAZ Regulation by Actin-Processing Factors. Cell 154, 1047–1059 (2013).

163. Lachowski, D. et al. FAK controls the mechanical activation of YAP, a transcriptional regulator required for durotaxis. FASEB J. 32, 1099–1107 (2018).

164. Desgrosellier, J. S. & Cheresh, D. A. Integrins in cancer: biological implications and therapeutic opportunities. Nat. Rev. Cancer 10, 9–22 (2010).

165. Sulzmaier, F. J., Jean, C. & Schlaepfer, D. D. FAK in cancer: mechanistic findings and clinical applications. Nat. Rev. Cancer 14, 598–610 (2014).

166. Wagers, A. J. & Weissman, I. L. Plasticity of Adult Stem Cells. Cell 116, 639–648 (2004).

167. Clevers, H. What is an adult stem cell? Science 350, 1319–20 (2015).

168. Rumman, M., Dhawan, J. & Kassem, M. Concise Review: Quiescence in Adult Stem Cells: Biological Significance and Relevance to Tissue Regeneration. Stem Cells 33, 2903–2912 (2015).

169. Cheung, T. H. & Rando, T. A. Molecular regulation of stem cell quiescence. Nat. Rev. Mol. Cell Biol. 14, 329–340 (2013).

170. Gattazzo, F., Urciuolo, A. & Bonaldo, P. Extracellular matrix: A dynamic microenvironment for stem cell niche. Biochim. Biophys. Acta - Gen. Subj. 1840, 2506–2519 (2014).

171. Brizzi, M. F., Tarone, G. & Defilippi, P. Extracellular matrix, integrins, and growth factors as tailors of the stem cell niche. Current Opinion in Cell Biology 24, 645–651 (2012).

172. Hynes, R. O. The extracellular matrix: not just pretty fibrils. Science 326, 1216–9 (2009).

173. Zanconato, F., Cordenonsi, M. & Piccolo, S. YAP/TAZ at the Roots of Cancer. Cancer Cell 29, 783–803 (2016).

174. McBeath, R., Pirone, D. M., Nelson, C. M., Bhadriraju, K. & Chen, C. S. Cell shape, cytoskeletal tension, and RhoA regulate stem cell lineage commitment. Dev. Cell 6, 483–95 (2004).

175. Mannaerts, I. et al. The Hippo pathway effector YAP controls mouse hepatic stellate cell activation. J. Hepatol. 63, 679–688 (2015).

176. Niklason, L. E. Understanding the Extracellular Matrix to Enhance Stem Cell-Based Tissue Regeneration. Cell Stem Cell 22, 302–305 (2018).

177. Hayashi, Y. & Furue, M. K. Biological Effects of Culture Substrates on Human Pluripotent Stem Cells. Stem Cells Int. 2016, 1–11 (2016).

178. Ludwig, T. E. et al. Derivation of human embryonic stem cells in defined conditions. Nat. Biotechnol. 24, 185–187 (2006).

179. Chen, G. et al. Chemically defined conditions for human iPSC derivation and culture. Nat. Methods 8, 424–429 (2011).

180. Hughes, C. S., Postovit, L. M. & Lajoie, G. A. Matrigel: A complex protein mixture required for optimal growth of cell culture. Proteomics 10, 1886–1890 (2010).

181. Kleinman, H. K. & Martin, G. R. Matrigel: Basement membrane matrix with biological activity. Semin. Cancer Biol. 15, 378–386 (2005).

182. Kleinman, H. K. et al. Basement membrane complexes with biological activity. Biochemistry 25, 312–8 (1986).

183. Rodin, S. et al. Long-term self-renewal of human pluripotent stem cells on human recombinant laminin-511. Nat. Biotechnol. 28, 611–615 (2010).

184. Miyazaki, T. et al. Recombinant human laminin isoforms can support the undifferentiated growth of human embryonic stem cells. Biochem. Biophys. Res. Commun. 375, 27–32 (2008).

185. Miyazaki, T. et al. Laminin E8 fragments support efficient adhesion and expansion of dissociated human pluripotent stem cells. Nat. Commun. 3, 1236 (2012).

186. Melkoumian, Z. et al. Synthetic peptide-acrylate surfaces for long-term self-renewal and cardiomyocyte differentiation of human embryonic stem cells. Nat. Biotechnol. 28, 606–610 (2010).

187. Villa-Diaz, L. G. et al. Synthetic polymer coatings for long-term growth of human embryonic stem cells. Nat. Biotechnol. 28, 581–583 (2010).

188. Higuchi, A. et al. Long-term xeno-free culture of human pluripotent stem cells on hydrogels with optimal elasticity. Sci. Rep. 5, 18136 (2016).

189. Sart, S., Ma, T. & Li, Y. Extracellular matrices decellularized from embryonic stem cells maintained their structure and signaling specificity. Tissue Eng. Part A 20, 54–66 (2014).

190. Evseenko, D. et al. Identification of the Critical Extracellular Matrix Proteins that Promote Human Embryonic Stem Cell Assembly. Stem Cells Dev. 18, 919–928 (2009).

191. Laperle, A. et al. α-5 Laminin Synthesized by Human Pluripotent Stem Cells Promotes Self-Renewal. Stem Cell Reports 5, 195–206 (2015).

192. Pook, M. et al. Changes in Laminin Expression Pattern during Early Differentiation of Human Embryonic Stem Cells. PLoS One 10, e0138346 (2015).

193. Rowland, T. J. et al. Roles of Integrins in Human Induced Pluripotent Stem Cell Growth on Matrigel and Vitronectin. Stem Cells Dev. 19, 1231–1240 (2010).

194. Villa-Diaz, L. G., Kim, J. K., Laperle, A., Palecek, S. P. & Krebsbach, P. H. Inhibition of Focal Adhesion Kinase Signaling by Integrin α6β1 Supports Human Pluripotent Stem Cell Self-Renewal. Stem Cells 34, 1753–1764 (2016).

195. Teramura, T. et al. Mechanical stimulation of cyclic tensile strain induces reduction of pluripotent related gene expressions via activation of Rho/ROCK and subsequent decreasing of AKT phosphorylation in human induced pluripotent stem cells. Biochem. Biophys. Res. Commun. 417, 836–841 (2012).

196. Kinehara, M. et al. Protein Kinase C Regulates Human Pluripotent Stem Cell Self-Renewal. PLoS One 8, e54122 (2013).

197. Vitillo, L., Baxter, M., Iskender, B., Whiting, P. & Kimber, S. J. Integrin-Associated Focal Adhesion Kinase Protects Human Embryonic Stem Cells from Apoptosis, Detachment, and Differentiation. Stem Cell Reports 7, 167–176 (2016).

198. Vitillo, L. & Kimber, S. J. Integrin and FAK Regulation of Human Pluripotent Stem Cells. Curr. stem cell reports 3, 358–365 (2017).

199. Sastry, S. K. et al. Quantitative changes in integrin and focal adhesion signaling regulate myoblast cell cycle withdrawal. J. Cell Biol. 144, 1295–309 (1999).

200. Kleinschmidt, E. G. & Schlaepfer, D. D. Focal adhesion kinase signaling in unexpected places. Curr. Opin. Cell Biol. 45, 24–30 (2017).

201. Lim, S.-T. S. Nuclear FAK: a new mode of gene regulation from cellular adhesions. Mol. Cells 36, 1–6 (2013).

202. Pakzad, M. et al. Presence of a ROCK Inhibitor in Extracellular Matrix Supports More Undifferentiated Growth of Feeder-Free Human Embryonic and Induced Pluripotent Stem Cells upon Passaging. Stem Cell Rev. Reports 6, 96–107 (2010).

203. Harb, N., Archer, T. K. & Sato, N. The Rho-Rock-Myosin Signaling Axis Determines Cell-Cell Integrity of Self-Renewing Pluripotent Stem Cells. PLoS One 3, e3001 (2008).

204. Chen, G., Hou, Z., Gulbranson, D. R. & Thomson, J. A. Actin-Myosin Contractility Is Responsible for the Reduced Viability of Dissociated Human Embryonic Stem Cells. Cell Stem Cell 7, 240–248 (2010).

205. Furue, M. et al. Leukemia inhibitory factor as an anti-apoptotic mitogen for pluripotent mouse embryonic stem cells in a serum-free medium without feeder cells. In Vitro Cell. Dev. Biol. Anim. 41, 19–28 (2005).

206. Singh, A. et al. Adhesion strength–based, label-free isolation of human pluripotent stem cells. Nat. Methods 10, 438–444 (2013).

207. Närvä, E. et al. A Strong Contractile Actin Fence and Large Adhesions Direct Human Pluripotent Colony Morphology and Adhesion. Stem Cell Reports 9, 67–76 (2017).

208. Qin, H. et al. Systematic Identification of Barriers to Human iPSC Generation. Cell 158, 449–461 (2014).

209. Vining, K. H. & Mooney, D. J. Mechanical forces direct stem cell behaviour in development and regeneration. Nat. Rev. Mol. Cell Biol. 18, 728–742 (2017).

210. Ohgushi, M., Minaguchi, M. & Sasai, Y. Rho-Signaling-Directed YAP/TAZ Activity Underlies the Long-Term Survival and Expansion of Human Embryonic Stem Cells. Cell Stem Cell 17, 448–461 (2015).

211. Taleahmad, S. et al. Low Focal Adhesion Signaling Promotes Ground State Pluripotency of Mouse Embryonic Stem Cells. J. Proteome Res. 16, 3585–3595 (2017).

212. Taleahmad, S. et al. Proteome Analysis of Ground State Pluripotency. Sci. Rep. 5, 17985 (2016).

213. Yu, L. et al. Low Cell-Matrix Adhesion Reveals Two Subtypes of Human Pluripotent Stem Cells. Stem Cell Reports (2018). doi:10.1016/J.STEMCR.2018.06.003

214. Schratt, G. et al. Serum response factor is crucial for actin cytoskeletal organization and focal adhesion assembly in embryonic stem cells. J. Cell Biol. 156, 737–50 (2002).

215. Ikeda, T. et al. Srf destabilizes cellular identity by suppressing cell-type-specific gene expression programs. Nat. Commun. 9, 1387 (2018).

216. Qin, H. et al. YAP Induces Human Naive Pluripotency. Cell Rep. 14, 2301–2312 (2016).

217. Sackmann, E. K., Fulton, A. L. & Beebe, D. J. The present and future role of microfluidics in biomedical research. Nature 507, 181–189 (2014).

218. Velve-Casquillas, G., Le Berre, M., Piel, M. & Tran, P. T. Microfluidic tools for cell biological research. Nano Today 5, 28–47 (2010).

219. Halldorsson, S., Lucumi, E., Gómez-Sjöberg, R. & Fleming, R. M. T. Advantages and challenges of microfluidic cell culture in polydimethylsiloxane devices. Biosensors and Bioelectronics 63, 218–231 (2015).

220. Gagliano, O. & Luni, C. Microfluidic technology enhances the potential of human pluripotent stem cells. Biochem. Biophys. Res. Commun. 473, 683–687 (2016).

221. Titmarsh, D., Hidalgo, A., Turner, J., Wolvetang, E. & Cooper-White, J. Optimization of flowrate for expansion of human embryonic stem cells in perfusion microbioreactors. Biotechnol. Bioeng. 108, 2894–2904 (2011).

222. Giobbe, G. G. et al. Functional differentiation of human pluripotent stem cells on a chip. Nat. Methods 12, 1–7 (2015).

223. Guild, J. et al. Embryonic Stem Cells Cultured in Microfluidic Chambers Take Control of Their Fate by Producing Endogenous Signals Including LIF. Stem Cells 34, 1501–1512 (2016).

224. Giulitti, S., Magrofuoco, E., Prevedello, L. & Elvassore, N. Optimal periodic perfusion strategy for robust long-term microfluidic cell culture. Lab Chip 13, 4430 (2013).

225. Warmflash, A., Sorre, B., Etoc, F., Siggia, E. D. & Brivanlou, A. H. A method to recapitulate early embryonic spatial patterning in human embryonic stem cells. Nat. Methods 11, 847–854 (2014).

226. Luni, C. et al. High-efficiency cellular reprogramming with microfluidics. Nat. Methods 13, 446–452 (2016).

227. Warren, L., Schlaeger, T. M. & Rossi, D. J. Highly Efficient Reprogramming to Pluripotency and Directed Differentiation of Human Cells with Synthetic Modified mRNA. Stem Cell 7, 618–630 (2010).

228. Warren, L., Ni, Y., Wang, J. & Guo, X. Feeder-free derivation of human induced pluripotent stem cells with messenger RNA. Sci Rep 2, 1–7 (2012).

229. Poleganov, M. A. et al. Efficient Reprogramming of Human Fibroblasts and Blood-Derived Endothelial Progenitor Cells Using Nonmodified RNA for Reprogramming and Immune Evasion. Hum. Gene Ther. 26, 751–766 (2015).

230. Anokye-Danso, F. et al. Highly Efficient miRNA-Mediated Reprogramming of Mouse and Human Somatic Cells to Pluripotency. Cell Stem Cell 8, 376–388 (2011).

231. Potter, S. S. Single-cell RNA sequencing for the study of development, physiology and disease. Nat. Rev. Nephrol. 14, 479–492 (2018).

232. Svensson, V., Vento-Tormo, R. & Teichmann, S. A. Exponential scaling of single-cell RNA-seq in the past decade. Nat. Protoc. 13, 599–604 (2018).

233. Haque, A., Engel, J., Teichmann, S. A. & Lönnberg, T. A practical guide to single-cell RNA-sequencing for biomedical research and clinical applications. Genome Med. 9, 75 (2017).

234. Kolodziejczyk, A. A., Kim, J. K., Svensson, V., Marioni, J. C. & Teichmann, S. A. The technology and biology of single-cell RNA sequencing. Mol. Cell 58, 610–20 (2015).

235. Tang, F. et al. mRNA-Seq whole-transcriptome analysis of a single cell. Nat. Methods 6, 377–382 (2009).

236. Zheng, G. X. Y. et al. Massively parallel digital transcriptional profiling of single cells. Nat. Commun. 8, 14049 (2017).

237. Halpern, K. B. et al. Single-cell spatial reconstruction reveals global division of labour in the mammalian liver. Nature 542, 1–5 (2017).

238. Macosko, E. Z. et al. Highly Parallel Genome-wide Expression Profiling of Individual Cells Using Nanoliter Droplets. Cell 161, 1202–1214 (2015).

239. Campbell, J. N. et al. A molecular census of arcuate hypothalamus and median eminence cell types. Nat. Neurosci. (2017). doi:10.1038/nn.4495

240. Cao, J. et al. Comprehensive single-cell transcriptional profiling of a multicellular organism. Science 357, 661–667 (2017).

241. Jaitin, D. A. et al. Dissecting Immune Circuits by Linking CRISPR-Pooled Screens with Single-Cell RNA-Seq. Cell 167, 1883–1896.e15 (2016).

242. Tsoucas, D. & Yuan, G. C. Recent progress in single-cell cancer genomics. Current Opinion in Genetics and Development 42, 22–32 (2017).

243. Tirosh, I. et al. Single-cell RNA-seq supports a developmental hierarchy in human oligodendroglioma. Nat. Publ. Gr. 539, (2016).

244. Fan, J. et al. Linking transcriptional and genetic tumor heterogeneity through allele analysis of single-cell RNA-seq data. Genome Res. 28, 1217–1227 (2018).

245. Moncada, R. et al. Building a tumor atlas: integrating single-cell RNA-Seq data with spatial transcriptomics in pancreatic ductal adenocarcinoma. bioRxiv 254375 (2018). doi:10.1101/254375

246. Zhao, T. et al. Single-Cell RNA-Seq Reveals Dynamic Early Embryonic-like Programs during Chemical Reprogramming. Cell Stem Cell 23, 31–45.e7 (2018).

247. Chu, L.-F. et al. Single-cell RNA-seq reveals novel regulators of human embryonic stem cell differentiation to definitive endoderm. Genome Biol. 17, 173 (2016).

248. Grün, D. Revealing routes of cellular differentiation by single-cell RNA-seq. Curr. Opin. Syst. Biol. 11, 9–17 (2018).

249. Klein, A. M. et al. Droplet barcoding for single-cell transcriptomics applied to embryonic stem cells. Cell 161, 1187–1201 (2015).

250. Karaiskos, N. et al. The Drosophila embryo at single-cell transcriptome resolution. Science 358, 194–199 (2017).

251. Trapnell, C. et al. The dynamics and regulators of cell fate decisions are revealed by pseudotemporal ordering of single cells. Nat. Biotechnol. 32, 381–386 (2014).

252. Cacchiarelli, D. et al. Aligning single-cell developmental and reprogramming trajectories identifies molecular determinants of reprogramming outcome. bioRxiv 122531 (2017). doi:10.1101/122531

253. Ziegenhain, C. et al. Comparative analysis of single-cell RNA sequencing methods. Mol. Cell 631–673 (2017). doi:10.1101/035758

254. Picelli, S. et al. Full-length RNA-seq from single cells using Smart-seq2. Nat. Protoc. 9, 171–81 (2014).

255. Zilionis, R. et al. Single-cell barcoding and sequencing using droplet microfluidics. Nat. Protoc. 12, 44–73 (2017).

256. Gierahn, T. M. et al. Seq-Well: portable, low-cost RNA sequencing of single cells at high throughput. Nat. Methods 14, 395–398 (2017).

257. Duffy, D. C., McDonald, J. C., Schueller, O. J. A. & Whitesides, G. M. Rapid prototyping of microfluidic systems in poly(dimethylsiloxane). Anal. Chem. 70, 4974–4984 (1998).

258. Symons, J. a, Alcamí, a & Smith, G. L. Vaccinia virus encodes a soluble type I interferon receptor of novel structure and broad species specificity. Cell 81, 551–560 (1995).

259. Turato, C. et al. SERPINB3 modulates TGF-B expression in chronic liver disease. Lab. Investig. 90, 1016–1023 (2010).

260. Turato, C. et al. Increased antiprotease activity of the SERPINB3 polymorphic variant SCCA-PD. Exp. Biol. Med. 236, 281–290 (2011).

261. Denk, W., Strickler, J. H. & Webb, W. W. Two-photon laser scanning fluorescence microscopy. Science 248, 73–6 (1990).

262. Zoumi, A., Yeh, A. & Tromberg, B. J. Imaging cells and extracellular matrix in vivo by using second-harmonic generation and two-photon excited fluorescence. Proc. Natl. Acad. Sci. U. S. A. 99, 11014–9 (2002).

263. Takahashi, K. et al. Induction of pluripotency in human somatic cells via a transient state resembling primitive streak-like mesendoderm. Nat. Commun. 5, 3678 (2014).

264. Turato, C. Implicazioni biologiche di SerpinB3 nella fibrosi epatica e nell'epatocarcinoma. (2011).

265. Hashimoto, K.-I., Kiyoshima, T., Matsuo, K., Ozeki, S. & Sakai, H. Effect of SCCA1 and SCCA2 on the Suppression of TNF-␣ -Induced Cell Death by Impeding the Release of Mitochondrial Cytochrome c in an Oral Squamous Cell Carcinoma Cell Line. Tumor Biol 26, 165–172 (2005).

266. Turato, C., Simonato, D., Quarta, S., Gatta, A. & Pontisso, P. MicroRNAs and SerpinB3 in hepatocellular carcinoma. Life Sci. 100, 9–17 (2014).

267. Catanzaro, J. M. et al. Elevated Expression of Squamous Cell Carcinoma Antigen (SCCA) Is Associated with Human Breast Carcinoma. PLoS One 6, (2011).

268. Sheshadri, N. et al. SCCA1/SERPINB3 promotes oncogenesis and epithelial-mesenchymal transition via the unfolded protein response and IL6 signaling. Cancer Res. 74, 6318–6329 (2014).

269. Villano, G. et al. Role of squamous cell carcinoma antigen-1 on liver cells after partial hepatectomy in transgenic mice. Int. J. Mol. Med. 25, 137–143 (2010).

270. Suminami, Y. et al. Inhibition of apoptosis in human tumour cells by the tumour-associated serpin, SCC antigen-1. Br. J. Cancer 82, 981–9 (2000).

271. Murakami, A. et al. Tumor-related protein, the squamous cell carcinoma antigen binds to the intracellular protein carbonyl reductase. Int. J. Oncol. 36, 1395–1400 (2010).

272. Murakami, A. et al. Relationship between decreased expression of squamous cell carcinoma antigen 2 and E-cadherin in primary cervical cancer lesions and lymph node metastasis. Oncol. Rep. 19, 99–104 (2008).

273. Nawata, S. et al. Electrophoretic analysis of the 'cross-class' interaction between novel inhibitory serpin, squamous cell carcinoma antigen-1 and cysteine proteinases. Electrophoresis 18, 784–789 (1997).

274. Higgins, W. J., Fox, D. M., Kowalski, P. S., Nielsen, J. E. & Worrall, D. M. Heparin enhances serpin inhibition of the cysteine protease cathepsin L. J. Biol. Chem. 285, 3722–3729 (2010).

275. Catanzaro, J. M. et al. Oncogenic Ras induces inflammatory cytokine production by upregulating the squamous cell carcinoma antigens SerpinB3/B4. Nat. Commun. 5, (2014).

276. Katagiri, C., Nakanishi, J., Kadoya, K. & Hibino, T. Serpin squamous cell carcinoma antigen inhibits UV-induced apoptosis via suppression of c-JUN NH2-terminal kinase. J. Cell Biol. 172, 983–990 (2006).

277. Quarta, S. et al. P.428 SCCA over-expression induces cell proliferation and down-regulation of the adhesion system. J. Clin. Virol. 36, S193 (2006).

278. Cappon, A. et al. The protease-inhibitor SerpinB3 modulate survival and Wnt pathway of inflammatory human monocytes. Dig. Liver Dis. 48, e27 (2016).

279. Villano, G. et al. SERPINB3 is associated with longer survival in transgenic mice. doi:10.1038/srep03056

280. Xia, H. Bin & Chen, X. G. Overexpression of hepatitis B virus-binding protein, squamous cell carcinoma antigen 1, extends retention of hepatitis B virus in mouse liver. Acta Biochim. Biophys. Sin. (Shanghai). 38, 484–491 (2006).

281. Sueoka, K. et al. Tumor-associated serpin, squamous cell carcinoma antigen stimulates matrix metalloproteinase-9 production in cervical squamous cell carcinoma cell lines. Int. J. Oncol. 27, 1345–1353 (2005).

282. Suminami, Y. et al. Suppression of a squamous cell carcinoma (SCC)-related serpin, SCC antigen, inhibits tumor growth with increased intratumor infiltration of natural killer cells. Cancer Res. 61, 1776–80 (2001).

283. Cannito, S. et al. HIF2-alpha neddylation as a selective SerpinB3-dependent mechanism leading to its increase. J. Hepatol. 62, S410 (2015).

284. Sun, Y., Sheshadri, N. & Zong, W. X. SERPINB3 and B4: From biochemistry to biology. Seminars in Cell and Developmental Biology 62, 170–177 (2017).

285. Ahmed, S. T. & Darnell, J. E. Serpin B3/B4, activated by STAT3, promote survival of squamous carcinoma cells. Biochem. Biophys. Res. Commun. 378, 821–825 (2009).

286. Song, K. J., Ahn, H.-J. & Nam, H.-W. Anti-Apoptotic Effects of SERPIN B3 and B4 via STAT6 Activation in Macrophages after Infection with Toxoplasma gondii. Korean J. Parasitol. 50, 1–6 (2012).

287. Moll, P., Ante, M., Seitz, A. & Reda, T. QuantSeq 3′ mRNA sequencing for RNA quantification. Nat. Methods 11, i–iii (2014).

288. Hu, Q., Luni, C. & Elvassore, N. Microfluidics for secretome analysis under enhanced endogenous signaling. Biochem. Biophys. Res. Commun. 497, 480–484 (2018).

289. Bierie, B. et al. Integrin-β4 identifies cancer stem cell-enriched populations of partially mesenchymal carcinoma cells. Proc. Natl. Acad. Sci. 114, E2337–E2346 (2017).

290. Miranda, A., Pericuesta, E., Ramírez, M. Á. & Gutierrez-Adan, A. Prion Protein Expression Regulates Embryonic Stem Cell Pluripotency and Differentiation. PLoS One 6, e18422 (2011).

291. Rezza, A. et al. Signaling Networks among Stem Cell Precursors, Transit-Amplifying Progenitors, and their Niche in Developing Hair Follicles. Cell Rep. 14, 3001–3018 (2016).

292. Smyth, I. et al. The extracellular matrix gene Frem1 is essential for the normal adhesion of the embryonic epidermis. Proc. Natl. Acad. Sci. 101, 13560–13565 (2004).

293. Hu, J. K.-H. et al. An FAK-YAP-mTOR Signaling Axis Regulates Stem Cell-Based Tissue Renewal in Mice. Cell Stem Cell 21, 91–106.e6 (2017).

294. Guarino, M. et al. Circulating SCCA–IgM complex is a useful biomarker to predict the outcome of therapy in hepatocellular carcinoma patients. Scand. J. Clin. Lab. Invest. 77, 448–453 (2017).

295. Pontisso, P. Role of SERPINB3 in hepatocellular carcinoma. Ann. Hepatol. 13, 722–727 (2014).

296. Rosowski, K. A., Mertz, A. F., Norcross, S., Dufresne, E. R. & Horsley, V. Edges of human embryonic stem cell colonies display distinct mechanical properties and differentiation potential. Sci. Rep. 5, 14218 (2015).

297. Narba, A. et al. The Matrisome: In Silico Definition and In Vivo Characterization by Proteomics of Normal and Tumor Extracellular Matrices. Molecular & cellular proteomics : MCP 11, (2012).